NASA Contractor Report - 166051

F-111 NATURAL LAMINAR FLOW GLOVE FLIGHT TEST DATA ANALYSIS AND BOUNDARY LAYER STABILITY ANALYSIS

(NASA-CR-166051) F-111 NATURAL LAMINAR FLOW GLOVE FLIGHT TEST DATA ANALYSIS AND BOUNDARY LAYER STABILITY ANALYSIS Contractor Report, Aug. 1981 - Jul. 1983 (Boeing Commercial Airplane Co.) 224 p HC A10/MF A01 CSCL 01C

N86-15305

Unclas
G3/05 16049

Preliminary Design Department

BOEING COMMERCIAL AIRPLANE COMPANY
P.O. BOX 3707, SEATTLE, WASHINGTON 98124

CONTRACT NAS1-15325
JANUARY 1984

FOR EARLY DOMESTIC DISSEMIN

PUBLICLY RELEASED ON JAN 1986

NASA

National Aeronautics and
Space Administration

Langley Research Center
Hampton, Virginia 23665

1. Report No. NASA CR-166051	2. Government Accession No.	3. Recipient's Catalog No.
4. Title and Subtitle F-111 NATURAL LAMINAR FLOW GLOVE FLIGHT TEST DATA ANALYSIS AND BOUNDARY LAYER STABILITY ANALYSIS		5. Report Date January 1984
		6. Performing Organization Code
7. Author(s) L. James Runyan, Brent H. Navran, and Rodger A. Rozendaal		8. Performing Organization Report No D6-51153
		10. Work Unit No.
9. Performing Organization Name and Address Boeing Commercial Airplane Company P.O. Box 3707 Seattle, WA 98124		11. Contract or Grant No. NAS1-15325
		13. Type of Report and Period Covered Contractor Report— August 1981 through July 1983
12. Sponsoring Agency Name and Address National Aeronautics and Space Administration Washington, D.C. 20546		14. Sponsoring Agency Code

15. Supplementary Notes

Technical Monitor: D. B. Middleton
                 NASA-Langley Research Center

16. Abstract

This report contains an analysis of 34 selected flight test data cases from a NASA flight program incorporating a natural laminar flow airfoil into partial wing gloves on the F-111 TACT airplane. This analysis determined the measured location of transition from laminar to turbulent flow. The report also contains the results of a boundary layer stability analysis of 25 of the selected cases in which the crossflow (C-F) and Tollmien-Schlichting (T-S) disturbance amplification factors were correlated with the measured transition location. The chord Reynolds numbers for these cases ranged from about 23 million to 29 million, the Mach numbers ranged from 0.80 to 0.85, and the glove leading-edge sweep angles ranged from 9 deg to 25 deg. The results indicate that the maximum extent of laminar flow varied from 56% chord at 9-deg sweep to 21% chord at 25-deg sweep on the upper surface, and from 51% chord at 16-deg sweep to 6% chord at 25-deg sweep on the lower surface. The results of the boundary layer stability analysis indicate that when both C-F and T-S disturbances are amplified, an interaction takes place that reduces the maximum amplification factor of either type of disturbance that can be tolerated without causing transition.

17. Key Words (Suggested by Author(s)) Boundary layer Natural laminar Cross flow disturbances flow (NLF) wing glove Flight test Thickness Reynolds Linear stability theory number Natural laminar flow (NLF) Tollmien-Schlichting disturbances	18. Distribution Statement FEDD distribution Subject Category 05

19. Security Classif. (of this report) Unclassified	20. Security Classif. (of this page) Unclassified	21. No. of Pages 237	22. Price

F-111 NATURAL LAMINAR FLOW GLOVE FLIGHT TEST DATA ANALYSIS AND BOUNDARY LAYER STABILITY ANALYSIS

Preliminary Design Department

BOEING COMMERCIAL AIRPLANE COMPANY
P.O. BOX 3707, SEATTLE, WA 98124

NATIONAL AERONAUTICS AND SPACE ADMINISTRATION
LANGLEY RESEARCH CENTER

FOREWORD

This report presents the results of the F-111 Natural Laminar Flow Glove Flight Test Data Analysis and Boundary Layer Stability Analysis. The work was conducted under NASA Contract NAS1-15325 from August 1981 through June 1982. Eight additional cases were analyzed in May, June, and July 1983. Two of the 25 data cases analyzed and included herein were funded by Boeing Independent Research and Development (IR&D). The contract was managed by the NASA Energy Efficient Transport Office (EETPO), which is headed by R. V. Hood, and is a part of the Aircraft Energy Efficiency (ACEE) program organization at Langley Research Center. D. B. Middleton was the technical monitor for the contract. The work was performed by the Preliminary Design department and the Technical Staff of the Boeing Commercial Airplane Company. Key contractor personnel responsible for this effort were:

G. W. Hanks
Program Manager

A. L. Nagel
Aerodynamics Supervision

G. E. Ledbetter
Project Manager

B. H. Navran
Aerodynamics

L. B. Gratzer
Technology Management

R. A. Rozendaal
Aerodynamics

W. M. Howard
Aerodynamics Supervision

L. J. Runyan
Aerodynamics

W. A. Blissell
Aerodynamics Supervision

D. A. Sikavi
Aerodynamics

W. D. Larsen
Aerodynamics

T. C. VerSteegh
Aerodynamics

CONTENTS

Page

FIGURES

FIGURES

TABLES

Page

1.0 SUMMARY

Airplane wing profile drag can be significantly reduced by designing the wing to have extended natural laminar flow (NLF). Extended NLF relies on favorable chordwise pressure gradients to stabilize the boundary layer and maintain laminar flow. The amount of natural laminar flow, however, depends on the Reynolds number, Mach number, and sweep angle.

A NASA flight program incorporating an NLF airfoil into partial wing gloves on the F-111 Transonic Aircraft Technology (TACT) airplane was conducted in mid-1980 to evaluate the extent of NLF at relatively high Reynolds numbers through a range of wing sweep angles. This report contains an analysis of 34 selected cases of flight test data from that program. From measured boundary layer velocity profiles, the analysis determined the location of transition from laminar to fully turbulent flow in the boundary layer. The report also contains the results of a boundary layer stability analysis of 25 selected cases in which crossflow and Tollmien-Schlichting disturbance amplification factors were correlated with the transition location. The chord Reynolds numbers for these cases ranged from 23 to 29 million, and the Mach numbers ranged from 0.80 to 0.85.

The results of the flight test data analysis show that the maximum extent of laminar flow varied from 56% chord at 9-deg sweep to 21% chord at 25-deg sweep on the upper surface, and from 51% chord at 9-deg sweep to 6% chord at 25-deg sweep on the lower surface. Because the transition location was not measured directly in this test but inferred from measured boundary layer velocity profiles, there is some uncertainty associated with these transition locations.

The results of the boundary layer stability analysis show that in cases for which crossflow amplification was zero, the Tollmein-Schlichting amplification factor at transition ranged from 7.8 to 12.9. None of the cases analyzed had zero T-S amplification. For the cases in which both types of disturbances are amplified, the results indicate that an interaction takes place reducing the maximum amplification factor of either type of disturbance that can be tolerated without causing transition. Many of the lower surface results showed transition at unexpectedly low amplification factors, indicating that transition was probably affected by external disturbances, such as engine noise or insect contamination.

The results of the boundary layer stability analysis should increase confidence in the results of future NLF design work. However, because of the limited flight data base and the uncertainty in transition location resulting from the type of instrumentation used on the glove, a more comprehensive flight test is needed. It is recommend the test a new flight test program be initiated to further explore the effects of wing sweep, lift coefficient, and Mach number and also the effects of Reynolds number and noise. The test should have improved instrumentation to now transition location directly and in real time.

2.0 INTRODUCTION

The recent rise in jet fuel prices has caused an increased interest in improving aircraft fuel efficiency. A promising way to achieve significant improvements is to design a wing to provide extensive laminar flow. NASA's Aircraft Energy Efficiency (ACEE) program has sponsored development of laminar flow technology for application to commercial transport airplanes. The ACEE studies (refs. 1, 2, and 3) show that with continuous chordwise suction, disturbances in the laminar boundary layer can be effectively controlled to sufficiently high Reynolds numbers and sweep angles to make laminar flow control (LFC) potentially feasible for use on large transports.

Investigations of natural laminar flow (NLF) (ref. 4) show that significant regions of laminar flow, although more limited than attainable with LFC, can be obtained on wings without suction if the pressure distribution is selected to retard disturbance growth in the laminar boundary layer. However, the range of sweep angles and Reynolds numbers at which NLF will work is limited. A flight test program to investigate these NLF limits was conducted by NASA-Dryden Flight Research Center. The flight vehicle was the F-111 Transonic Aircraft Technology (TACT) airplane fitted with partial wing gloves designed for extended laminar flow.

The best methods currently available for designing laminar flow wings are b   on linear boundary layer stability theory. This theory is used to calculate the growth of disturbances in the boundary layer. The two primary types of disturbances that are usually critical are the crossflow (C-F) mode and the Tollmien-Schlichting (T-S) mode. In previous applications of the theory, transition has been assumed to occur when the factor by which either disturbance has been amplified exceeds some allowable value. It has been suggested that a criterion based on an appropriate relationship between amplification factors for T-S and C-F disturbances should be used. Because the linear stability theory is used in combination with some form of transition criterion to predict the transition point, this amplification criterion is a key element of the laminar flow wing design method and must be established by correlation between theory and experimental data.

Only a limited amount of experimental data are available from full-scale flight tests of partially laminarized wings (refs. 5, 6, 7, and 8). These previous flight test programs provided useful data for laminar flow research and for the calibration of

theoretical methods. However, the F-111 NLF glove flight test was the first systematic flight test investigation of the effect of sweep on high-speed laminar boundary layer transition. As a result, this is the first set of flight test data that can provide guidance concerning the way C-F and T-S disturbances interact to cause transition.

2.1 OBJECTIVES

The objectives of this study were—

o   To analyze F-111 NLF glove flight test data (pressure distributions and boundary layer velocity profiles) for 34 selected cases (flight conditions) to determine the location of boundary layer transition from laminar to fully turbulent flow.

o   To analyze the boundary layer stability of 25 of the selected flight test cases and correlate C-F and T-S disturbance amplification factors with the transition location for each case.

o   To use these results to assess the interaction of C-F and T-S disturbances during the transition process.

2.2 APPROACH

2.2.1 Flight Test Data Analysis

The flight test data consisted of pressure distributions and boundary layer velocity profiles measured at a single spanwise station on the glove. For each case, in addition to the natural transition flight, at least one flight was made in which transition was forced with a trip strip at a known chordwise location on the glove. By computing the displacement-thickness Reynolds number f om the measured velocity profile for each of these forced transition flights and comparing it to that of the natural transition flight, the natural transition location for a given case was determined. Theoretical boundary layer calculations were used to aid in the analysis. Details of the analysis method are given in Appendix A.

2.2.2 Boundary Layer Stability Analysis

The boundary layer stability analysis was performed using Boeing computer programs with input data consisting of measured pressure distributions, Reynolds numbers, Mach numbers and glove sweep angles. This analysis yielded the maximum disturbance amplification factor as a function of chordwise location for both C-F and T-S disturbances. The measured transition location for each case (as determined in the first part of the study) was then used to determine the C-F and T-S disturbance amplification factors at transition for each case.

3.0 SYMBOLS AND ABBREVIATIONS

3.1 ACRONYMS

C-F	crossflow
DELTA	boundary layer thickness (height above surface at which velocity is 99% of local freestream velocity)
KS	component of dimensional wave number parallel to the leading edge
LFC	laminar flow control
NCF	crossflow disturbance amplification factor
NLF	natural laminar flow
NTS	Tollmien-Schlichting disturbance amplification factor
RDTH	displacement thickness Reynolds number
REC	Reynolds number based on chord
TACT	Transonic Aircraft Technology
T-S	Tollmien-Schlichting
TRANS	transition location, x/c

3.2 MATHEMATICAL SYMBOLS

A	disturbance amplitude
A_o	disturbance amplitude at neutral stability point
c	chord
$\bar{c}$	average chord
C_L	airplane lift coefficient
C_p	pressure coefficient
C_{p_N}	pressure coefficient based on velocity normal to glove leading edge
$\alpha^*_{r_s} = KS$	component of dimensional wavenumber in direction of glove leading edge
$\ln A/A_o$	amplification factor
M	Mach number
N	disturbance amplification factor ($\ln A/A_o$)
p	pressure
q	dynamic pressure
$R_\delta^* = RDTH$	displacement thickness Reynolds number ($U_e \delta^*/\nu$)

Re_c	Reynolds number based on chord ($U_\infty c/\nu$)
s/c	normalized arc length from leading edge along glove surface
U_e	velocity at edge of boundary layer
U_∞	undisturbed reference velocity
u	component of velocity parallel to boundary layer rake
u'	component of velocity parallel to local potential flow direction
w'	component of velocity normal to local potential flow direction
x/c	normalized distance from leading edge along airfoil chord
y	distance above glove surface
y/c	normalized airfoil ordinate
α	angle of attack
δ	boundary layer thickness (height above surface at which velocity is 99% of local freestream velocity)
δ^*	boundary layer displacement thickness
Λ	sweep angle
ν	dynamic viscosity coefficient

3.3 SUBSCRIPTS

e	denotes edge of boundary layer
L	lower surface
LE	leading edge
N	normal to glove leading edge
TE	trailing edge
TR	transition
U	upper surface
∞	undisturbed reference condition

4.0 CONFIGURATION AND FLIGHT TEST DESCRIPTION

A program initiated by NASA-Dryden Flight Research Center (DFRC) resulted in the design of a natural laminar (NFL) flow airfoil. This NLF airfoil was developed jointly by NASA-Dryden Flight Research and Langley Research Centers as a part of the Aircraft Energy Efficiency (ACEE) program. The airfoil was designed to have favorable pressure gradients over 50% of the lower surface and 65% of the upper surface. A partial wing glove incorporating this airfoil was designed by NASA to fit over the outer wing panels of the variable sweep F-111 Transonic Aircraft Technology (TACT) airplane. A photograph of the F-111 with NLF gloves in flight and a planform view of the glove and airplane are shown in Figure 1. A sketch of the NLF airfoil is shown in Figure 2. Airfoil coordinates are given in Appendix B.

The glove airfoil section was defined to be streamwise for a leading-edge sweep angle of 10 deg. The glove leading-edge sweep angle was controllable from 9 to 26 deg.

Both wings of the F-111 were fitted with NLF gloves. The right glove was instrumented to measure pressure distributions and boundary layer velocity profiles. A row of upper and lower surface pressure orifices was located at the midspan of the glove. The left glove was added for symmetry.

A boundary layer rake was located at 90% of the chord on both the upper and lower surfaces for the first 17 flights, and at 60% chord on the upper surface, and 50% chord on the lower surface for the last two flights. The boundary layer rakes were 4 inches high and consisted of 18 pressure probes each. The boundary layer rakes and the pressure orifice rows were aligned in the streamwise position relative to the flow for a wing sweep of 10 deg.

The boundary layer velocity profiles measured by the rakes were the primary means of determining the transition location for each case. In order to calibrate data derived from the measured velocity profile for natural transition (clean wing) against the boundary layer transition location, flights were made for which transition was forced by a boundary layer trip strip attached to the surface of the wing. Forced transition flights were made with the trip at 5% chord when the rakes were in the forward location, and for five trip locations ranging from 5% to 50% chord when the rakes were at 90% chord.

9
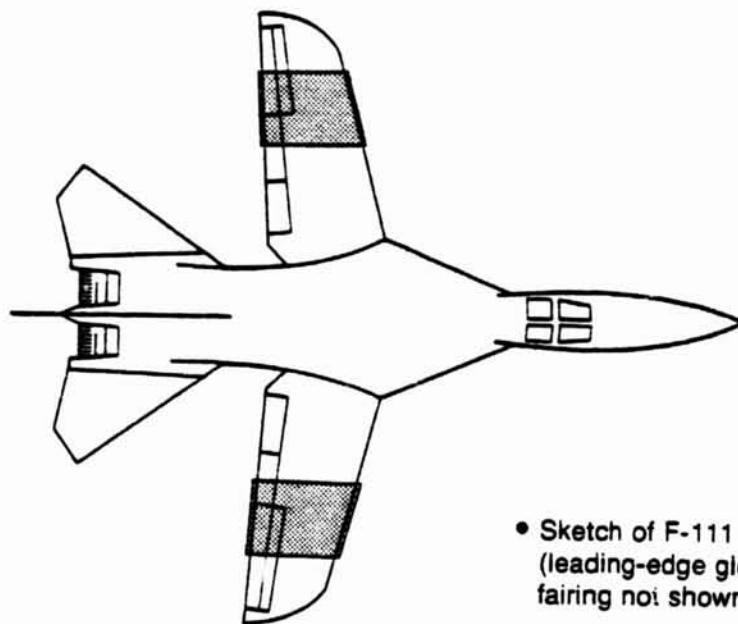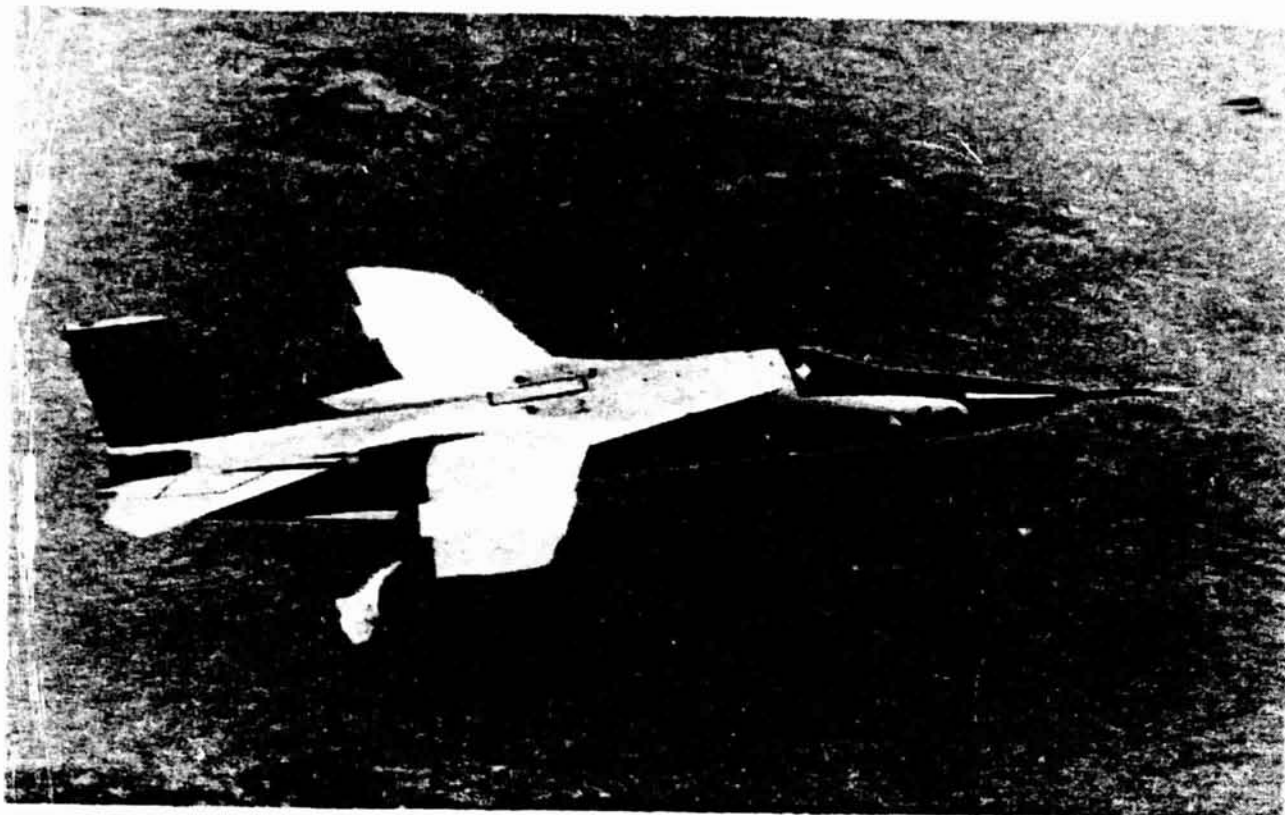
- Sketch of F-111
  (leading-edge glove
  fairing not shown)

Figure 1.   F-111 With NLF Glove

• Airfoil NLAM78

$\Lambda_{LE} = 10$ deg

$\Lambda_{TE} = -1.28$ deg

1.83 m
(6 ft)

• $\bar{c} = 3.06$ m (10.03 ft)

• $C_L = 0.50$
• $M = 0.770$
• $Re_c = 25 \times 10^6$

C_P

x/c
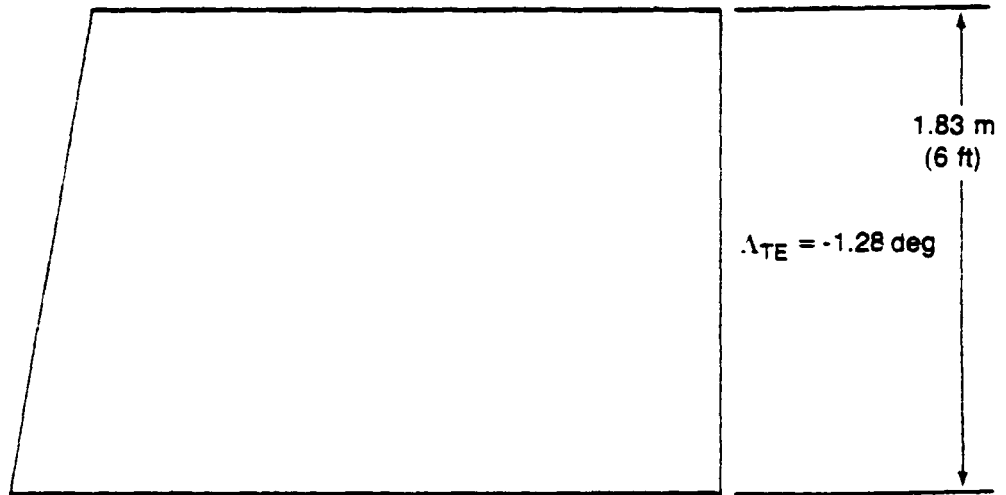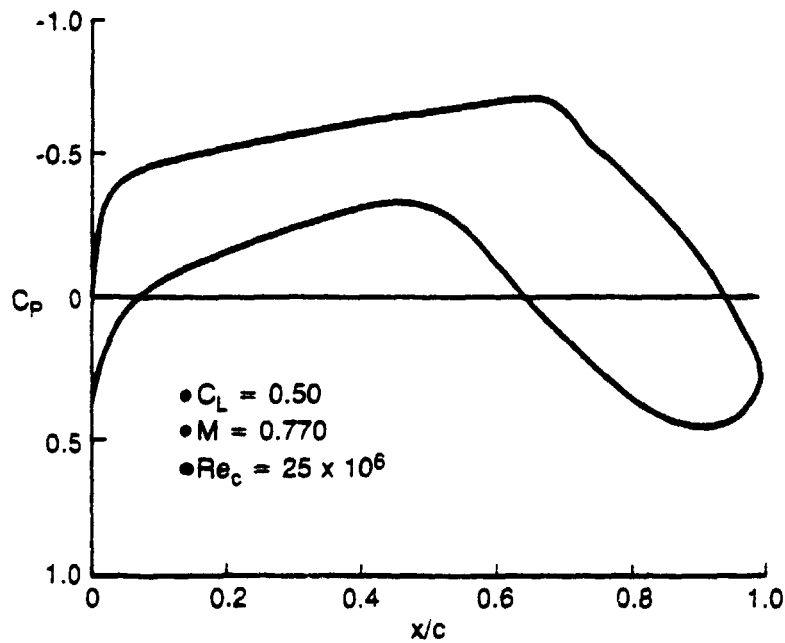
Figure 2. F-111 NLF Glove Geometry and Calculated Pressure

Nineteen flights were made at altitudes of either 9144m (30 000 ft) or 7620m (25 000 ft) and at Mach numbers ranging from 0.80 to 0.85. The resulting Reynolds numbers, based on the average chord of the glove, varied from about 23 million at 9144m (30 000 ft) to about 29 million at 7620m (25 000 ft). The glove leading-edge sweep angle varied from 9 to 26 deg.

5.0 FLIGHT TEST DATA ANALYSIS

5.1 METHOD OF ANALYSIS

A total of 34 cases were selected for analysis in the present study. A single case consisted of one glove surface (either upper or lower) at a specified flight condition and sweep angle. The measured data for each case consisted of the pressure distribution and the boundary layer velocity profile at the rake location for the natural transition (clean wing) flight and for 1 to 5 forced transition flights in which the boundary layer was tripped at specified locations. The objective of this analysis was to determine the transition location for the clean wing flight for each case. Because there is less uncertainty involved in determining δ^* than in determining δ from the measured velocity profiles, R_δ^* (at the rake location) was chosen as the best nondimensional parameter for correlation with the transition location. The forced transition flights allowed the trend of R_δ^* with transition location to be determined. The value of R_δ^* corresponding to the clean wing flight was then used to determine the natural transition location. The method of analysis is summarized in Figure 3 and discussed in Appendix A.

As shown in Figure 3, step 1 was to determine the displacement thickness Reynolds number (R_δ^*) for the clean wing flight from its measured velocity profile. A Boeing boundary layer program, A552, was then used to compute the expected trend of R_δ^* (at the rake location) with changes in the transition location for the clean wing flight conditions (step 2). A552 is a computer program for finite-difference calculation of compressible laminar or turbulent boundary layers on infinite (untapered) swept wings. Primary inputs to the program are the pressure distribution normal to the leading edge, Reynolds number, and Mach number. The primary outputs are the boundary layer temperature profile and the boundary layer velocity profiles, which are parallel and perpendicular to the local potential flow streamline. In step 3, A552 was used to compute R_δ^* at the rake location with various specified transition locations and with the flight conditions corresponding to those of the appropriate forced transition flight. The R_δ^* values were then determined for each of the forced transition flights from the measured velocity profiles (step 4). These R_δ^* values were then adjusted (step 5) to clean wing flight conditions by shifting by the difference in R_δ^* between step 2 and step 3. In step 6 a line was faired through the results of step 5 using the step 2 A552 results as a guide to the slope of the line. The location at which this line

Step	Condition
① ▬ ▬ ▬	Ⓑ
② ⊙	Ⓑ
③ ◉	Ⓐ
④ ◈	Ⓐ
⑤ ▣	Ⓑ
⑥ ▬ · ▬ · ▬	Ⓑ

Ⓐ = Conditions when forced transition flight test data points were taken: M, Re, pressure distribution, α, Λ

Ⓑ = Conditions when clean wing flight test data were taken M, Re_c, pressure distribution, α, Λ

④ Flight test data with forced transition at various positions — condition Ⓐ

⑥ Fairing — condition Ⓑ

⑤ Flight test transition data adjusted from condition Ⓐ to condition Ⓑ by shifting by amount of ◉ to ⊙

R_{δ^*}, displacement thickness Reynolds No.

① Flight test measured R_{δ^*} for clean—wing—condition Ⓑ

⑦ Final transition point = intersection of fairing of points with measured R_{δ^*} for clean wing—condition Ⓑ

③ A552 analysis with transition position specified — condition Ⓐ

② A552 analysis with transition position specified — condition Ⓑ

Transition position, % chord

Figure 3. Data Analysis Method

intersected the line of step 1 corresponds to the transition location for this case (step 7). The scatter in the adjusted test data for the forced transition flights (step 5) resulted in some uncertainty in the transition location. The amount of scatter varied from case to case, as shown in Appendix C.

5.2 RESULTS

A summary of the results for all 34 cases is given in Table 1. The extent of laminar flow was found to vary from 0% (case 7) to 56% (case 16). In general, the upper surface results at a given sweep angle show a greater extent of laminar flow than on the lower surface. The variation of transition location with sweep angle is shown in Figure 4. On the upper surface, the maximum extent of laminar flow varies from 56% chord at a sweep angle of 9 deg to 21% chord at a sweep angle of 25 deg. On the lower surface, the maximum extent of laminar flow varies from 51% chord at a sweep angle of 15 deg to 6% chord at a sweep angle of 25 deg. The lower surface cases that show transition at 31% chord or greater are from flight 146 and do not seem to follow the trend of the other lower surface cases. These were cases 26 through 34 and, as shown in Appendix C, the flight test results do not show anything unusual. However, as can be seen from Table 1, 10 of the 20 lower surface cases analyzed are from various data runs taken during flight 161. It is possible that the large extent of laminar flow for cases 26 through 34 is an indication that external disturbances (possibly insect contamination) may have affected the transition location for all cases from flight 161, but not for cases 26 through 34, which are from flight 146.

Because the lift coefficient varied from case to case, no conclusions can be drawn from the results concerning the effect of Reynolds number. Because there was some scatter in the flight test data used to determine the transition location for each case, some uncertainty was associated with each of the estimated transition locations. The magnitude of this uncertainty was not estimated.

The extent of laminar flow on the upper surface would probably have been greater if bumps (waves) in the pressure distribution had not been present. These bumps are present only at certain flight conditions and are apparently caused by shocks propagating onto the glove from the inboard wing, not by defects (such as waves) in the glove itself.

Table 1. F-111 NLF Glove: Summary of Results

Case	Surface	Rake, %	Flight	Run	Λ, deg	M	α, deg	C_L	$Re_c \times 10^{-6}$	s/c_{trans}, %	N_{T-S}	N_{C-F}
1	Lower	50	161	15	9.0	0.82	4.54	0.416	23.1	20	-	-
2		50	161	2	9.0	0.81	5.13	0.501	22.7	20	0.8	0.6
3		50	161	20	16.0	0.83	4.66	0.387	28.2	14	0.7	6.3
4		50	161	7	15.9	0.83	4.83	0.397	23.3	12	-	-
5		50	161	25	18.8	0.83	4.75	0.377	28.1	8	-	-
6		50	161	11	19.0	0.83	5.02	0.394	23.3	13	0.4	4.8
7		50	161	281	22.0	0.85	4.19	0.285	29.0	0	-	-
8		50	161	112	21.7	0.84	5.08	0.382	23.6	8	0.4	7.0
9		50	161	23	25.2	0.85	4.08	0.275	28.9	2	-	-
10	Lower	50	161	12	25.0	0.85	5.23	0.373	23.9	6	-	-
11	Upper	60	161	15	9.0	0.82	4.54	0.416	23.1	46	-	-
12		60	161	7	15.9	0.83	4.83	0.397	23.3	23	3.4	2.1
13		60	161	25	18.8	0.83	4.75	0.377	27.1	17	3.8	4.5
14		60	161	28	22.0	0.85	4.80	0.358	28.9	7	-	-
15		60	161	12	25.2	0.85	5.23	0.373	23.9	21	4.6	5.3
16		90	147	8A	9.0	0.82	4.15	0.379	23.1	56	7.8	0
17		90	155	18	9.0	0.82	4.62	0.432	27.9	55	8.7	0
18		90	158	3	9.0	0.82	5.24	0.504	23.0	45	12.9	0
19		90	147	14	16.1	0.83	4.58	0.379	23.3	36	5.4	2.2
20		90	147	15	16.1	0.83	5.02	0.436	23.3	42	6.6	2.0
21		90	147	16	16.1	0.83	5.90	0.550	23.4	43	6.6	2.2
22		90	158	23	25.2	0.85	4.28	0.276	28.9	20	5.5	6.7
23		90	147	21	25.1	0.85	4.88	0.357	23.8	18	-	-
24	Upper	90	155	13	25.2	0.82	5.72	0.429	23.8	15	4.4	7.0
25	Lower	90	155	3A	9.0	0.82	4.54	0.416	23.0	23	1.5	0.3
26	Lower	90	146	18	15.6	0.83	4.28	0.353	23.4	51	.	~5

Table 1. F-111 NLF Glove: Summary of Results (Concluded)

Case	Surface	Rake, %	Flight	Run	Λ, deg	M	α, deg	C_L	$Re_c \times 10^6$	s/c_{trans}, %	N_{T-S}	N_{C-F}
27	Lower	90	146	2	10	0.80	4.77	0.425	22.8	31	2.3	0.9
28				3	10	0.81	4.60	0.407	23.1	38	1.6	1.0
29				4	10	0.82	4.65	0.414	23.4	34	0.9	0.9
30				8	10	0.81	3.89	0.322	26.9	48	3.4	1.6
31				9	10	0.82	3.83	0.314	27.3	49	2.1	1.6
32				17A	15	0.83	3.87	0.292	27.7	51	*	6.6
33				17B	15	0.83	4.76	0.415	27.9	51	*	5.5
34				18B	16	0.83	5.00	0.447	23.2	51	*	6.4

*For these cases, T-S amplification varies so rapidly near the transition point (due to adverse local pressure gradient) that reliable values cannot be given
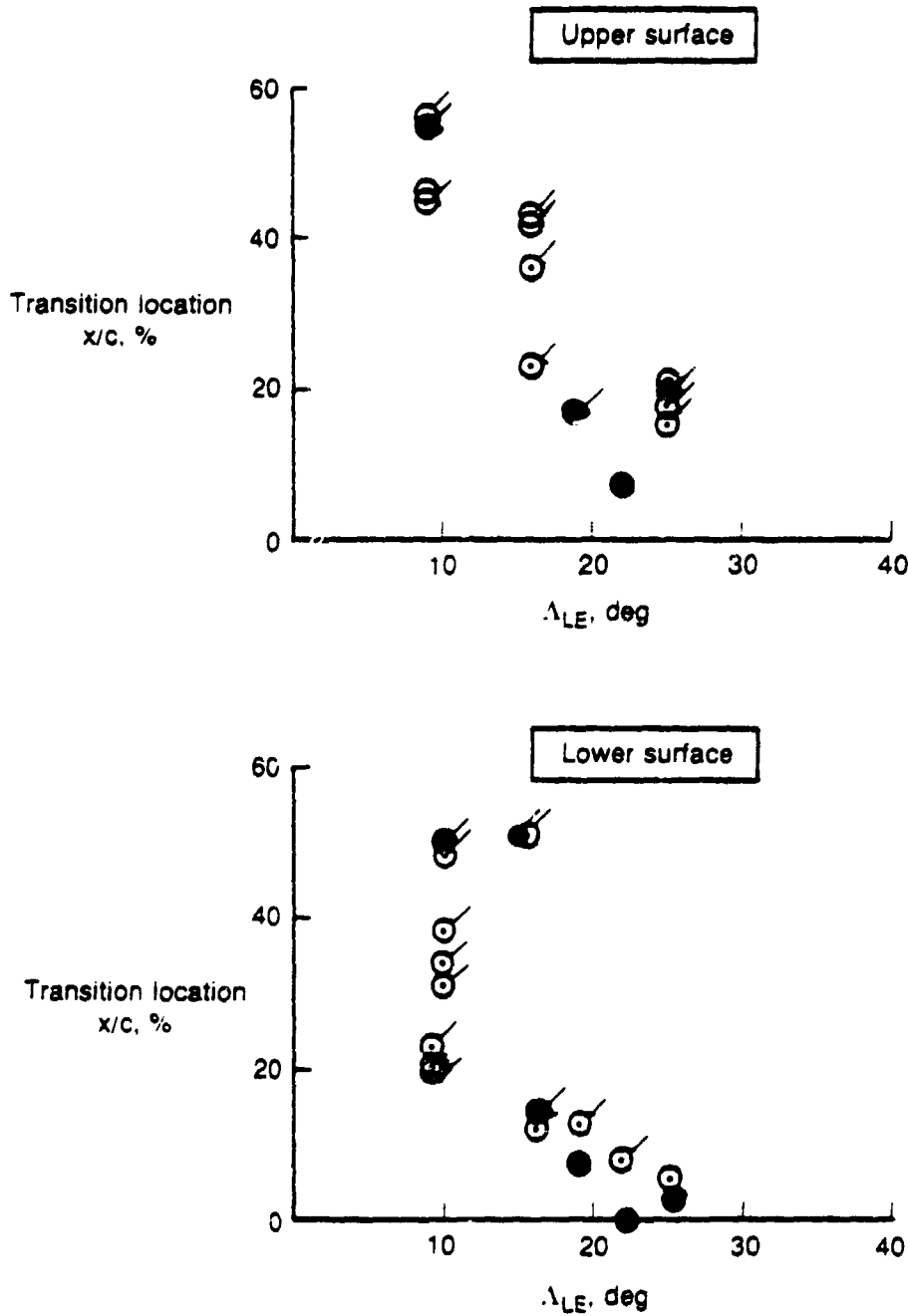
Figure 4. *Transition Location Versus Sweep*

Details of the case by case analysis, including pressure distributions and boundary layer velocity profiles, are in Appendix C.

6.0 BOUNDARY LAYER STABILITY ANALYSIS

Nearly all previous laminar flow flight test investigations dealt with either low sweep configurations (leading-edge sweep angles of about 10 deg or less), in which Tollmien-Schlichting (T-S) disturbances were the primary cause of transition, or high sweep configurations (leading-edge sweep angles of 30 deg or larger), in which crossflow (C-F) disturbances were the primary cause of transition. Because the F-111 data cover a range of sweep angles from low to high, there are many cases in which both amplified C-F disturbances and amplified T-S disturbances are present at the transition location. Because of these cases, these results provide insight into how the C-F and T-S disturbances interact during the boundary layer transition process. To understand this interaction, a boundary layer stability analysis was performed for 25 of the F-111 data cases.

6.1 LINEAR STABILITY THEORY

Current methods of predicting boundary layer transition are based on the linear boundary layer stability theory (refs. 9 to 16). The basic premise of this theory is that transition is caused by the amplification of initially small boundary layer disturbances as they propagate downstream. The rate at which a disturbance is amplified depends on its frequency and propagation direction. When the amplitude of the disturbance becomes large enough, it will begin to cause distortions of the mean flow of the laminar boundary layer, eventually resulting in transition to turbulent flow. Although the later stages of transition are beyond the scope of the theory, it still provides the best currently available basis for correlating transition data.

By solving the equations for linearized three-dimensional boundary layer stability (ref. 14), the amplification rate of small disturbances in the boundary layer can be computed at each point along the surface. The ratio of the disturbance amplitude, A, at any point to its amplitude, A_o, at the neutral stability point can be computed by integrating the amplification rate along the wing surface. The quantity $\ln A/A_o$ is called the amplification factor. By correlating measured transition locations with computed amplification factors for many cases, the amplification factor at which transition is likely to occur for a given disturbance environment can be inferred. The amplification factor can then be used to predict the transition location for a case in which that location has not been measured. Thus, the determination of the allowable

amplification factor for the primary disturbance modes is the key to useful application of the method.

On a high-speed swept wing there are four basic types of laminar boundary layer instabilities to be considered (refs. 17 and 18). These are: (1) T-S, (2) C-F, (3) Taylor-Goertler, and (4) leading-edge attachment line stability.

T-S instability has a direction of propagation (direction of wavenumber vector) close to the local freestream direction. Amplification of T-S disturbances is small in regions of favorable pressure gradient and large in regions of adverse pressure gradient.

A C-F instability has a direction of propagation nearly perpendicular to the local freestream direction. C-F in the boundary layer results from the combination of wing sweep and pressure gradient and is most severe in the wing leading-edge and trailing-edge regions, where pressure gradients are largest.

Taylor-Goertler instability occurs primarily in the flow over concave surfaces. Because the F-111 natural laminar flow (NLF) glove does not have concave surfaces in the region designed to have laminar flow, this type of instability was not considered in this study.

Attachment line instability refers to the behavior of the boundary layer along the forward stagnation or attachment line; i.e., the focus of points for which the chordwise velocity is zero. The boundary layer flow along the attachment line can be either laminar or turbulent depending on Reynolds number and environment, as described in Reference 18. If the attachment line flow does become turbulent, the flow over the wing will be turbulent also.

Detailed stability calculations are not required to assess attachment line instability; the boundary layer state depends primarily on the boundary layer thickness Reynolds number. However, there is an intermediate Reynolds number range where the boundary layer can be either laminar or turbulent depending on environment and flow history.

The potential for attachment line transition on the F-111 NLF glove is analyzed in Reference 19. The intermediate Reynolds number range mentioned in the preceding paragraph occurs at sweep angles of 23 to 35 deg for the F-111 laminar flow glove test conditions and wing geometry.

None of the 25 cases selected for the boundary layer stability analysis had transition at the leading edge, so attachment line instability apparently was not a problem in these cases.

6.1.1 Previous Studies

In previous studies, various linear boundary layer stability methods were calibrated against wind tunnel and flight test data. Variation from study to study in the amplification factors at transition is to be expected, because the calculation methods and the flow environment, both of which affect the amplification factors at transition, varied from study to study. Jaffe et al. (ref. 9) found that T-S transition correlated with an amplification factor of 10. Srokowski and Orzag (ref. 11) used an envelope method to analyze wind tunnel data and found that T-S-caused transition correlated with an amplification factor of 12 and C-F-caused transition correlated with amplification factors ranging from 10 to 11. In the envelope method, the disturbance frequency was kept fixed as the disturbance propagated downstream, but the disturbance wavelength was allowed to vary to maximize the disturbance amplification rate at each point along the wing. Runyan and George-Falvy (ref. 16) used a constant wave angle method and found that C-F-caused transition corresponded to an amplification factor of 12 and T-S-caused transition corresponded to an amplification factor of 15. The T-S result of 15 was based on a case for which the disturbance environment was favorable (sailplane in free flight). This value, therefore, is probably an upper bound that may be difficult to achieve in cases where engine noise or other disturbance source is present.

The previous studies did not assess the possible interaction of T-S and C-F disturbances during the process leading to transition. This assessment was the primary objective of the boundary layer stability analysis conducted in this study.

6.1.2 Method of Current Study

The procedure for the overall stability analysis is illustrated in Figure 5. The boundary layer characteristics are analyzed using a Boeing boundary layer program, A552. The boundary layer temperature and velocity profiles, which are the primary output of A552, become the primary input to the stability program, which is a Boeing modification of a computer program known as the MACK code (ref. 20). This program solves the boundary layer stability equations for three-dimensional, linearized, parallel flow for a perfect gas and can calculate either spatial (used in this study) or temporal stability. The program was used to calculate disturbance growth curves, such as those shown in Figure 5. (For a discussion of spatial versus temporal stability, see ref. 10.)

The disturbance growth direction used to compute amplification factors was along the local potential flow streamline. Mack (ref. 14) determined that this was a satisfactory approximation to the actual growth direction, which is equal to the real part of the group velocity angle. The MACK code can compute either incompressible or compressible stability. In the present study, compressible stability was used for all the calculations. The sixth order equations (which neglect dissipation) were used instead of the complete eighth order equations. This use resulted in a significant reduction in computation time, and, as shown by Mack (ref. 14), results given by the sixth order equations for a transonic swept wing differed from those of the eighth order equations by only a few percentage points.

T-S disturbances were followed downstream, keeping frequency and wave angle fixed. Relative to the local stream direction, this wave angle was 40 deg on the upper surface and 25 deg on the lower surface, where the local Mach number is lower. These wave angles were determined by varying the wave angle at fixed locations on the upper and lower surfaces for selected cases. They correspond closely to the wave angles for maximum disturbance amplification. This is assumed to be true for similar cases analyzed in this study.

C-F disturbances were followed downstream, keeping the frequency fixed and letting the wave angle vary in accordance with the irrotationality condition applied to the wavenumber vector, as proposed by Mack (ref. 10). In case 3, a comparison was made between the C-F amplification factor at transition obtained using the constant wave angle approach (ref. 16) to follow crossflow disturbances downstream, and the factor

24

- Boeing laminar boundary layer code
  - Infinite swept wing
  - Compressible

↓

Boundary layer
velocity profiles
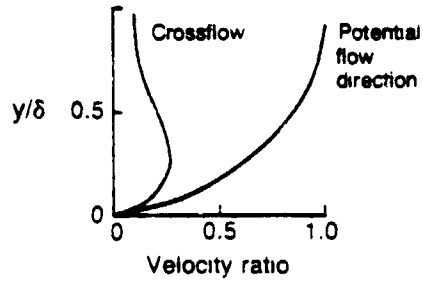
● Modified MACK stability code (Boeing)

  - Spatial or temporal stability
  - Compressible or incompressible

↓

Boundary layer
stability analysis
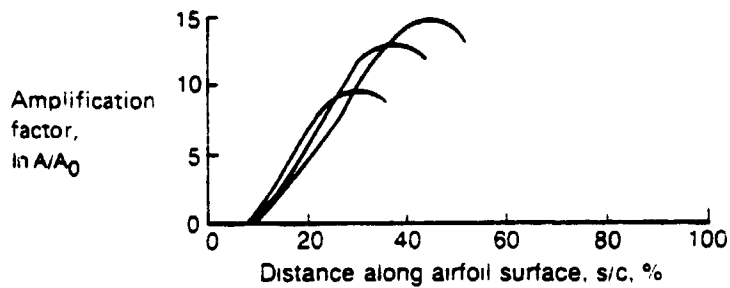
Figure 5. Stability Analysis Procedure

obtained using the irrotationality condition. The constant wave angle approach resulted in an amplification factor of 6 at transition; the irrotationality condition resulted in a value of 7.

Both Mack (ref. 14) and Srokowski and Orzag (ref. 11) found stationary crossflow disturbances (zero frequency) to be the most highly amplified. Mack showed that application of the irrotationality condition to stationary crossflow disturbances resulted in nearly constant wavelength disturbances, except for a small region of rapid change near the leading edge. Hefner and Bushnell (ref. 21) studied a number of cases and found that the most highly amplified crossflow disturbances sometimes did not occur at or near zero frequency but at significantly higher frequencies.

The effect of frequency on crossflow disturbance amplification was studied for case 21. The application of the irrotationality condition to a 939-Hz disturbance resulted in 13% higher amplification than did application of the irrotationality condition to a stationary crossflow disturbance. Although this result indicates that slightly higher crossflow amplification factors might have resulted for some cases if higher frequency disturbances had been analyzed, it is unlikely that the basic conclusions of the study would have been affected. Furthermore, any transition criterion is only applicable to the method used to derive it. The one derived here is, therefore, applicable to the commonly used method of considering only stationary crossflow disturbances.

As shown by Mack (ref. 14), the result of applying the irrotationality condition to an infinite swept wing analysis is that the spanwise (in the direction of the wing leading edge) component of the dimensional wavenumber, $\alpha^*_{r_s}$, must remain constant as the disturbance propagates downstream. Therefore, in defining the envelope of C-F disturbances, disturbances having a range of $\alpha^*_{r_s}$ values are followed downstream, with the frequency kept at zero.

6.2 RESULTS

Twenty-five cases were selected for the boundary layer stability analysis. These cases were selected because of their potential to provide insight into the interaction between T-S and C-F disturbances. Fourteen of the cases studied were for the lower surface of the glove, and the other 11 were for the upper surface.

The compressible C-F and T-S stability envelopes, with corresponding pressure distributions, are shown in the following figures. For T-S disturbances, the lines represent the envelope of a range of T-S disturbance frequencies. For the C-F disturbances, the lines represent the envelope of crossflow disturbances with a range of values of the spanwise component of the dimensional wavenumber, $\alpha^*_{r_s}$. Detailed disturbance growth curves for each case are in Appendix D.

The transition location for each case, the determination of which was described in Section 5.0, is used with the C-F and T-S envelopes to determine the C-F and T-S amplification factors at transition. These amplification factors are given in Table 1.

Cases 2 and 3 (figs. 6 and 7) are lower surface cases. Case 2 has a Reynolds number of 22.7 million and a sweep angle of only 9.0 deg. As a result, case 2 has very low C-F amplification factors. Case 3 has a higher sweep angle (16.0 deg) and a higher Reynolds number (28.2 million) than case 2, and as a result, it has much higher C-F amplification factors. At transition, case 3 has a C-F amplification factor of 6.3, compared with 0.6 for case 2. Neither case 2 nor case 3 show much amplification of T-S disturbances with amplification factors at transition of 0.8 for case 2 and 0.7 for case 3.

Cases 6 and 8 (figs. 8 and 9) are also lower surface cases. Case 6 has a sweep angle of 19.0 deg and Reynolds number of 23.3 million, and case 8 has a sweep angle of 21.7 deg and Reynolds number of 23.6 million. As shown in Table 1, case 6 has at transition a C-F amplification factor of 4.8 and a T-S of 0.4, and case 8 has at transition a C-F amplification factor of 7.0 and a T-S of 0.4.

Cases 12, 13, and 15 (figs. 10, 11, and 12) are upper surface cases for which the boundary layer rake was in the forward location (60% chord). The cases all show significant amplification of both C-F and T-S disturbances at transition.

Cases 16 through 24 are also upper surface cases but for flights having the aft-rake location (90% chord). Cases 16, 17, and 18 (figs. 13, 14, and 15), which all correspond to a very low sweep angle of about 9 deg, have no C-F amplification and large T-S amplification factors. Cases 19, 20, and 21 (figs. 16, 17, and 18), which all have a sweep angle of about 16 deg, have some crossflow amplification, but it is still less than

PRESSURE DISTRIBUTION

C_{p_N}

s/c

COMPRESSIBLE STABILITY

ln A/A_0

— C-F
--- T-S

o LOWER SURFACE
o TRANSITION AT S/C=.20
o SWEEP=9.0 DEG.
o REC=22.7 MILLION
o MACH NO.=.81
o CL=.501
o FLIGHT 161, RUN 2

s/c
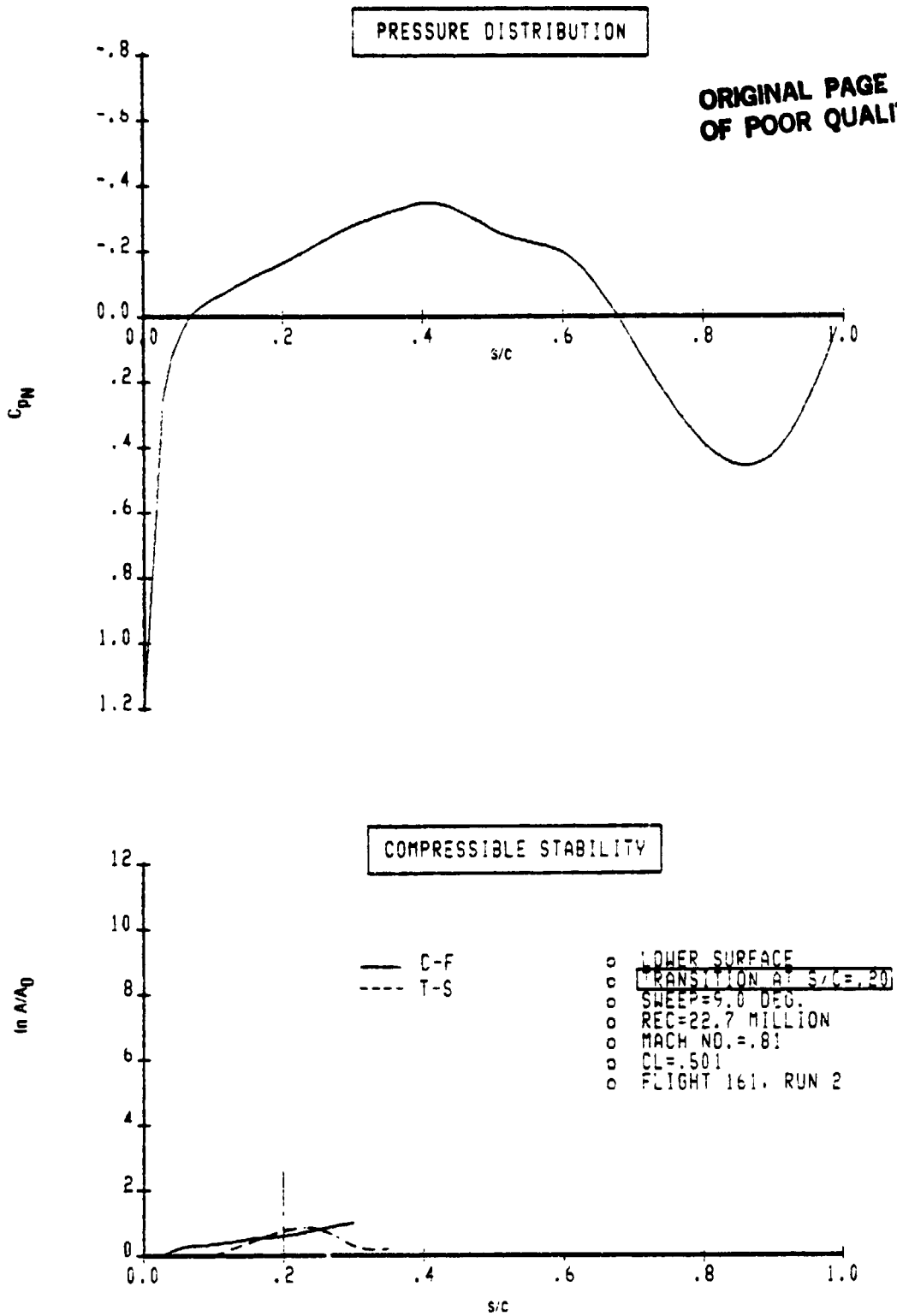
Figure 6. Case 2 Stability Envelopes

PRESSURE DISTRIBUTION

COMPRESSIBLE STABILITY

—— C-F
---- T-S

o LOWER SURFACE
o TRANSITION AT S/C=.14
o SWEEP=16.0 DEG.
o REC=28.2 MILLION
o MACH NO.=.83
o CL=.387
o FLIGHT 161, RUN 20
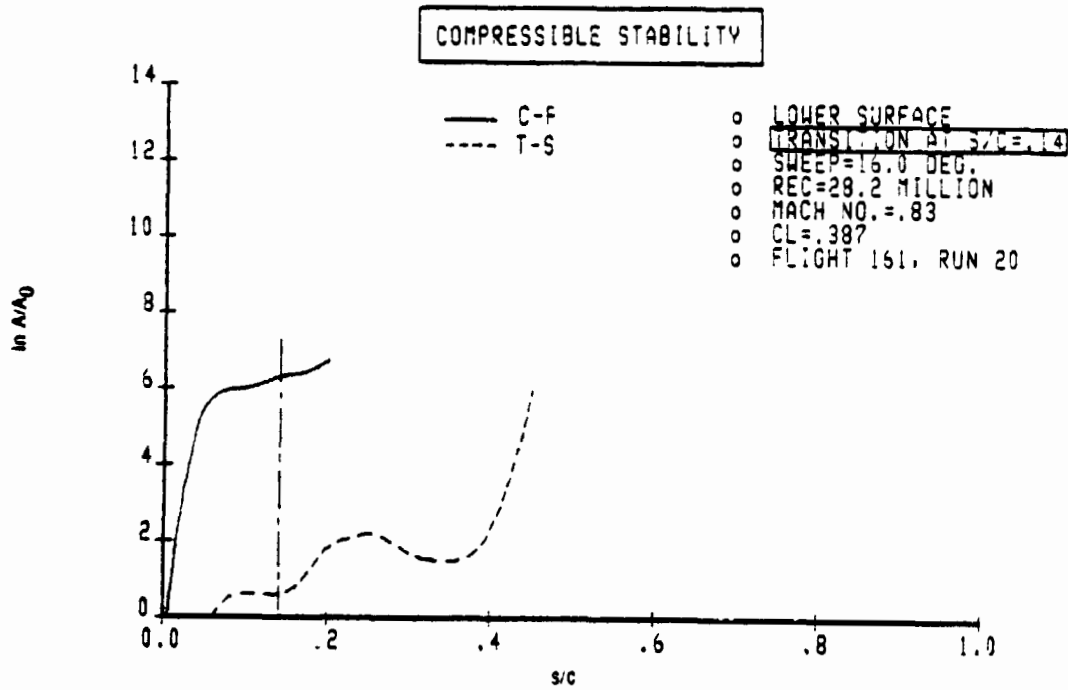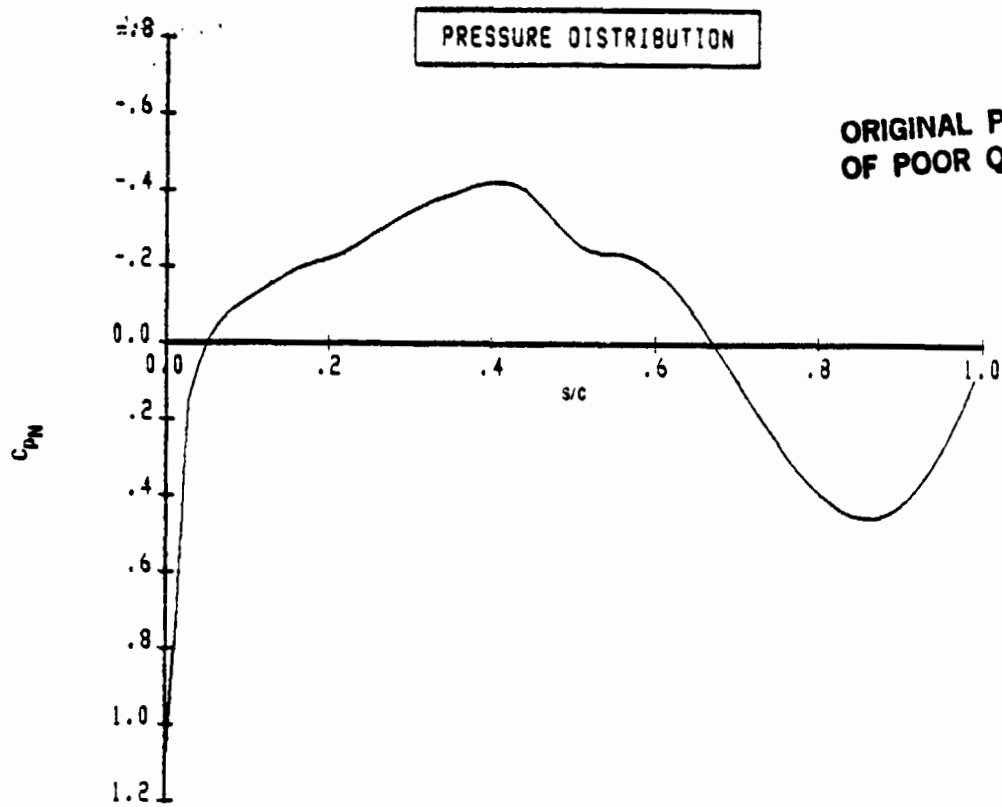
Figure 7. Case 3 Stability Envelopes

PRESSURE DISTRIBUTION

COMPRESSIBLE STABILITY

— C-F
---- T-S

o LOWER SURFACE
o TRANSITION AT S/C=.13
o SWEEP=19.0 DEG.
o REC=23.3 MILLION
o MACH NO.=.83
o CL=.394
o FLIGHT 161, RUN 11
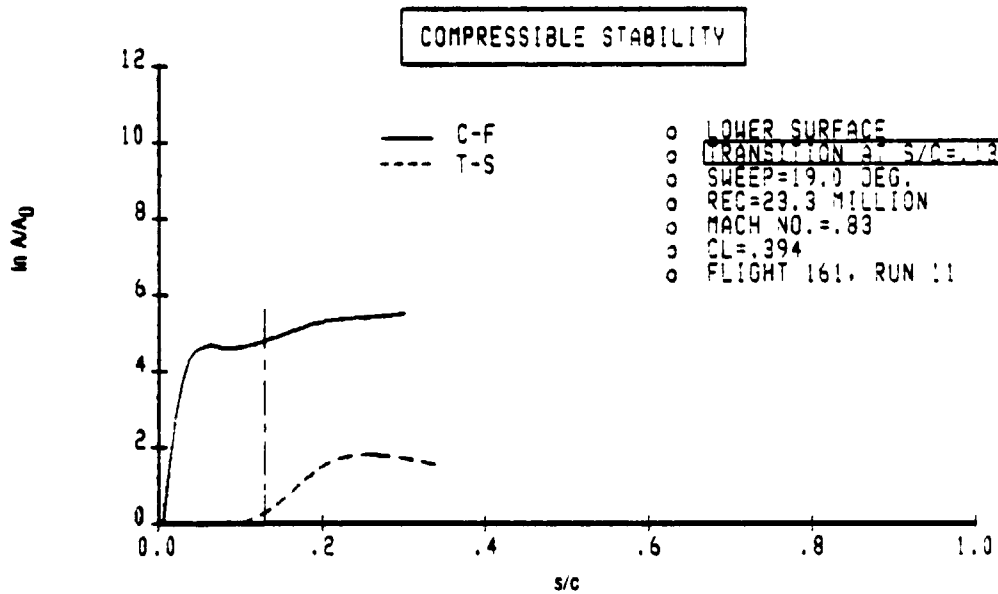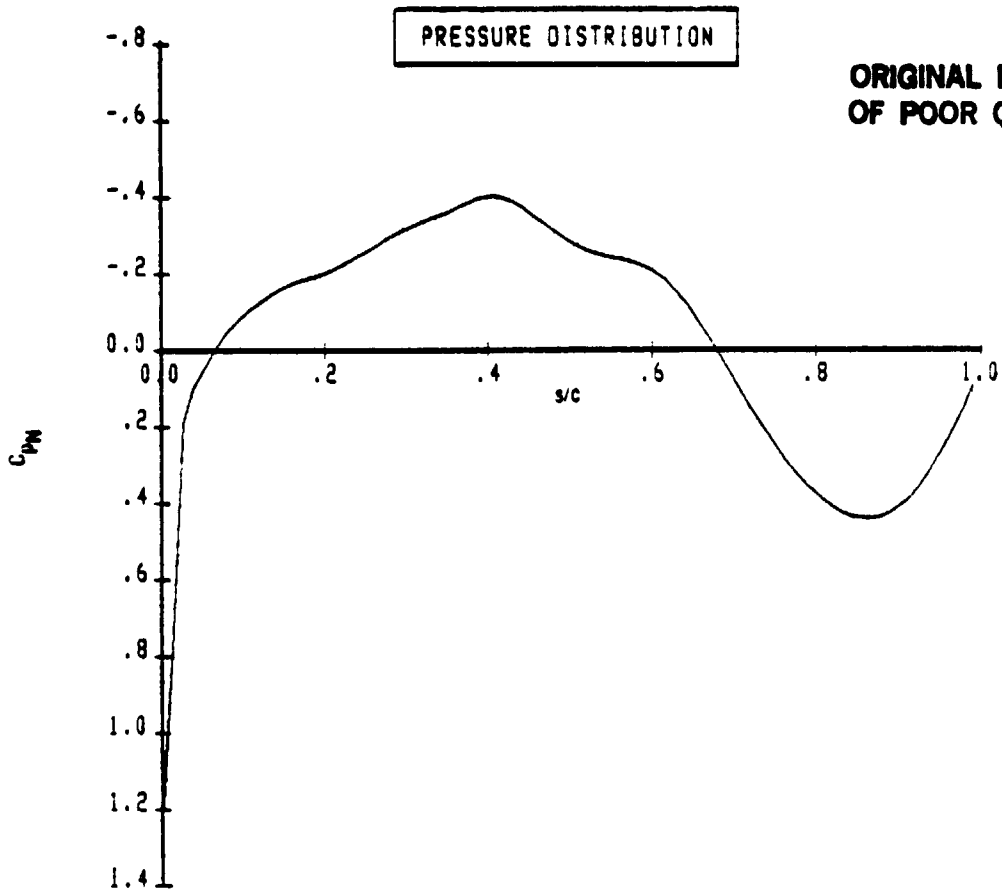
Figure 8. Case 6 Stability Envelopes

PRESSURE DISTRIBUTION

COMPRESSIBLE STABILITY

C-F
T-S

o LOWER SURFACE
o TRANSITION AT S/C=.18
o SWEEP=21.7 DEG.
o REC=23.6 MILLION
o MACH NO.=.84
o CL=.382
o FLIGHT 161, RUN 112
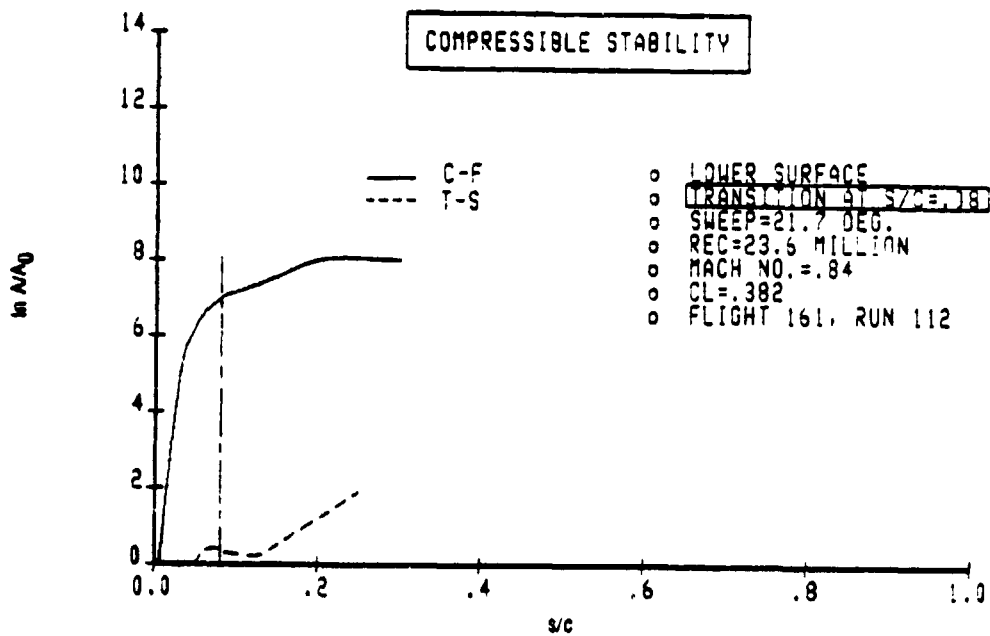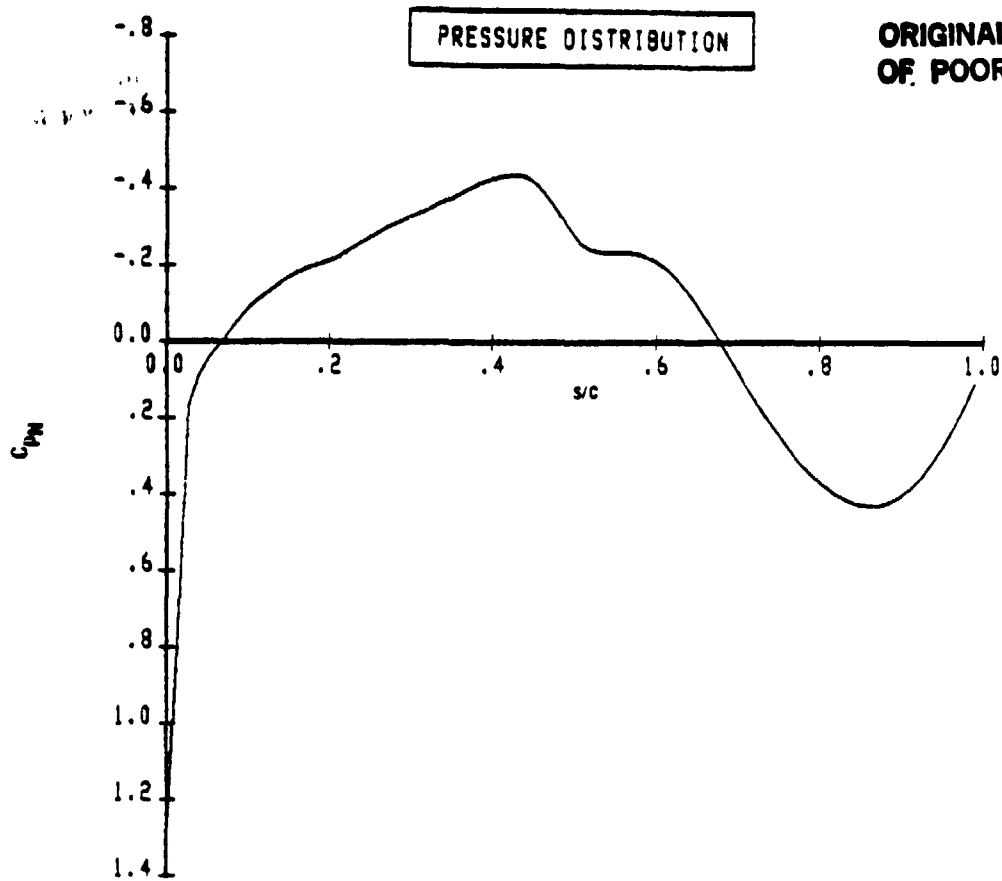
Figure 9. Case 8 Stability Envelopes

PRESSURE DISTRIBUTION

COMPRESSIBLE STABILITY

C-F

T-S

o UPPER SURFACE
o TRANSITION @ S/C=.21
o SWEEP=15.9 DEG.
o REC=23.3 MILLION
o MACH NO.=.83
o CL=.397
o FLIGHT 161, RUN 7
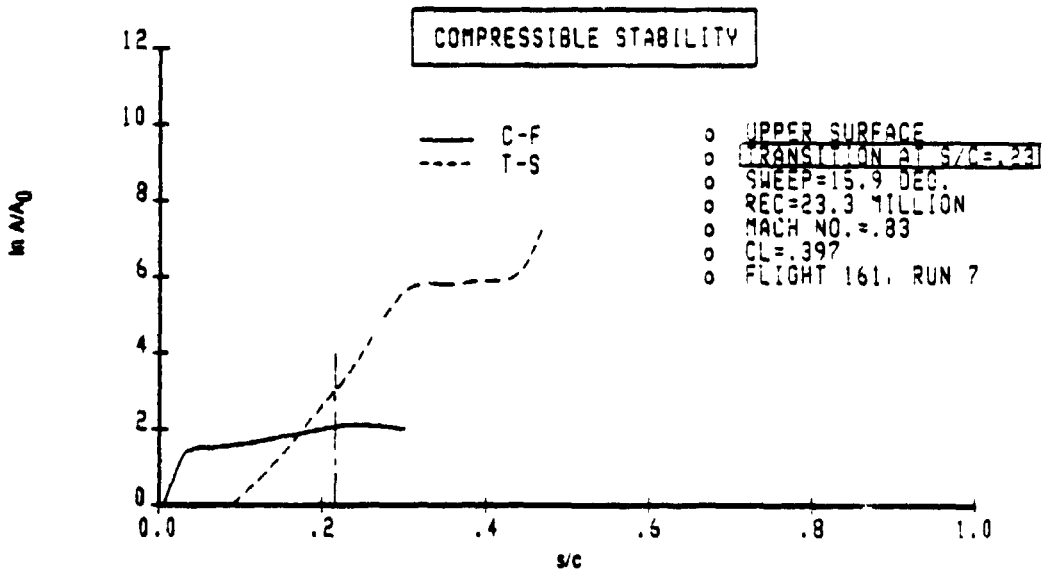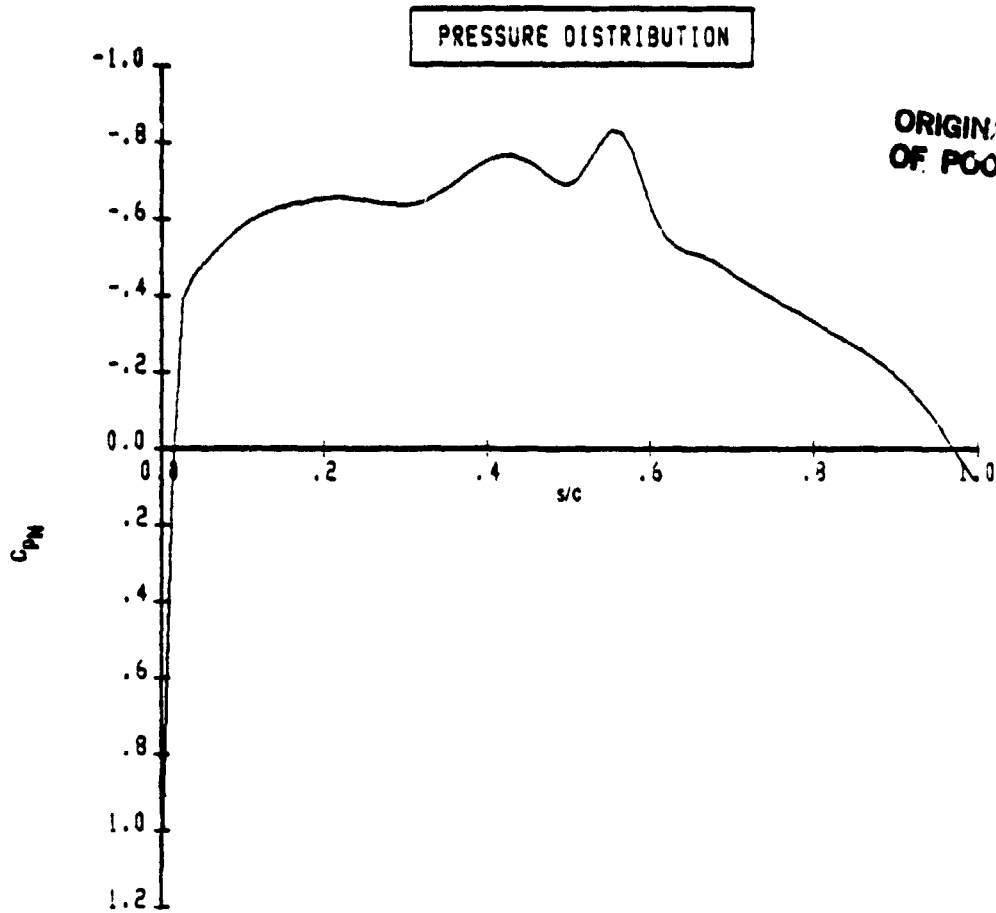
Figure 10. Case 12 Stability Envelopes

PRESSURE DISTRIBUTION

C_{PN}

s/c

COMPRESSIBLE STABILITY

ln A/A$_0$

—— C-F
---- T-S

UPPER SURFACE
TRANSITION @ S/C=.17
SWEEP=18.9 DEG.
REC=27.1 MILLION
MACH NO.=.33
CL=.377
FLIGHT 161, RUN 25

s/c
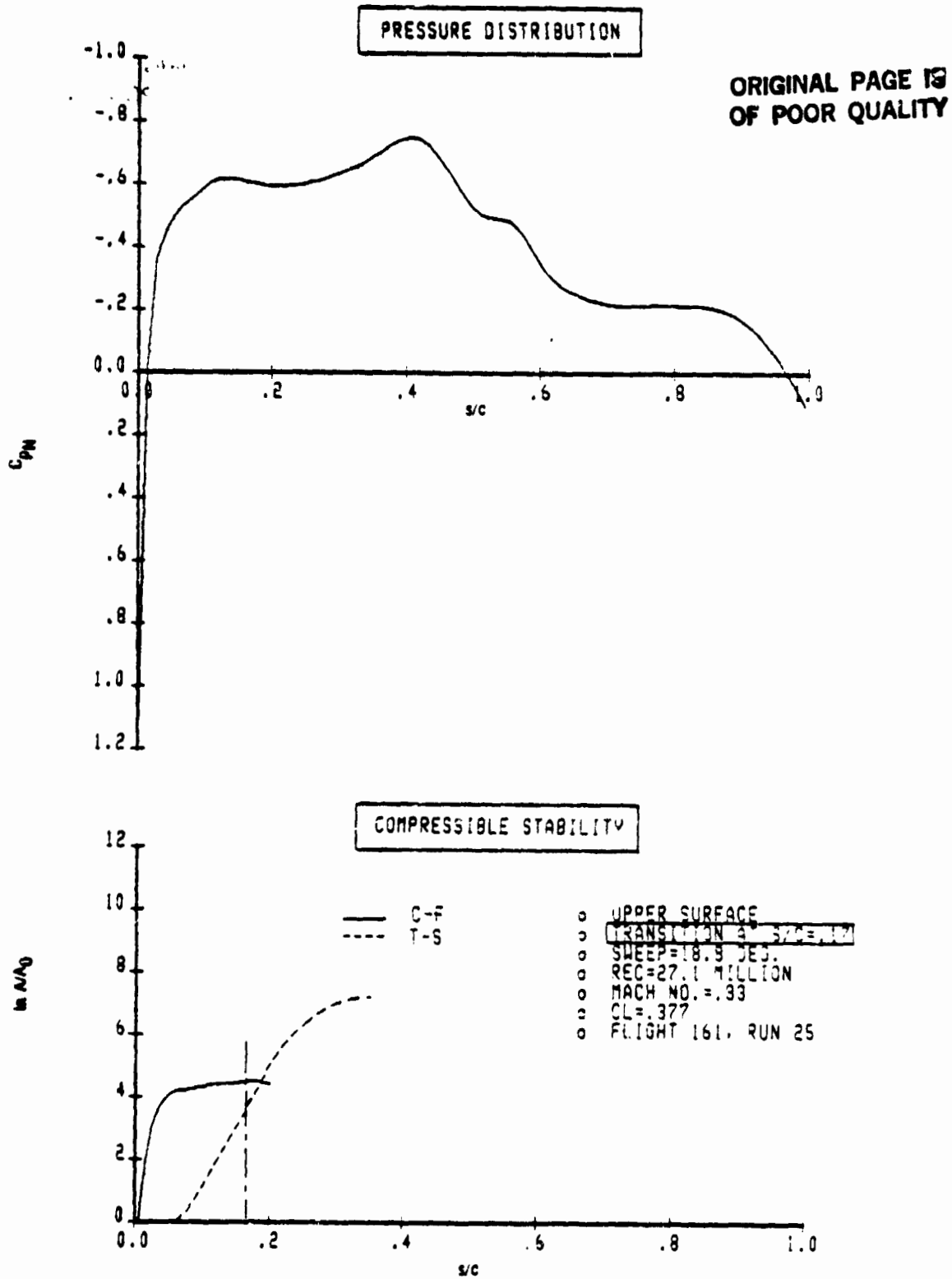
Figure 11. Case 13 Stability Envelopes

33
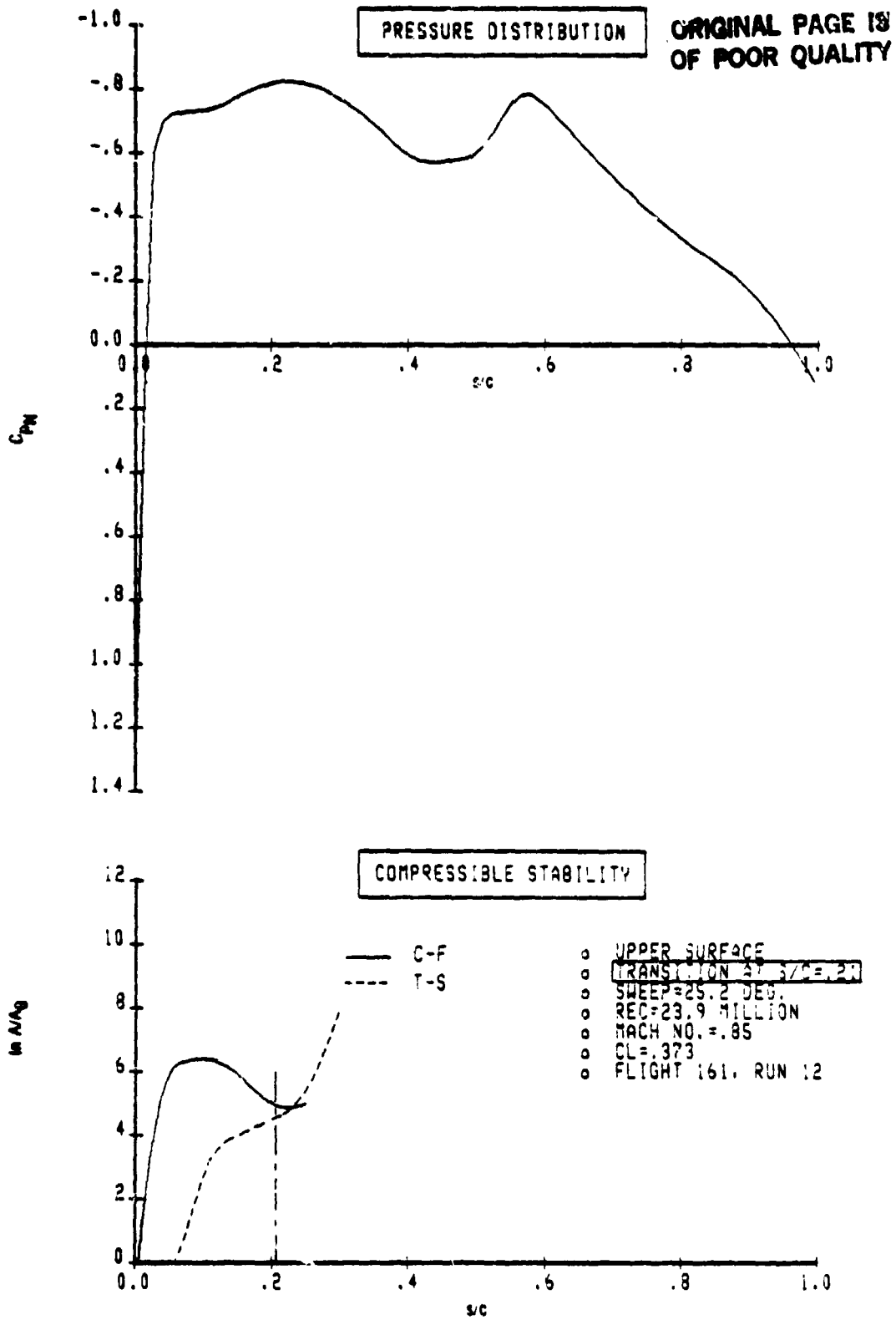
Figure 12. Case 15 Stability Envelopes

PRESSURE DISTRIBUTION

COMPRESSIBLE STABILITY

—— C-F
---- T-S

o UPPER SURFACE
o TRANSITION AT S/C=.56
o SWEEP=9.0 DEG.
o REC=23.1 MILLION
o MACH NO.=.82
o CL=.379
o FLIGHT 147, RUN 9A
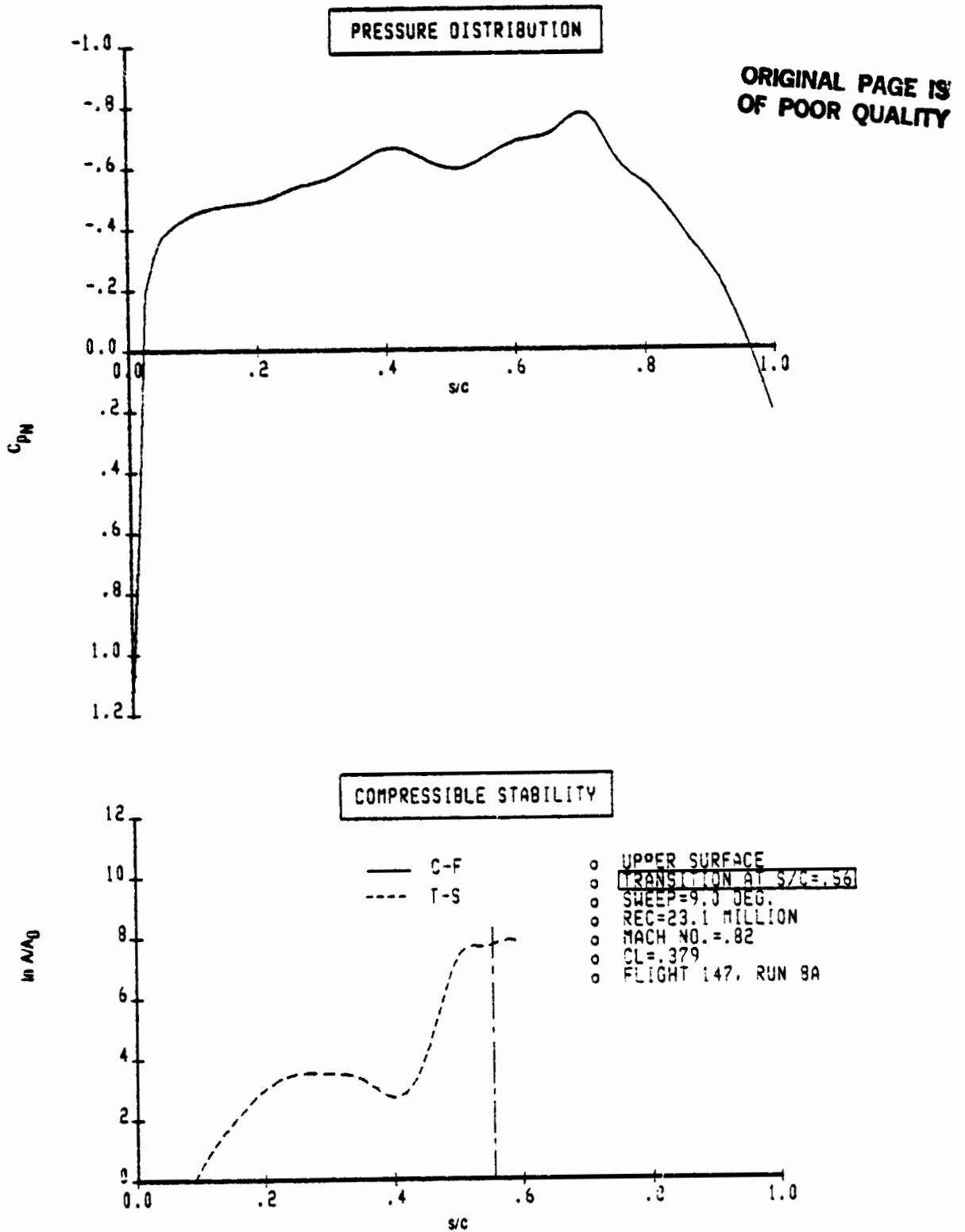
Figure 13. Case 16 Stability Envelopes

PRESSURE DISTRIBUTION

COMPRESSIBLE STABILITY
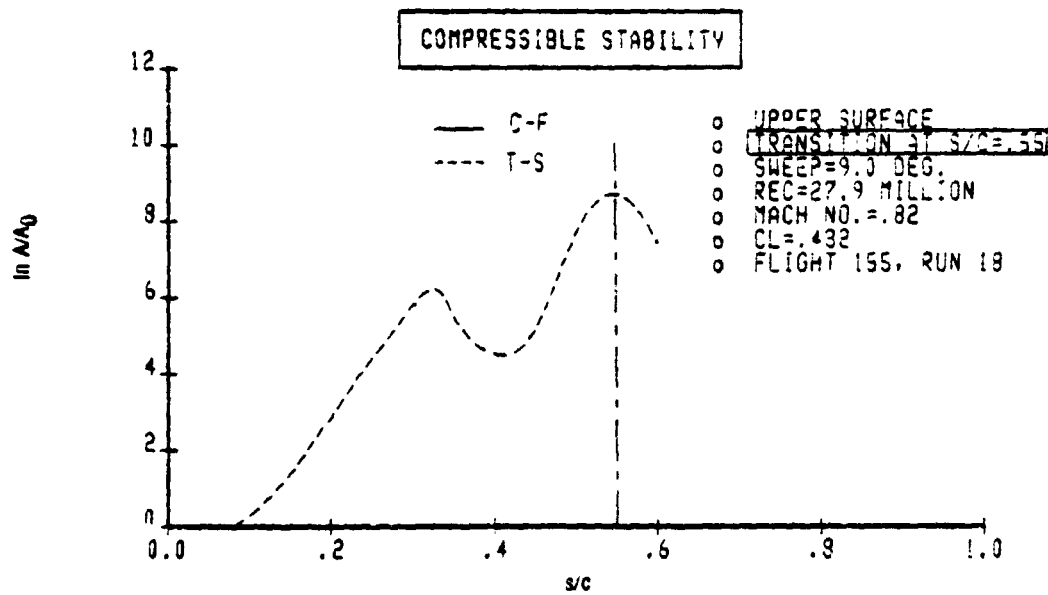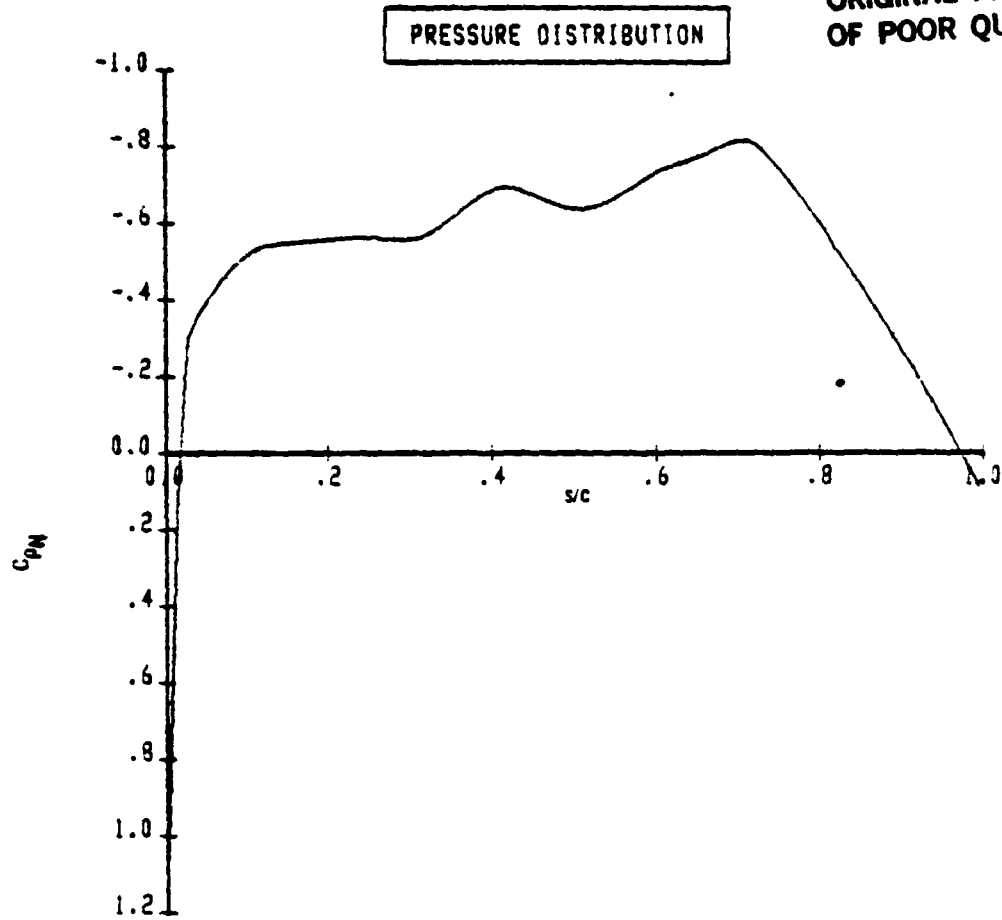
Figure 14. Case 17 Stability Envelopes
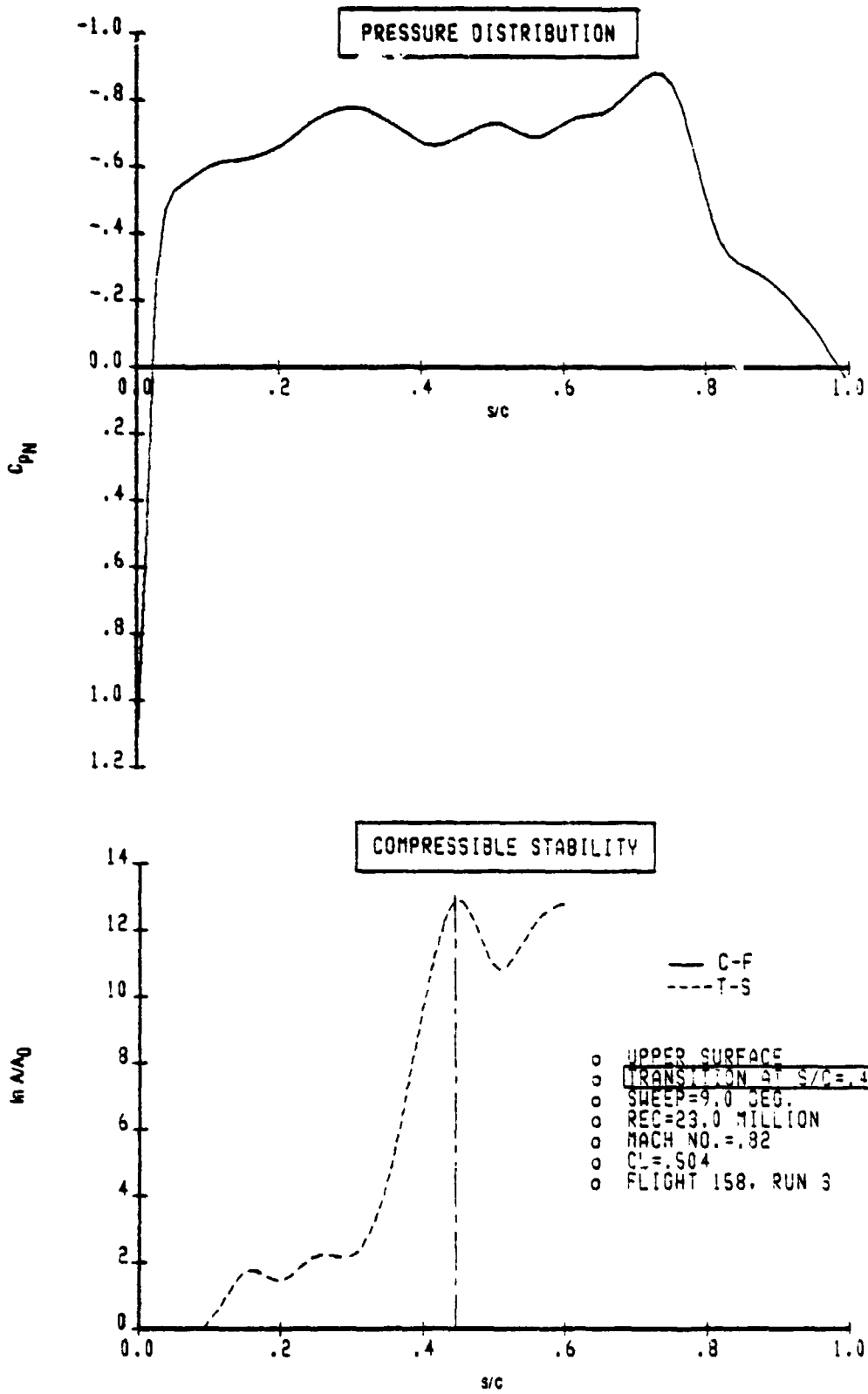
Figure 15. Case 18 Stability Envelopes

PRESSURE DISTRIBUTION

C_{p_N}

s/c

COMPRESSIBLE STABILITY

$\ln A/A_0$

—— C-F
---- T-S

UPPER SURFACE
TRANSITION AT S/C=.36
SWEEP=16.1 DEG.
REC=23.3 MILLION
MACH NO.=.83
CL=.379
FLIGHT 147, RUN 14

s/c
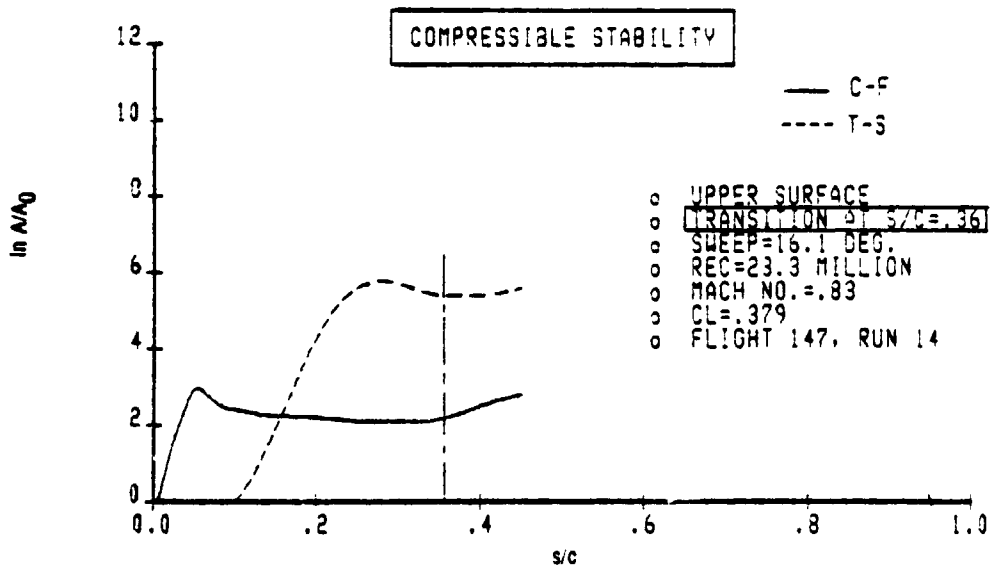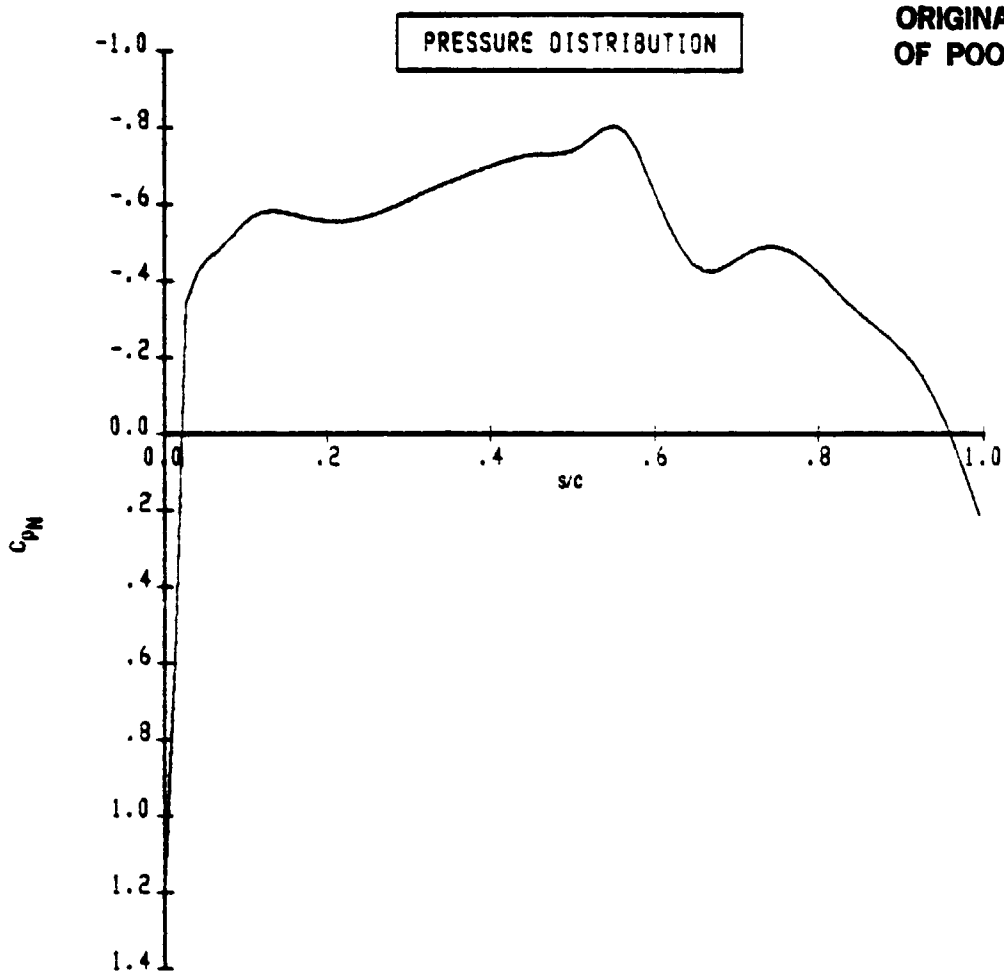
Figure 16. Case 19 Stability Envelopes

PRESSURE DISTRIBUTION

c_{p_N}

s/c

COMPRESSIBLE STABILITY

$\ln A/A_0$

—— C-F

---- T-S

o UPPER SURFACE
o TRANSITION AT S/C=.42
o SWEEP=16.1 DEG.
o REC=23.3 MILLION
o MACH NO.=.83
o CL=.436
o FLIGHT 147, RUN 15

s/c
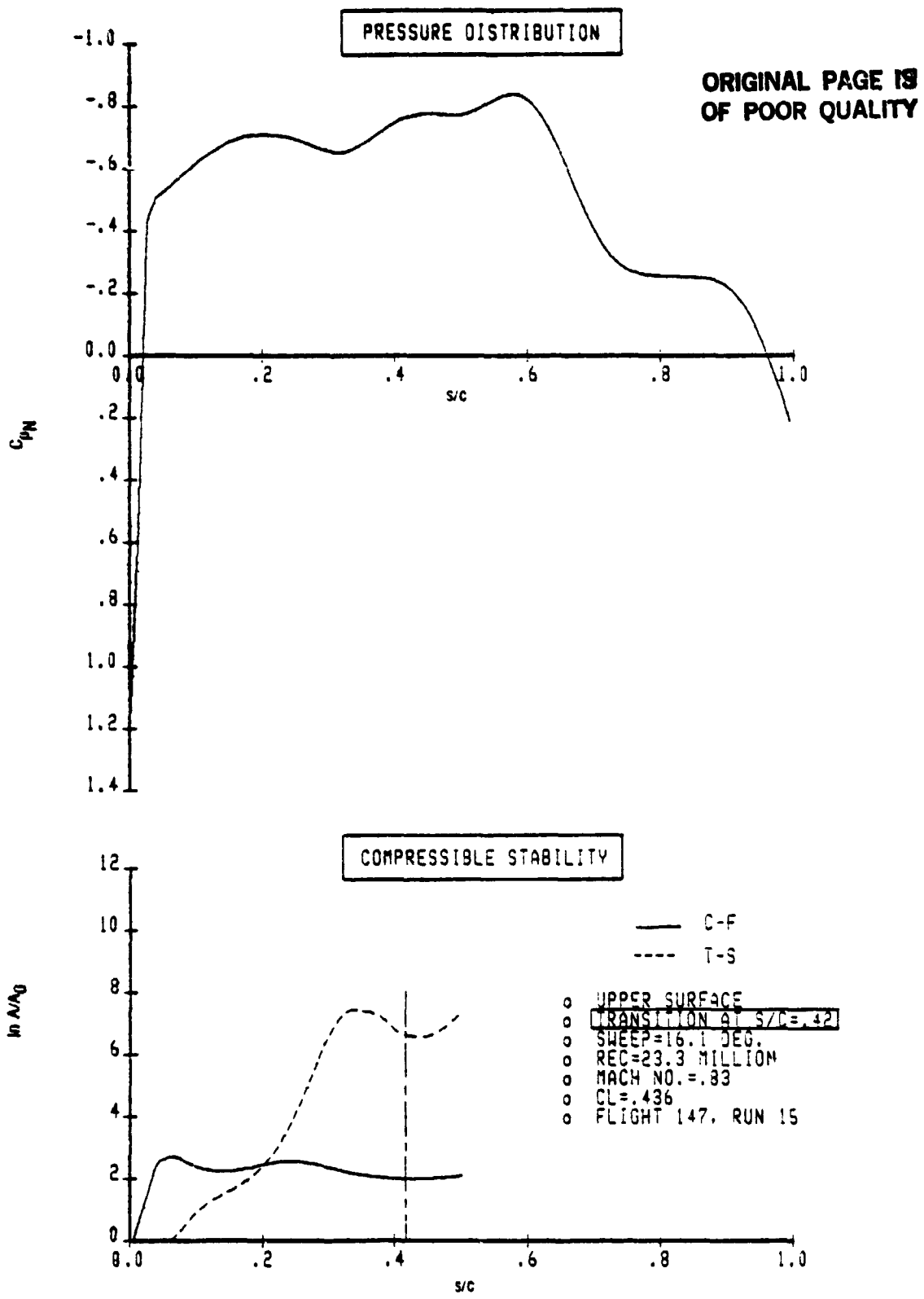
Figure 17. Case 20 Stability Envelopes
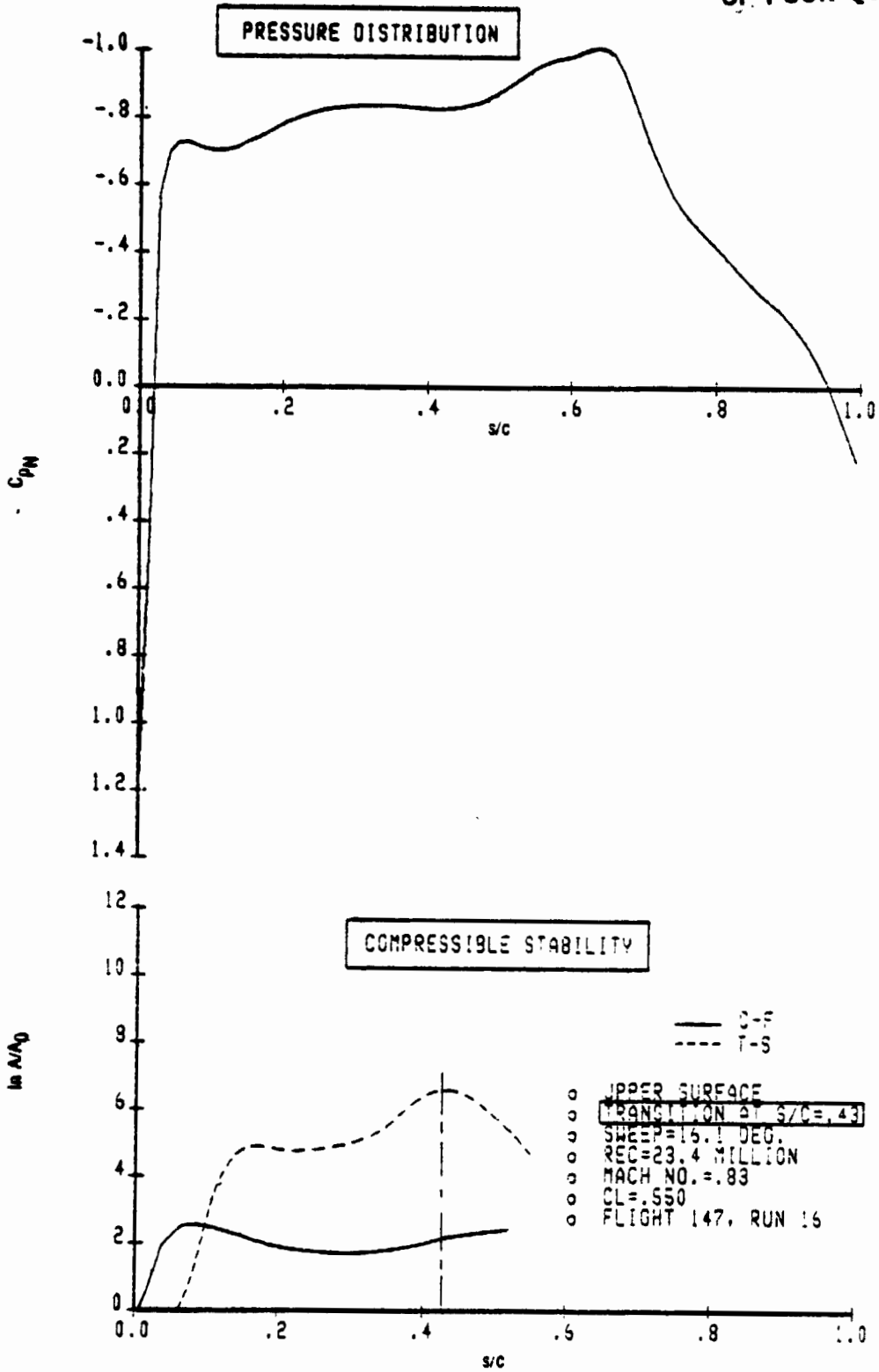
Figure 18. Case 21 Stability Envelopes

the T-S amplification. Cases 22 and 24 (figs. 19 and 20), which both have sweep angles of about 25 deg, have large amplification of both C-F and T-S disturbances.

Cases 25 through 34 (figs. 21 thorugh 30) are for the lower surface with the rake in the aft location. The sweep angle varies from 9 to 16 deg for these cases. Crossflow amplification was not calculated for cases 28, 29, and 30 because they were at low sweep angles and were almost duplicates of other cases. For cases 28 and 29, the crossflow results of case 27 were used, and for case 30 the crossflow results of case 31 were used. The T-S amplification factors for those cases that had transition at about 51% chord could only be estimated due to the rapid change in T-S amplification in that area. The transition could have been caused by laminar separation or the rapid growth of T-S disturbances due to the adverse pressure gradient. The cases from flight 146, cases 26 through 34, show much longer laminar runs than the other lower surface cases, but the amplification factors at transition are generally not a great deal higher. Stability analyses alone do not show why that one flight had the longer lower surface laminar runs.

In Figure 31, the T-S amplification factor at transition (NTS) has been plotted versus the C-F amplification factor at transition (NCF) for each of the cases analyzed. As indicated in the figure, different symbols have been used for the upper surface-aft rake cases, the upper surface-forward rake cases, and the lower surface cases.

It should be noted that the measured boundary layer velocity profiles for cases 16, 17, and 18 (shown in figs. B-30, B-31, and B-32 in app. B) indicate that there may be some flow separation or incipient flow separation at the rake location. However, this does not necessarily invalidate the use of the data for these three cases. If the velocity profile data still show the correct trend with change in forced transition location, then the clean wing profile data can be expected to give a valid estimate of the transition location. It can be seen from figures B-30, B-31, and B-32 that the boundary layer thickness δ varies in a reasonable manner with changes in the forced transition location. Also, Figures C-16, C-17, and C-18 in Appendix C show that the trend of measured displacement thickness Reynolds number, RDTH with forced transition location is in general agreement with the A552 estimate, with no more scatter than is present for most of the other cases. Furthermore, a comparison of the boundary layer thickness for a given forced transition location between any of cases 16 through 18 (figs. B-30, B-31, and B-32) with any of cases 19 through 21 (figs. B-33, B-34, and

PRESSURE DISTRIBUTION

COMPRESSIBLE STABILITY

——— C-F
- - - - T-S

o UPPER SURFACE
o TRANSITION AT S/C=.20
o SWEEP=25.2 DEG.
o REC=28.9 MILLION
o MACH NO.-.85
o CL=.276
o FLIGHT 158, RUN 23
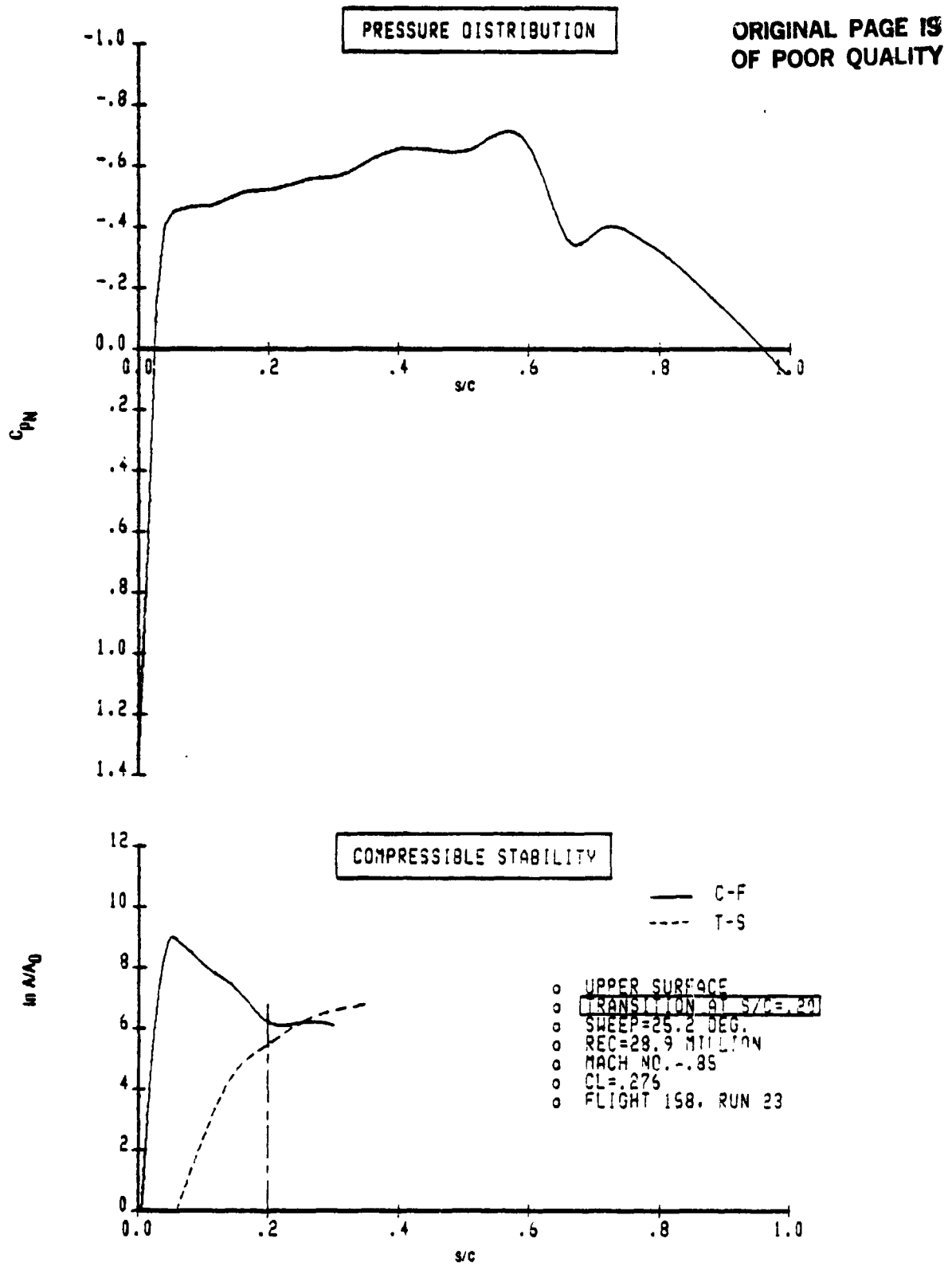
Figure 19. Case 22 Stability Envelopes

Figure 20. Case 24 Stability Envelopes

PRESSURE DISTRIBUTION

COMPRESSIBLE STABILITY

— C-F

---- T-S

o LOWER SURFACE
o TRANSITION AT S/C=.23
o SWEEP=9.0 DEG.
o REC=23.0 MILLION
o MACH NO.=.82
o CL=.416
o FLIGHT 155, RUN 3A

Figure 21. Case 25 Stability Envelopes

PRESSURE DISTRIBUTION

COMPRESSIBLE STABILITY

C-F
T-S

LOWER SURFACE
TRANSITION AT S/C=.5
SWEEP=15.6 DEG.
REC=23.4 MILLION
MACH NO.=.83
CL=.353
FLIGHT 146, RUN 18

Figure 22. Case 26 Stability Envelopes

PRESSURE DISTRIBUTION

COMPRESSIBLE STABILITY

———— C-F
– – – T-S

- LOWER SURFACE
- TRANSITION AT S/C = .31
- SWEEP = 10 DEG.
- REC = 22.9 MILLION
- MACH NO. = .80
- CL = .425
- FLIGHT 146, RUN 2
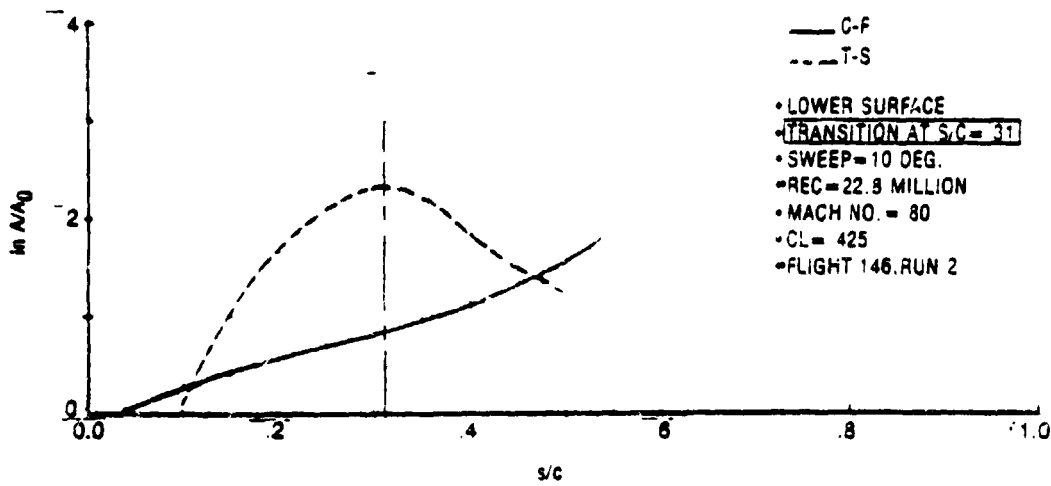
Figure 23. Case 27 Stability Envelopes

PRESSURE DISTRIBUTION

COMPRESSIBLE STABILITY

- C-F
- - - - T-S
- LOWER SURFACE
- TRANSITION AT S/C = .38
- SWEEP = 10 DEG.
- REC = 23.1 MILLION
- MACH NO. = .81
- CL = 407
- FLIGHT 146, RUN 3

C-F ENVELOPE FOR CASE 27 USED
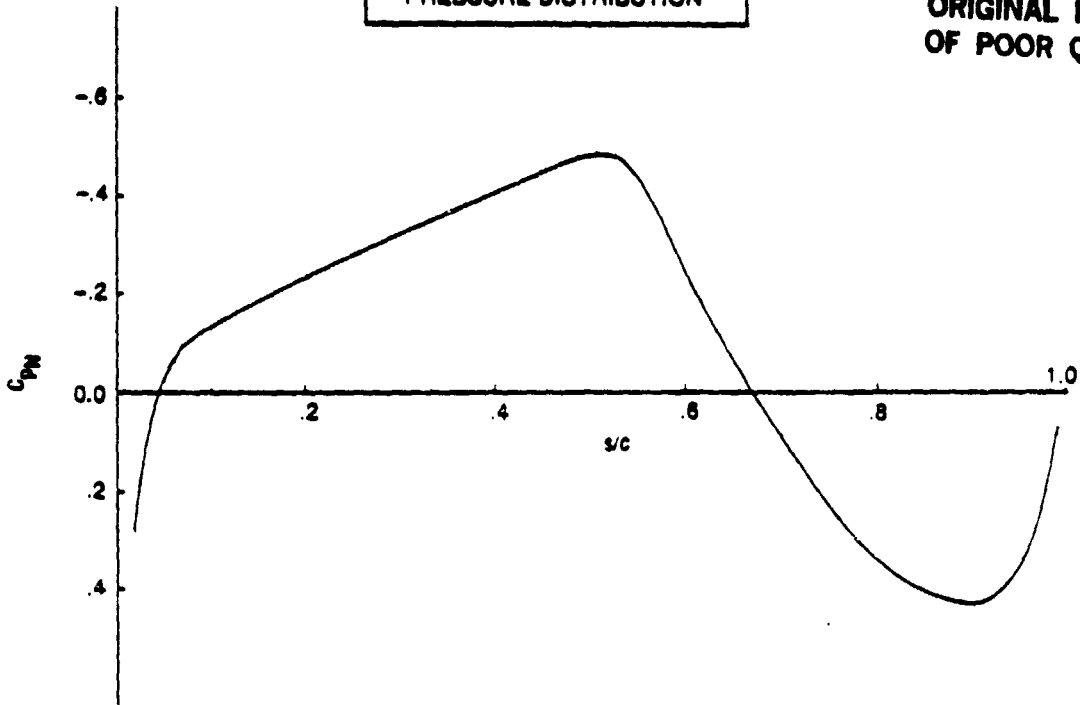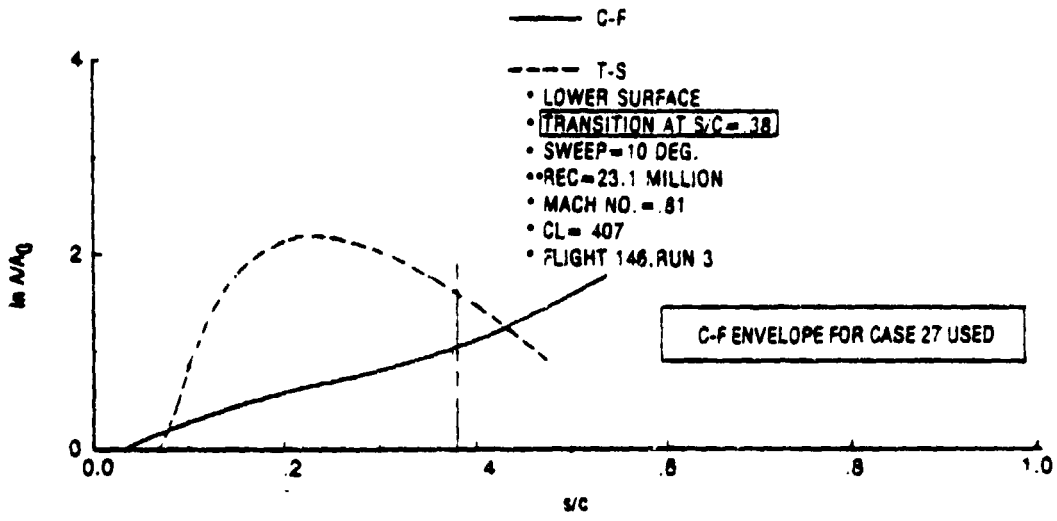
Figure 24. Case 28 Stability Envelopes

PRESSURE DISTRIBUTION

COMPRESSIBLE STABILITY

—————— C-F

— — — — T-S
- LOWER SURFACE
- TRANSITION AT S/C = 34
- SWEEP = 10 DEG.
- REC = 23.4 MILLION
- MACH NO. = 82
- CL = 414
- FLIGHT 148, RUN 4

C-F ENVELOPE FOR CASE 27 USED
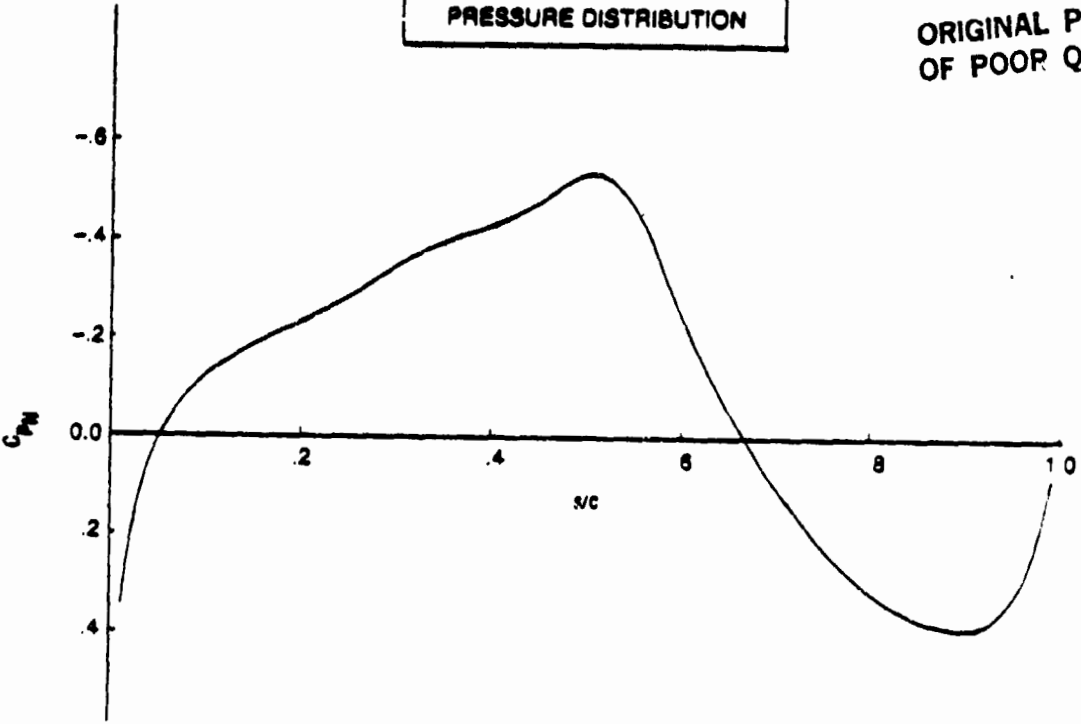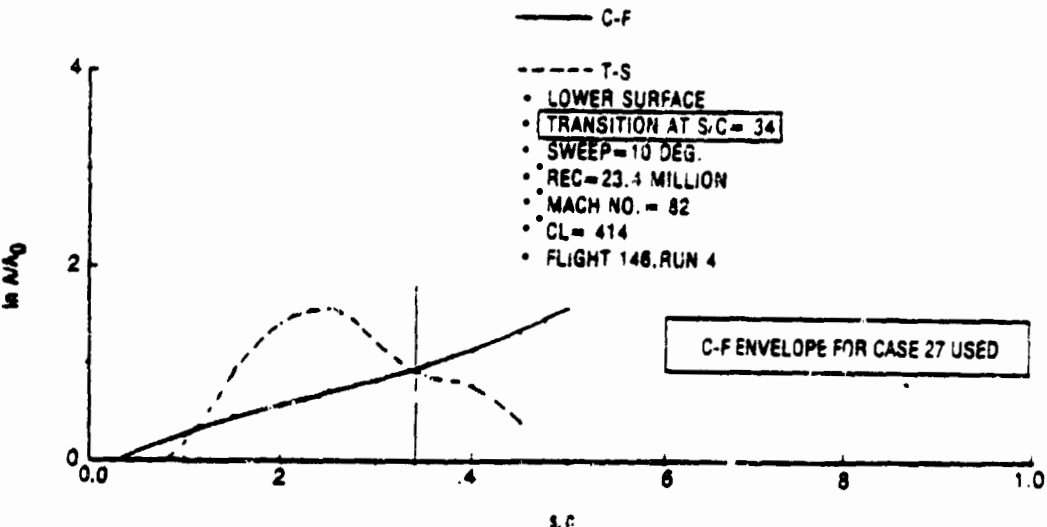
Figure 25. Case 29 Stability Envelopes

43
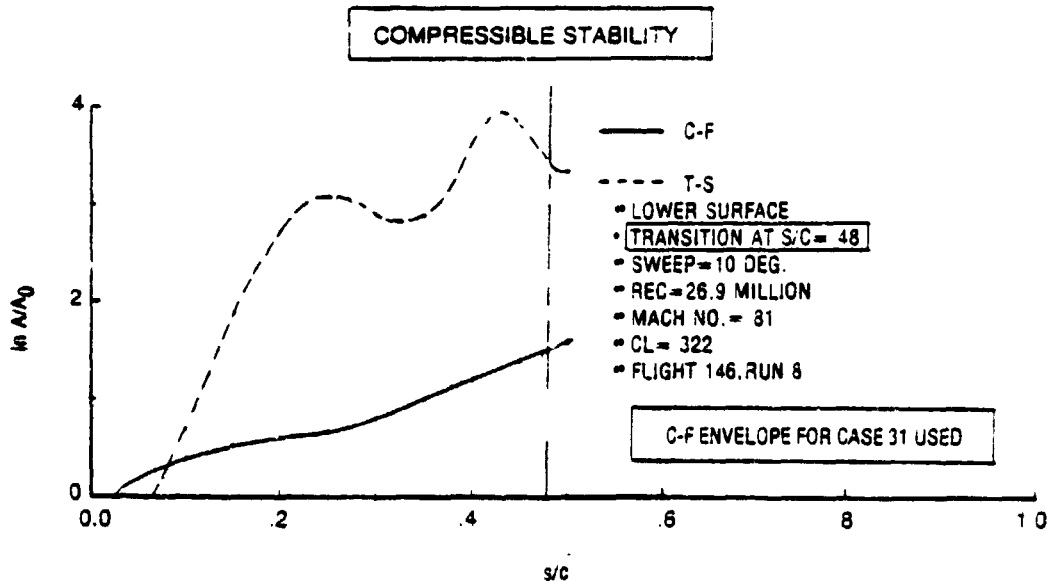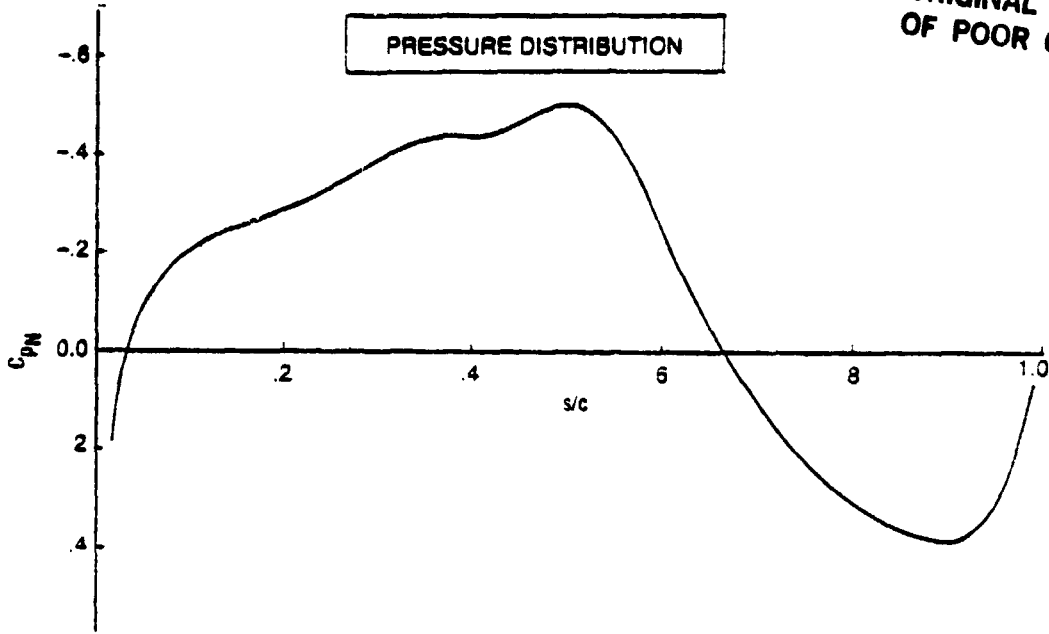
Figure 26. Case 30 Stability Envelopes

PRESSURE DISTRIBUTION

COMPRESSIBLE STABILITY

- C-F
- T-S
- LOWER SURFACE
- TRANSITION AT S/C = .49
- SWEEP = 10 DEG.
- REC = 27 3 MILLION
- MACH NO. = 82
- CL = .314
- FLIGHT 146, RUN 9
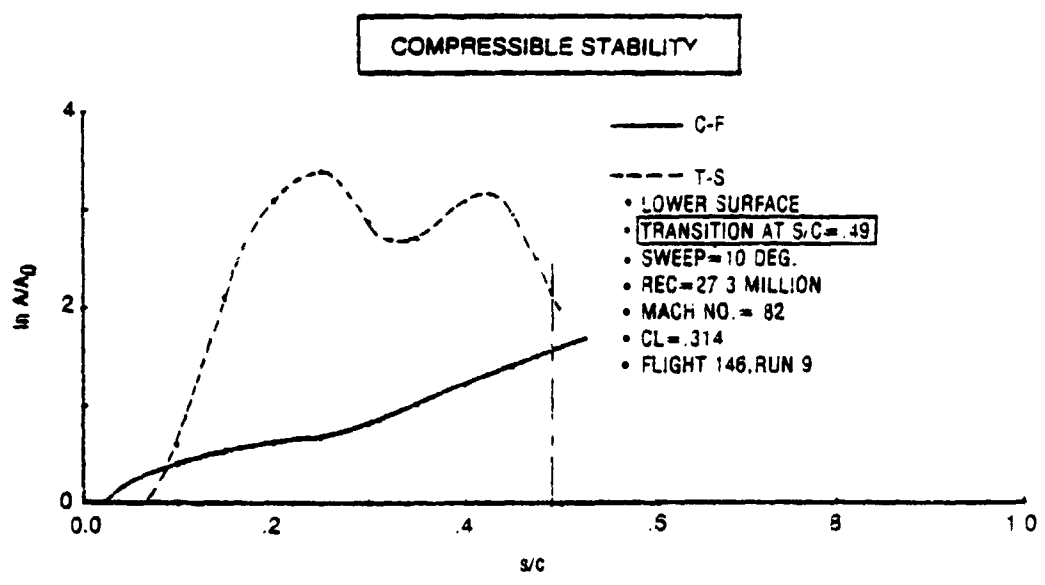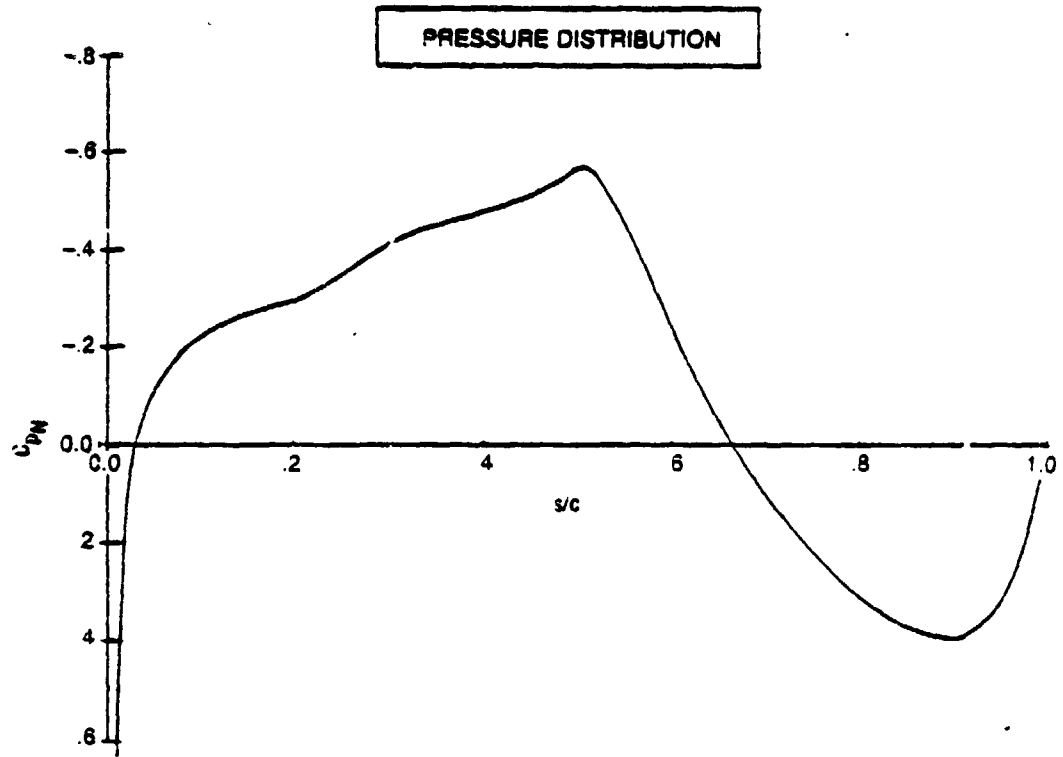
Figure 27. Case 31 Stability Envelopes

PRESSURE DISTRIBUTION

COMPRESSIBLE STABILITY

C-F

T-S
- LOWER SURFACE
- TRANSITION AT S/C = 51
- SWEEP = 15 DEG.
- REC = 27.7 MILLION
- MACH NO. = .83
- CL = 292
- FLIGHT 146, RUN 17A

Figure 28. Case 32 Stability Envelopes

PRESSURE DISTRIBUTION

C_{p_N}

-.8

-.6

-.4

-.2

0.0

.2

.4

6

.2   .4   .6   .8   1.0

S/C

COMPRESSIBLE STABILITY

$\ln A/A_0$

6

4

2

0

———— C-F

- - - - T-S
** LOWER SURFACE
** TRANSITION AT S/C= 51
** SWEEP=15 DEG.
** REC=27 9 MILLION
** MACH NO. = 83
* CL= 415
* FLIGHT 146, RUN 178

0.0   2   .4   .6   8   1.0

S/C

Figure 29. Case 33 Stability Envelopes

52

PRESSURE DISTRIBUTION

COMPRESSIBLE STABILITY

C-F

T-S
- LOWER SURFACE
- TRANSITION AT S/C = .51
- SWEEP = 16 DEG.
- REC = 23.2 MILLION
- MACH NO. = .83
- CL = .447
- FLIGHT 146, RUN 188

Figure 30. Case 34 Stability Envelopes

F-111 TRANSITION N-FACTORS

○ UPPER SURFACE, AFT RAKE
▽ UPPER SURFACE, FORWARD RAKE
◇ LOWER SURFACE
- SEE DISCUSSION ON
  PAGE 41.

Figure 31. Transition Amplification Factors

B-35), which are not separated, shows that cases 16 through 18, in general, have slightly thinner boundary layers than cases 19 through 21. This is the expected trend, given that the primary difference is that cases 19 though 21 are for 16-deg sweep instead of the 9-deg sweep for cases 16 though 18. If severe separation were present for cases 16 through 18, they would have had much thicker boundary layers at the rake location than cases 19 through 21. These observations indicate that the separation in cases 16 through 18 did not begin very far ahead of the rakes and is not severe enough to invalidate the use of the data.

In Figure 32, envelopes have been drawn around all the upper surface points and all the lower surface points shown in Figure 31. It can be seen that there is a considerable difference between the upper and the lower surfaces. If the external disturbance conditions were the same on both surfaces, theory indicates that they should both show the same amplification factor trends at transition. However, the lower surface shows transition at much lower C-F and T-S amplification factor combinations than does the upper surface. This indicates that larger external disturbances may have been present in the lower surface environment than were present in the upper surface environment.

As discussed in Section 5.2, all lower surface cases that were analyzed except cases 25 through 34 were based on data taken during flight 161. It is possible that the external disturbances that affected data taken during flight 161 were not present during flight 146, on which cases 26 through 34 are based, resulting in the much larger extent of laminar flow for these cases. For example, case 26 (flight 146) showed 51% chord laminar flow, whereas case 4 (flight 161) at the same Reynolds number and sweep and with a similar pressure distribution up to 40% chord, showed only 12% laminar flow. This comparison suggests that some form of contamination was present during flight 161 that was not present during flight 146. This is also supported by the fact that all three upper surface cases taken from flight 161 (cases 12, 13, and 15) show lower disturbance growth factors relative to the other upper surface cases in Figure 31. Determining the source of the external disturbances is highly speculative because there is insufficient evidence to support any specific cause.

The possibility of engine noise causing the lower surface to have transition with low amplification factors was considered by examining case 25. As shown in the photograph in Figure 33, the engine inlet on the F-111 is located aft of the leading edge at the side-of-body. Thus, the lower surface could be exposed to engine inlet
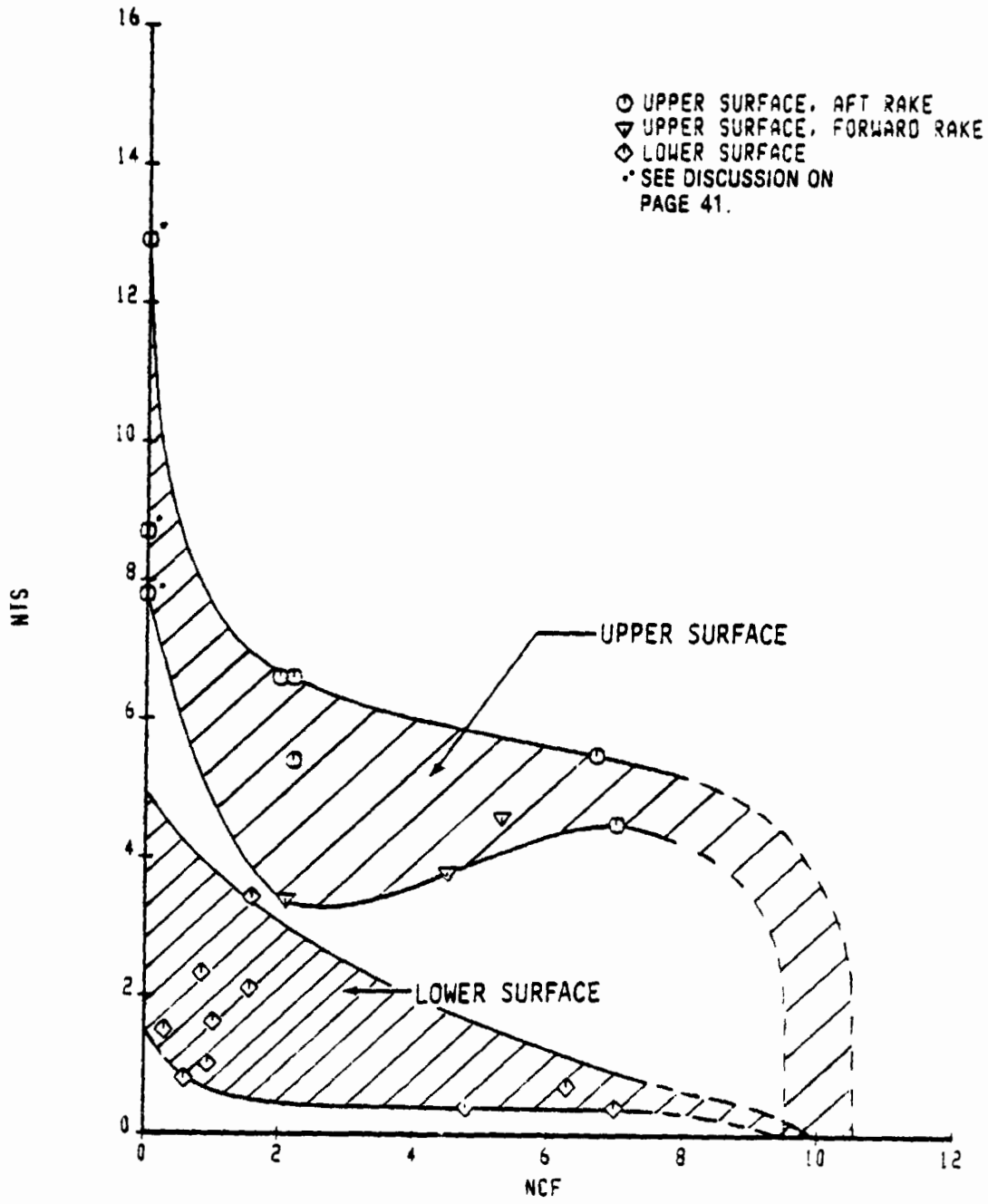
Figure 32. Transition Amplification Factor Envelopes on Upper and Lower Surfaces

Figure 33. F-111 in Flight Showing Wing-Inlet Relationship

noise, especially at high Mach numbers, but the upper surface would be shielded from such noise. Engine noise could excite T-S disturbances, because such noise tends to have peak energy in the same frequency range as most highly amplified T-S disturbances (2000 to 8000 Hz). C-F disturbances probably would be affected less than T-S disturbances because their highest amplification usually occurs at lower frequencies. This might result in the type of envelope shown in Figure 32 for the lower surface, because T-S disturbances of large initial amplitude require much less amplification before causing transition than do the normally infinitesimal disturbances. Although the possibility of engine noise contamination on the lower surface is plausible, there was no apparent effect on transition location when the engine on the right-hand wing of the F-111 was throttled back for case 25. The results of case 25 thus raise doubts about this hypothesis.

In addition to external disturbances, the low transition amplification factors for the lower surface may be due to a change in the C-F and T-S interaction for areas of lower velocity like wing lower surfaces. Overall, the results provide the following insights: (1) The results indicate that T-S and C-F disturbances interact to reduce the amplification factors of T-S and C-F disturbances at transition relative to those occurring when transition is caused by a single type of disturbance. (2) Although firm conclusions cannot be drawn because of the limited number of points, it appears that, as the C-F amplification factor at transition increases from 0 to 2, there is a significant decrease in the corresponding T-S amplification factor at transition. The corresponding effect on the C-F amplification factor at transition when the T-S amplification factor at transition increases from 0 to 2 appears to be much smaller.

The points included in the upper surface envelope of Figure 32 include both forward-rake cases, for which only one forced transition calibration flight was made, and aft-rake cases for which five forced transition calibration flights were made. Because of the more exact calibration of the aft-rake cases, there is a higher degree of confidence in the measured transition locations for these cases. Figure 34 shows the envelope of only these upper surface, aft-rake results.

The envelopes in Figures 32 and 34 are shown intersecting the C-F axis at a level greater than nine. This fairing of the curve was guided by the results of case 22 shown in Figure 19. In that case the C-F envelope rises rapidly to a peak value of about 9 at 5% chord, at which point the T-S amplification factor is 0. Because this is well ahead
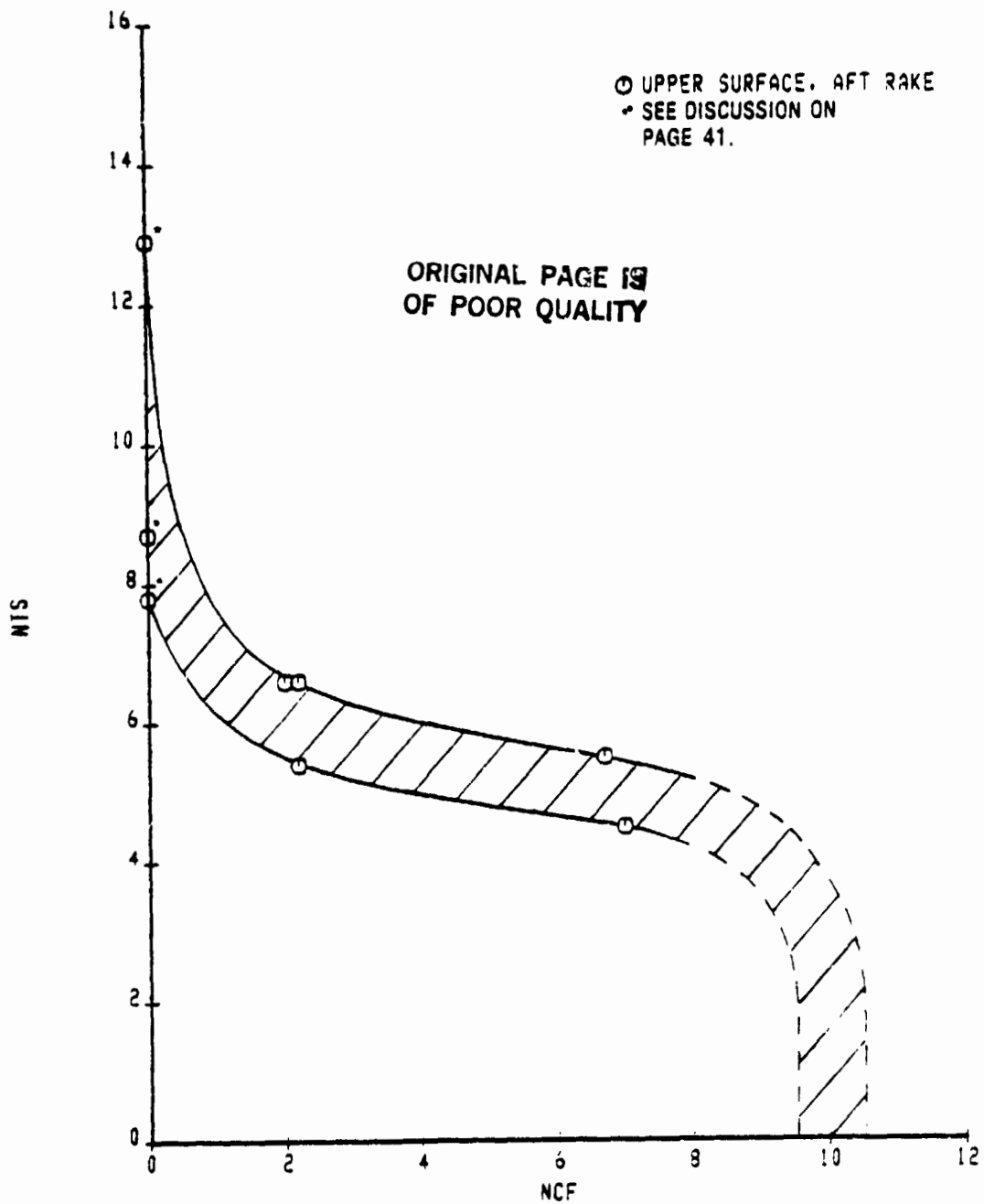
Figure 34. Transition Amplification Factor Envelope Upper Surface, Aft Rake Only

·of the transition location at 20% chord, these values indicate that a C-F amplification factor of 9, in the absence of T-S disturbances does not cause transition.

Figure 35 shows the envelope of the upper surface, aft-rake results along with the range of amplification factors (N-factors) found in previous studies for T-S-caused transition and for C-F-caused transition. These results were obtained using several different methods, which contributes to the large range of scatter. Also shown is the assumption used in the Hybrid Laminar Flow Control (HLFC) study (ref. 22). The range of amplification factors for pure T-S transition found in the current study is within the range of previous results. The HLFC assumption is optimistic for cases where T-S disturbances are the primary cause of transition and conservative for cases where C-F disturbances are the primary cause.

Figure 36 shows the effect of assuming a $\pm 5\%$ x/c uncertainty in the transition location. As would be expected, the envelope widens. However, it should be noted that, because of the shape of the T-S and C-F disturbance envelopes for the cases involved, there is very little change in the size of the band for low C-F amplification factors.

Figure 37 shows the trajectories followed by several aft-rake cases in the NTS-NCF plane. Cases 16, 17, and 18 follow the NTS axis from its origin to their respective transition locations because none of these cases have any significant crossflow amplification. Cases 19, 20, and 21 follow the NCF axis out to a level of about 2.5 at which point the trajectories begin to move up in a direction generally parallel to the NTS axis, indicating that the C-F amplification factors remain fairly constant as the T-S disturbances grow. Case 22 follows the NCF axis to a value of about 9 before the T-S disturbances begin to be amplified. The NCF values then begin to decrease as NTS increases. Case 24 is similar to case 22 except that case 24 reaches an NCF value of only about 7.5 before T-S disturbances begin to be amplified. The trace of lower surface case 33 also is shown in Figure 37, although the point of transition cannot be accurately determined because of the rapid increase in NTS at the transition location. Cases 19, 20, and 30 show a drop from peak NTS levels to that level at transition. This could indicate that transition actually occurred forward of the locations given by the transition analyses or that the mechanism causing transition cannot be fully explained by linear stability analyses. Nevertheless, if linear theory is used to establish a transition criteria, it seems reasonable to include the maximum
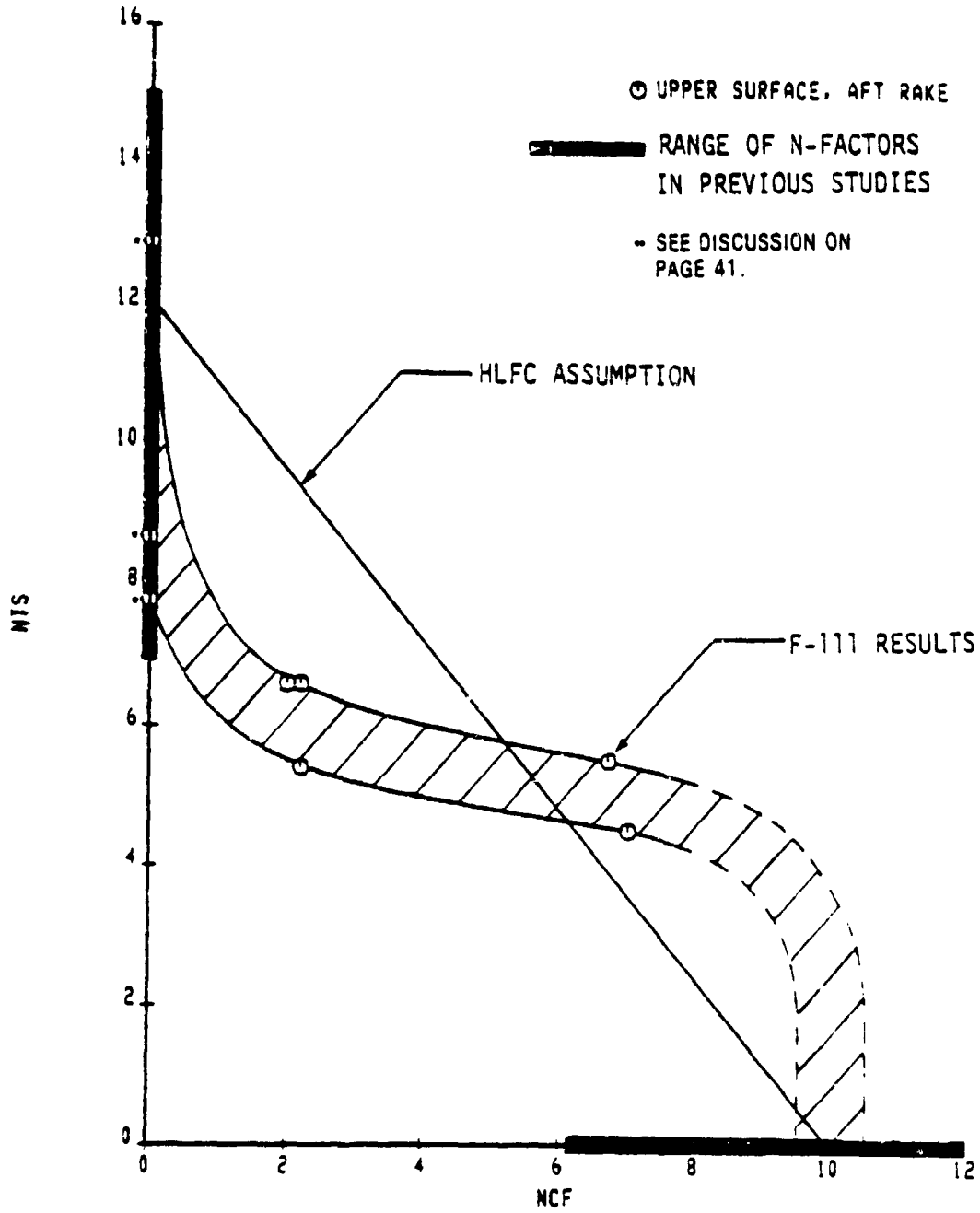
Figure 35. Transition Amplification Factor Envelope and Results of Previous Studies

F-111 TRANSITION N-FACTORS
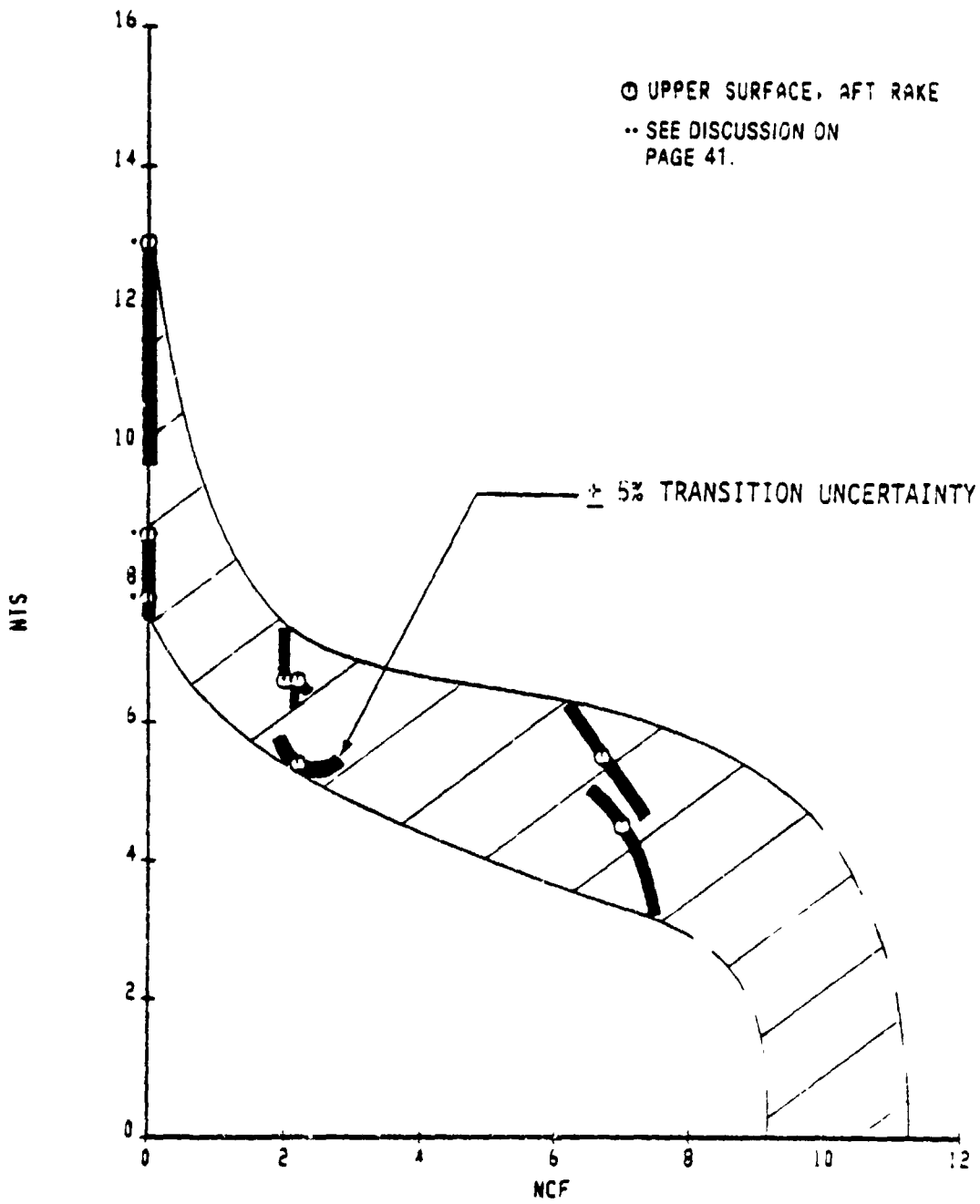
Figure 36. Transition Amplification Factor Envelope for ± 5% Transition Uncertainty
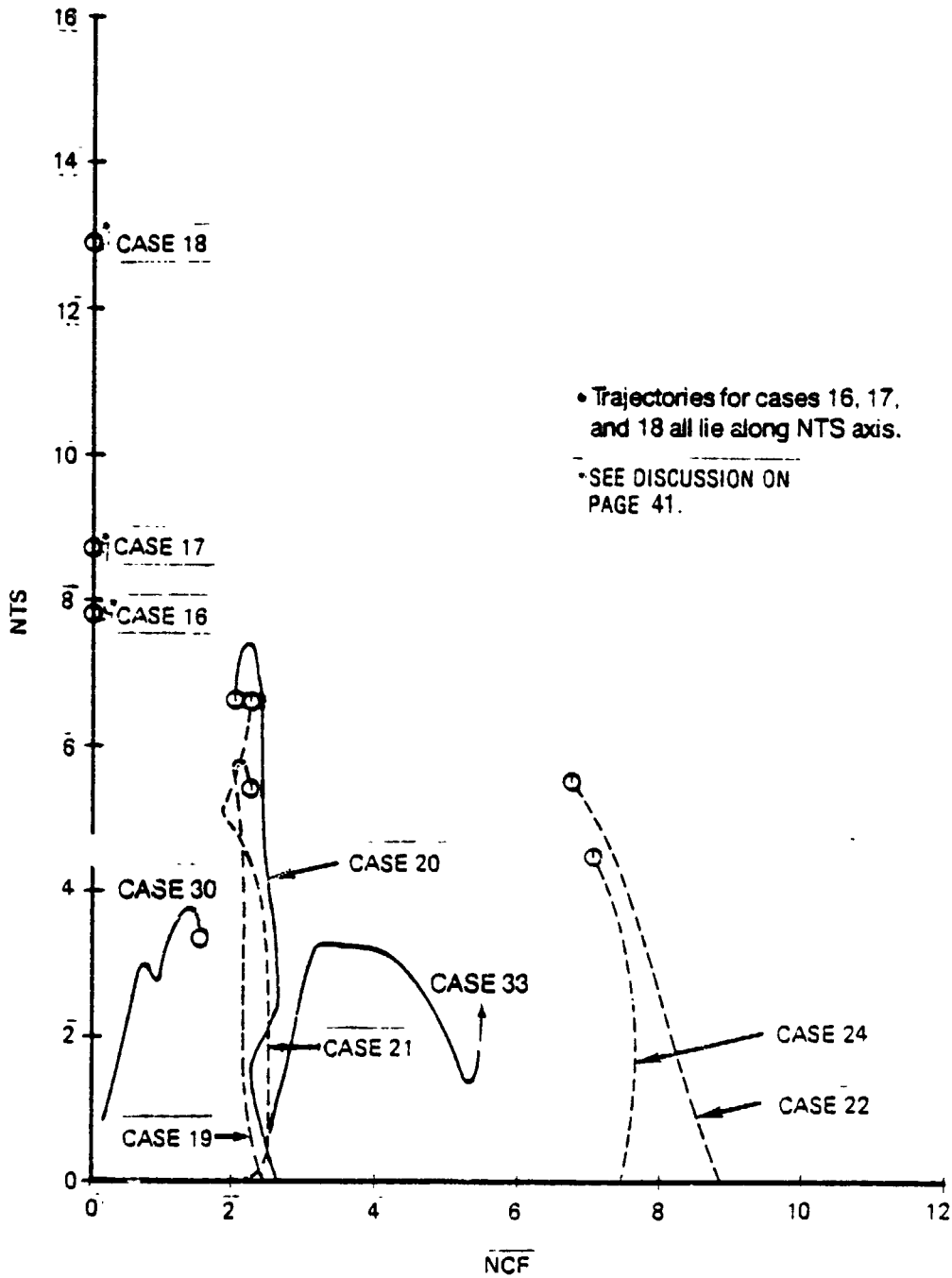
Figure 37. Amplification Factor Trajectories

63

values of the NTS-NCF traces of cases 20, 30, and 33 in determining the transition criteria envelopes. The change that this makes to the envelopes shown in Figure 32 is illustrated in Figure 38.

In Reference 19, a stability analysis of the F-111 NLF glove at selected flight conditions was made before the flight test and was based on wind-tunnel-measured pressure distributions. The differences between the results of that study and the results of the current study can be attributed to differences between the actual pressure distributions measured in flight and those measured in the wind tunnel. The bumps in the midchord region of the upper surface flight-test pressure distributions did not occur in the wind tunnel test. The effect of these bumps can be seen by comparing the results of case 16 of the current study, which had a bump, with the results of case 2 of Reference 19, which did not have a bump. Case 16 had a leading-edge sweep angle of 9.0 deg and a chord Reynolds number of 23.1 million. Case 2 of Reference 19 had a leading-edge sweep angle of 10 deg and a chord Reynolds number of 25.0 million. Transition for case 16 was at 56% chord, where the T-S amplification factor was 7.8 and the C-F amplification factor was 0. At 56% chord, case 2 had a T-S amplification factor of about 3.5 and a C-F amplification factor of about 2.0. Thus, for case 16, the bump resulted in an adverse pressure gradient that accelerated the growth of T-S disturbances and damped out the growth of C-F disturbances.

When there were no bumps in the pressure distribution, the current results are similar to those of Reference 19. An example of this is seen by comparing case 22 of the current study to case 5 of Reference 19. Case 22 had a leading-edge sweep angle of 25.2 deg and a chord Reynolds number of 28.9 million. Case 5 had a leading-edge sweep angle of 26.0 deg and a chord Reynolds number of 25.0 million. Case 22 had a transition location of 20% chord, where the T-S amplification factor was 5.5 and the C-F amplification factor was 6.7. At 20% chord, case 5 of Reference 16 had a T-S amplification factor of about 6 and a C-F amplification factor of about 7. Thus, the results of the current stability analysis and those of Reference 19 are similar except for differences resulting from pressure distribution changes.
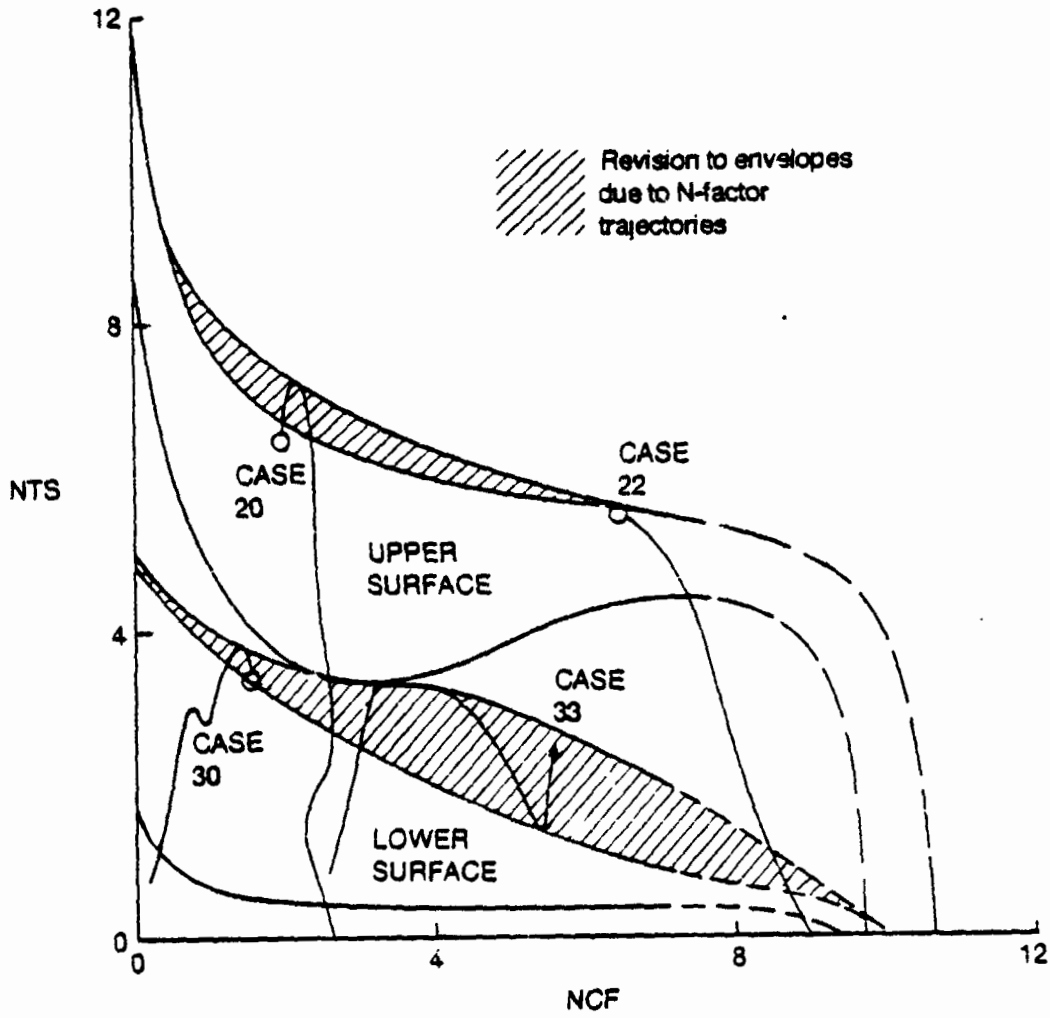
Figure 38. Revision to Amplification Factor Envelopes

7.0 CONCLUSIONS AND RECOMMENDATIONS

7.1 CONCLUSIONS

The analysis of 34 selected cases of F-111 flight test data to determine the measured transition location and the analysis of boundary layer stability of 25 of those 34 cases indicate the following:

o The maximum extent of laminar flow attained on the upper surface varies from 56% chord at 9-deg sweep to 21% chord at 25-deg sweep, with chord Reynolds numbers in the range from 23 to 28 million. The maximum extent of laminar flow attained on the lower surface varies from 51% chord at 16-deg sweep to 6% chord at 25-deg sweep.

o Results of the stability analyses show that when both crossflow (C-F) and Tollmien-Schlichting (T-S) disturbances are amplified, they interact and reduce the maximum amplification factor of either disturbance that can be tolerated without causing transition. This interaction may produce even greater reductions on the lower surface where velocities are lower.

o The stability analyses for the upper and lower surfaces show significantly different theoretical amplification factors at transition. There is no theoretical explanation of this difference but it could be due to extraneous disturbances such as noise or surface contamination. The airplane geometry would tend to shield the upper surface from engine noise.

o There is uncertainty associated with the measured transition locations, because the transition location was inferred from measured boundary layer velocity profiles and was not measured directly. The magnitude of this uncertainty was not estimated.

7.2 RECOMMENDATIONS

o Engine noise levels at the glove location on the F-111 TACT airplane should be measured on both the upper and lower surface so that the possibility of noise contamination on the glove lower surface can be investigated.

o   Because of the significant fuel savings potential of laminar flow aircraft, it is recommended that a new flight test program be initiated to further explore the effects of wing geometry and flight conditions. The test also should consider changes in the following areas:

   o   Improved instrumentation, namely, transition detection using flush hot-film surface probes mounted in an array that will provide information on the extent of laminar flow.

   o   Measurement of the noise intensity on the glove upper and lower surface in flight.

   o   Recording of insect contamination after each flight and possibly the implementation of some preventive measures.

   o   Larger variations in Reynolds number and Mach number.

   o   A glove with a larger spanwise extent to minimize the effect of the inboard wing on the glove.

8.0 REFERENCES

1. Boeing Commercial Airplane Company, "Evaluation of Laminar Flow Control System Concepts for Subsonic Commercial Transport Aircraft," NASA CR-158976, December 1978.

2. Lockheed-Georgia Company, "Evaluation of Laminar Flow Control System Concepts for Subsonic Commercial Transport Aircraft," NASA CR-159253, September 1980.

3. McDonnell Douglas Company, "Evaluation of Laminar Flow Control System Concepts for Subsonic Commercial Transport Aircraft," NASA CR-159252, December 1982.

4. Boeing Commercial Airplane Company, "Natural Laminar Flow Airfoil Analysis and Trade Studies," NASA CR-159029, May 1979.

5. Smith, F. and Higton, D. J., "Flight Tests on King Cobra FZ.440 to Investigate the Practical Requirements for the Achievement of Low Profile Drag Coefficients on a Low Drag Aerofoil," RAE Rept. Aero. 2073, (ARC9043), August 1945.

6. Pfenninger, W. and Groth, E., "Low Drag Boundary Layer Suction Experiments in Flight on a Wing Glove of an F94A Airplane with Suction Through a Large Number of Fine Slots," Boundary Layer and Flow Control, edited by G. V. Lachman, Vol. 2, pp. 981-999, 1961.

7. Fowell, L. R. and Antonatos, P. P., "Some Results from the X-21 Program, Part 2; Laminar Flow Control Flight Test Results on the X-21," AGARD-ograph 97, Pt. IV, May 1965.

8. Raspet, August and George-Falvy, Dezso, "Boundary Layer Studies on the Phoenix Sailplane," paper presented at the VIII Congress of O.S.T.I.V., Koln, Germany, June 1960.

9. Jaffe, N. A., Okamura, T. T., and Smith, A. M. O., "Determination of Amplification Factors and Their Application to Predicting Transition," AIAA Journal, Vol. 8, pp. 301-308, February 1970.

10. Mack, L. M., "Transition Prediction and Linear Stability Theory," presented at AGARD Fluid Dynamics Panel Symposium on Laminar Turbulent Transition, Copenhagen, Denmark, May 2-4, 1977.

11. Srokowski, A. J. and Orzag, S. A., "Mass Flow Requirements for LFC Wing Design," AIAA Paper 77-1222, AIAA Aircraft Systems and Technology Meeting, Seattle, Washington, August 22-24, 1977.

12. Nayfeh, A. H., "Stability of Three-Dimensional Boundary Layers," AIAA Paper 79-0262, AIAA 17th Aerospace Sciences Meeting, New Orleans, La., January 15-17, 1979.

13. Cebeci, T. and Stewartson, K., "On Stability and Transition in Three-Dimensional Flows," AIAA Paper 79-0263, AIAA 17th Aerospace Sciences Meeting, New Orleans, La., January 15-17, 1979.

14. Mack, L. M., "On the Stability of the Boundary Layer on a Transonic Swept Wing," AIAA Paper 79-0264, AIAA 17th Aerospace Sciences Meeting, New Orleans, La., January 15-17, 1979.

15. Lekoudis, S. G., "Stability of Three-Dimensional Compressible Boundary Layers Over Wings With Suction," AIAA Paper 79-0265, AIAA 17th Aerospace Sciences Meeting, New Orleans, La., January 15-17, 1979.

16. Runyan, L. J. and George-Falvy, D., "Amplification Factors at Transition on an Unswept Wing in Free Flight and on a Swept Wing in Wind Tunnel," AIAA Paper 79-0267, AIAA 17th Aerospace Sciences Meeting, New Orleans, La., January 15-17, 1979.

17. Boltz, F. W., Kenyon, G. C., and Allen, C. Q., "Effects of Sweep Angle on the Boundary Layer Stability Characteristics of an Untapered Wing at Low Speeds," NASA TN D-338, 1960.

18. Pfenninger, W., "Flow Problems of Swept Low-Drag Suction Wings of Practical Construction at High Reynolds Numbers," Annals of the N.Y. Academy of Sciences, Vol. 154, Art. 2, pp. 672-703, November 1968.

19. Runyan, L. James and Steers, Louis L., "Boundary Layer Stability Analysis of a Natural Laminar Flow Glove on the F-111 TACT Airplane," Viscous Flow Drag Reduction, Vol. 72, Progress in Astronautics and Aeronautics, pp. 17-32, 1980.

20. Mack, L. M., "Computation of the Stability of the Laminar Compressible Boundary Layer," Methods in Computational Physics, edited by B. Adler, Academic Press, N.Y., pp. 247-299, 1965.

21. Hefner, Jerry N. and Bushnell, Dennis M., "Status of Linear Boundary Layer Stability Theory and the e^n Method, With Emphasis on Swept-Wing Applications," NASA Technical Paper 1645, April 1980.

22. Boeing Commercial Airplane Co., "Hybrid Laminar Flow Control Study, Final Technical Report," NASA CR 165930, 1982.

23. Dagenhart, J. Ray, "Amplified Crossflow Disturbances in the Laminar Boundary Layer on Swept Wings With Suction," NASA Technical Paper 1902, November 1981.

APPENDIX A

DETAILS OF METHOD OF ANALYSIS

FIGURES

PRECEDING PAGE BLANK NOT FILMED

PAGE A 2

APPENDIX A: DETAILS OF METHOD OF ANALYSIS

This appendix describes the method used to determine the transition location for each case. The measured data for a given case consist of the pressure distribution, the boundary layer velocity profile at the rake location for the clean wing (natural transition) flight and for one to five forced transition flights in which the boundary layer was tripped at specified locations, and flight conditions for each flight. The analysis objective was to determine the transition location for the clean wing flight for each case.

The following is a step-by-step description of the method of analysis. Case 19 is used as a sample.

Step 1: The first step in the method is to compute the boundary layer displacement thickness (at the rake location), δ^*, for the clean wing flight and for each of the forced transition flights from the measured boundary layer velocity profiles. Figure A-1 shows all the measured velocity profiles for Case 19 and the calculated values of δ^*. The values of δ^* are later converted to measured R_δ^* values using the A552 results from steps 2 and 3:

$$R_{\delta}{}^*{}_{MEAS} = \frac{\delta^*{}_{MEAS}}{\delta^*{}_{A552}} \cdot R_{\delta}{}^*{}_{A552}$$

where $R_\delta{}^*{}_{A552}$ and $\delta^*{}_{A552}$ are the values calculated in either step 2 or step 3 for the pressure distribution corresponding to $R_\delta{}^*{}_{MEAS}$. Thus, if $R_\delta{}^*{}_{MEAS}$ is for the case with forced transition at 5%, the values of $\delta^*{}_{A552}$ and $R_\delta{}^*{}_{A552}$ used will be from the run based on the pressure distribution for forced transition at 5%.

Step 2: The second step in the method is to analytically predict the values of $R_\delta{}^*$ (using program A552) at the applicable rake location for the pressure distribution corresponding to the clean wing flight. The clean wing pressure distribution is shown in Figure A-2, along with pressure distributions for the forced transition flights.

Up to six different A552 runs (depending on the case) are made using the clean wing pressure distribution. The only change from run to run is the location at which transition is specified in the program. The six transition locations specified are 5%, 20%, 30%, 40%, 50%, and 65% chord or the location of minimum pressure (whichever
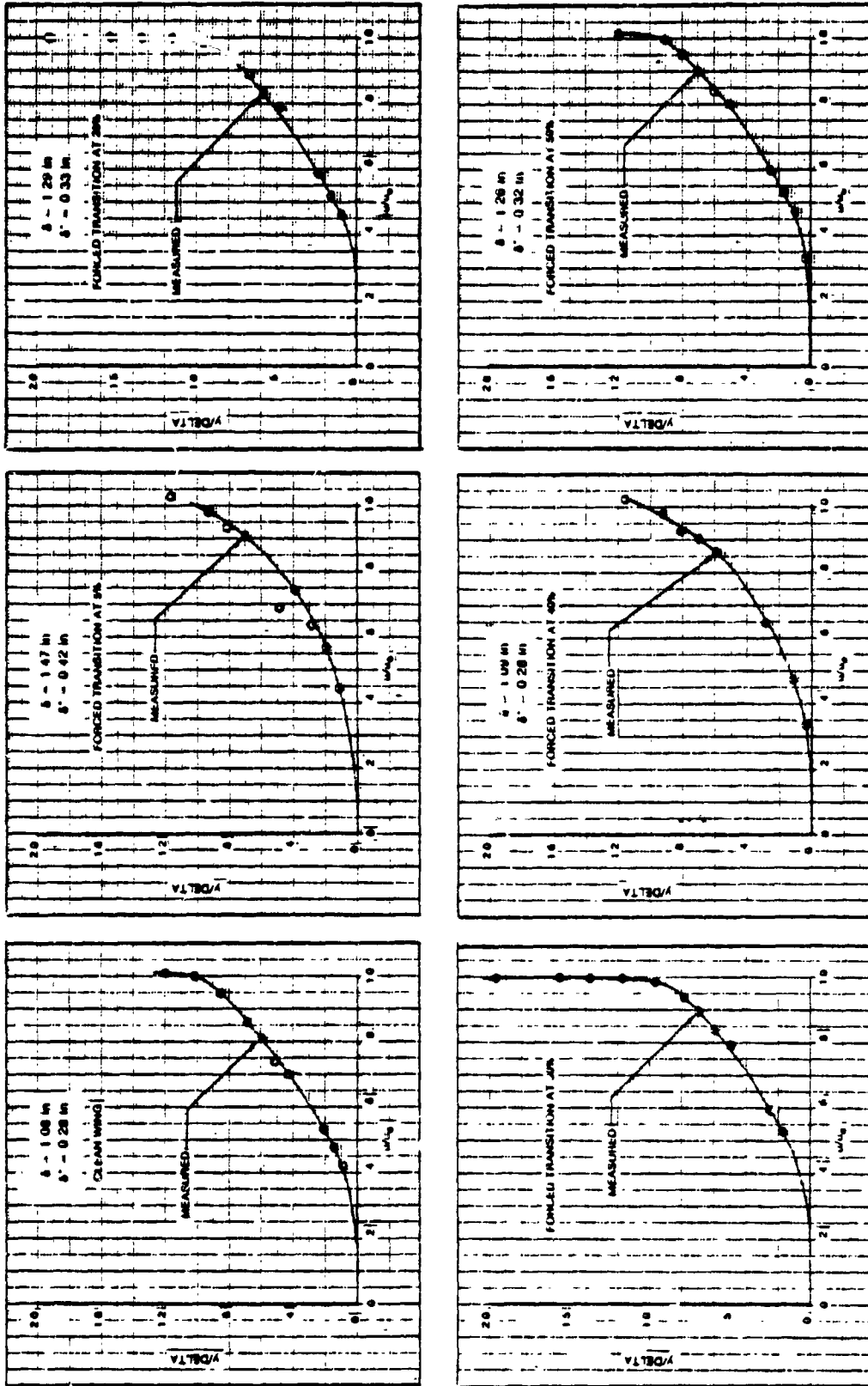
Figure A-1. Measured Velocity Profiles Case 19 .

CASE: 19
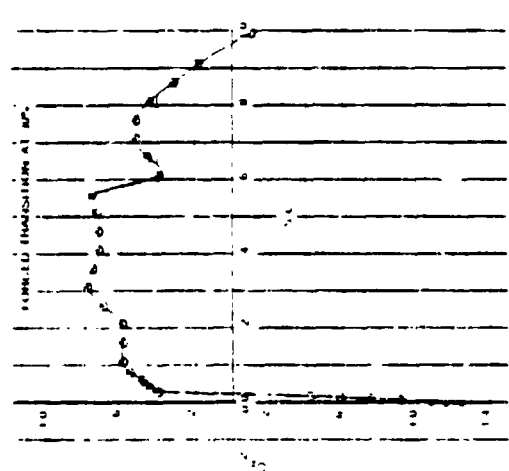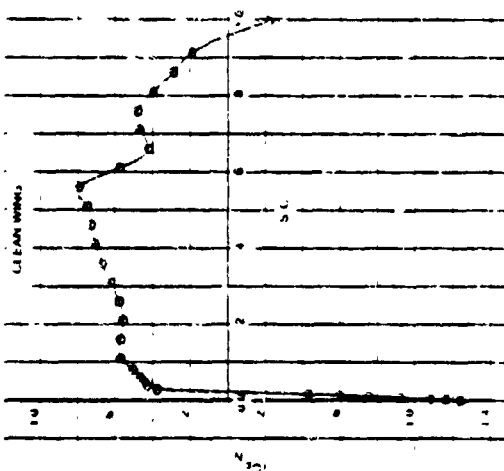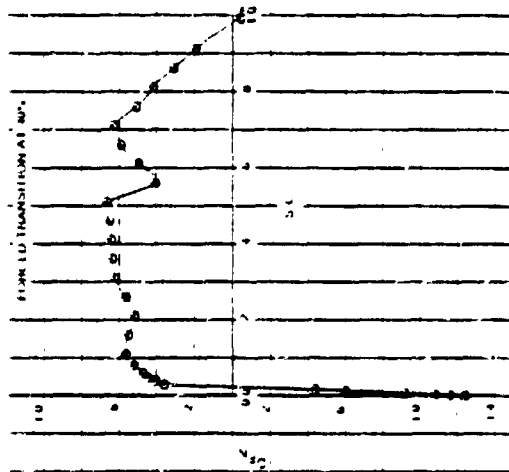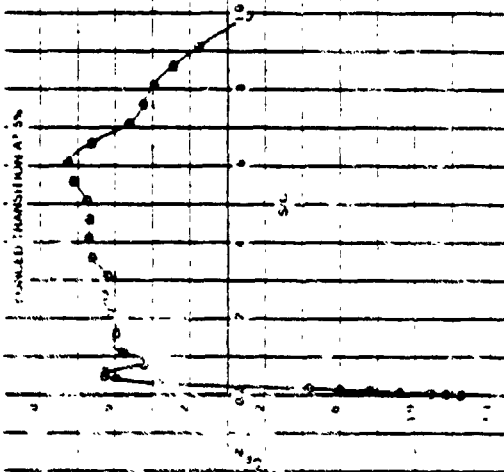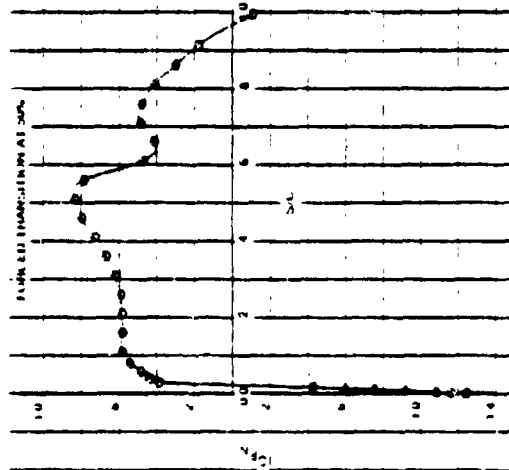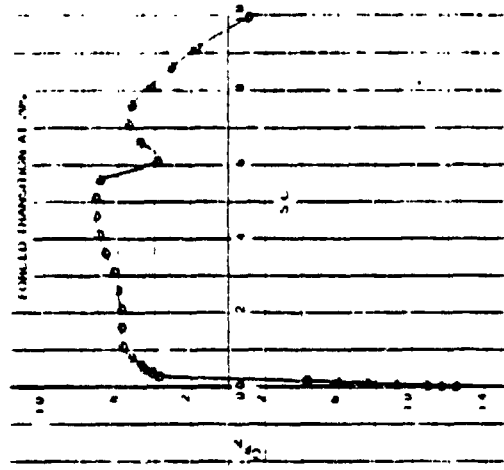
Figure A-2.   Measured Pressure Distributions Case 19

A-7

is further forward). The reason for varying the transition location is to determine how δ^* and R_δ^* at the rake location should vary as the transition location varies. Figure A-3 shows the results of this clean wing A552 analysis.

Step 3: Program A552 is used to analytically predict R_δ^* at the rake location for the forced transition pressure distributions. Only one A552 run is made for each forced transition pressure distribution with the Reynolds number and Mach number specified in A552 being those at which the pressure distribution was measured. The transition location specified in A552 corresponds to the location of the trip strip on the glove for the particular flight being analyzed. The reason for analyzing each of these cases in A552 is to account for the effect of pressure distribution and Reynolds number differences between the clean wing flight and the forced transition flights. Figure A-2 shows significant differences in pressure distribution from flight to flight. Also, some of the flights were made at an altitude of about 30,000 ft, resulting in a chord Reynolds number of about 23 million, and other flights were made at an altitude of about 25,000 ft, resulting in a chord Reynolds number of about 28 million. To be of use in evaluating the clean wing results, the forced transition results must be adjusted to account for any differences in pressure distribution and Reynolds number because the values of δ^* and R_δ^* at the rake location are functions of both. Figure A-4 shows the A552 results for forced transition pressure distributions to allow comparison with the corresponding R_δ^* values for the clean wing pressure distribution. The difference between the two sets of data varies with transition location. The difference between the two R_δ^* values for a given transition location is used in step 4 to adjust the measured value of R_δ^* for the forced transition cases to the clean wing pressure distribution.

In Figure A-5 the measured values of R_δ^* for forced transition flights and the clean wing flight have been added to the results shown in Figure A-4. The clean wing measured result is shown as a dashed line because only R_δ^* is known; the transition location is not known.

Step 4: In this step the measured R_δ^* values for the forced transition flights shown in Figure A-5 are adjusted to a clean wing. At a given transition location, the adjustment applied to the measured R_δ^* is as follows:

Specified transition location	δ^* (in.)	RDTH (R_{δ}^*)
.05	.335	66654
.20	.288	57276
.30	.253	50341
.40	.214	42629
.50	.173	34324
.55	.152	30229

$Re_c = 23.3 \times 10^6$

$M = .828$
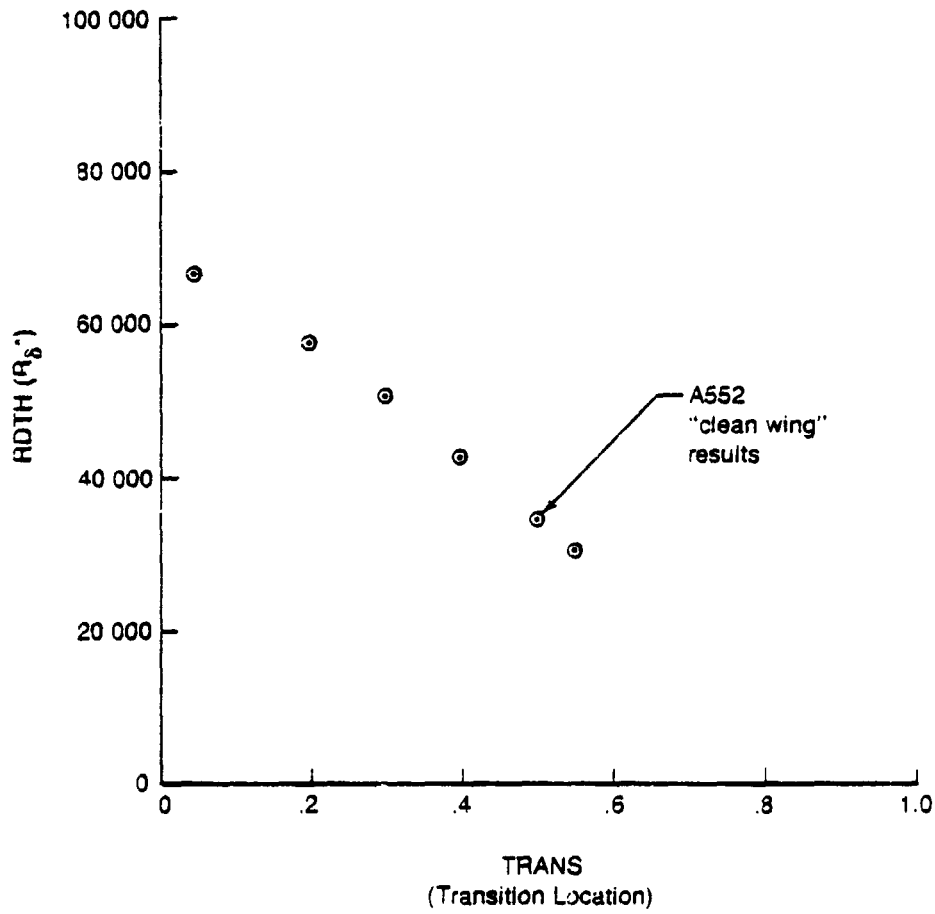
Figure A-3. Results from A552 Analysis of "Clean Wing" Pressure Distribution

Forced transition location	δ^* (in.)	RDTH (R_{δ}^*)
.05	.383	76272
.20	.285	68366
.30	.254	60863
.40	.212	42193
.50	.175	34721
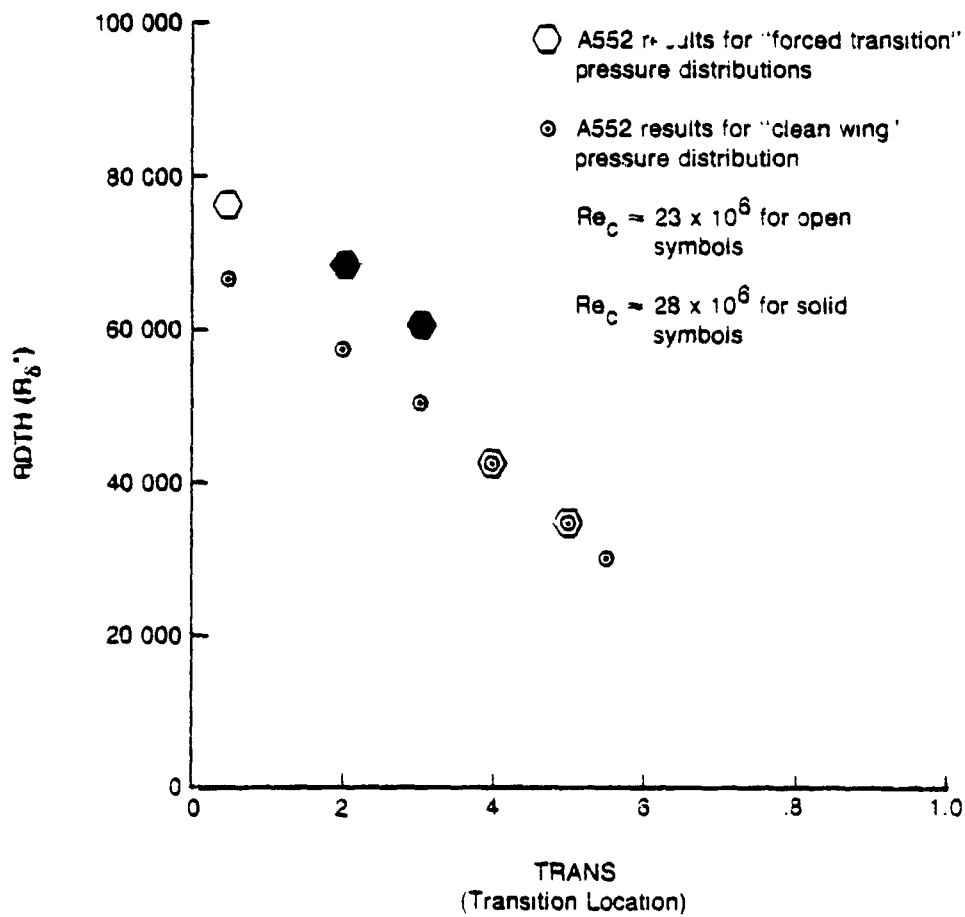
Figure A-4. A552 Results for "Forced Transition" and "Clean Wing" Pressure Distributions

————— ————— Measured R_δ' for "clean
wing" flight (transition
location unknown)

◇ Measured data for "forced
transition" flights (raw data –
not adjusted to "clean wing" basis)

⊙ A552 results for "forced transi-
tion" pressure distributions

⊙ A552 results for "clean wing"
pressure distribution

$Re_c \approx 23 \times 10^6$ for open
symbols

$Re_c \approx 28 \times 10^6$ for solid
symbols
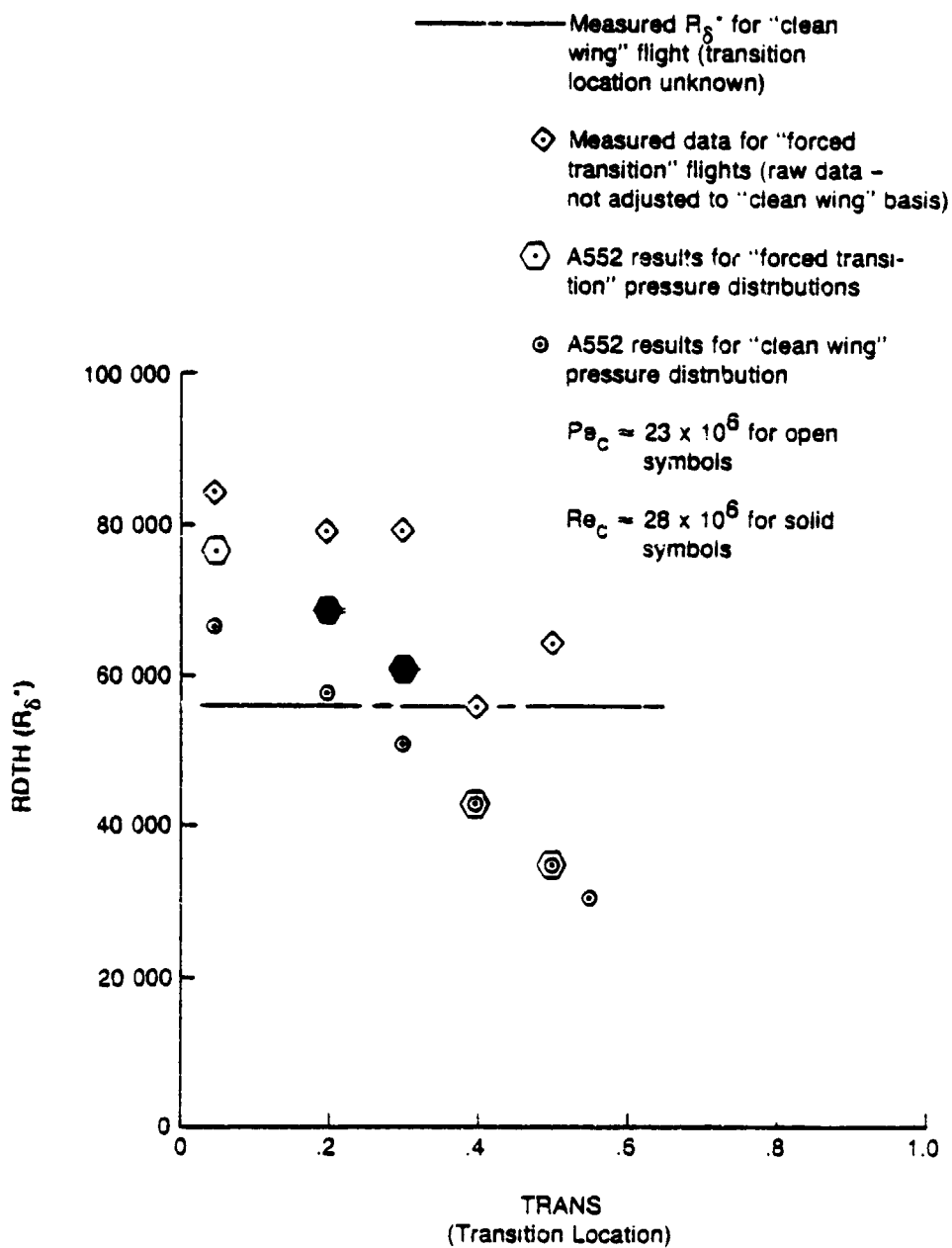
Figure A-5.   Results From Step 3

$$R_{\delta}^{*}{}_{\substack{\text{MEAS}\\\text{ADJ}}} = R_{\delta}^{*}{}_{\substack{\text{MEAS}\\\text{FORCED}}} - R_{\delta}^{*}{}_{\substack{\text{A552}\\\text{FORCED}}} - R_{\delta}^{*}{}_{\substack{\text{A552}\\\text{CLEAN}}}$$

In terms of the symbols used in Figure A-5, the "◇" symbol is adjusted downward by the difference between the "⊙" symbol and the "⊚" symbol. No adjustment is applied to the measured clean wing data (dashed line). The results of this step are plotted in Figure A-6.

Step 5: This is the final step. The A552 results for the clean wing pressure distribution are used to guide the fairing of a curve through the "▫" symbols in Figure A-6. The intersection of this curve with the line corresponding to the measured R_{δ}^{*} for the clean wing gives the estimated transition location for the clean wing, which is the final result of the analysis ("△" symbol) in Figure A-7. The measured data point for forced transition at 50% chord is higher than would be expected. This characteristic occurred in many cases for which the transition location was forward of 50% chord (see cases 18, 19, 20, 21 and 24). It is expected that the curve should flatten out aft of the transition point. Therefore, the data point at 50% chord for those cases was not allowed to influence the fairing of the curve. The forced transition data points having flight Reynolds numbers approximately the same as that of the clean wing were weighted more heavily in the fairing of the curve than the others.

The difference in Figure A-7 between the measured results ("▫" symbols) and the A552 results ("⊙" symbols) is probably due to a number of factors (the size of this difference varies from case to case):

o   Any three-dimensional effects resulting from wing taper and the relatively small span of the glove will not be accounted for in A552. In flight, the transition location probably varied with spanwise location on the glove, because the transition line usually takes the form of a series of turbulent wedges that eventually merge. Because the rake was located at the midspan of the glove, the data shown in this document reflect the transition point at that spanwise location. However, because A552 assumes a constant transition location along the span, there may be three-dimensional boundary layer thickness effects that A552 cannot model.
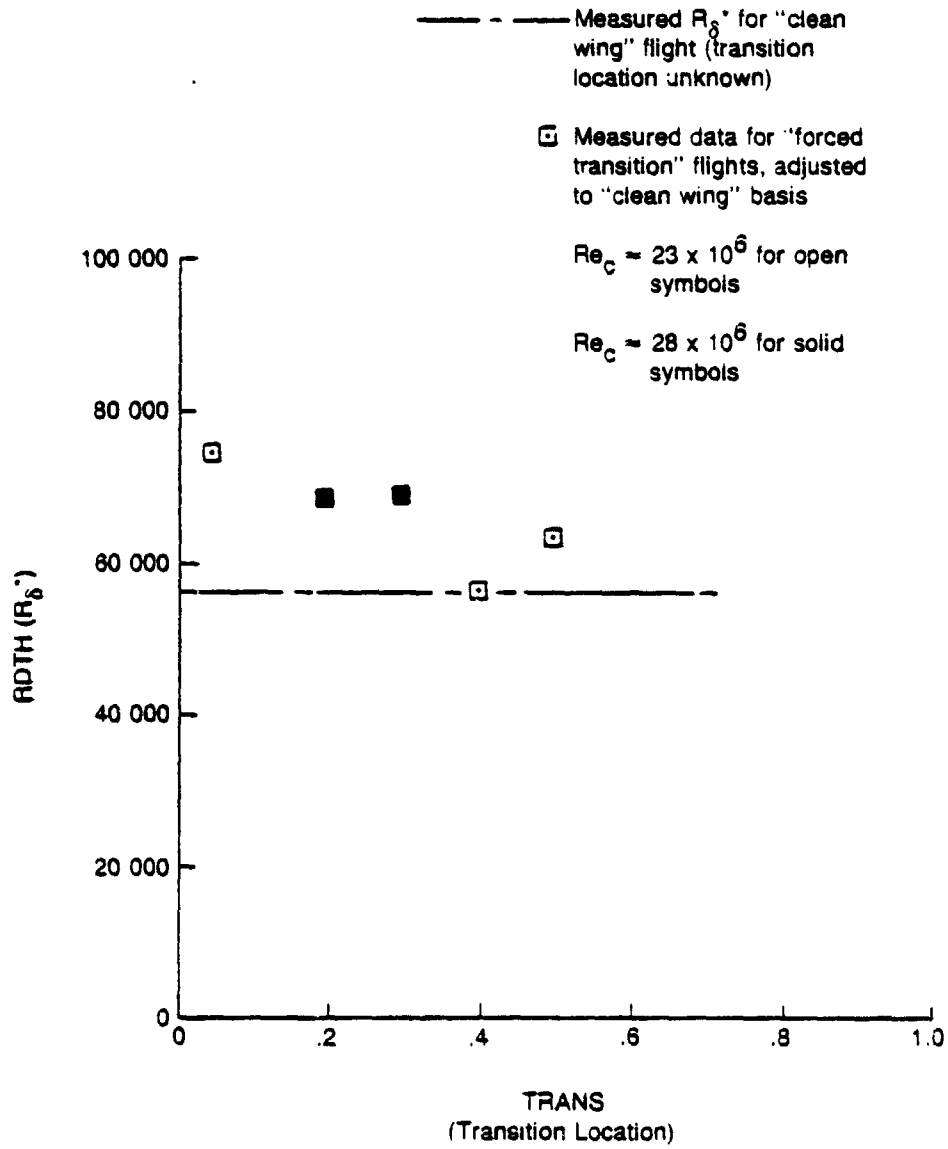
Figure A-6.   Results From Step 4

– – – – – – – Faired curve through "□"

─────── ─── Measured $R_\delta{}^*$ for "clean wing" flight data

□ Measured data for "forced transition" flights adjusted to "clean wing" basis

⊙ A552 results for "clean wing" pressure distribution

△ Estimated transition location for "clean wing" (final result of analysis)

$\overline{Re_c \approx 23 \times 10^6}$ for open symbols

$Re_c \approx 28 \times 10^6$ for solid symbols

RDTH ($R_\delta{}'$)

TRANS
(Transition Location)
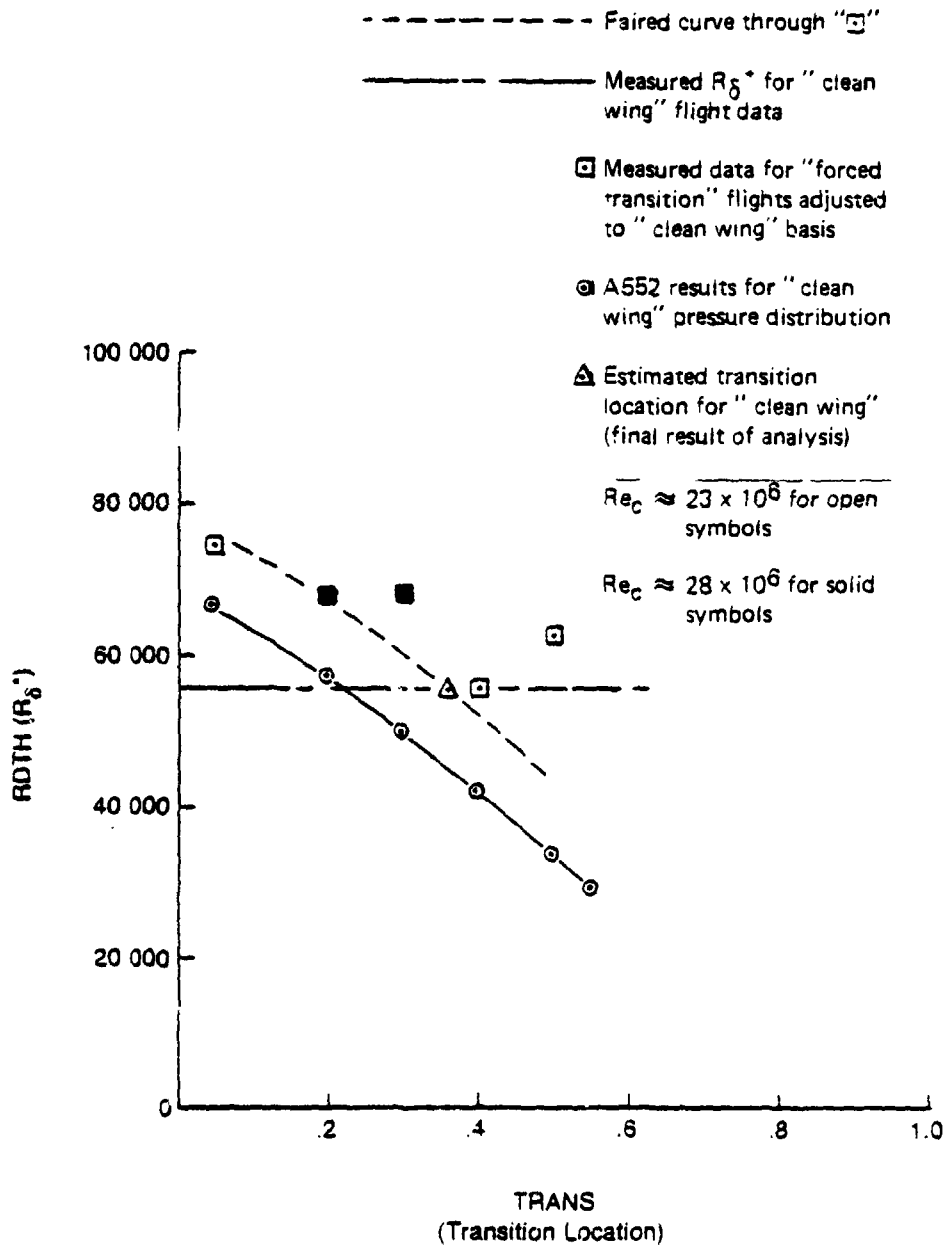
Figure A-7.   Results From Step 5

o   In some cases, especially aft of 60% chord, there was considerable judgment involved in determining what the pressure distribution should look like because the measured points were rather sparse. (The pressure distributions shown in this document include the enriched points, which were added to the measured data. However, the tabulated pressure distributions in app. B contain only the measured data points.)

o   There may be differences caused by the presence of shock waves in the pressure distribution and by disturbances introduced by the trip strips, which A552 cannot properly model.

Even though there are differences in the level of $R_\delta{}^*$ between A552 and the measured results, there is no evidence to indicate that the variation of $R_\delta{}^*$ with transition location computed using A552 is not accurate. In case 21, for example, where there was very little scatter in the flight test data, there is good agreement between the measured variation of $R_\delta{}^*$ with transition location and that computed by A552. Furthermore, in all other cases with multiple forced transition data points (cases 16 through 26), the use of A552 results to guide in the fairing of the curve through the measured data points apparently resulted in a reasonable fairing of the data.

APPENDIX B

FLIGHT TEST DATA AND AIRFOIL COORDINATES

FIGURES

FIGURES

FIGURES

APPENDIX B: FLIGHT TEST DATA AND AIRFOIL COORDINATES

The figures in this appendix show the measured pressure distributions and boundary layer velocity profiles for all 34 cases included in the current study. A552-calculated velocity profiles were used to guide the fairing of curves through the measured profile points and are shown for cases 1 through 17. For these cases, the measured profiles are shown as a solid line, and the A552 results, as a series of circles. For cases 18 through 34, only the measured profiles are shown, including the individual measured points through which the curves were faired. The coordinates of the glove airfoil, NLAM78, are also given. The pressure distributions shown in some of these plots include interpolated points that were not actually measured. Tabulations of the measured pressure distributions for the clean wing flights are given here and include only those values actually measured.
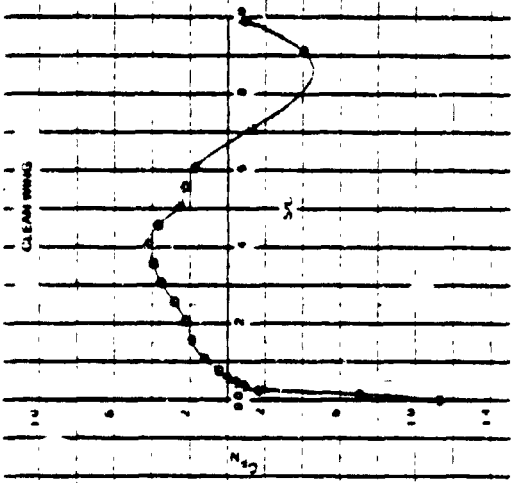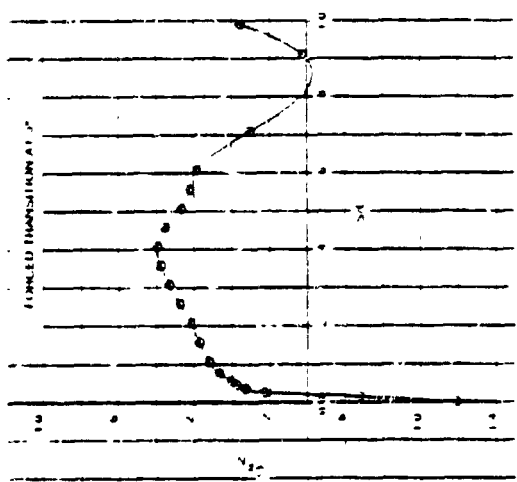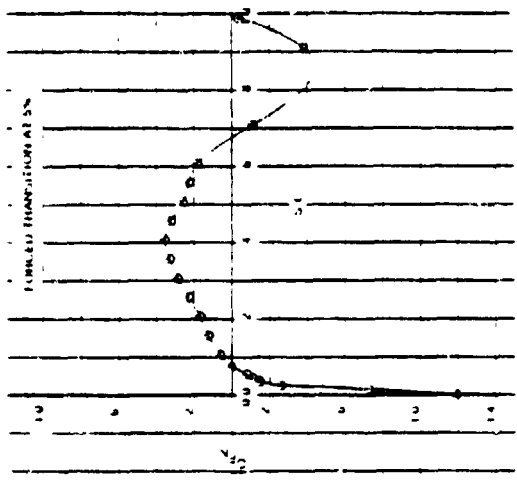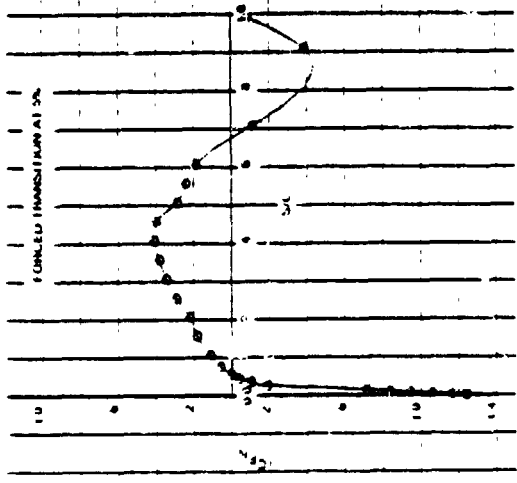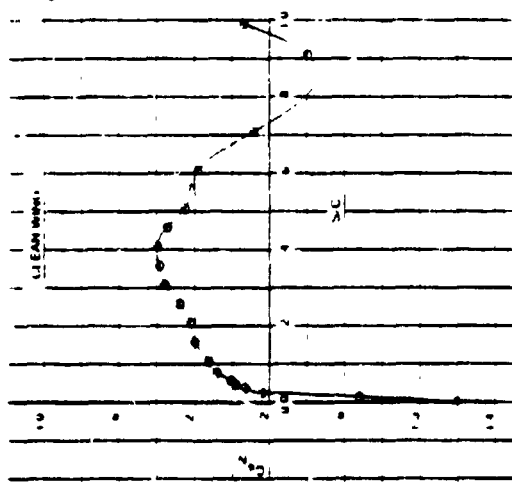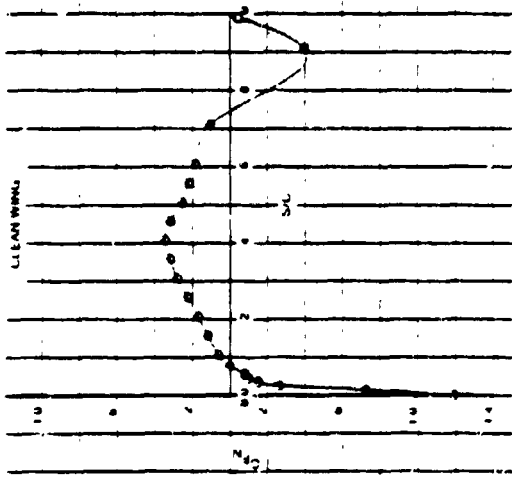
Figure B-1. Measured Pressure Distributions: F-111 NLF Glove, Cases 1, 2, and 3
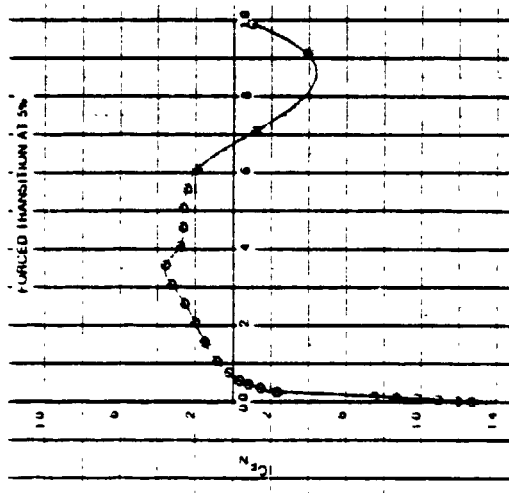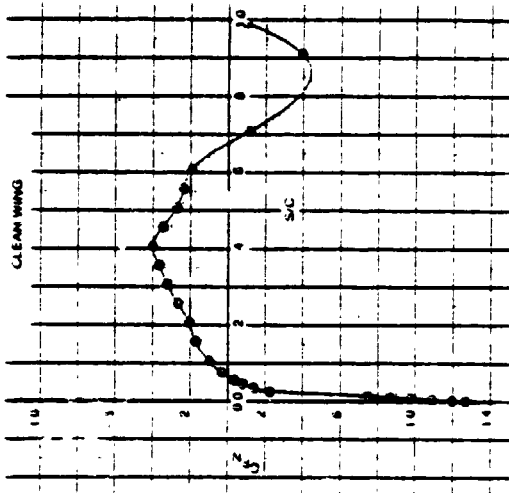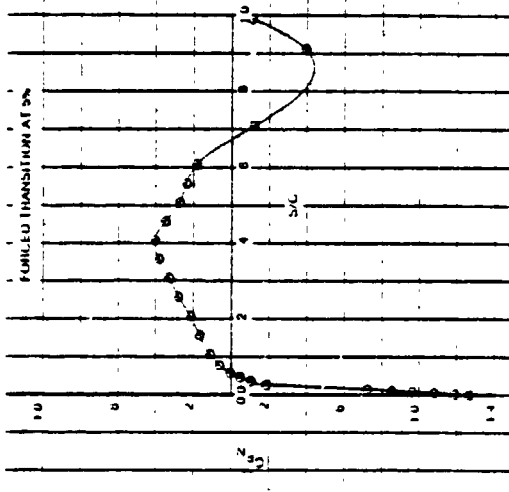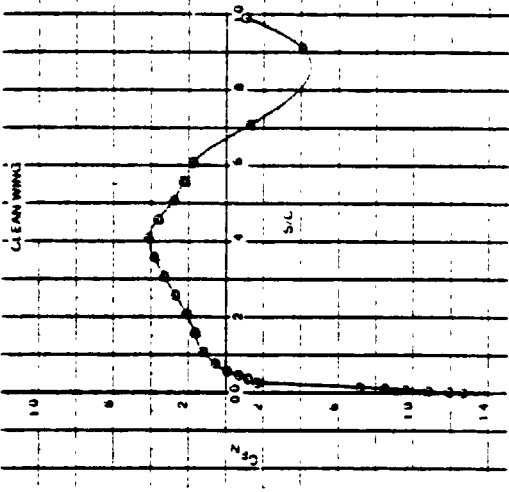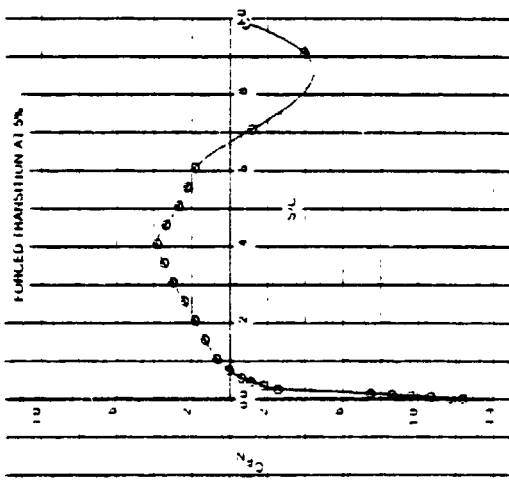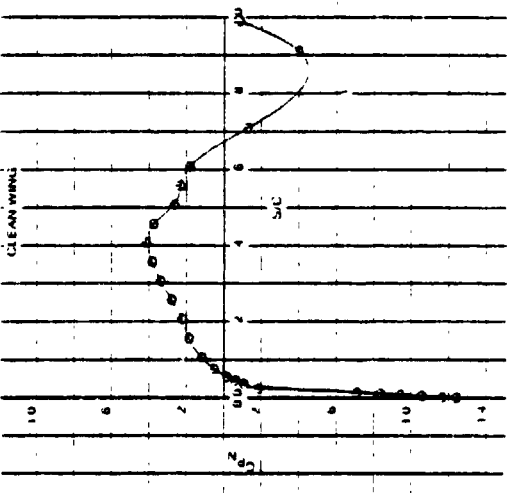
Figure B-2. Measured Pressure Distributions: F-111 NLF Glove, Cases 4, 5, and 6
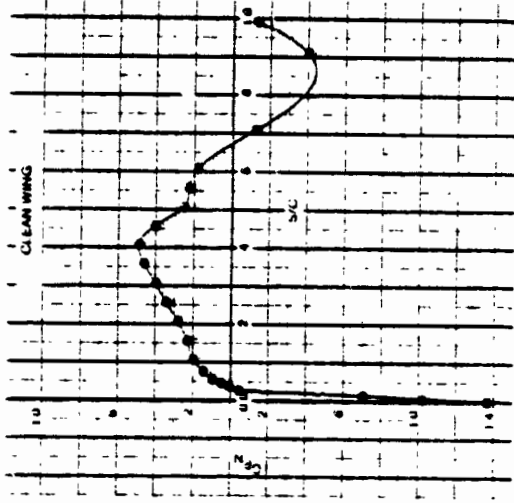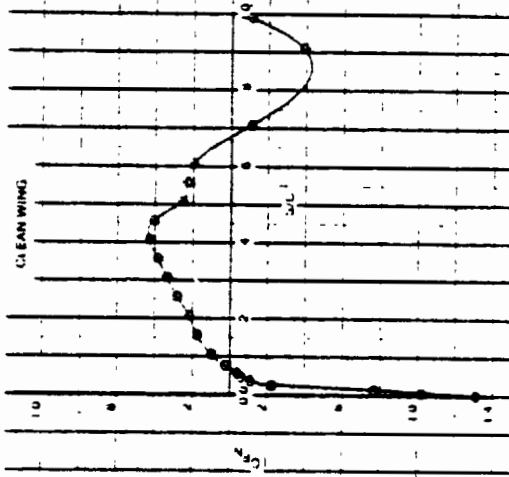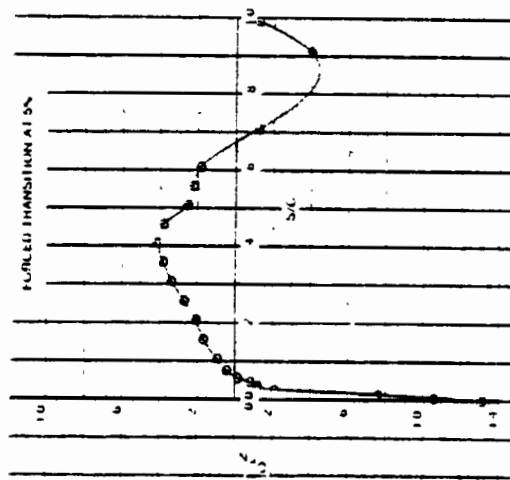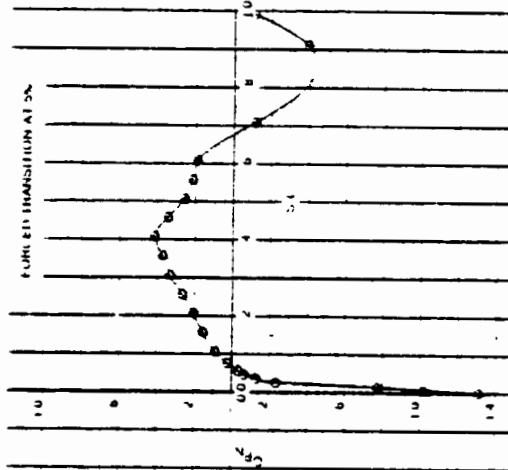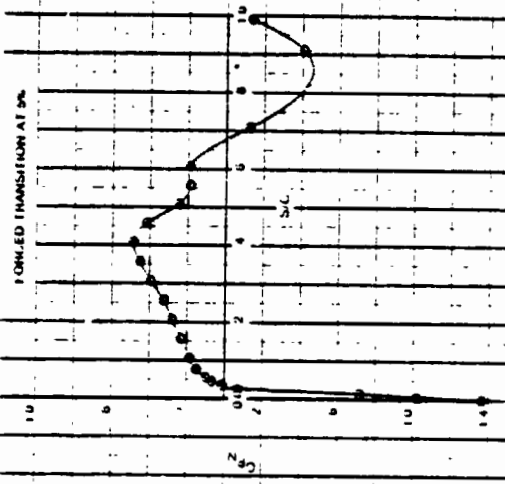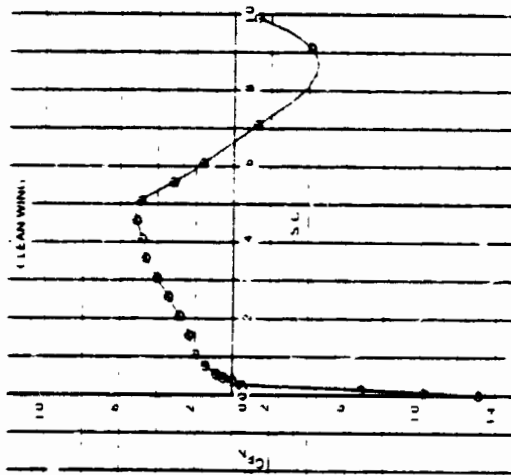
Figure B-3. Measured Pressure Distributions: F-111 NLF Glove, Cases 7, 8, and 9
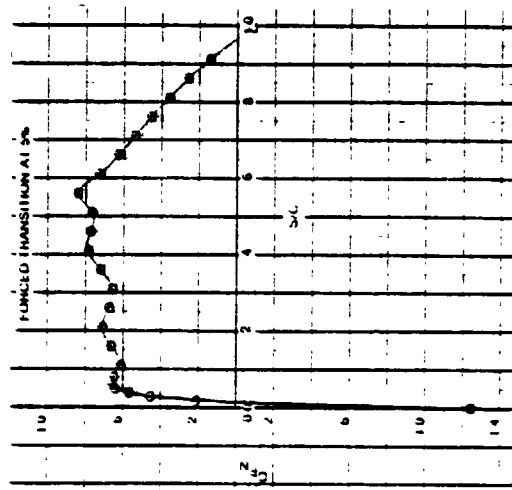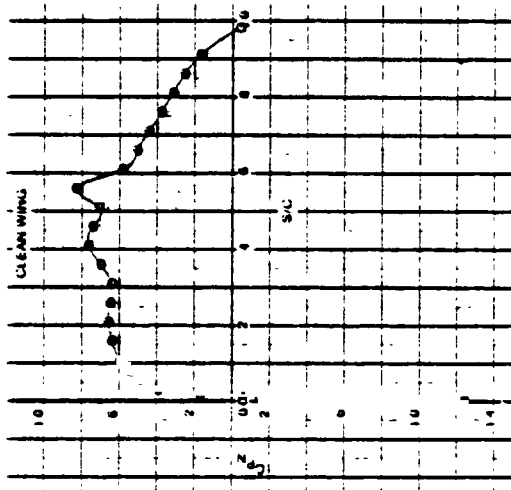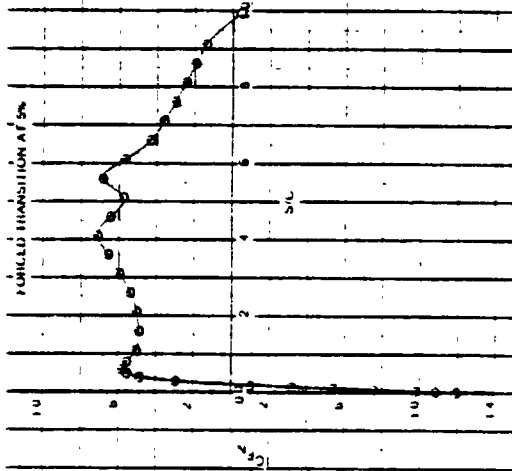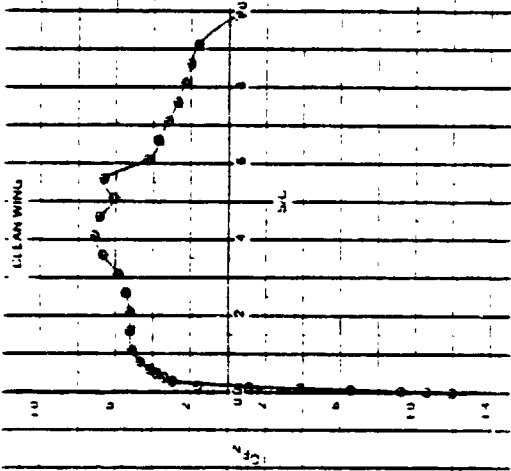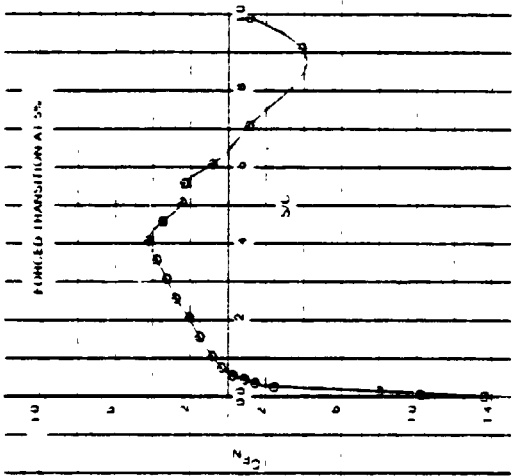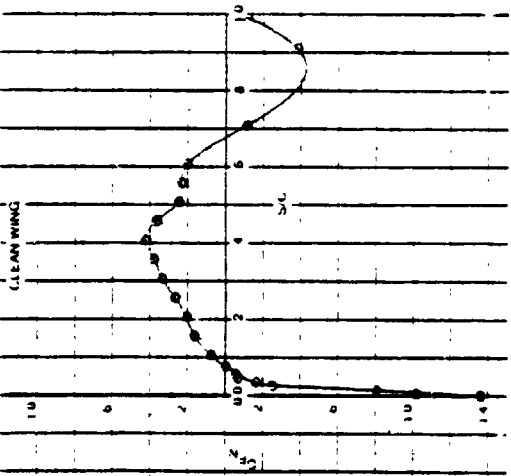
Figure B-4. Measured Pressure Distributions: F-111 NLF Glove, Cases 10, 11, and 12
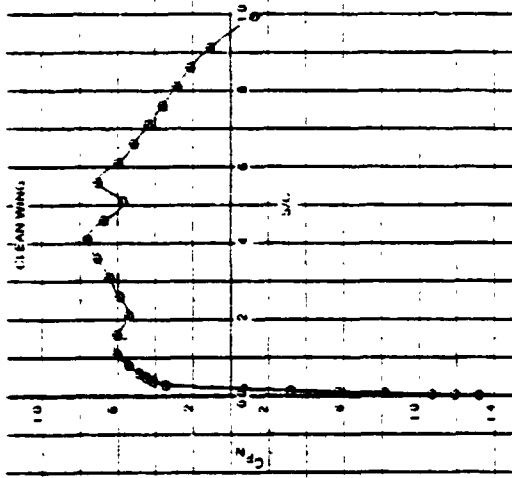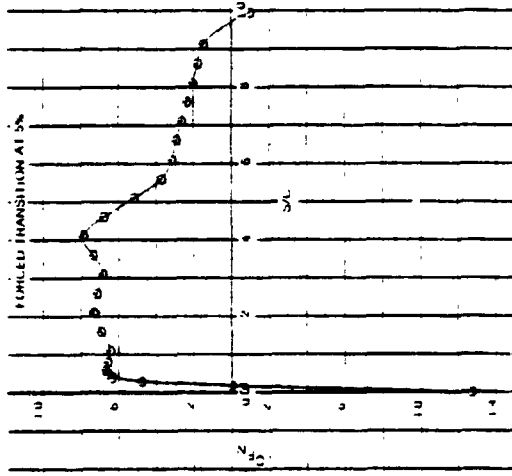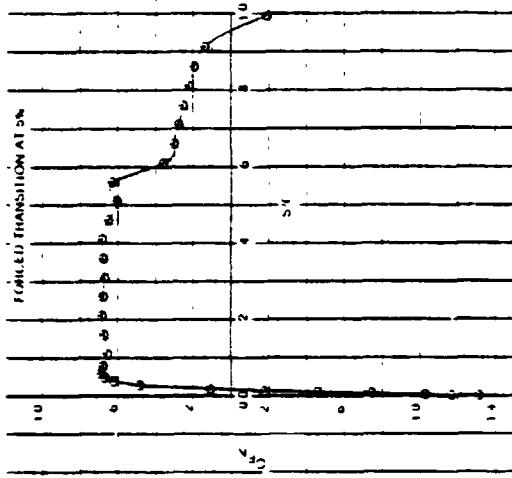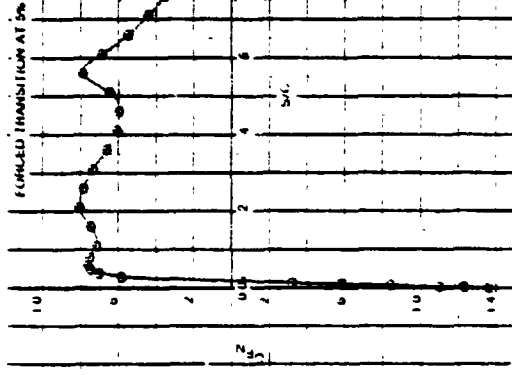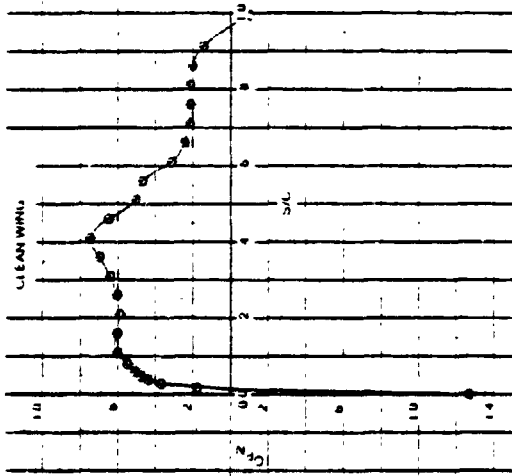
Figure B-5. Measured Pressure Distributions: F-111 NLF Glove, Cases 13, 14, and 15
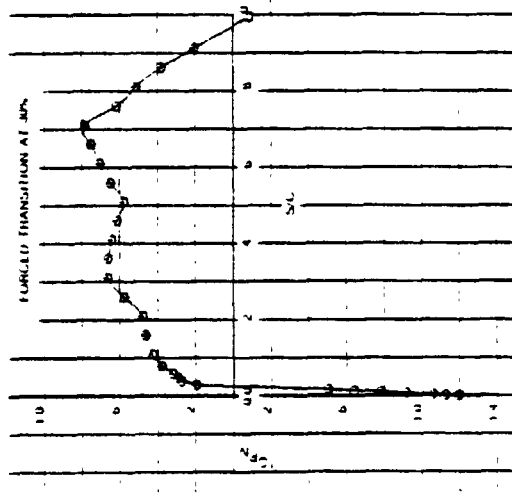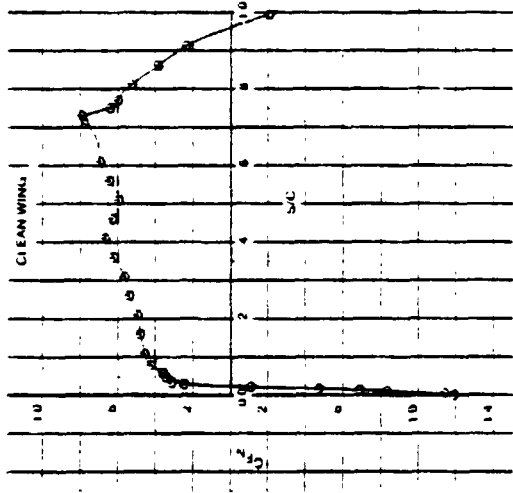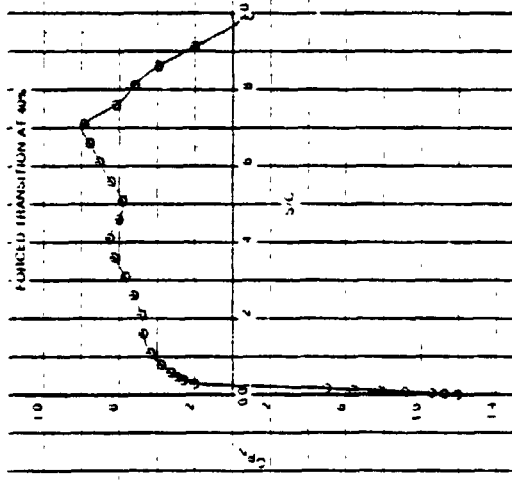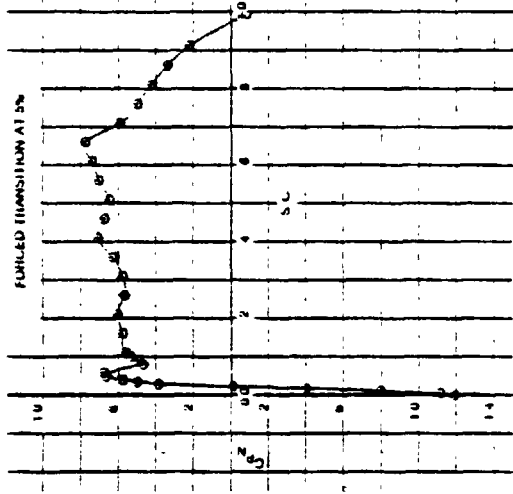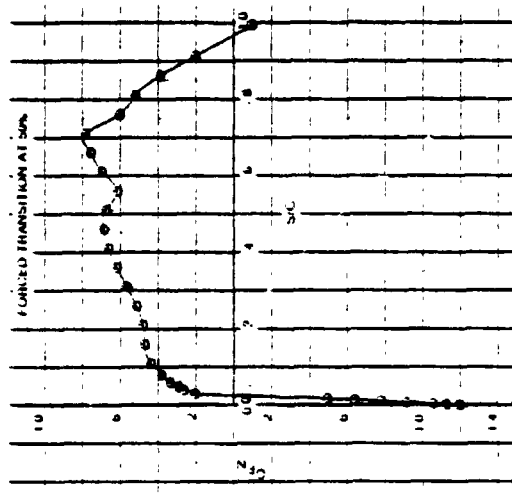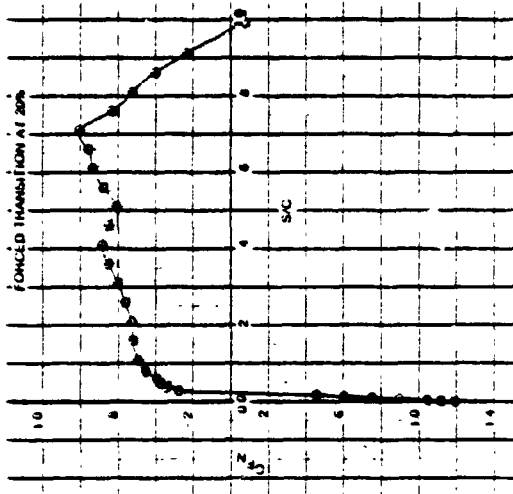
CASE: 16

Figure B-6. Measured Pressure Distributions: F-111 NLF Glove, Case 16

CASE: 17
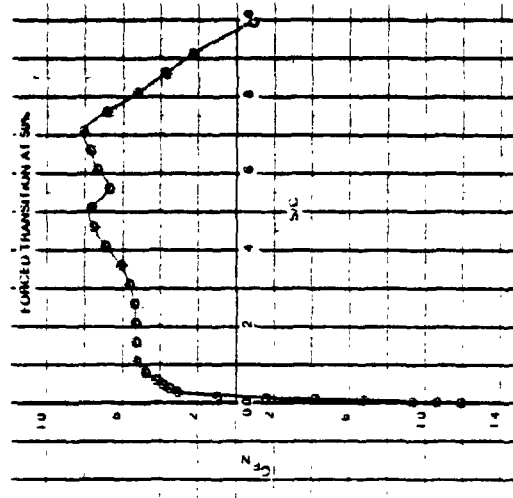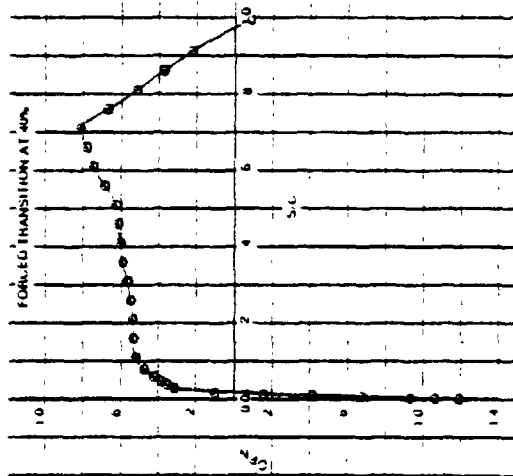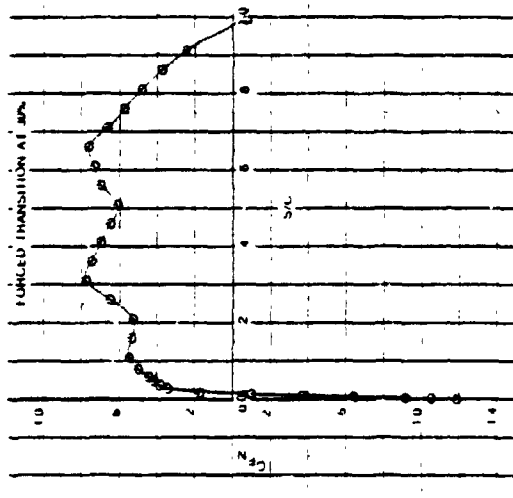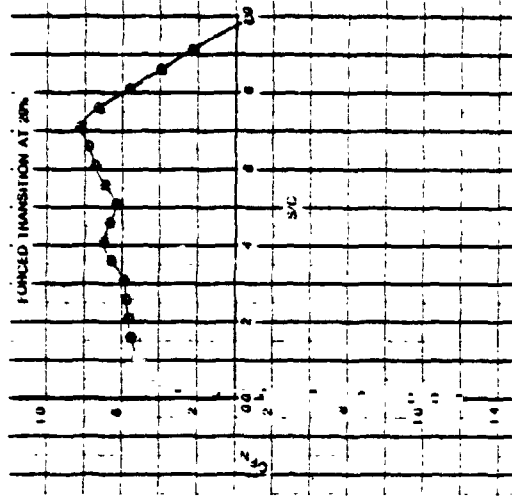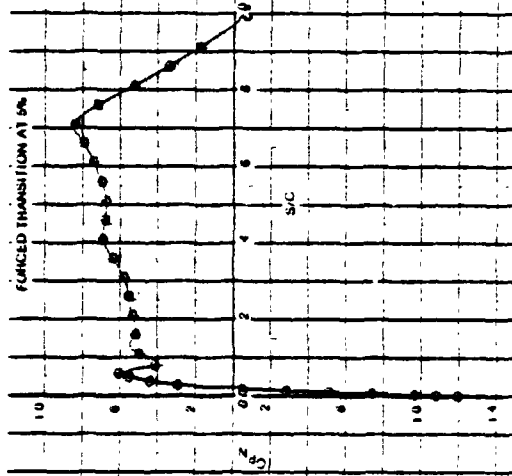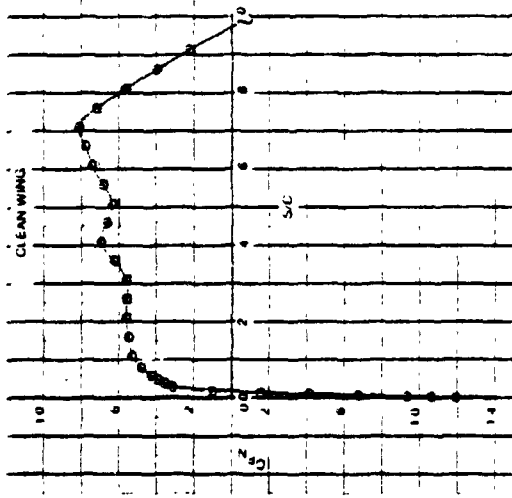
Figure B-7. Measured Pressure Distributions: F-111 NLF Glove, Case 17
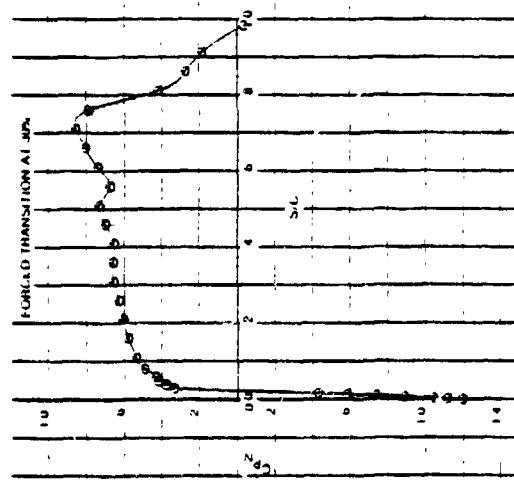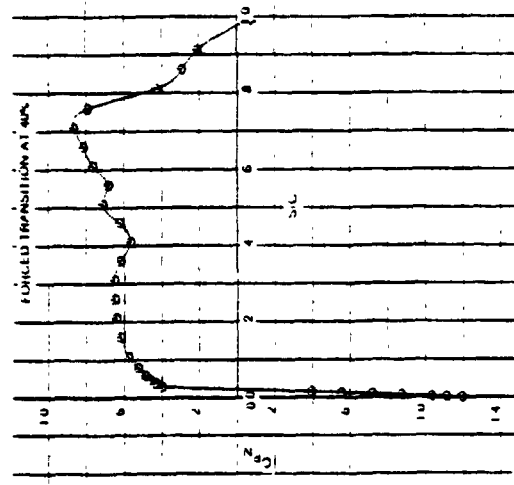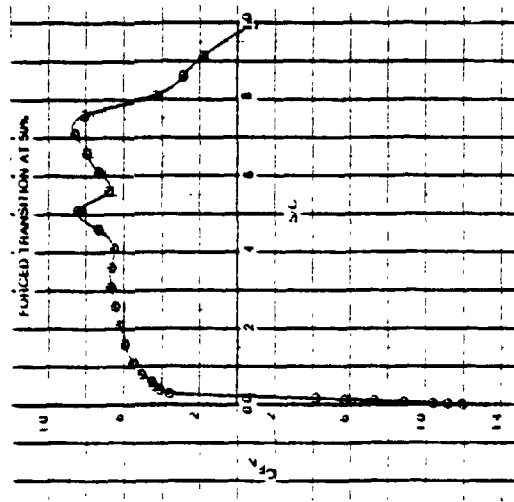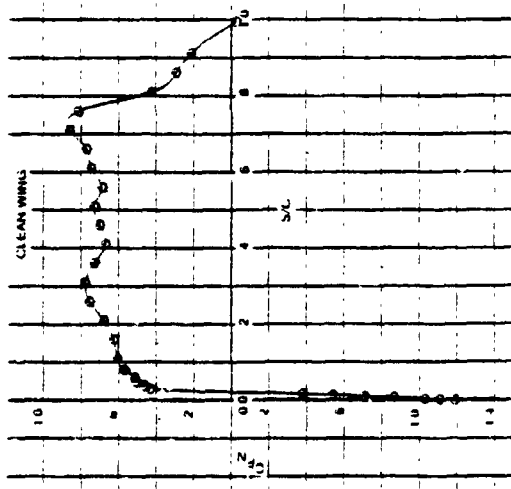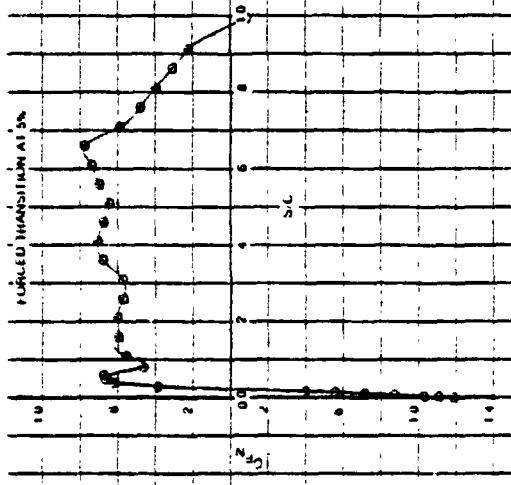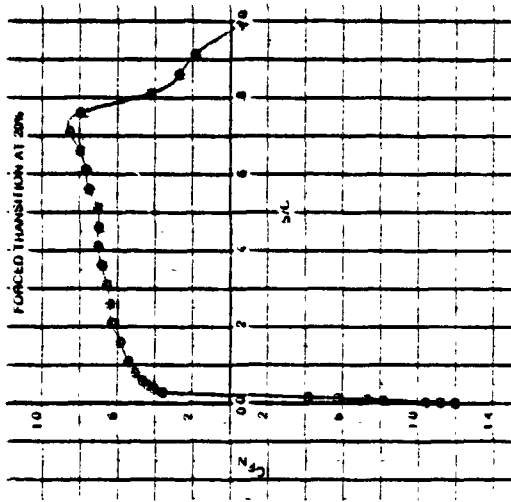
CASE: 18

Figure B-8. Measured Pressure Distributions: F-111 NLF Glove, Case 18
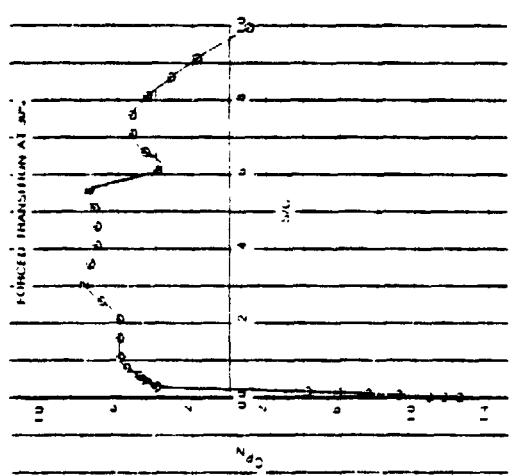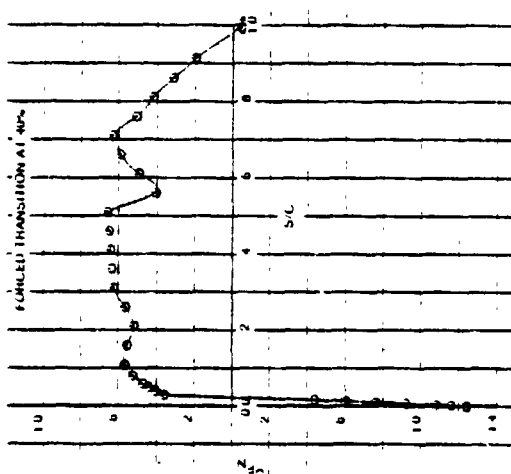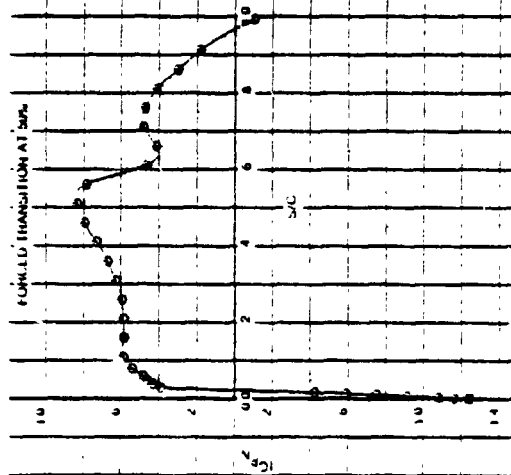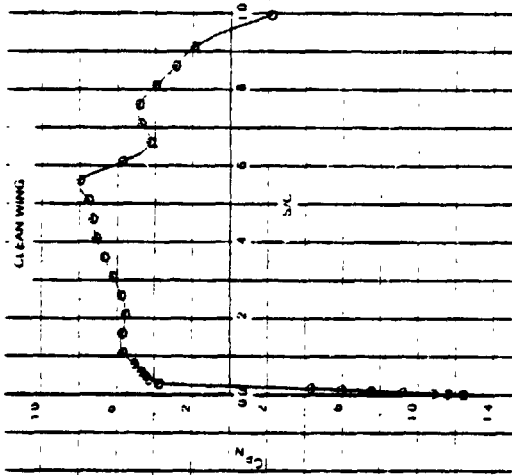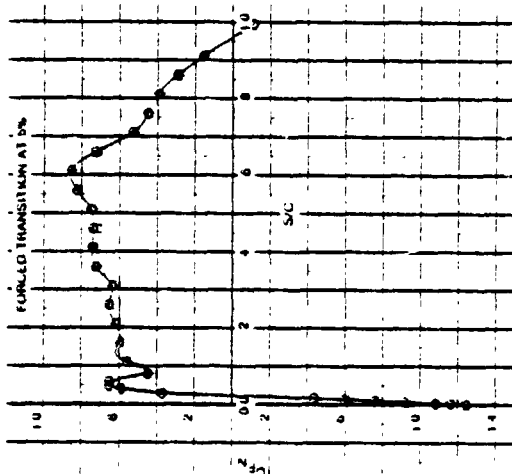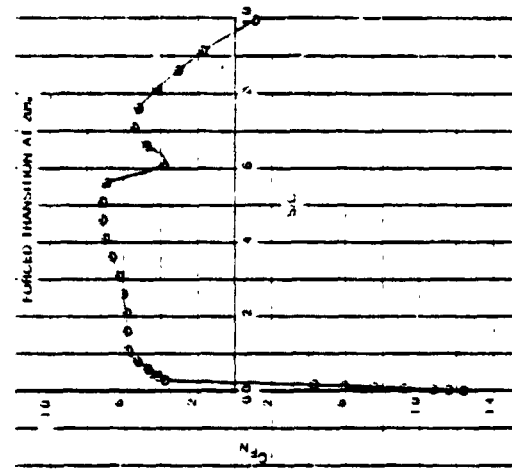
CASE: 19

Figure B-9. Measured Pressure Distributions: F-111 NLF Glove, Case 19
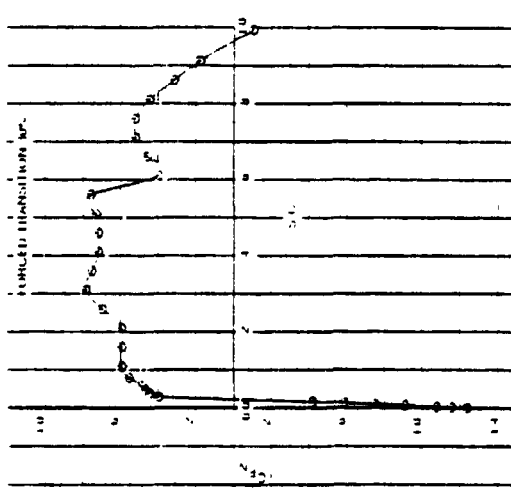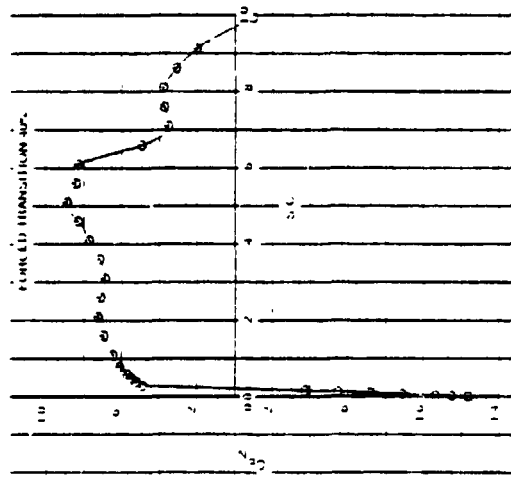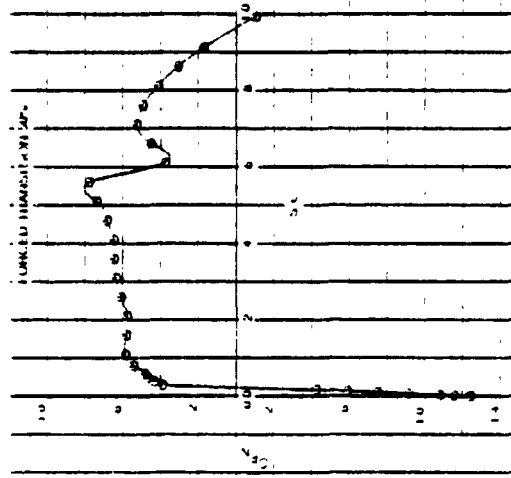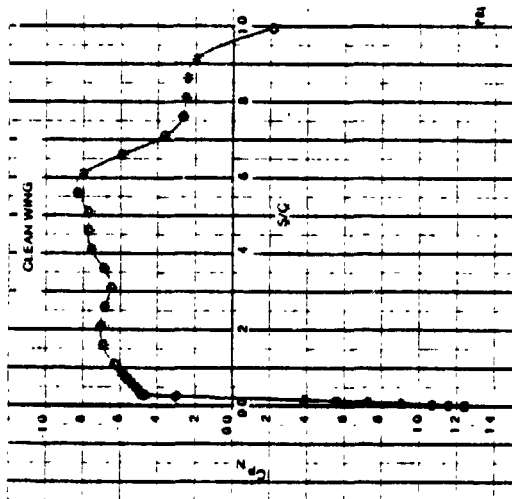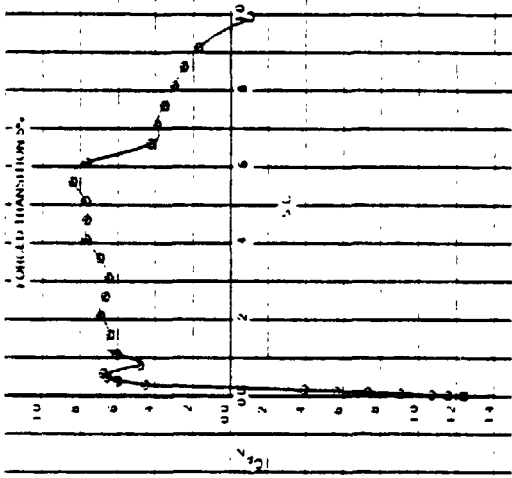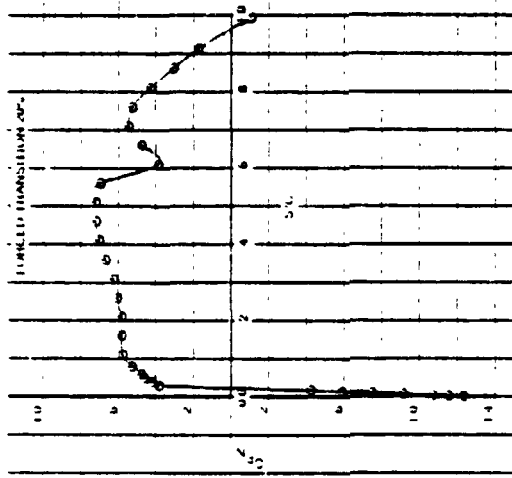
Figure B-10. Measured Pressure Distributions: F-111 NLF Glove, Case 20

CASE: 20
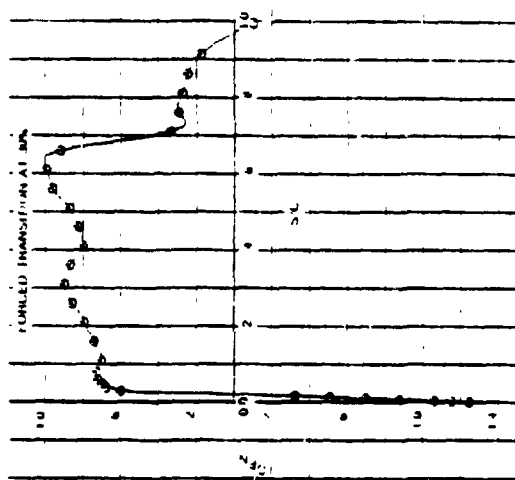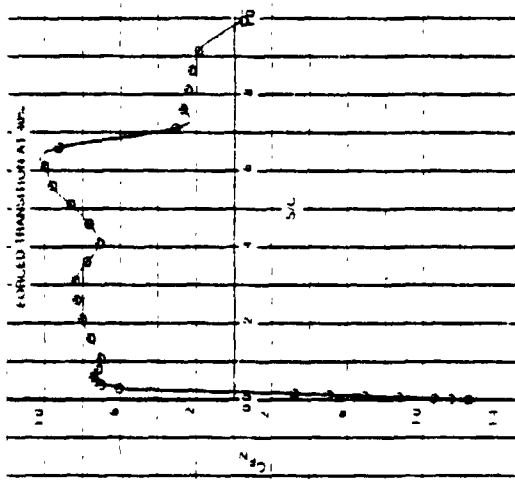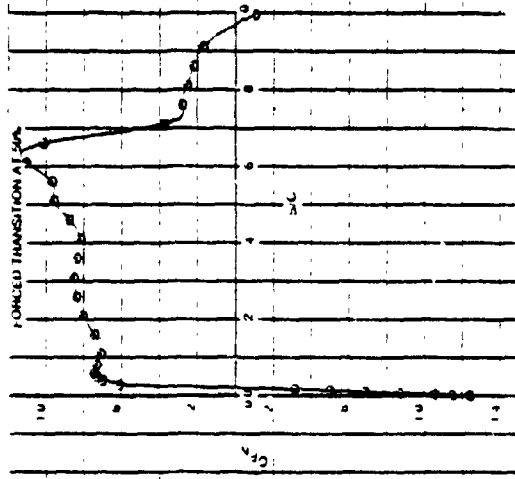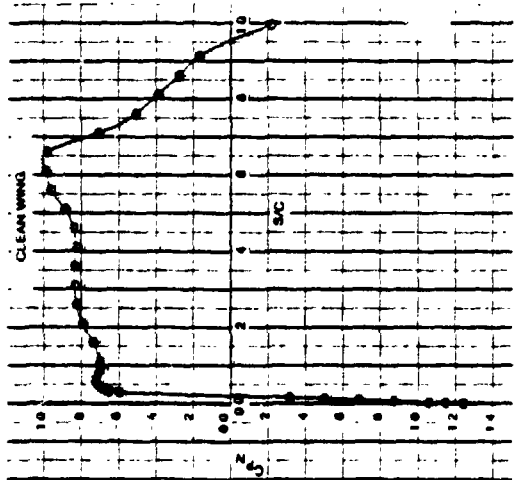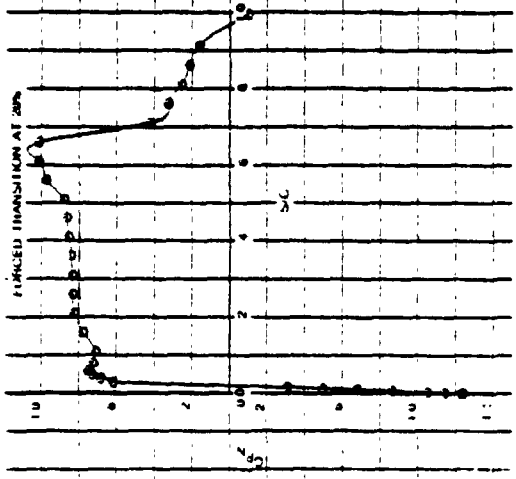
CASE: 21

Figure B-11. Measured Pressure Distributions: F-111 NLF Glove, Case 21
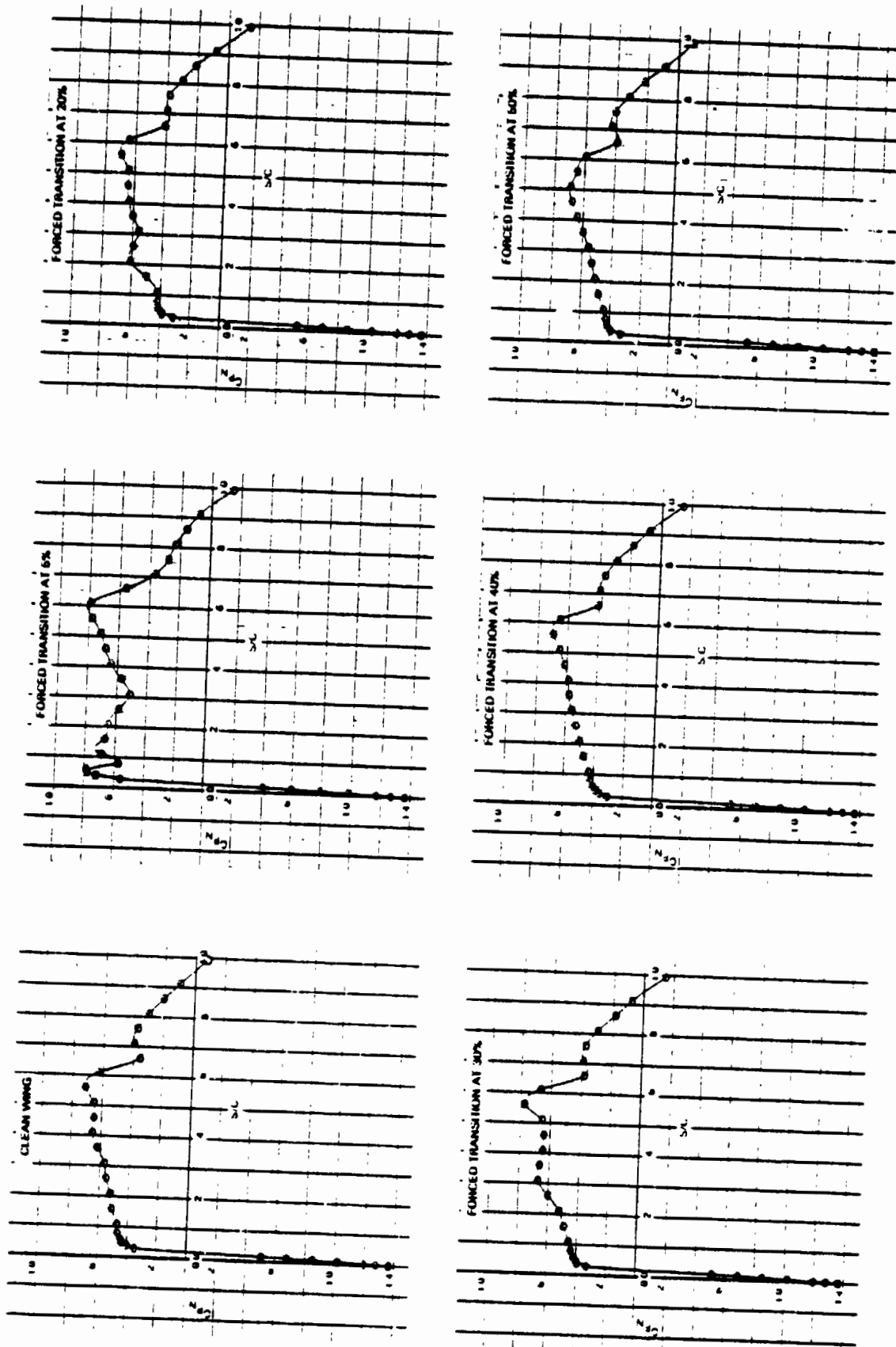
Figure B-12. Measured Pressure Distributions: F-111 NLF Glove, Case 22
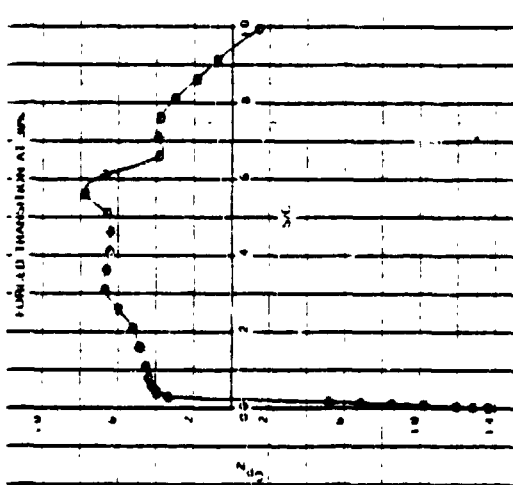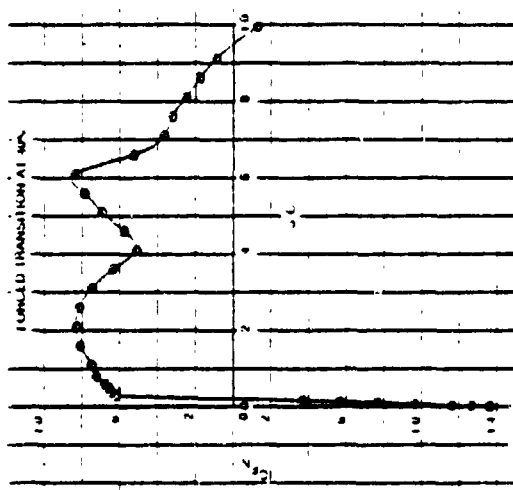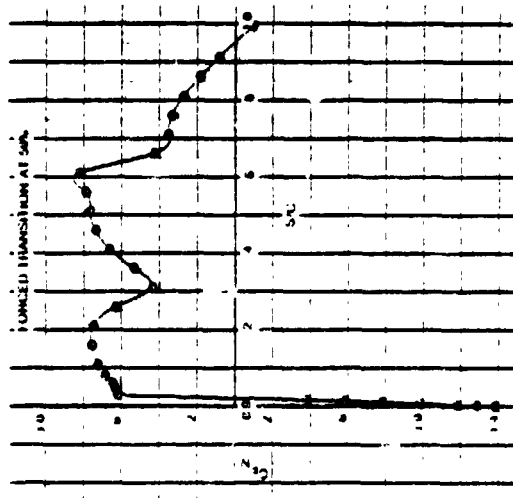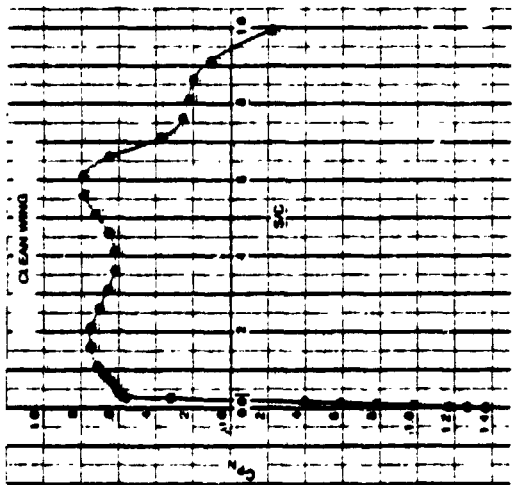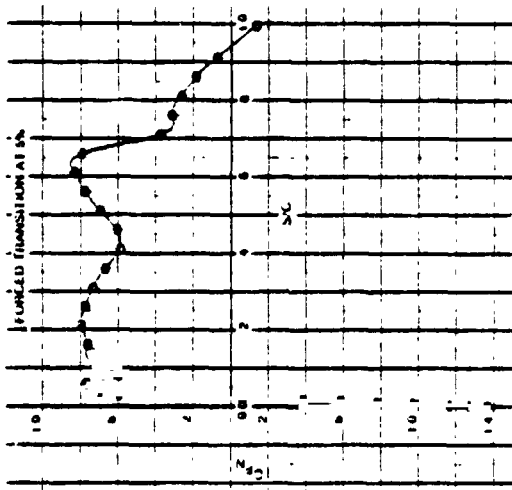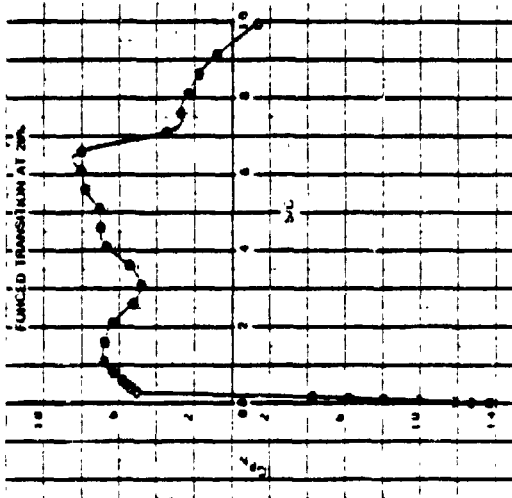
CASE: 23

Figure B-13. Measured Pressure Distributions: F-111 NLF Glove, Case 23
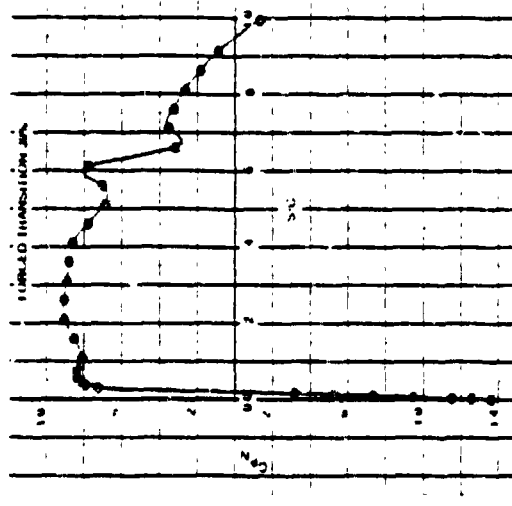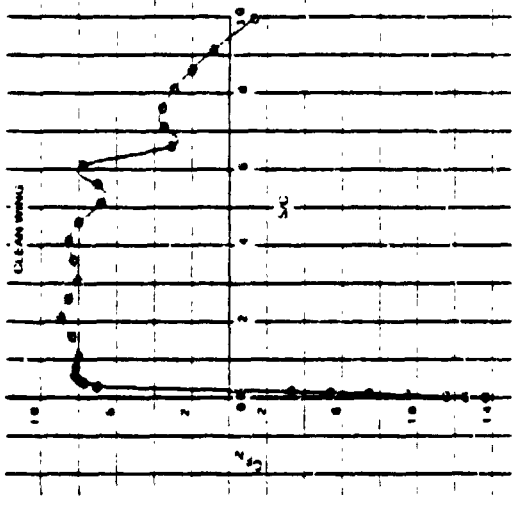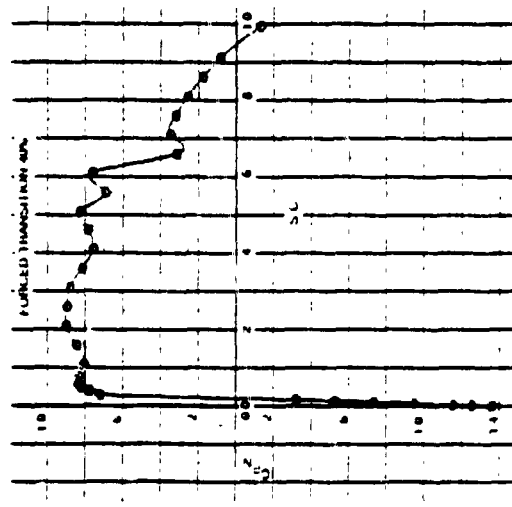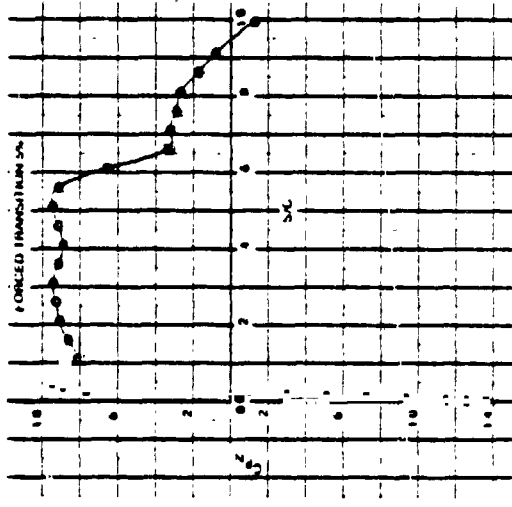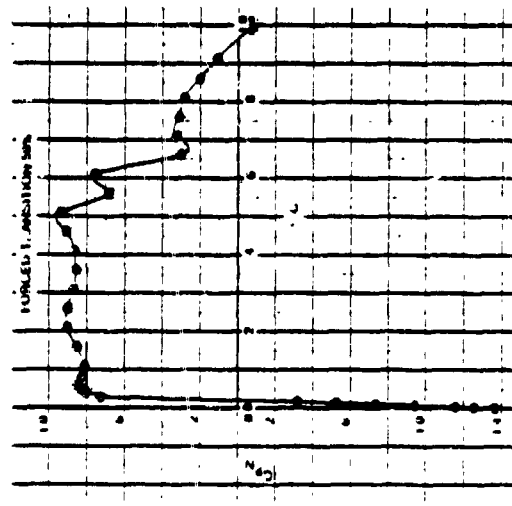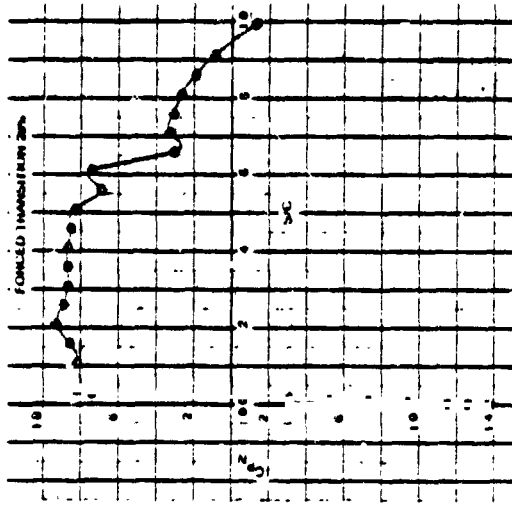
CASE: 24

Figure B-14. Measured Pressure Distributions: F-111 NLF Glove, Case 24
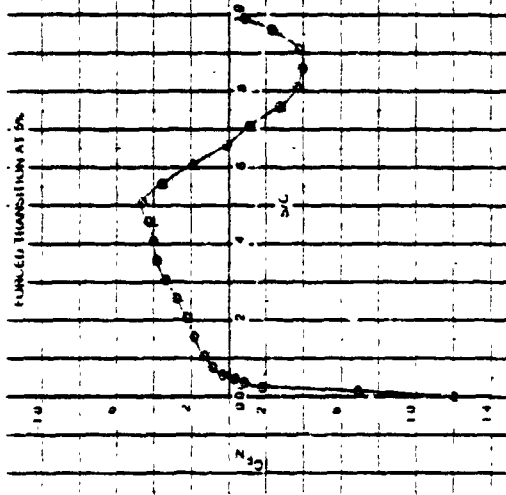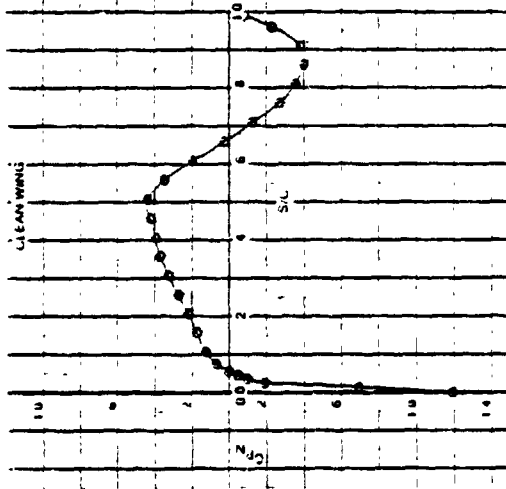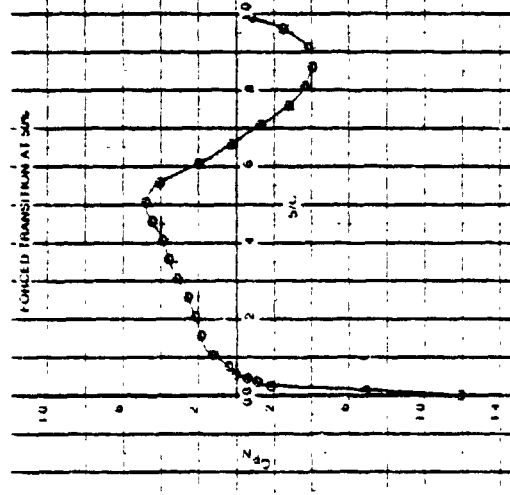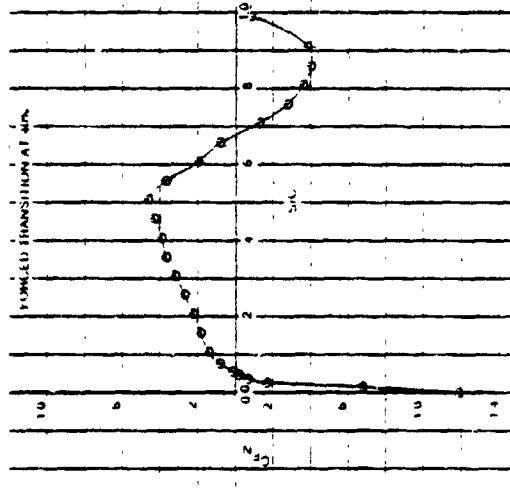
CASE: 25

Figure B-15. Measured Pressure Distributions: F-111 NLF Glove, Case 25
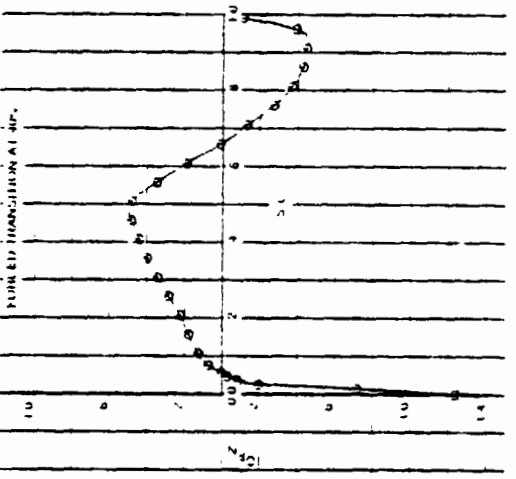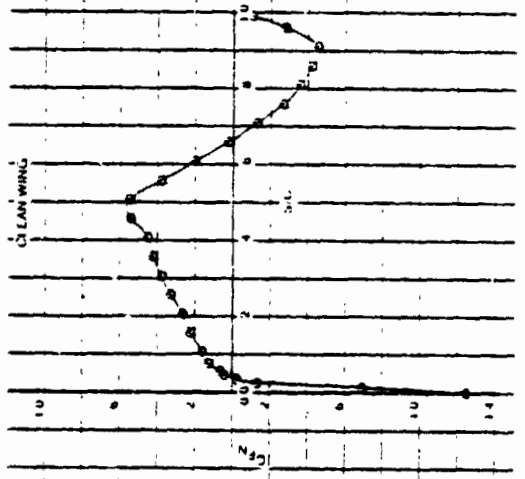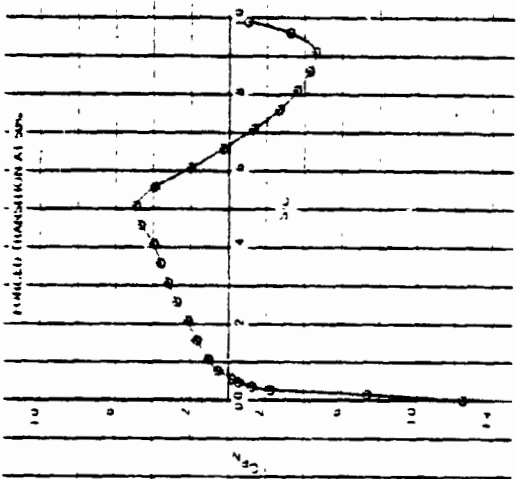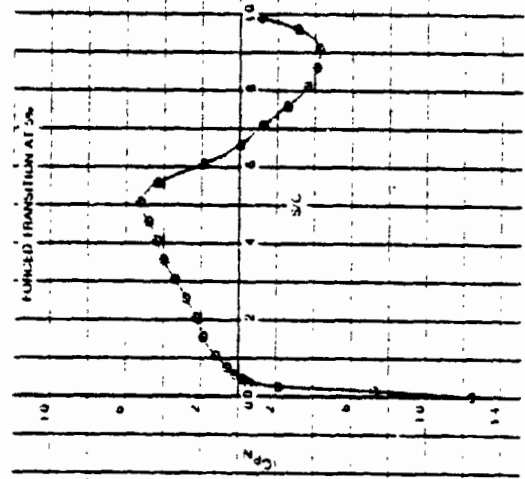
CASE: 26

Figure B-16. *Measured Pressure Distributions: F-111 NLF Glove, Case 26*
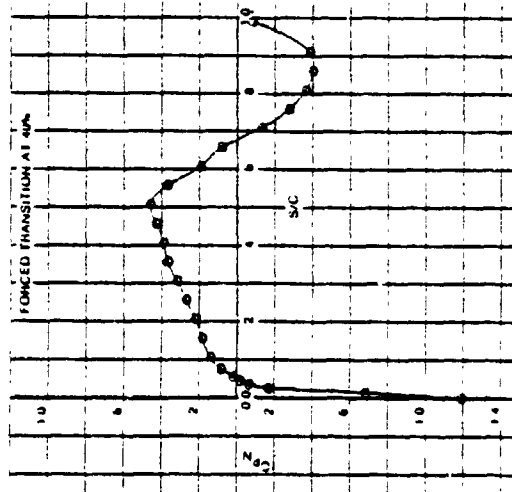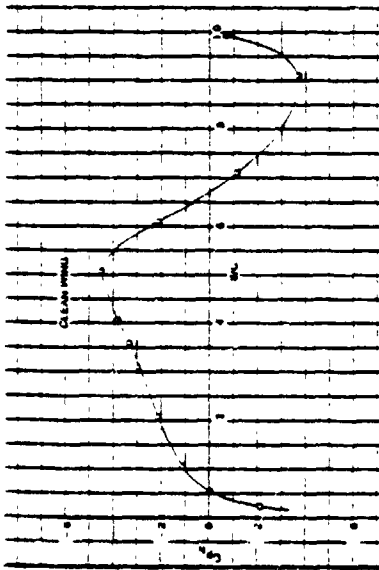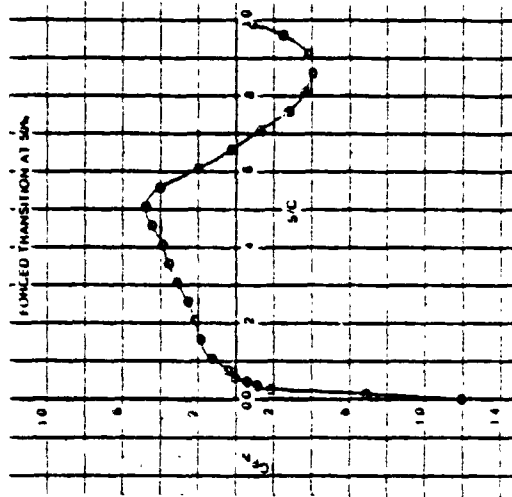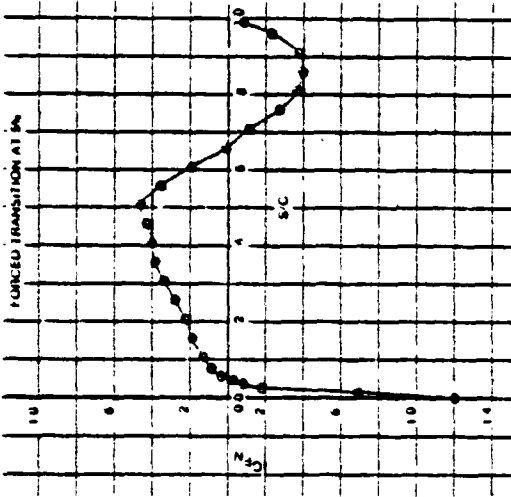
CASE: 27

Figure B-17. Measured Pressure Distributions: F-111 NLF Glove, Case 27

CASE: 28
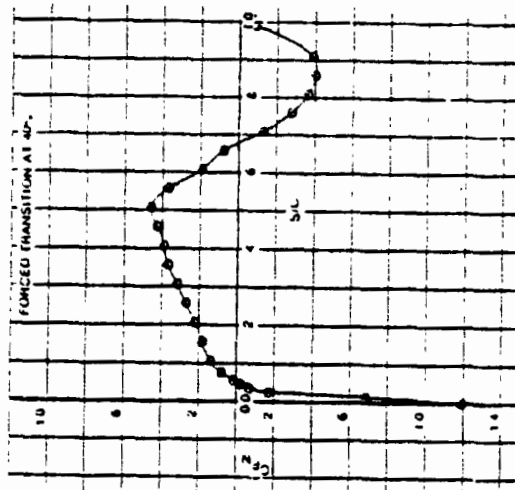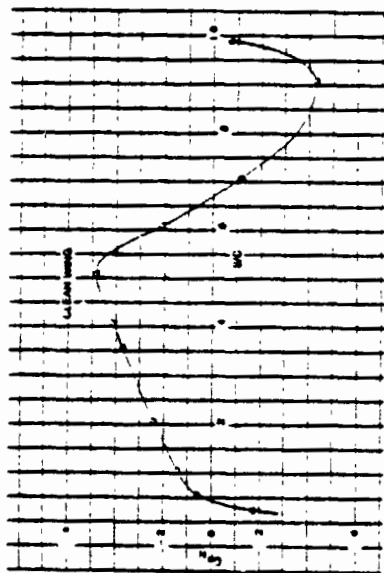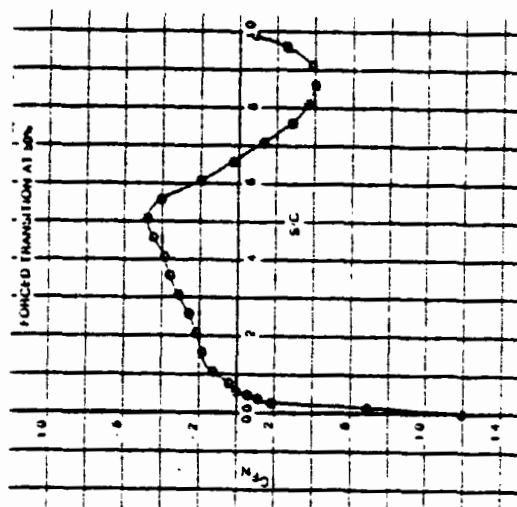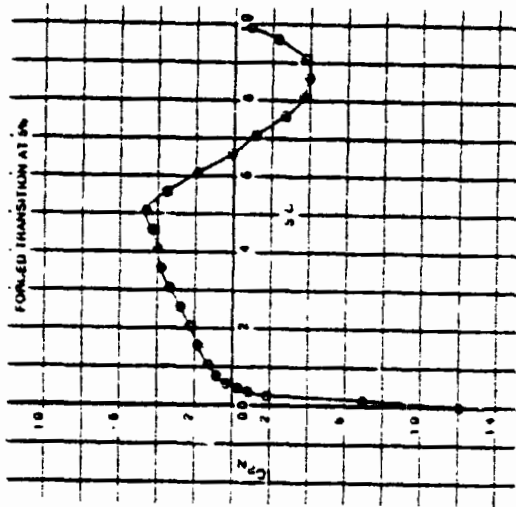
Figure B-18. Measured Pressure Distributions: F-111 NLF Glove, Case 28

CASE: 29
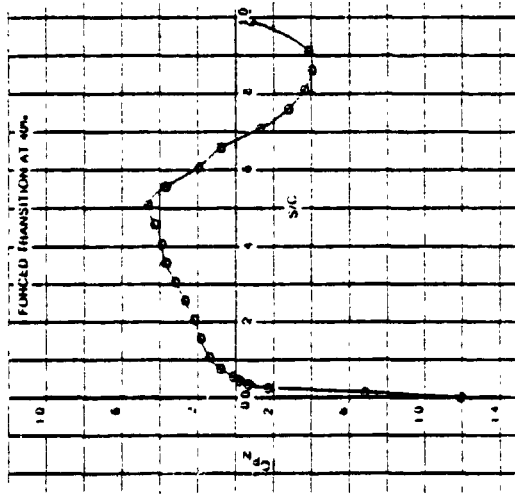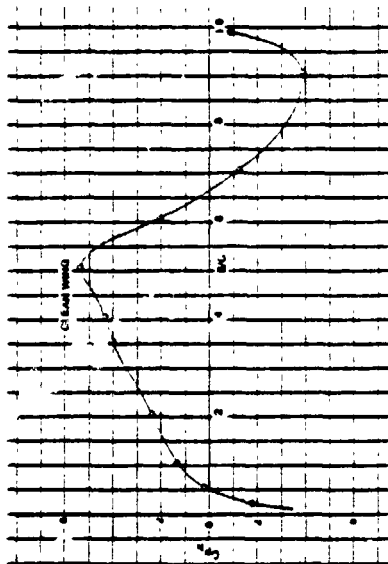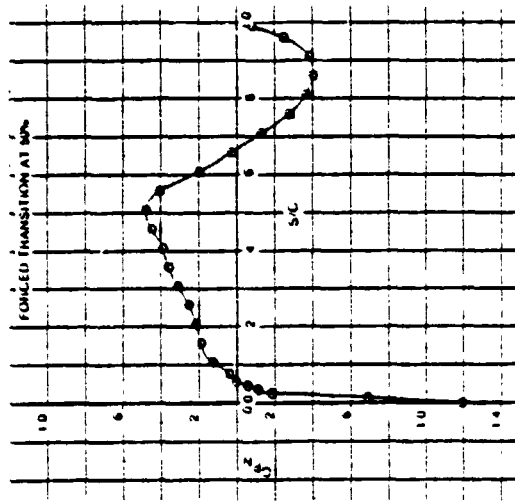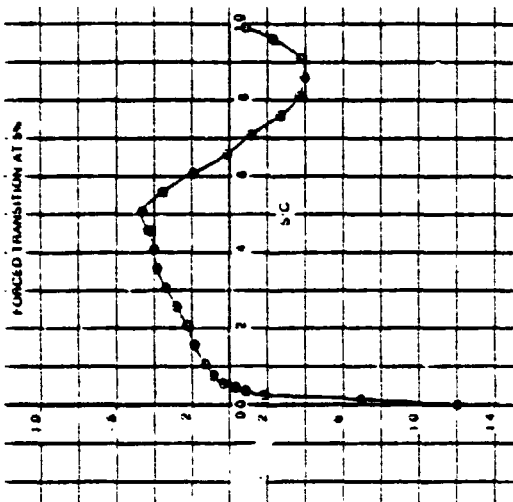
Figure B-19. Measured Pressure Distributions: F-111 NLF Glove, Case 29
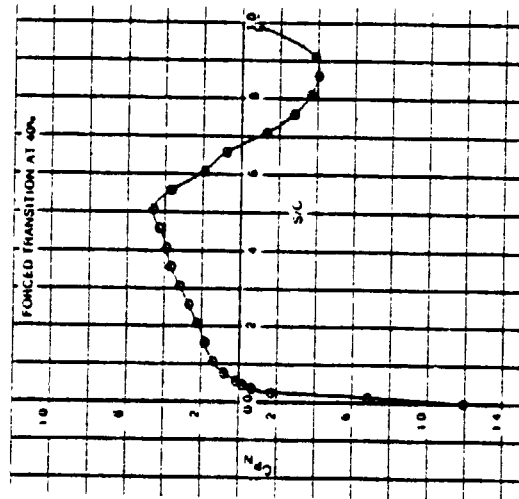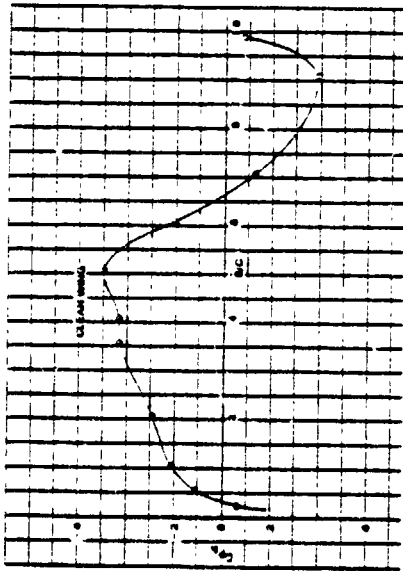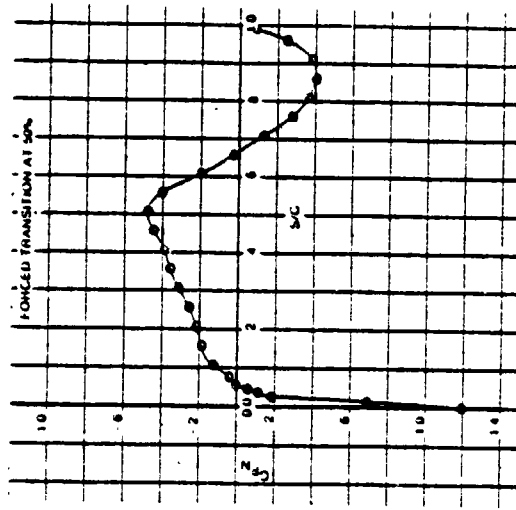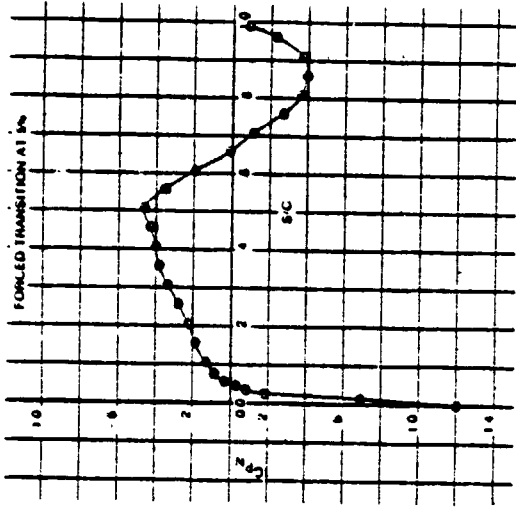
CASE: 30

Figure B-20. Measured Pressure Distributions: F-111 NLF Glove, Case 30
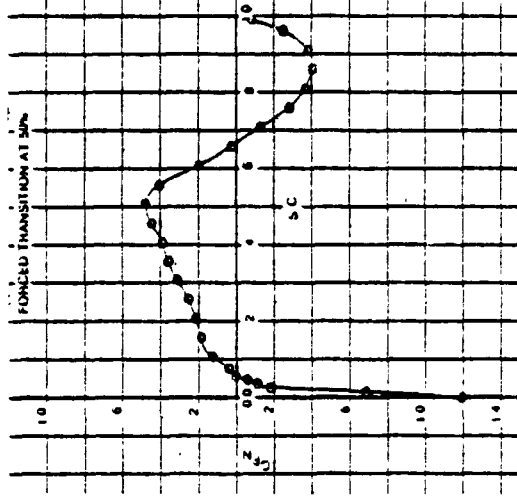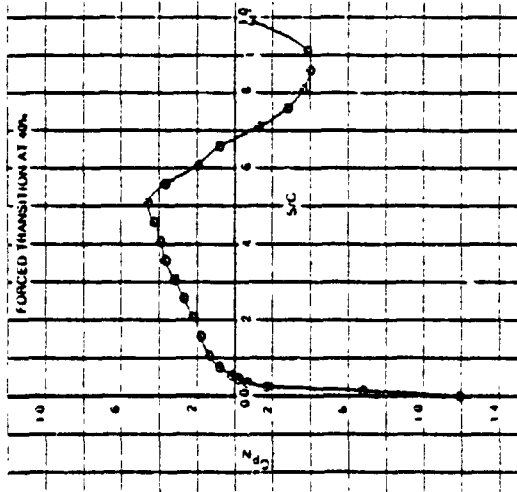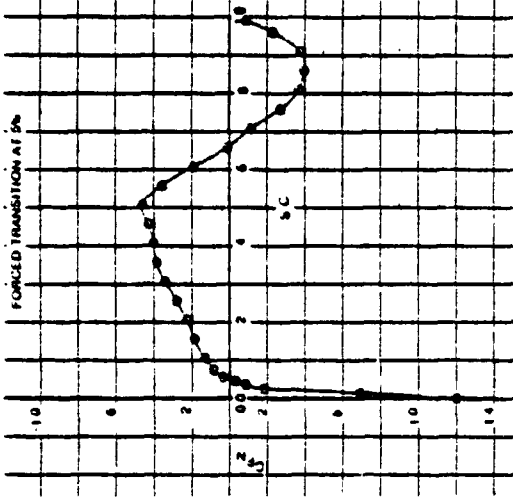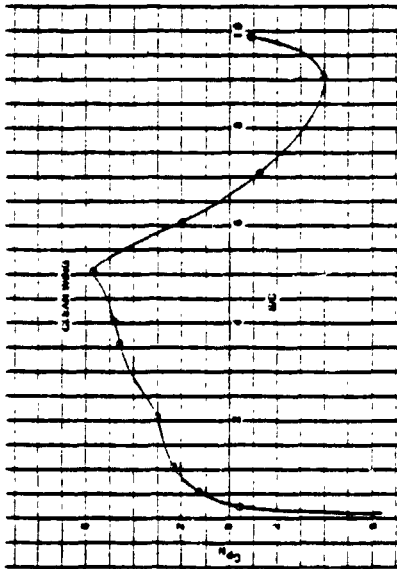
CASE: 31

Figure B-21. Measured Pressure Distributions: F-111 NLF Glove, Case 31
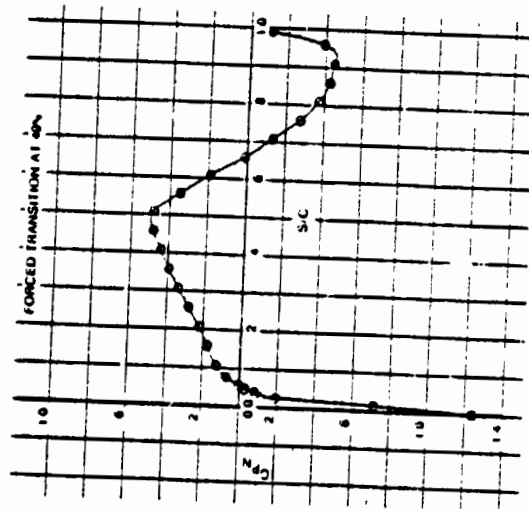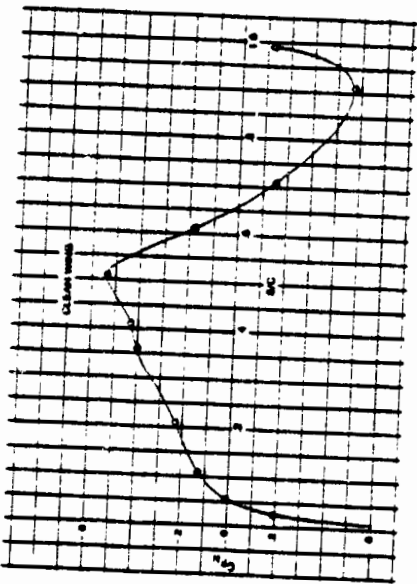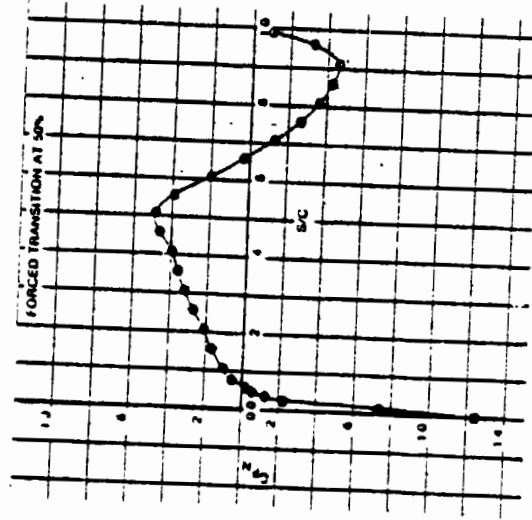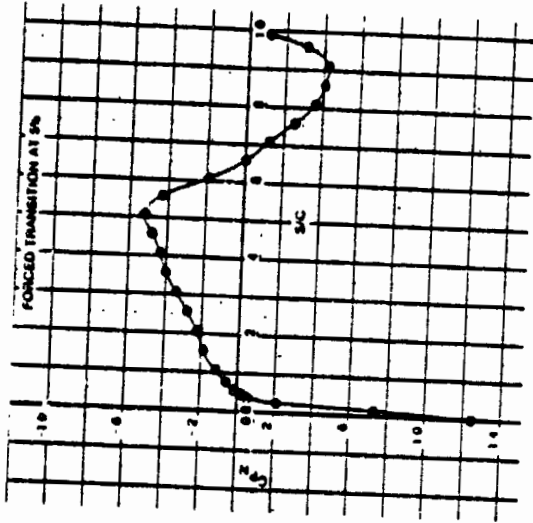
CASE: 32

Figure B-22. Measured Pressure Distributions: F-111 NLF Glove, Case 32
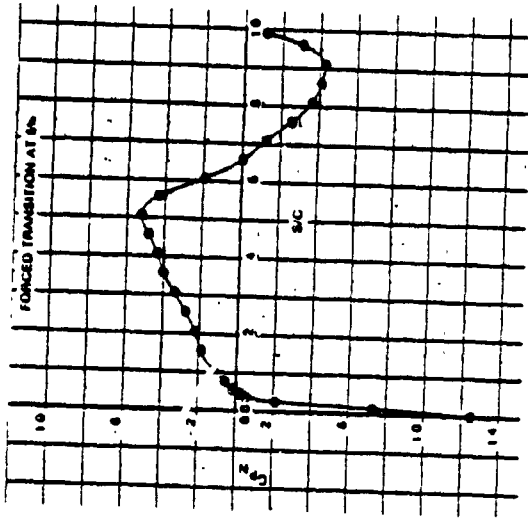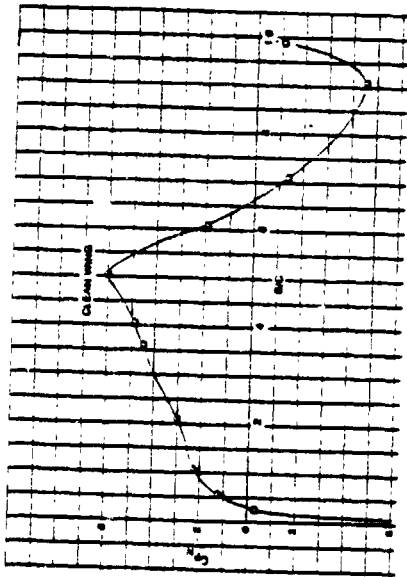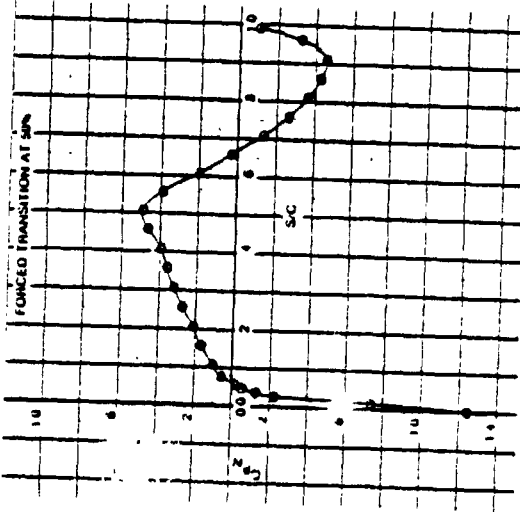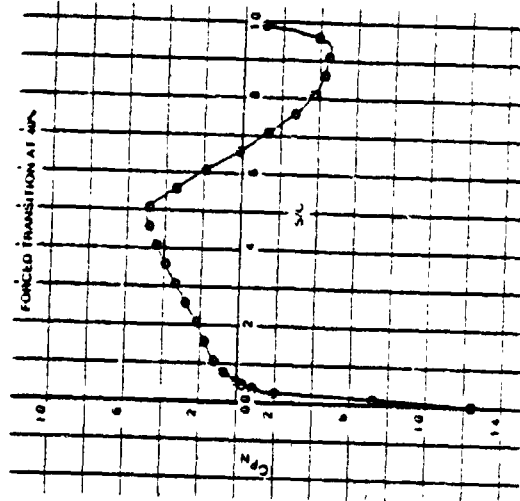
CASE: 33

Figure B-23. Measured Pressure Distributions: F-111 NLF Glove, Case 33

CASE: 34
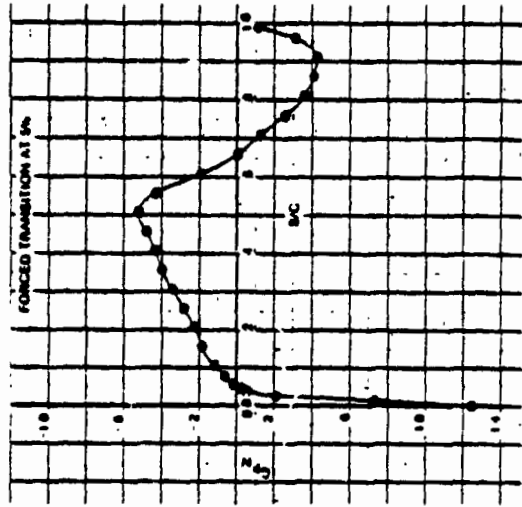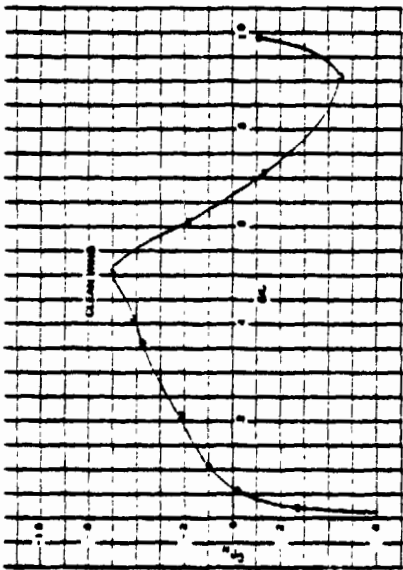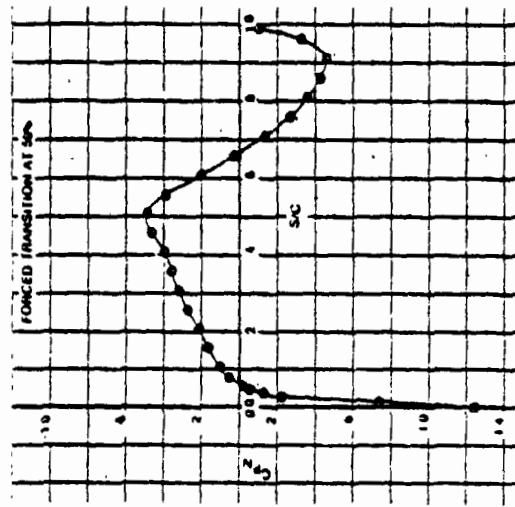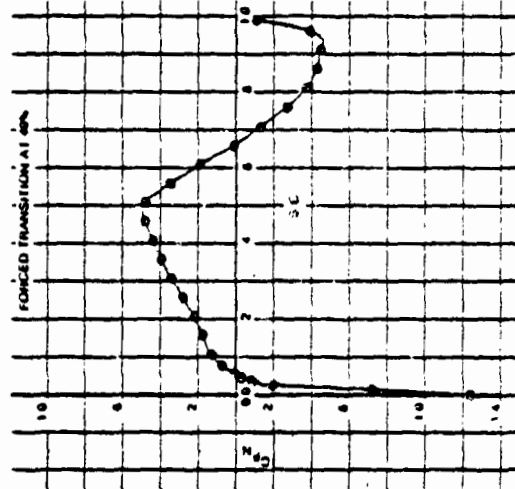
Figure B-24. Measured Pressure Distributions: F-111 NLF Glove, Case 34
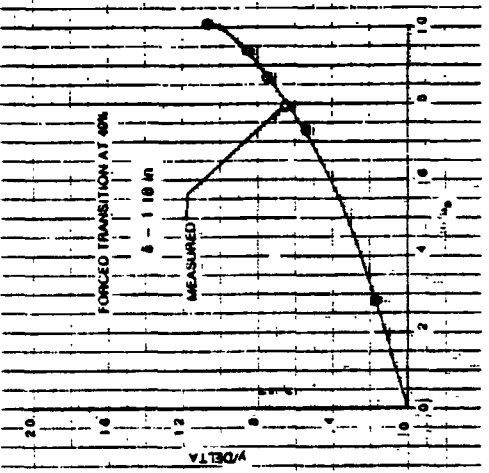
Figure B-25. Measured Velocity Profiles: F-111 NLF Glove, Cases 1, 2, and 3
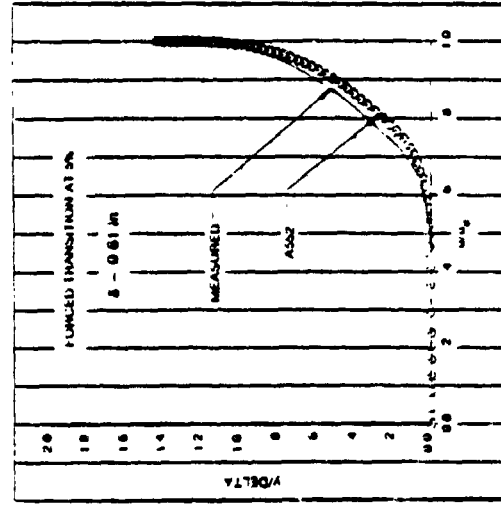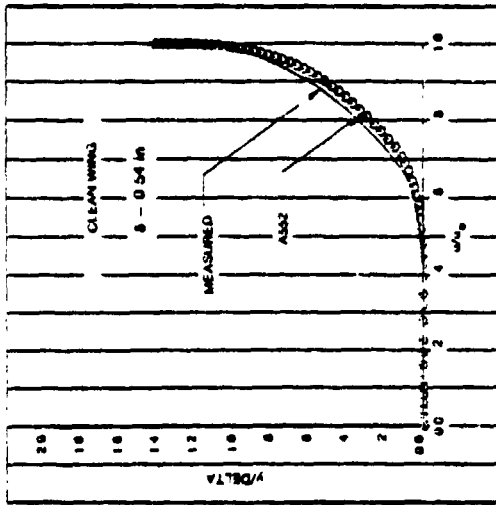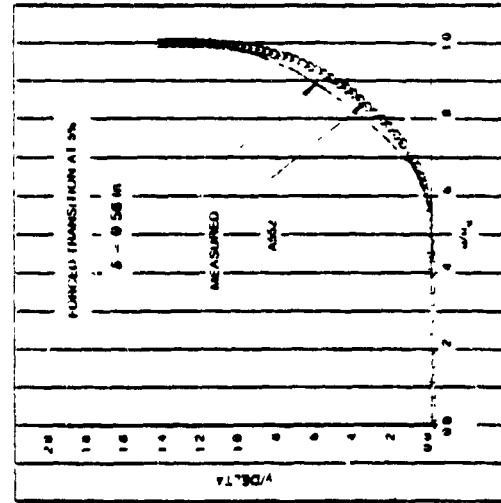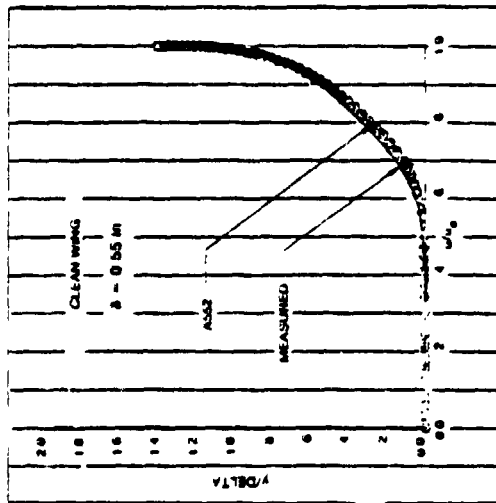
Figure B-26. Measured Velocity Profiles: F-111 NLF Glove, Cases 4, 5, and 6
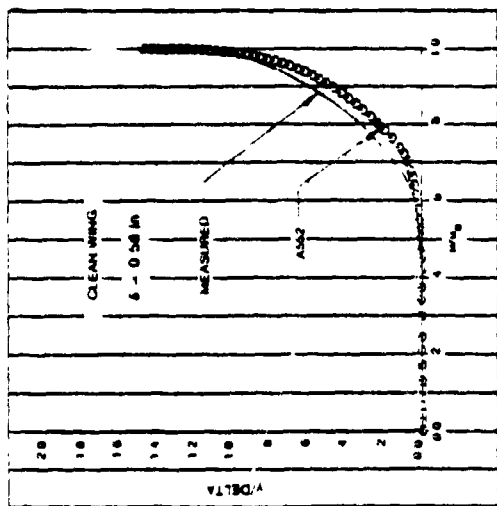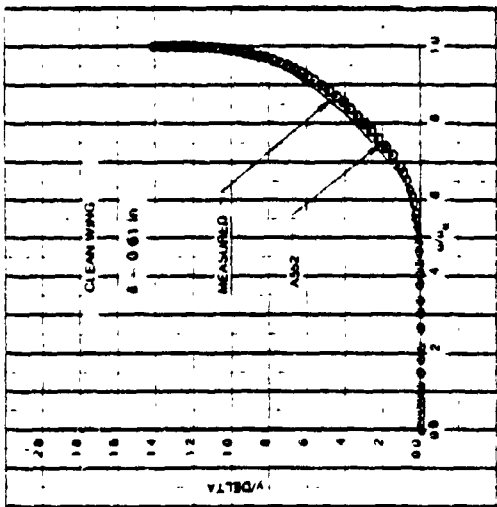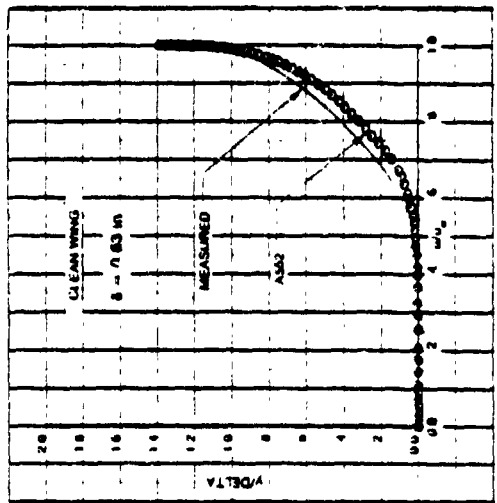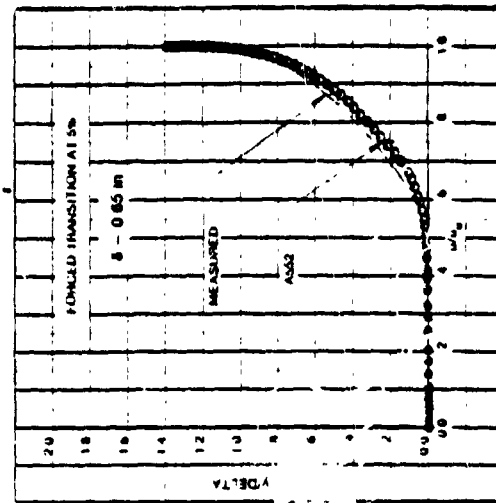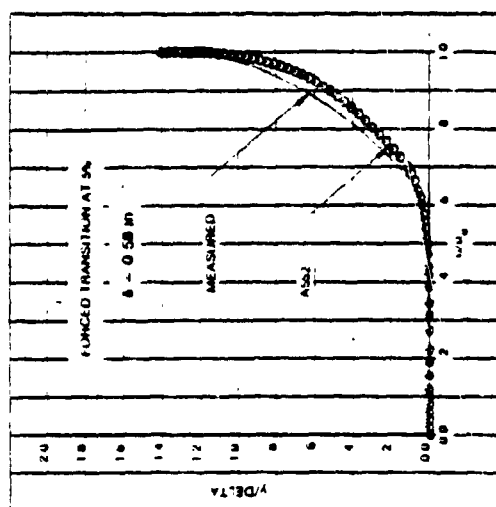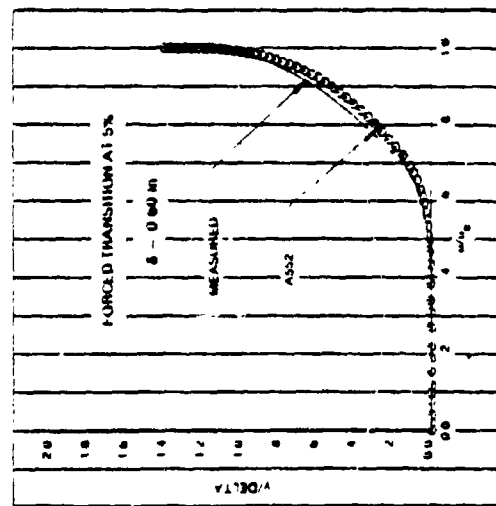
Figure B-27. Measured Velocity Profiles: F-111 NLF Glove, Cases 7, 8, and 9
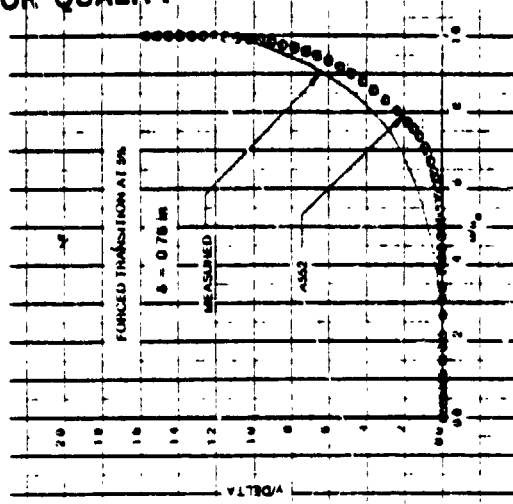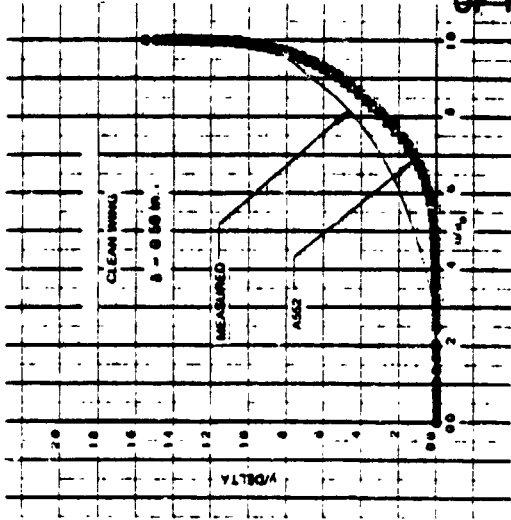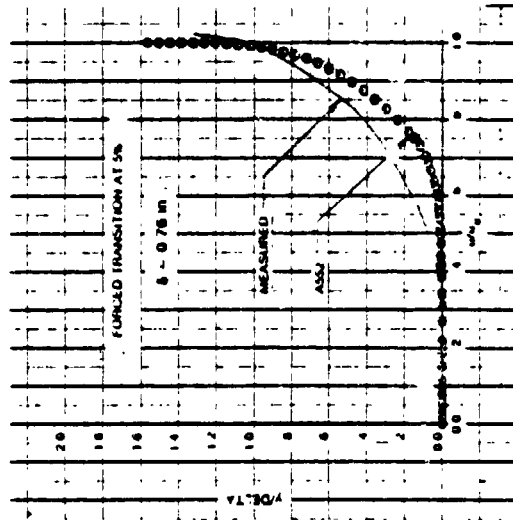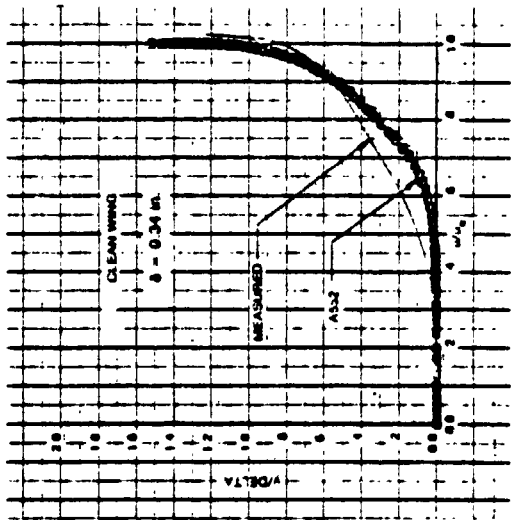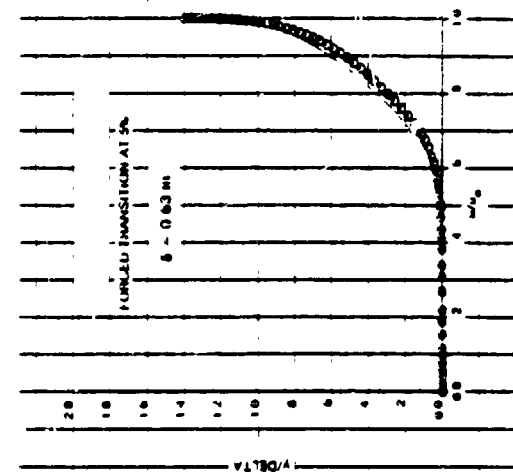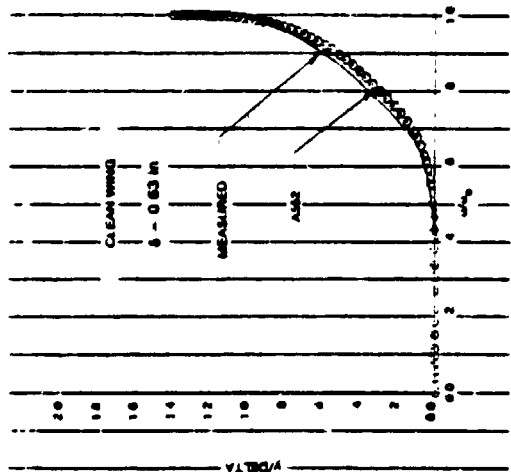
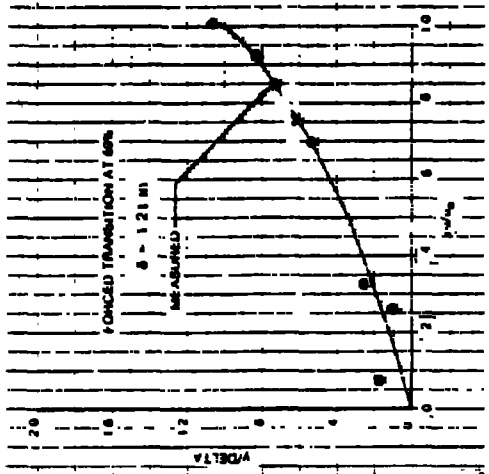Figure B-28. Measured Velocity Profiles: F-111 NLF Glove, Cases 10, 11, and 12

Figure B-29.   Measured Velocity Profiles: F-111 NLF Glove, Cases 13, 14, and 15

CASE: 16
RAKE AT 90%
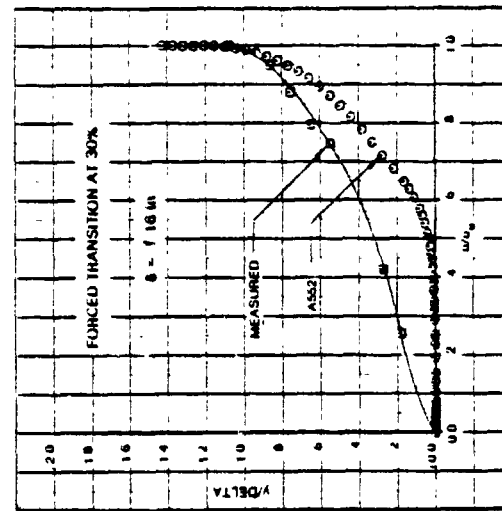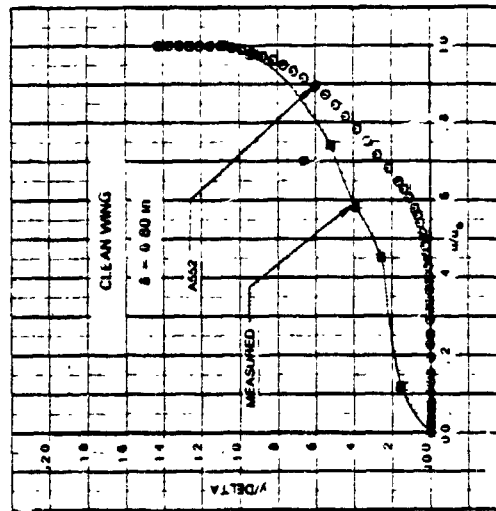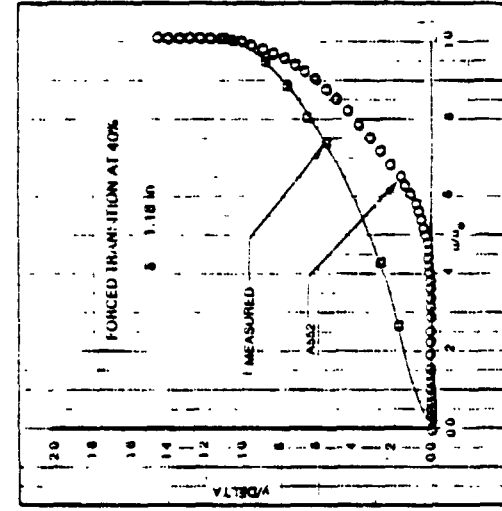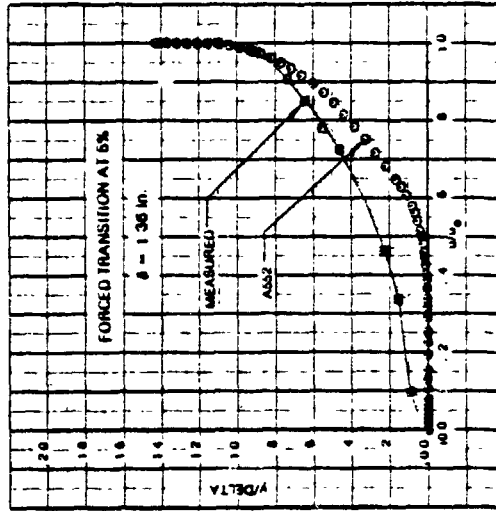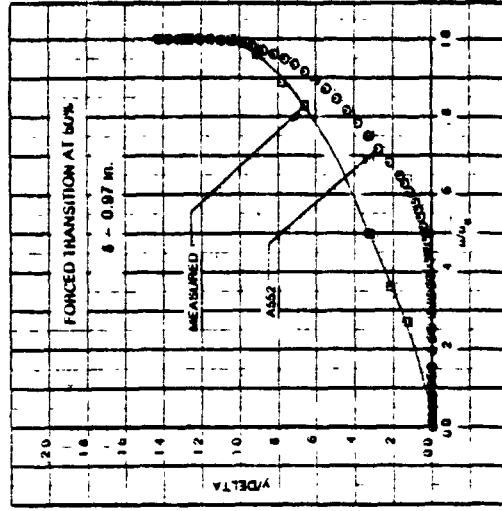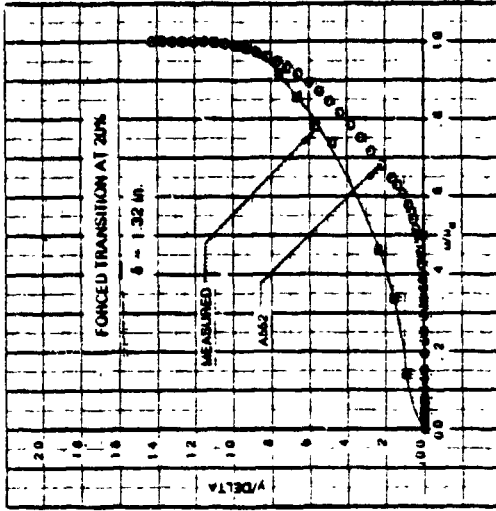
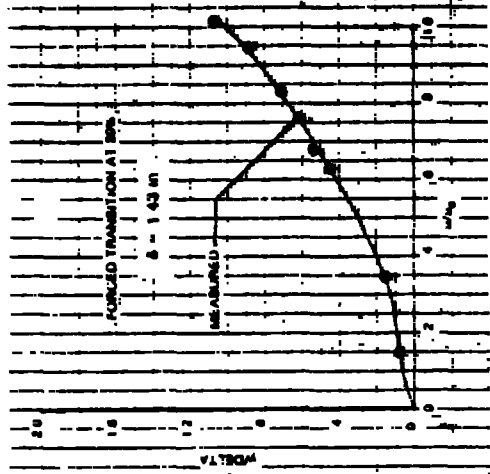Figure B-30. *Measured Velocity Profiles: F-111 NLF Glove, Case 16*
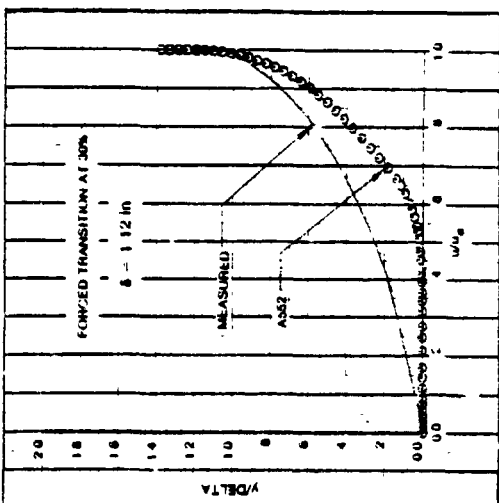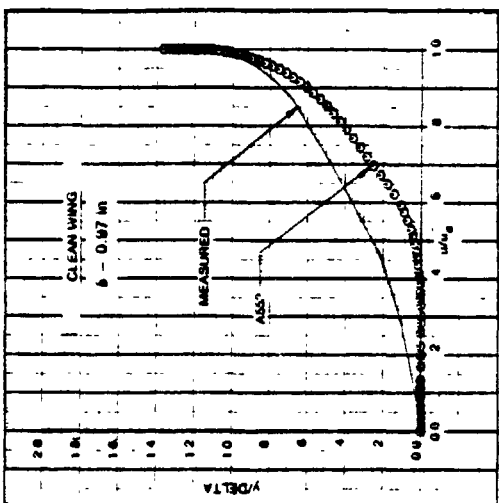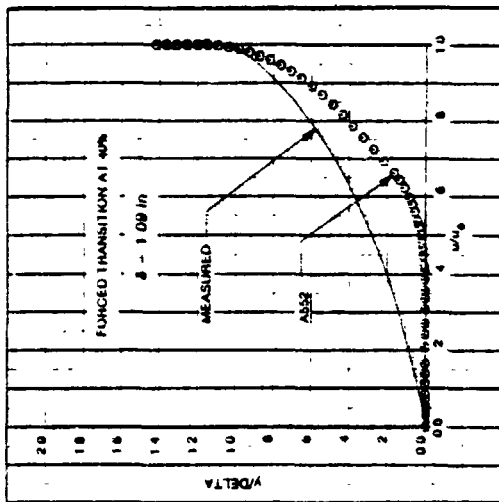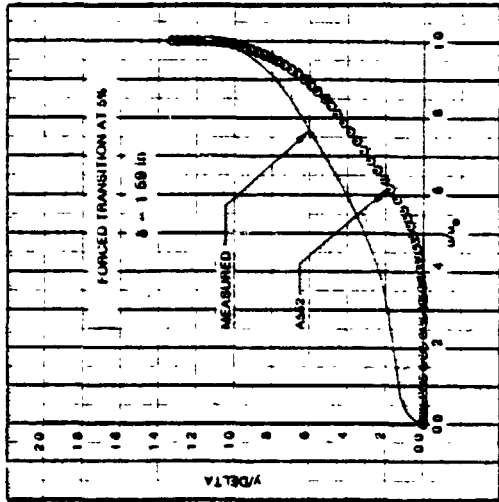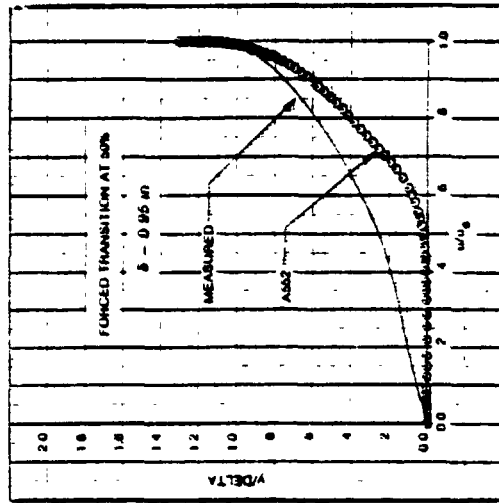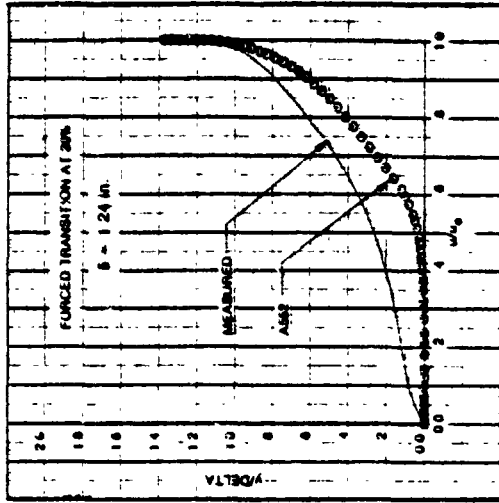
Figure B-31. Measured Velocity Profiles: F-111 NLF Glove, Case 17
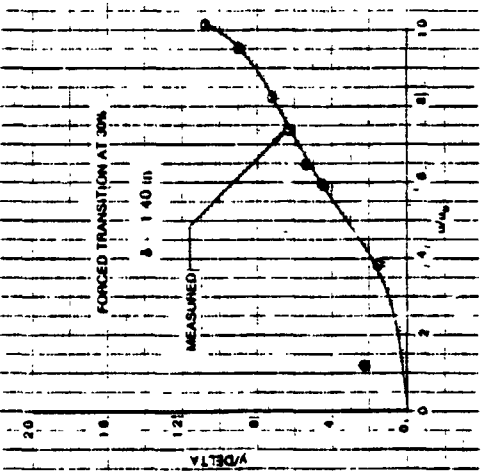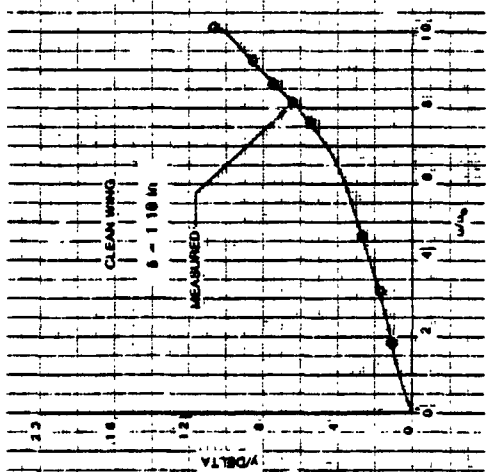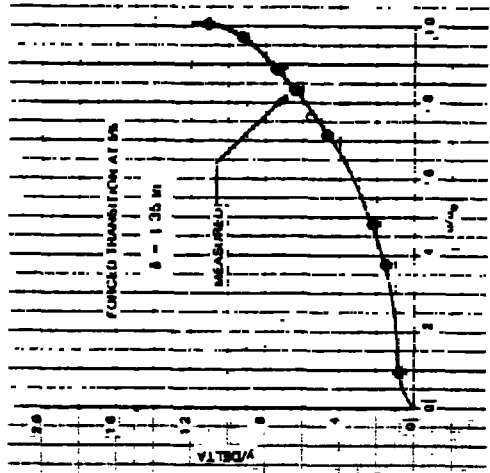
CASE: 18
RAKE AT 90%

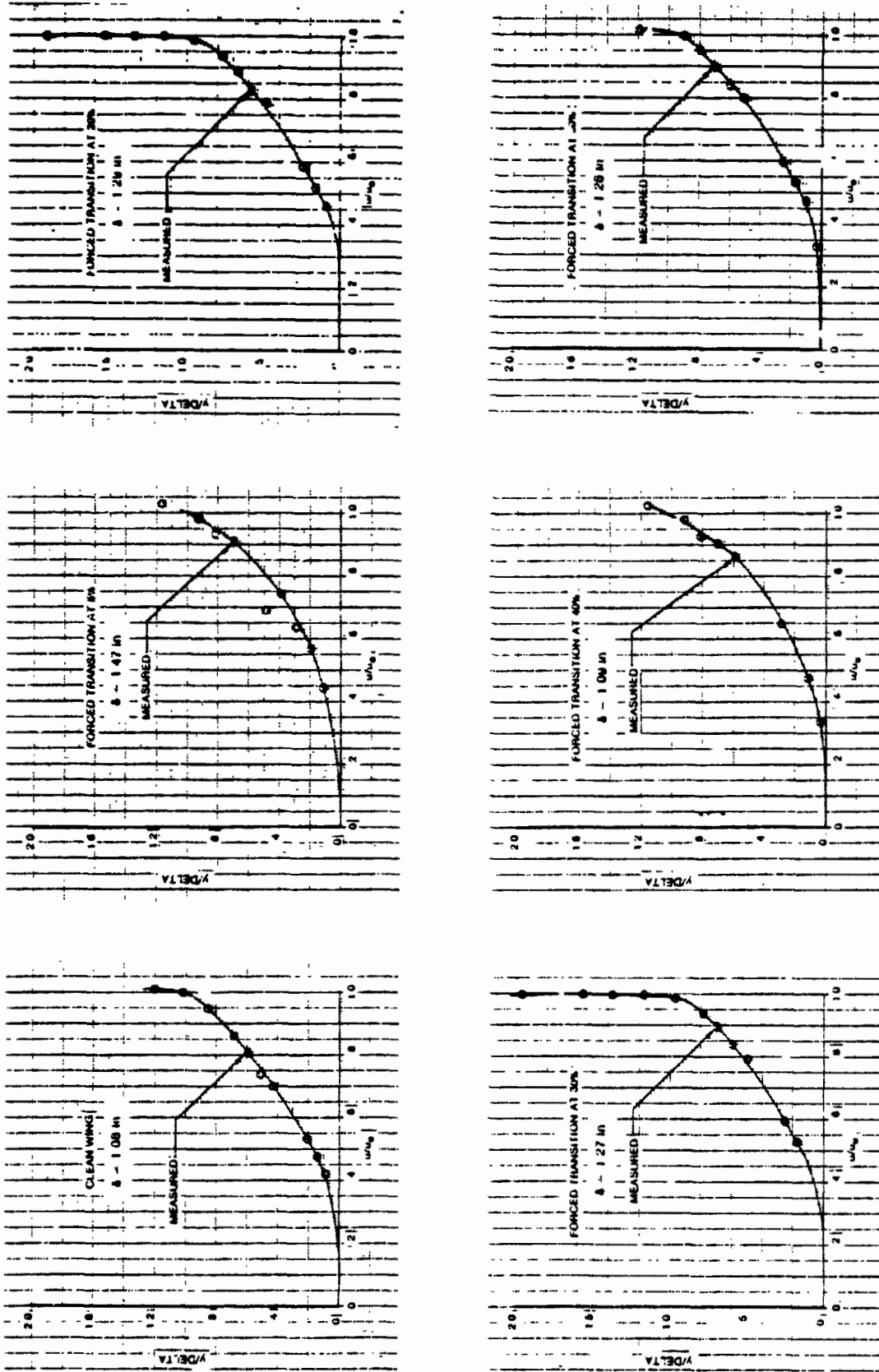Figure B-32. Measured Velocity Profiles: F-111 NLF Glove, Case 18

Figure B-33. Measured Velocity Profiles: F-111 NLF Glove, Case 19

CASE: 20
RAKE AT 90%
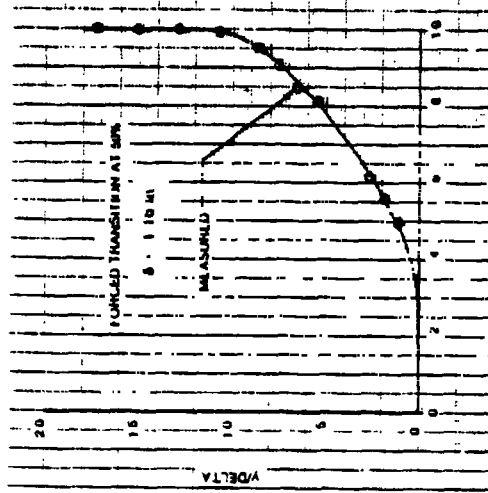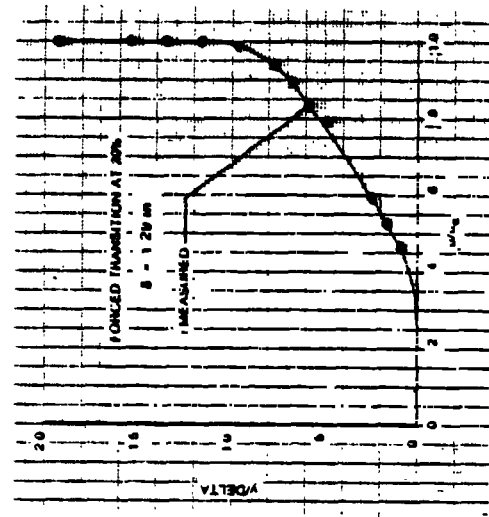
Figure B-34. Measured Velocity Profiles: F-111 NLF Glove, Case 20
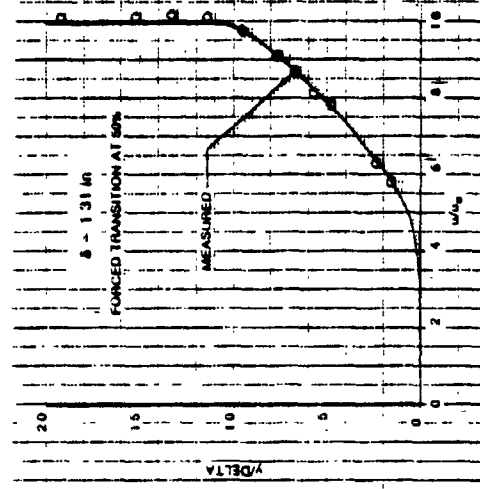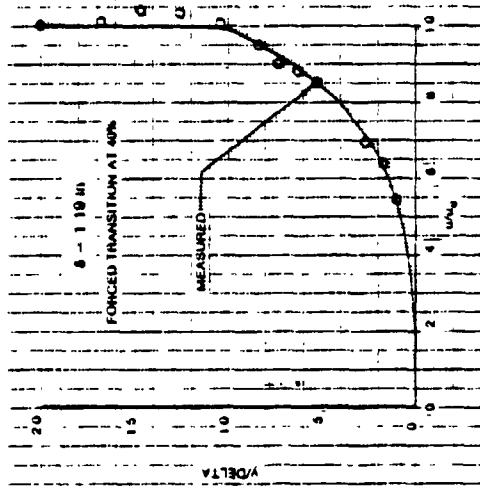
Figure B-35. Measured Velocity Profiles: F-111 NLF Glove, Case 21

CASE: 22
RAKE AT 90%
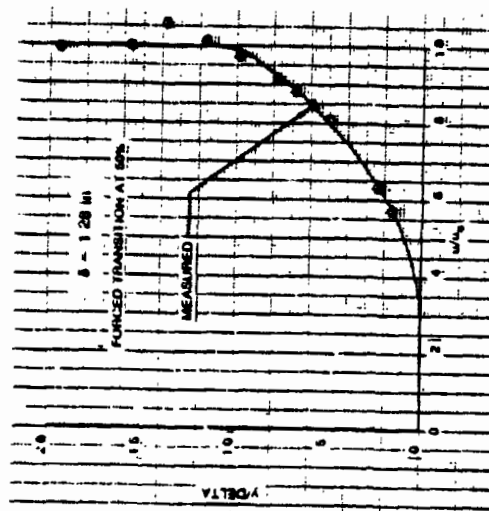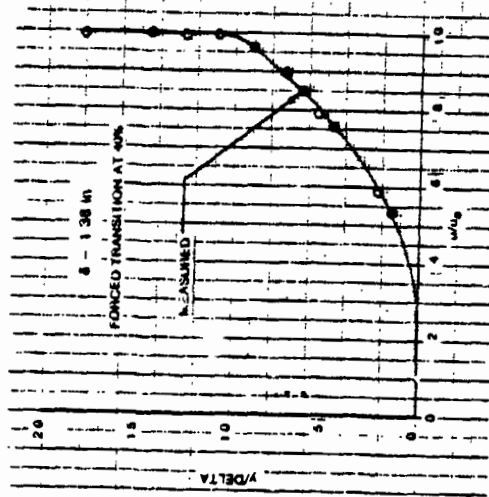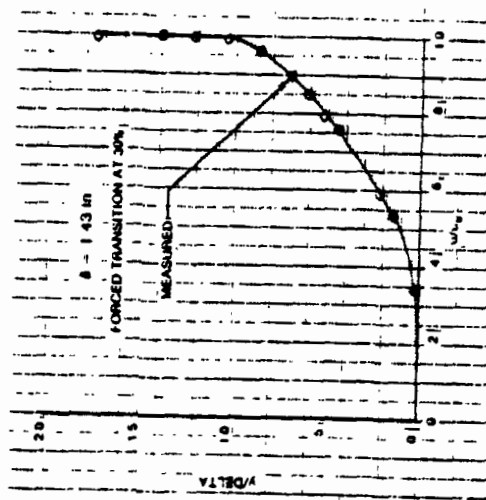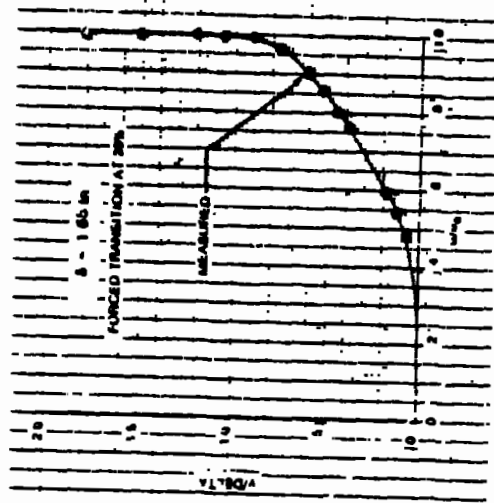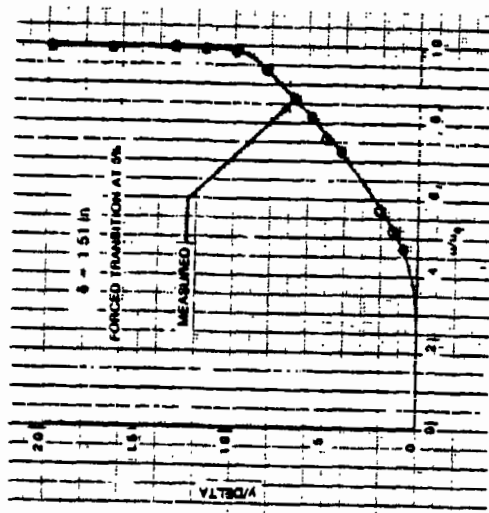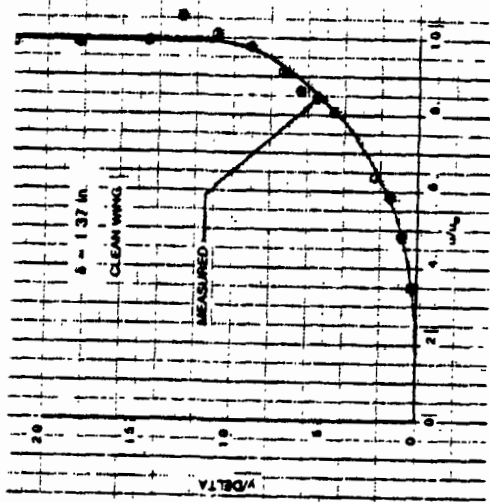
Figure B-36. Measured Velocity Profiles: F-111 NLF Glove, Case 22
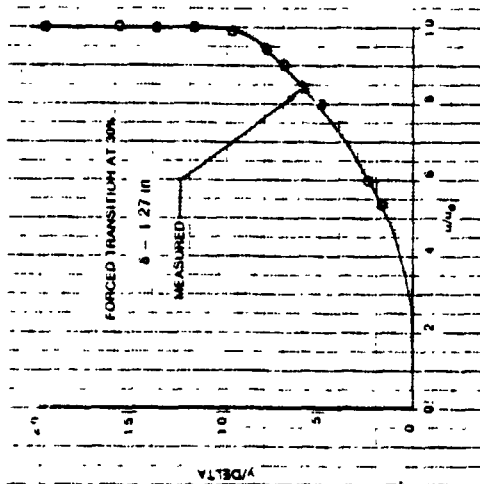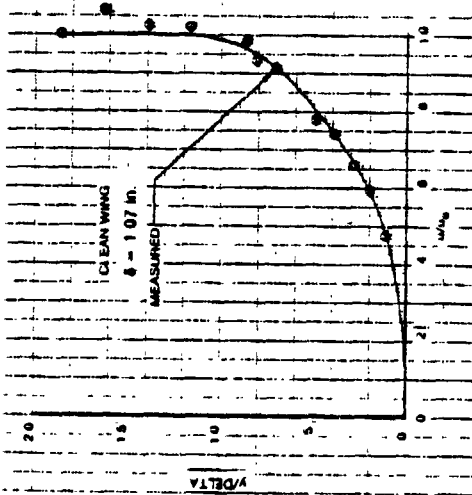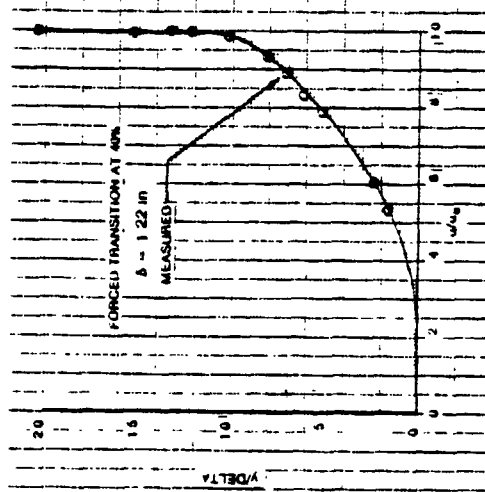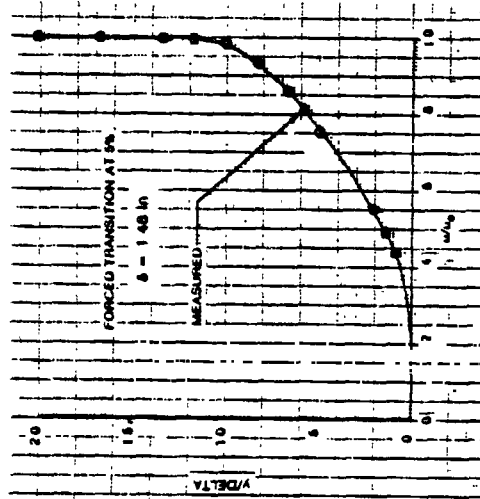
CASE: 23
RAKE AT 90%
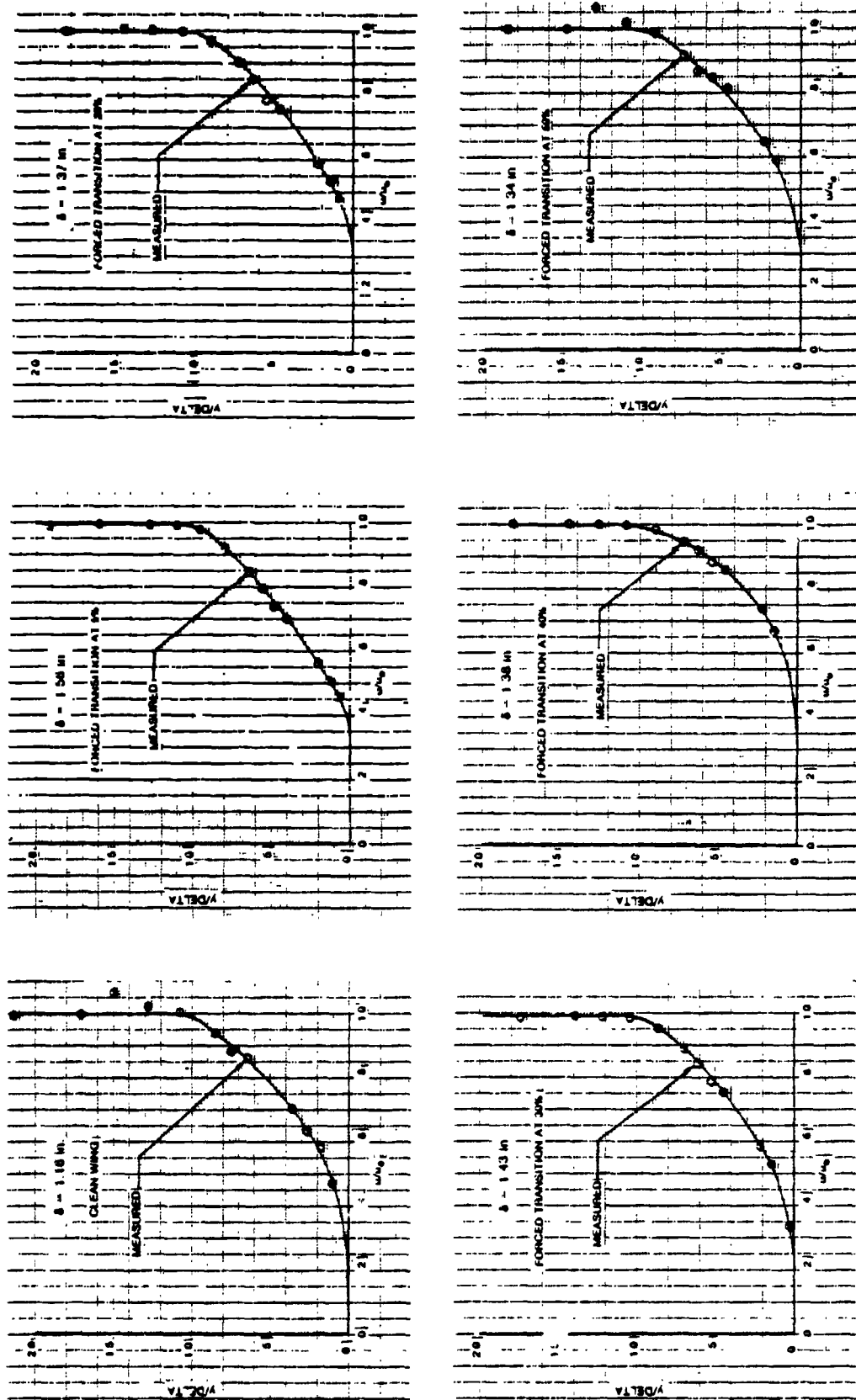
Figure B-37. Measured Velocity Profiles: F-111 NLF Glove, Case 23

CASE: 24
RAKE AT 90%
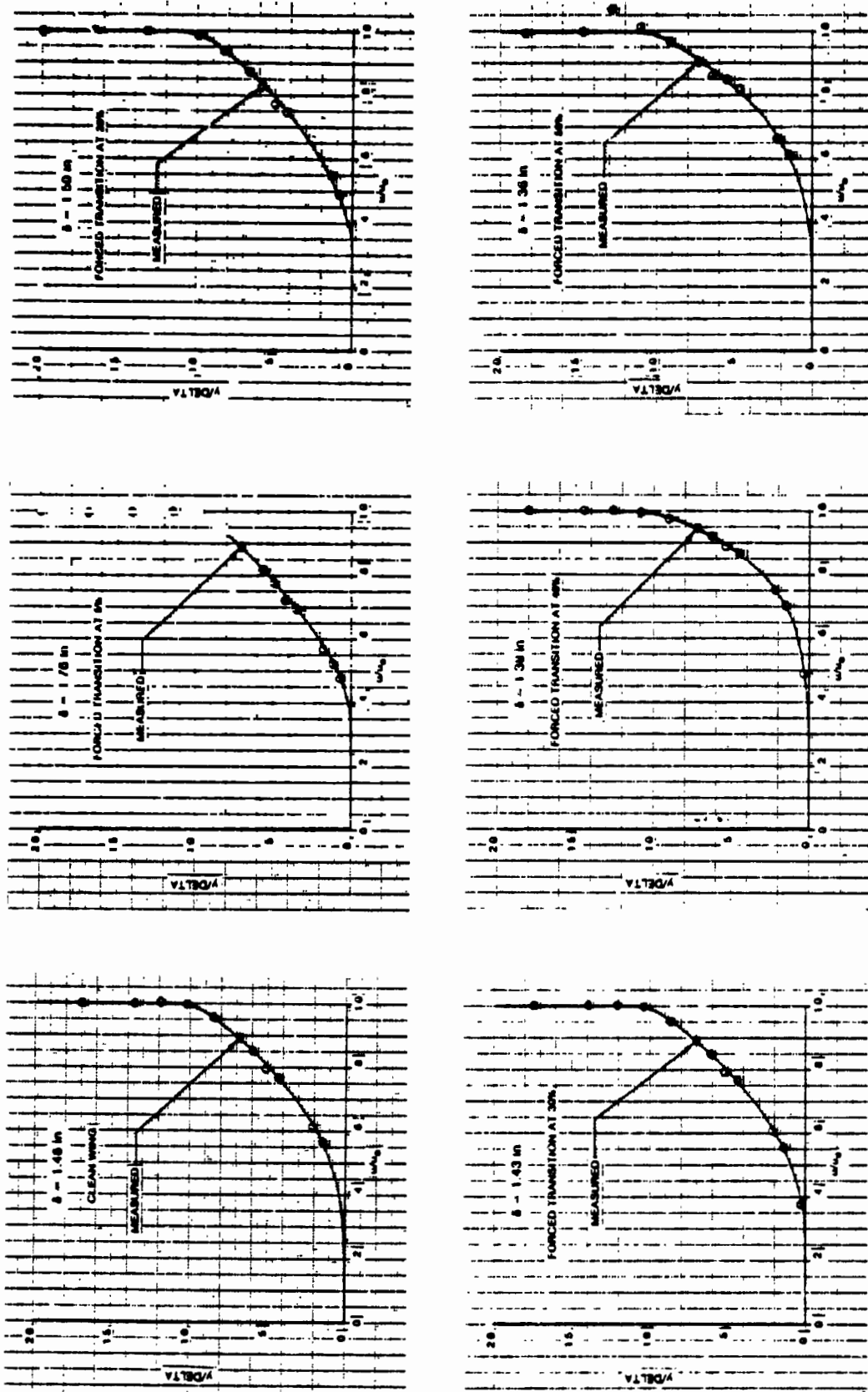
Figure B-38. Measured Velocity Profiles: F-111 NLF Glove, Case 24

CASE: 25
RAKE AT 90%
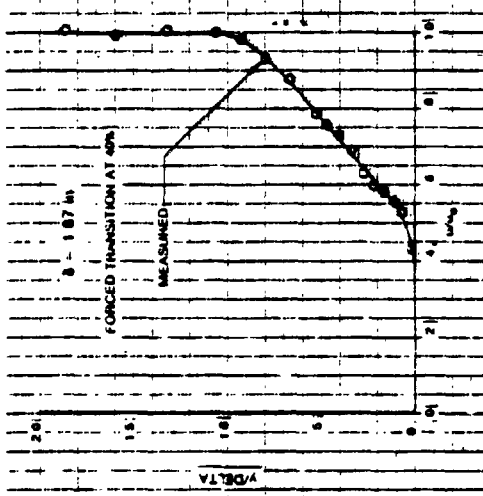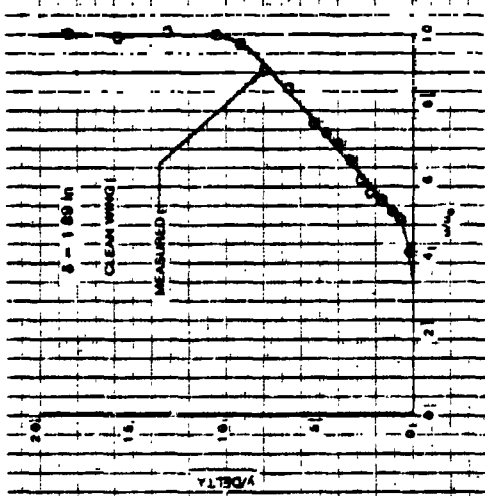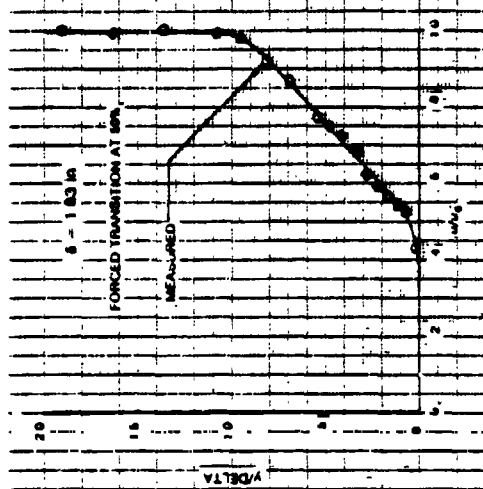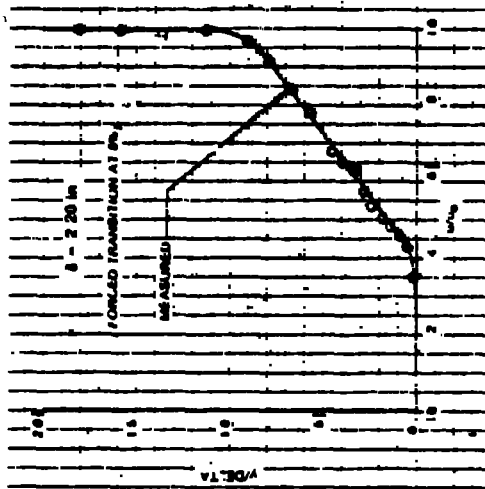
Figure B-39. Measured Velocity Profiles: F-111 NLF Glove, Case 25

CASE: 26
RAKE AT 90%
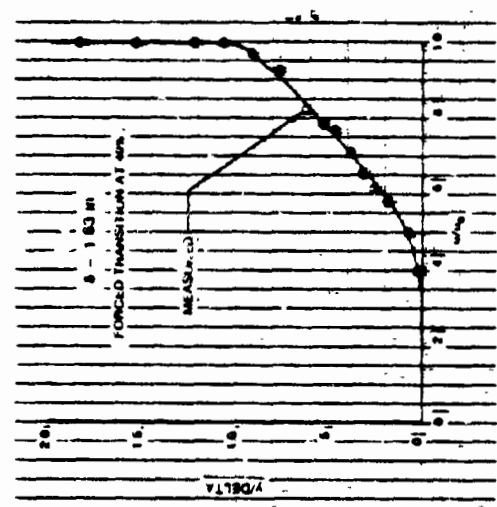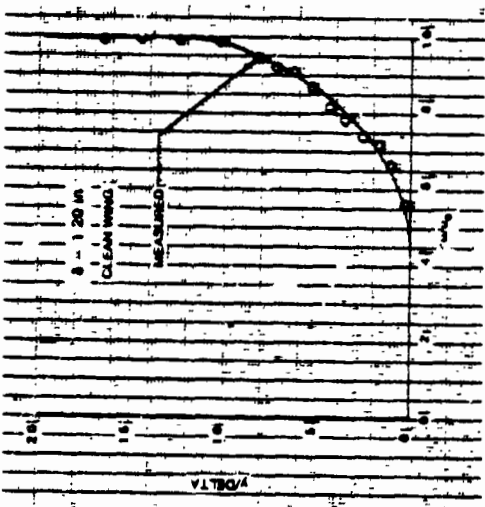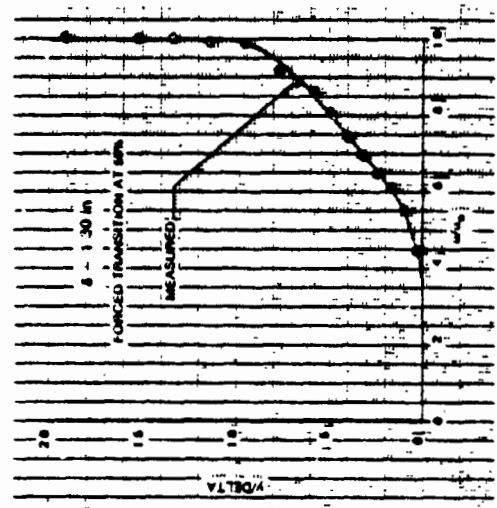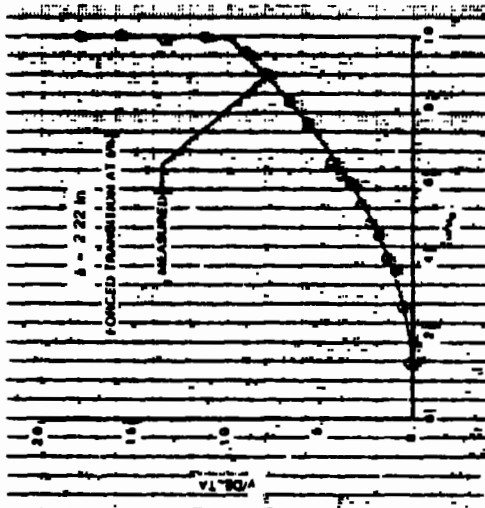
Figure B-40. Measured Velocity Profiles: F-111 NLF Glove, Case 26

CASE: 27
RAKE AT 90%
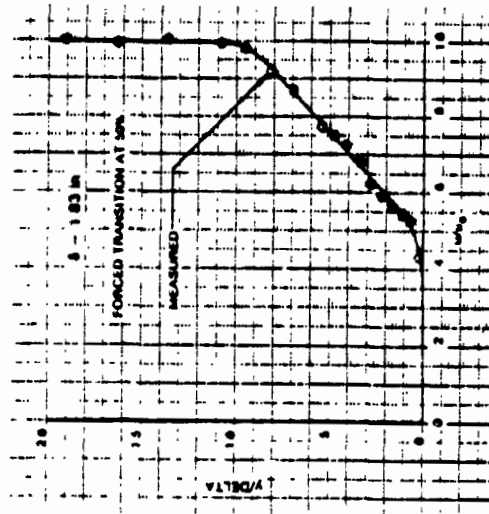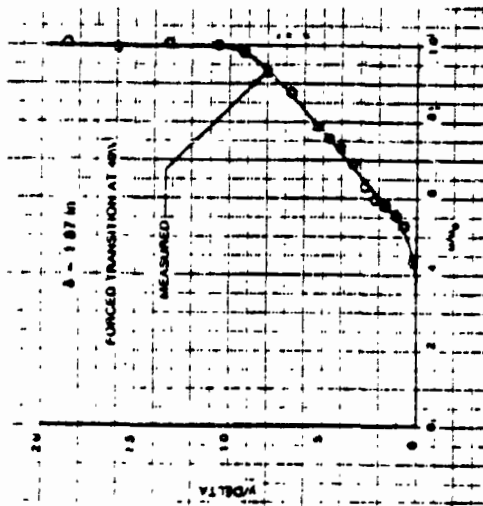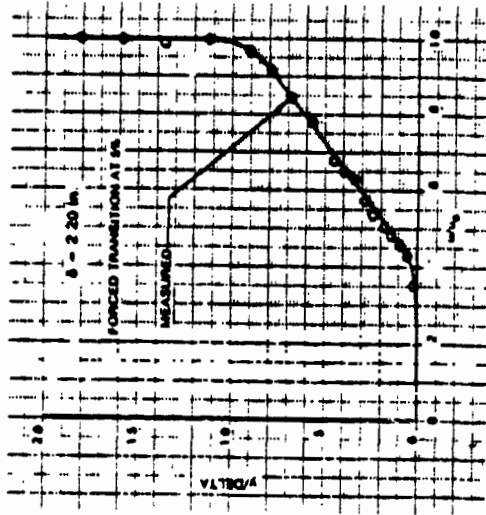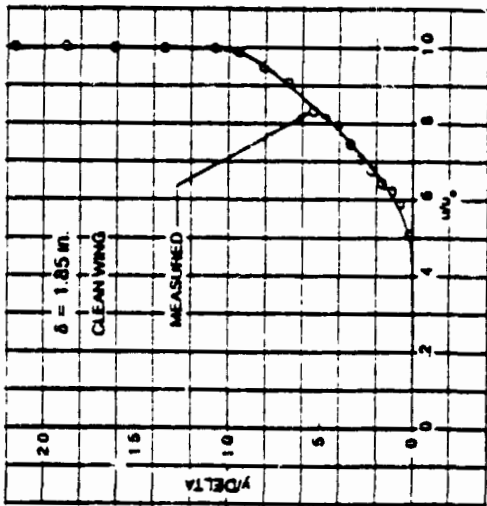
Figure B-41. Measured Velocity Profiles: F-111 NLF Glove, Case 27
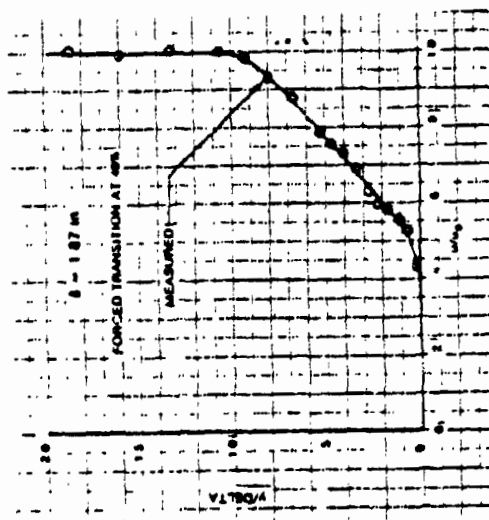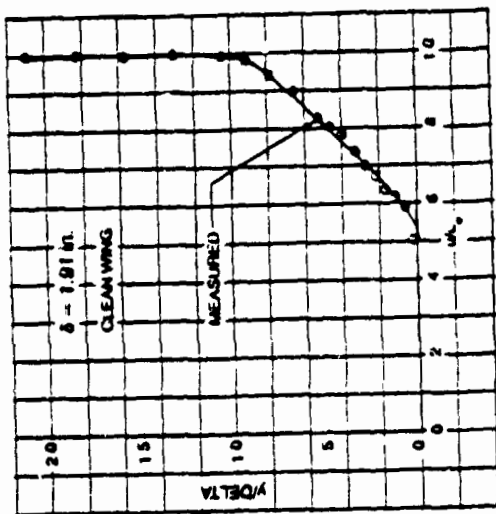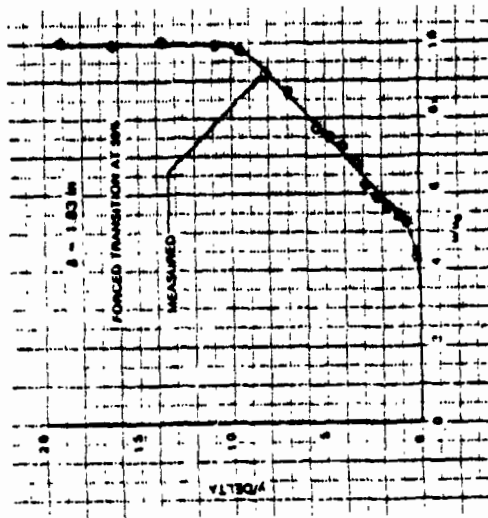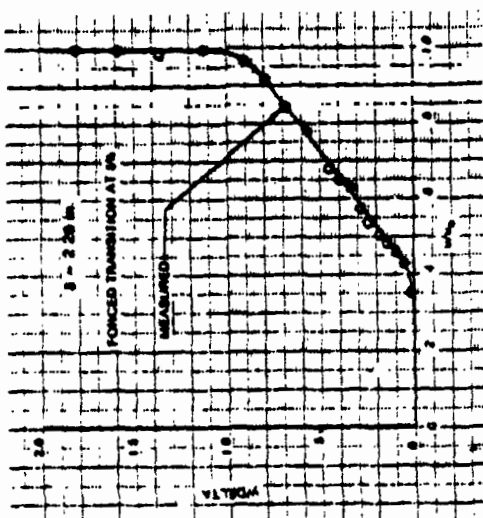
Figure B-42. Measured Velocity Profiles: F-111 NLF Glove, Case 28
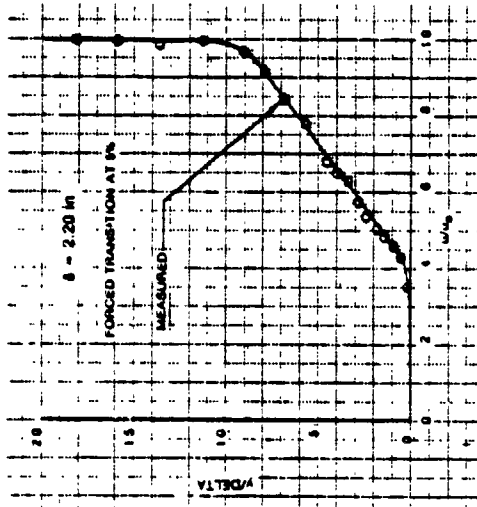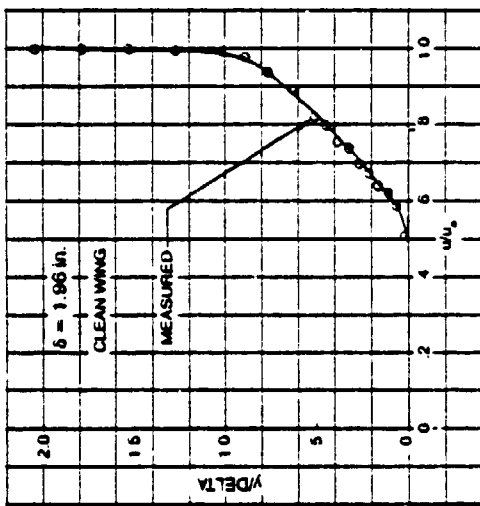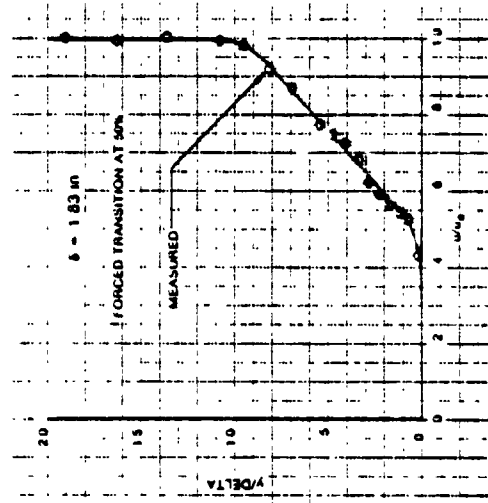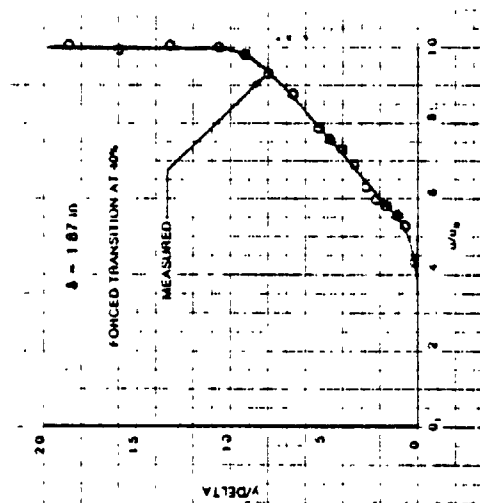
Figure B-43. Measured Velocity Profiles: F-111 NLF Glove, Case 29
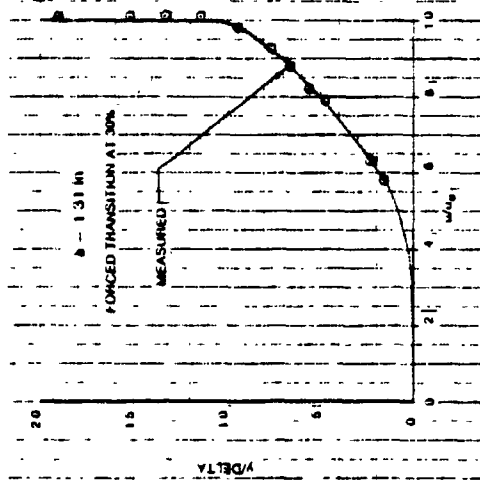
CASE: 30
RAKE AT 90%
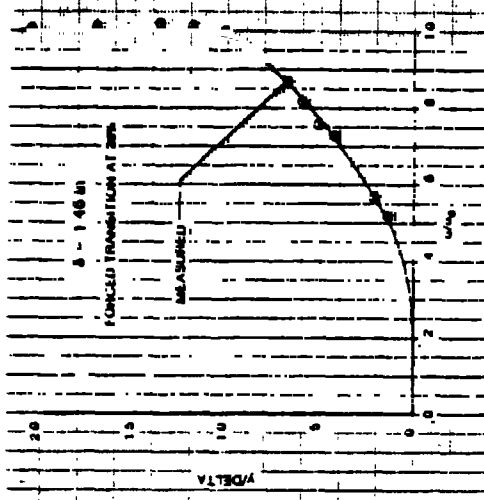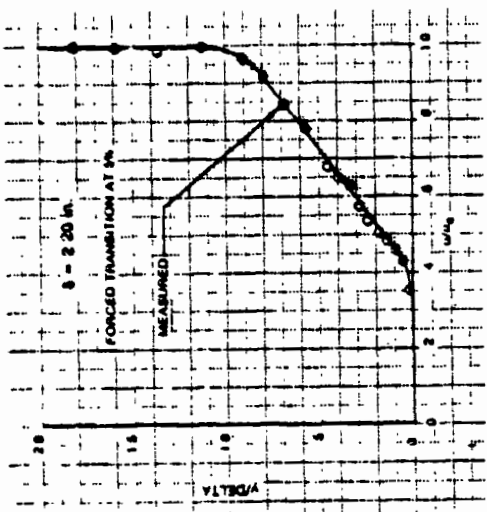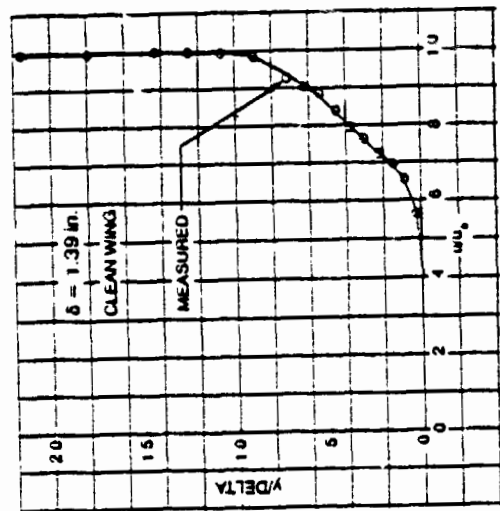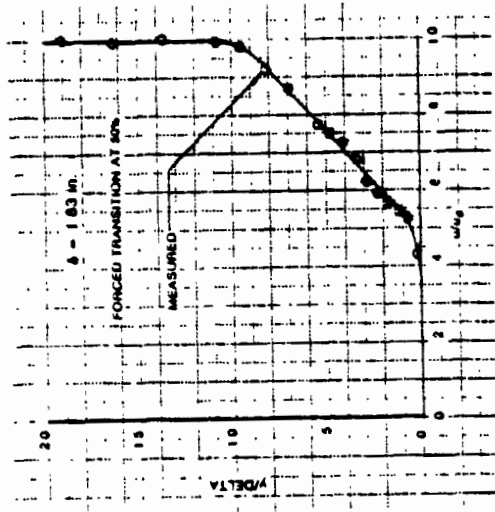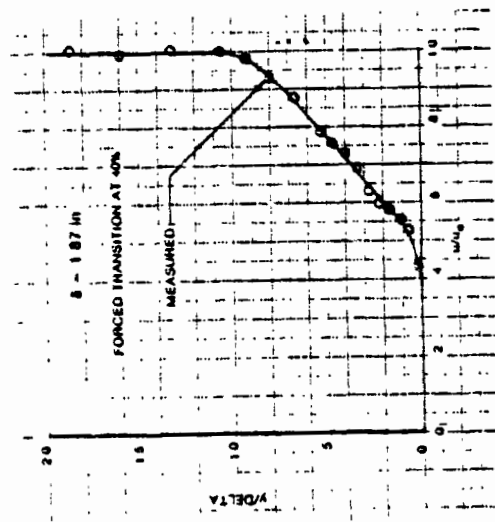
Figure B-44. Measured Velocity Profiles: F-111 NLF Glove, Case 30

CASE: 31
RAKE AT 90%
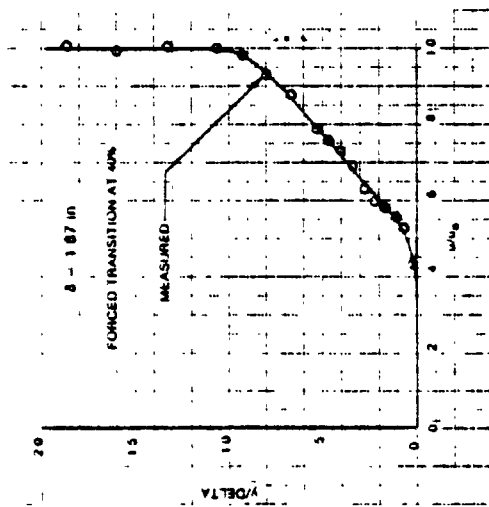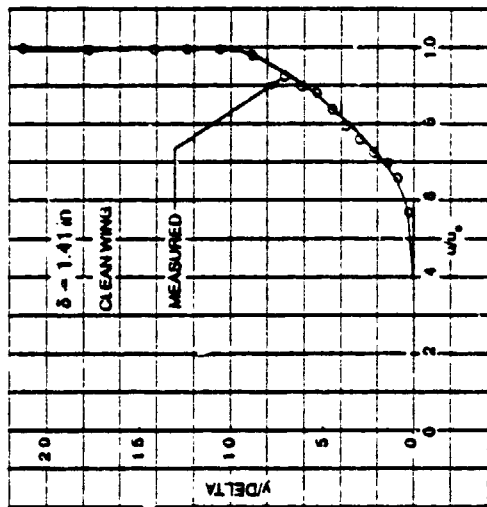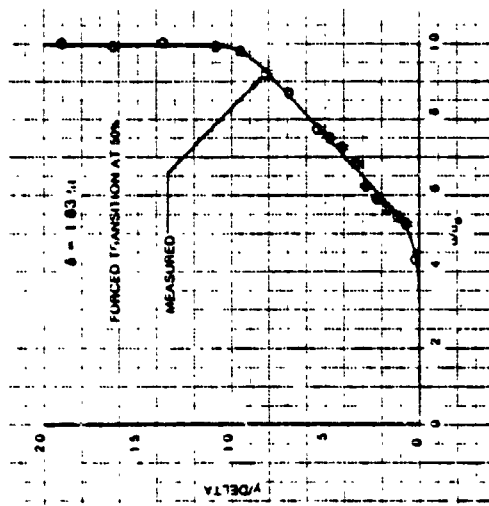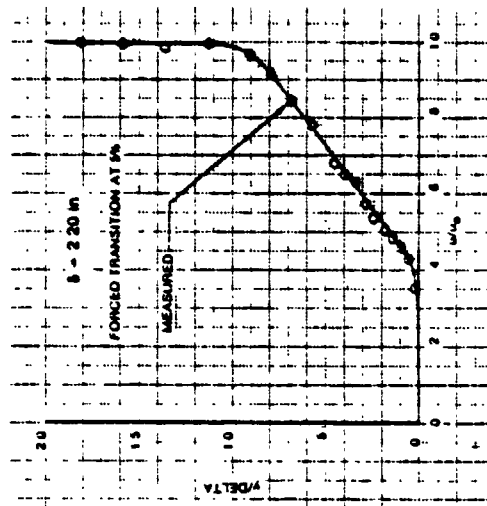
Figure B-45. Measured Velocity Profiles: F-111 NLF Glove, Case 31

CASE: 32
RAKE AT 90%
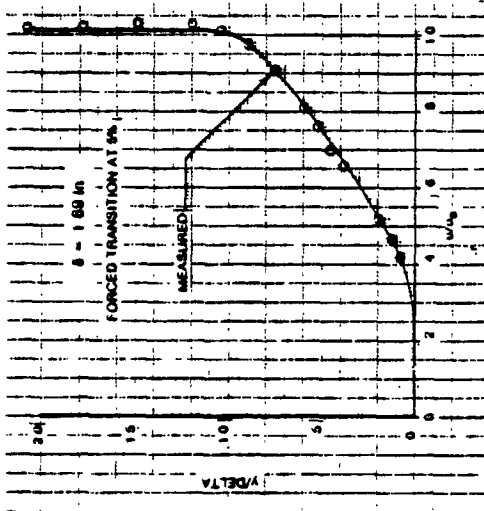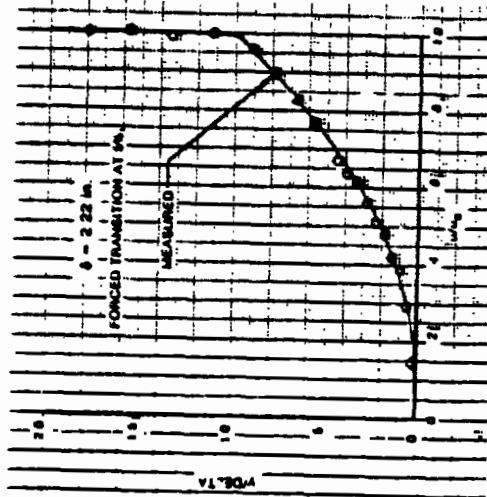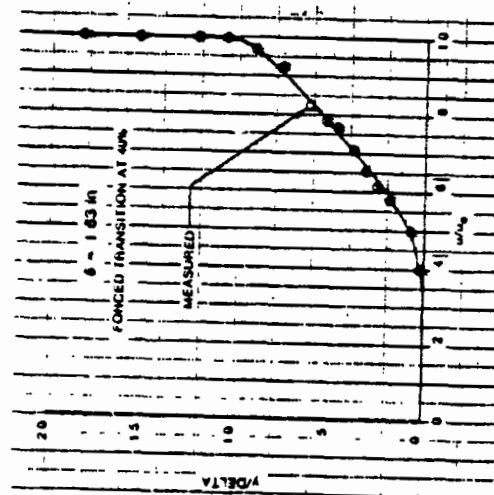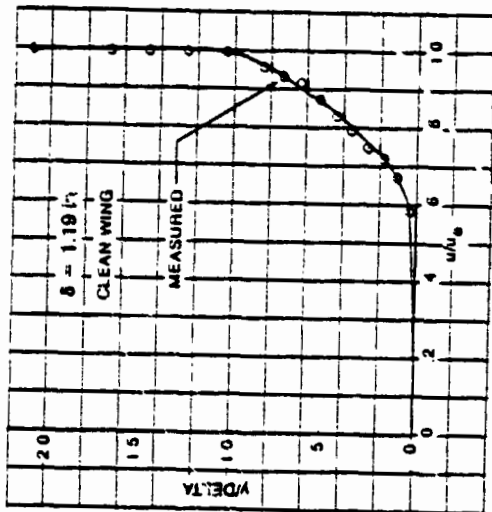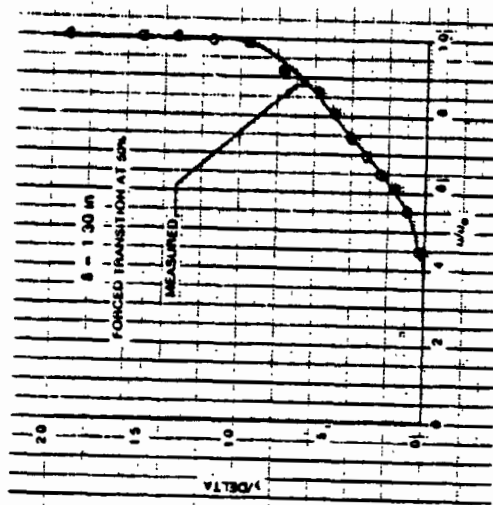

Figure B-46. Measured Velocity Profiles: F-111 NLF Glove, Case 32

CASE: 33
RAKE AT 90%
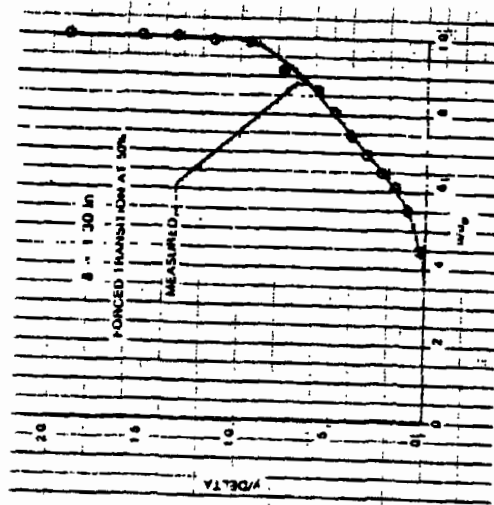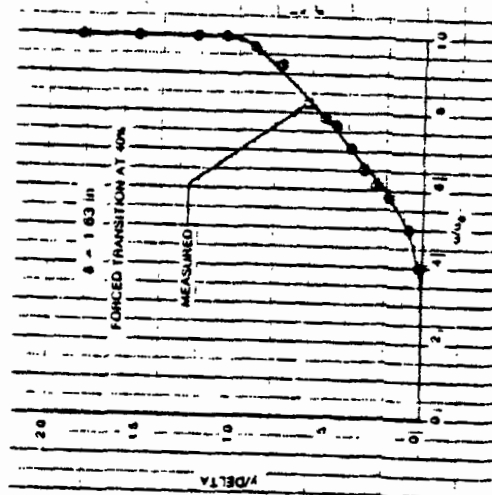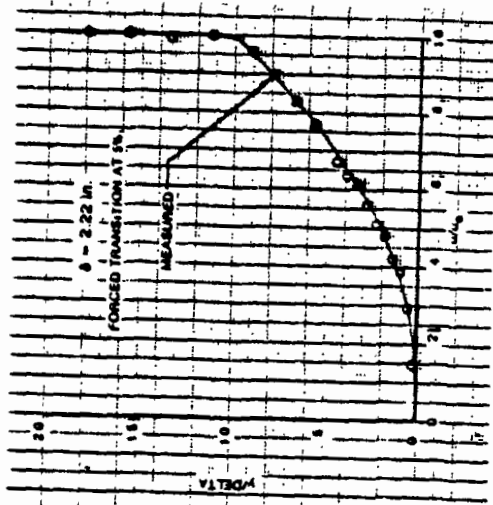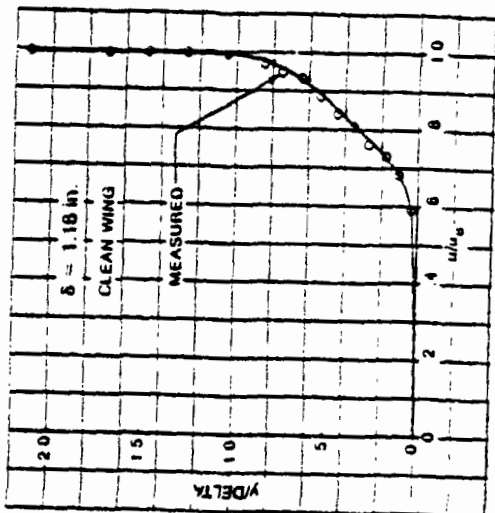
Figure B-47. Measured Velocity Profiles: F-111 NLF Glove, Case 33
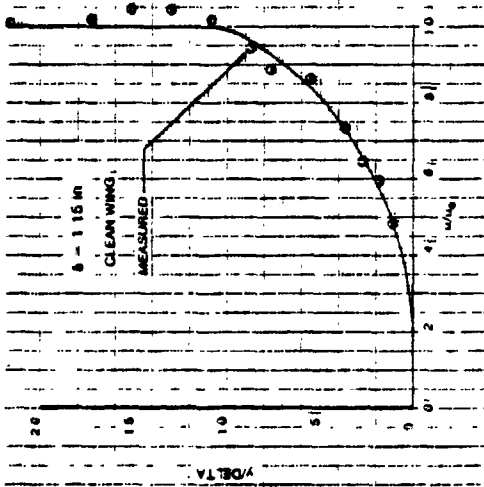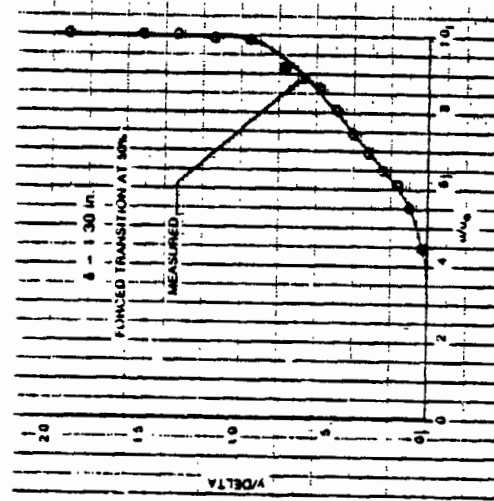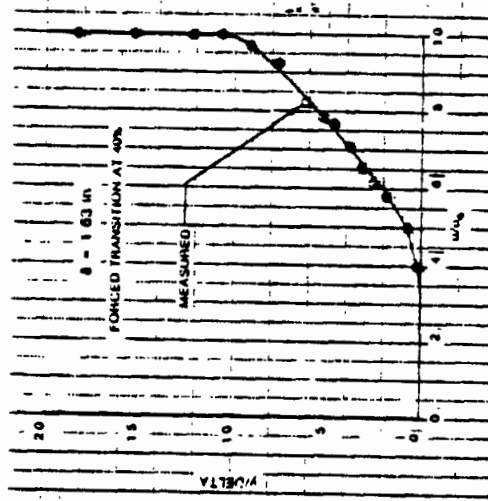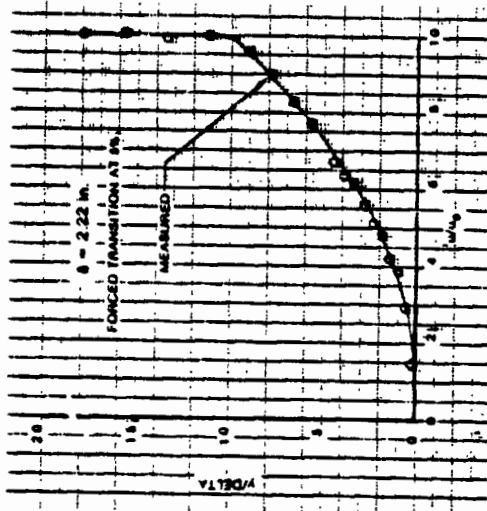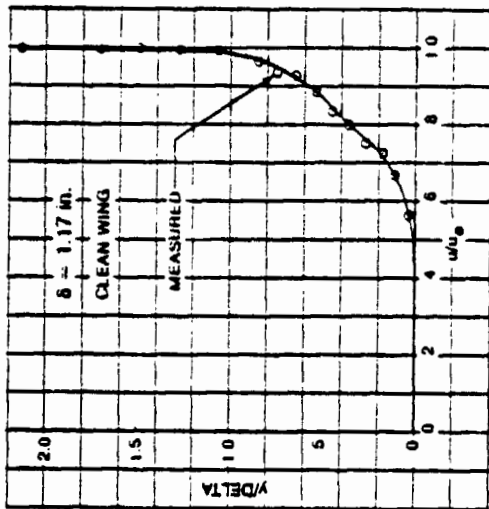
Figure B-48. Measured Velocity Profiles: F-111 NLF Glove, Case 34

| Upper surface				Lower surface	
X/C, U	Y/C, U	X/C, U	Y/C, U	X/C, L	Y/C, L
0.000000	0.000000	.557380	.053030	0.000000	0.000000
.000100	.002410	.575760	.052570	.001200	-.003410
.000800	.004440	.593930	.052030	.002000	-.004380
.002310	.006490	.612020	.051390	.003000	-.005340
.004410	.008530	.647610	.049850	.005000	-.006730
.007190	.010550	.665160	.048930	.008000	-.008340
.010670	.012540	.682560	.047930	.012000	-.010080
.014850	.014520	.716810	.045520	.018000	-.012250
.019730	.016450	.733510	.044120	.024000	-.014130
.025310	.018360	.750060	.042570	.032000	-.016340
.031590	.020250	.782080	.039180	.040000	-.013290
.038550	.022110	.812610	.035260	.050000	-.020470
.046190	.023920	.827250	.033210	.060000	-.022420
.054500	.025700	.855220	.028880	.070000	-.024200
.063470	.027440	.881410	.024360	.080000	-.025840
.073090	.029160	.905560	.019860	.100000	-.028780
.083340	.030840	.927470	.015350	.120000	-.031340
.094190	.032470	.955620	.009210	.140000	-.033670
.105650	.034070	.970040	.005750	.160000	-.035800
.117670	.035620	1.000000	-.002090	.190000	-.038700
.130270	.037120			.220000	-.041230
.143400	.038570			.260000	-.044060
.157060	.039980			.300000	-.046290
.171210	.041340			.350000	-.048230
.185840	.042630			.400000	-.049150
.200910	.043880			.450000	-.048900
216420	.045060			.500000	-.047200
.232320	.046190			.550000	-.043500
.248610	.047240			.600000	-.038010
.265240	.048240			.650000	-.031130
.282210	.049150			700000	-.023720
.299480	.050000			.740000	-.017680
.317030	.050770			.770000	-.013310
.334830	.051470			.800000	-.009350
.352860	.052100			.830000	-.005970
.371090	.052630			.850000	-.004130
.389480	.053060			.870000	-.002770
.408010	.053410			.890000	-.001910
426640	.053670			.910000	-.001660
.445330	.053850			.930000	-.002000
.464660	.053950			.950000	-.002930
.482800	.053950			.970000	-.004530
.501530	.053860			.080000	-.005580
.520230	.053680			.990000	-.006800
.538860	.053410			1.000000	-.008190

Table B-1.   NLAM78 Airfoil Coordinates, F-111 NLF Glove

Case 2	
x/c	Cp
.020	.254
.050	.075
.100	-.061
.200	-.169
.350	-.316
.400	-.342
.500	-.255
.600	-.184
.700	.107
.900	.391
.980	.038

Case 3	
x/c	Cp
.020	.158
.050	-.002
.100	-.117
.200	-.215
.350	-.374
.400	-.402
.500	-.244
.600	-.167
.700	.120
.900	.381
.980	.086

Case 6	
x/c	Cp
.020	.205
.050	.033
.100	-.094
.200	-.191
.350	-.339
.400	-.372
.500	-.252
.600	-.182
.700	.103
.900	.361
.980	.088

Case 8	
x/c	Cp
.020	.199
.050	.032
.100	-.187
.200	-.195
.350	-.344
.400	-.385
.500	-.233
.600	-.178
.700	.097
.900	.342
.980	.096

Table B-2. Measured Cp vs x/c: F-111 NLF Glove, Cases 2, 3, 6, and 8

Case 12		Case 13		Case 15	
x/c	C_p	x/c	C_p	x/c	C_p
.020	-.373	.050	-.474	.020	-.520
.050	-.471	.100	-.559	.050	-.622
.100	-.565	.200	-.547	.100	-.632
.200	-.622	.300	-.594	.200	-.706
.300	-.607	.400	-.692	.300	-.648
.400	-.724	.500	-.467	.400	-.498
.500	-.668	.550	-.436	.500	-.534
.550	-.790	.600	-.293	.550	-.666
.600	-.554	.900	-.136	.600	-.625
.900	-.156	.980	.094	.900	-.120
.980	.074			.980	.099

Case 16		Case 17	
x/c	C_p	x/c	C_p
.020	-.245	.020	-.312
.050	-.356	.050	-.418
.100	-.449	.100	-.523
.200	-.488	.200	-.553
.300	-.557	.300	-.555
.400	-.657	.400	-.686
.500	-.588	.500	-.629
.550	-.633	.550	-.671
.600	-.682	.600	-.733
.650	-.742	.650	-.770
.700	-.766	.700	-.805
.900	-.232	.900	-.225
.980	.201	.980	.086

Table B-3. Measured Cp vs x/c: F-111 NLF Glove, Cases 12, 13, 15, 16, and 17

Case 18			Case 19	
x/c	C_p		x/c	C_p
.020	-.428		.020	-.357
.050	-.510		.050	-.441
.100	-.600		.070	-.415
.200	-.667		.100	-.540
.300	-.767		.200	-.526
.400	-.659		.300	-.590
500	-.721		.400	-.671
.550	-.681		.500	-.712
.600	-.736		.550	-.755
.650	-.780		.600	-.545
.700	-.853		.650	-.402
.900	-.210		.700	-.447
.980	.026		.900	-.182
			.980	.202

Case 20			Case 21	
x/c	C_p		x/c	C_p
.020	-.450		.020	-.579
.050	-.510		.050	-.690
.070	-.467		.100	-.665
.100	-.599		.200	-.751
.200	-.671		.300	-.793
.300	-.617		.400	-.784
.400	-.719		.500	-.845
.500	-.738		.550	-.912
.550	-.789		.600	-.940
.600	-.761		.660	-.934
.650	-.565		.700	-.673
.700	-.345		.900	-.159
900	-.191		.980	.207
.980	.202			

Table B-4.   Measured Cp vs x/c: F-111 NLF Glove, Cases 18, 19, 20, and 21

Case 22			Case 24	
x/c	C_p		x/c	C_p
.020	-.300		.020	-.603
.050	-.382		.050	-.705
.100	-.403		.100	-.688
.200	-.450		.200	-.768
.300	-.488		.300	-.695
.400	-.563		.400	-.736
.500	-.560		.500	-.586
.550	-.610		.550	-.604
.600	-.538		.600	-.667
.650	-.303		.660	-.266
.700	-.340		.700	-.299
.900	-.087		.900	-.077
.900	.071		.980	.109
.980				

Case 25			Case 26	
x/c	C_p		x/c	C_p
.020	.185		.020	.125
.050	-.002		.050	-.061
.100	-.127		.100	-.155
.200	-.218		.200	-.253
.350	-.365		.300	-.404
.400	-.395		.400	-.429
.500	-.436		.500	-.522
.600	-.199		.600	-.193
.700	.121		.700	.122
.900	.376		.900	.430
.980	.080		.980	.097

Table B-5. Measured Cp vs x/c: F-111 NLF Glove, Cases 22, 24, 25, and 26

Case 27			Case 28	
x/c	C_p		x/c	C_p
.020	.208		.020	.172
.050	.004		.050	-.026
.100	-.109		.100	-.139
.200	-.210		.200	-.237
.350	-.326		.350	-.364
.400	-.374		.400	-.406
.500	-.442		.500	-.477
.600	-.211		.600	-.208
.700	.112		.700	.116
.900	.364		.900	.373
.980	.065		.980	.069

Case 29			Case 30	
x/c	C_p		x/c	C_p
.020	.175		.020	.059
.050	-.020		.050	-.111
.100	-.137		.100	-.213
.200	-.233		.200	-.288
.350	-.395		.350	-.427
.400	-.425		.400	-.428
.500	-.531		.500	-.493
.600	-.203		.600	-.201
.700	.121		.700	.125
.900	.381		.900	.381
.980	.079		.980	.078

Table B-6. Measured Cp vs x/c: F-111 NLF Glove, Cases 22, 24, 25, and 26

Case 31	
x/c	C_p
.020	.044
.050	-.123
.100	-.228
.200	-.303
.350	-.449
.400	-.467
.500	-.563
.600	-.197
.700	.125
.900	.389
.980	.085

Case 32	
x/c	C_p
.020	.186
.050	-.005
.100	-.120
.200	-.221
.350	-.386
.400	-.408
.500	-.521
.600	-.175
.700	.139
.900	.442
.980	.109

Case 33	
x/c	C_p
.020	.041
.050	-.120
.100	-.218
.200	-.297
.350	-.438
.400	-.457
.500	-.573
.600	-.184
.700	.133
.900	.435
.980	.107

Case 34	
x/c	C_p
.020	.225
.050	.018
.100	-.092
.200	-.207
.350	-.354
.400	-.384
.500	-.478
.600	-.194
.700	.124
.900	.427
.980	.097

Table B-7. Measured Cp vs x/c: F-111 NLF Glove, Cases 22, 24, 25, and 26

APPENDIX C

DETAILS OF FLIGHT TEST DATA ANALYSIS

Page

APPENDIX C: DETAILS OF FLIGHT TEST DATA ANALYSIS

This appendix contains a case-by-case analysis of the 34 selected cases of F-111 flight test data, using the method described in Appendix A, to determine the extent of laminar flow achieved.

Case 1:

This case was for the lower surface with the rake at 50% chord. The sweep angle was 9.0 deg, and the airplane lift coefficient (C_L) was 0.416. Figure C-1 shows the plot of displacement thickness Reynolds number at the rake location (RDTH) versus transition location for this case. The circular symbols are based on results of Boeing's boundary layer program, A552, for a clean wing (natural transition) pressure distribution (flight 161, run 15). The square symbol corresponds to the inferred displacement thickness Reynolds number for flight 162, run 15, in which transition was forced at 5% chord. The pressure distribution for that flight is shown in Appendix B. The triangular symbol corresponds to the inferred displacement thickness Reynolds number for the clean wing flight and indicates that transition was at 20% chord.

Case 2:

This case was for the lower surface with the rake at 50% chord. The sweep angle was 9.0 deg, and C_L was 0.501. Figure C-2 shows the plot of displacement thickness Reynolds number at the rake location versus transition location. Transition was at 20% chord.

Case 3:

This case was for the lower surface with the rake at 50% chord. The sweep angle was 16.0 deg, and C_L was 0.387. Figure C-3 shows the plot of displacement thickness Reynolds number at the rake location versus the transition location. The forced transition flight was at a chord Reynolds number of about 23 million compared with a chord Reynolds number of about 23 million for the clean wing. However, A552 was used to adjust (see app. A) the measured displacement thickness Reynolds number for the forced transition flight to correspond to a chord Reynolds number of 23 million. Transition was at 14% chord.

CLEAN WING
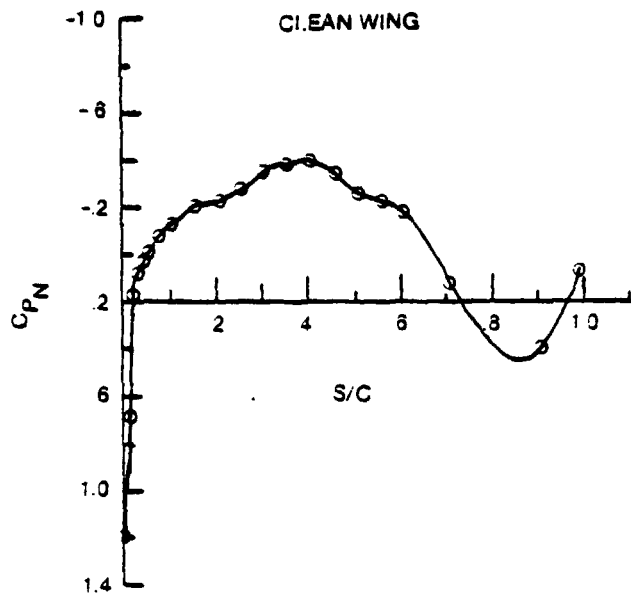
CASE 1
FLIGHT 161 RUN 15
LOWER SURFACE
$\Lambda = 9°$ M = 82. C_L = 416
RAKE AT 50%
TRANSITION AT 20%

O A552
△ MEASURED DATA FOR CLEAN WING
□ MEASURED DATA FOR FORCED TRANSITION

$Re_c \approx 23 \times 10^6$ FOR OPEN SYMBOLS
$Re_c \approx 28 \times 10^6$ FOR SOLID SYMBOLS

Figure C-1.   Transition Determination, Case 1 F-111 NLF Glove

- CASE 2
- FLIGHT 161, RUN 2
- LOWER SURFACE
- $\Lambda = 9°$, M = 81, C_L = 501
- RAKE AT 50%
- TRANSITION AT 20%

○ A552
△ MEASURED DATA FOR CLEAN WING
□ MEASURED DATA FOR FORCED TRANSITION

$Re_c = 23 \times 10^6$ FOR OPEN SYMBOLS
$Re_c = 28 \times 10^6$ FOR SOLID SYMBOLS
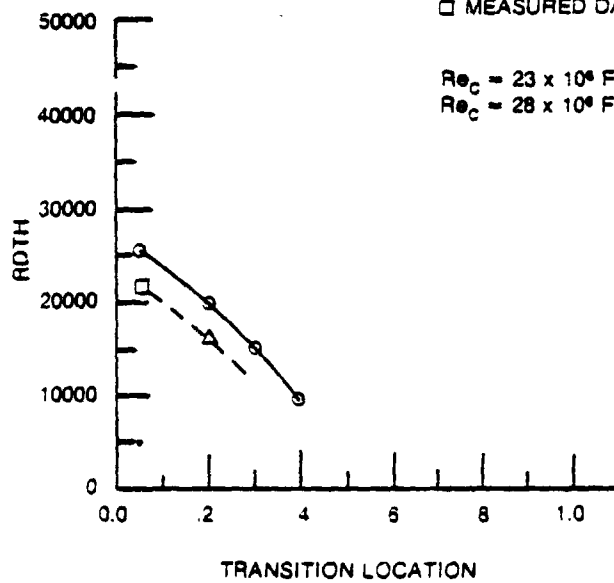
Figure C-2. Transition Determination, Case 2 F-111 NLF Glove
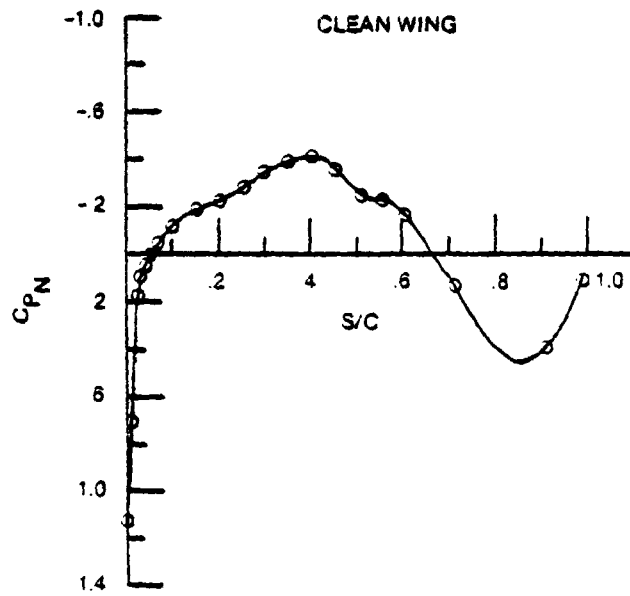
- CASE 3
- FLIGHT 161. RUN 20
- LOWER SURFACE
- $\Lambda = 16°$, M = 83, $C_L = 387$
- RAKE AT 50%
- TRANSITION AT 14%

○ A552
△ MEASURED DATA FOR CLEAN WING
□ MEASURED DATA FOR FORCED TRANSITION

$Re_c = 23 \times 10^6$ FOR OPEN SYMBOLS
$Re_c = 28 \times 10^6$ FOR SOLID SYMBOLS
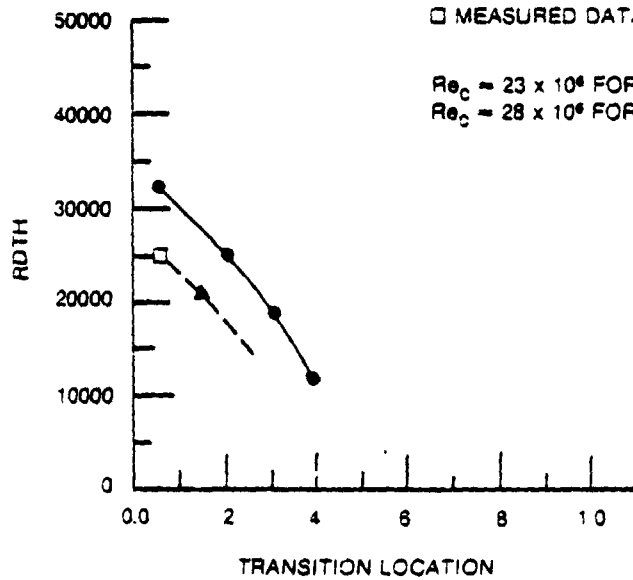
Figure C-3.   Transition Determination, Case 3 F-111 NLF Glove

Case 4:

This case was for the lower surface with the rake at 50% chord. The sweep angle was 15.9 deg, and C_L was 0.397. Displacement thickness Reynolds number at the rake location versus the transition location is plotted in Figure C-4. Transition was at 12% chord.

Case 5:

This case was for the lower surface with the rake at 50% chord. The sweep angle was 18.8 deg, and C_L was 0.377. Displacement thickness Reynolds number at the rake location versus the transition location is plotted in Figure C-5. Transition was at 8% chord.

Case 6:

This case was for the lower surface with the rake at 50% chord. The sweep angle was 19.0 deg, and C_L was 0.394. Displacement thickness Reynolds number at the rake location versus the transition location is plotted in Figure C-6. Transition was at 13% chord.

Case 7:

This case was for the lower surface with the rake at 50% chord. The sweep angle was 22.0 deg, and C_L was 0.285. Displacement thickness at the rake location versus the transition location is plotted in Figure C-7. Transition was at 0% chord.

The combination of high chord Reynolds number (29.0 million) and low C_L (which resulted in steeper pressure gradients in the forward region) probably caused very large crossflow disturbance growth rates. However, it is not likely that crossflow disturbances could have caused transition at 0% chord. It probably occurred at 1% to 2% chord rather than at 0%. Also, as discussed in Section 4.2, it is possible that insect contamination or engine noise contributed to the early transition.

CLEAN WING
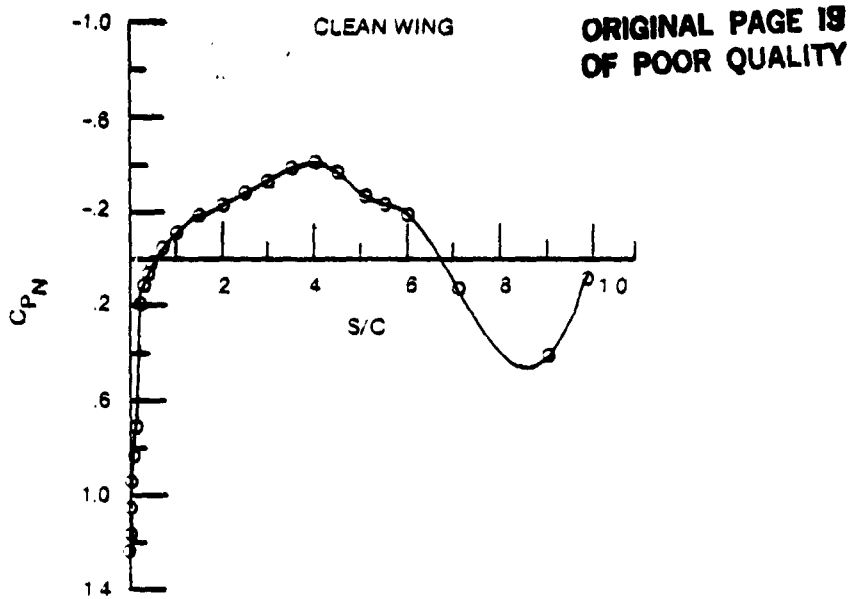
- CASE 4
- FLIGHT 161 RUN 7
- LOWER SURFACE
- Λ = 16°, M = .83, C_L = .397
- RAKE AT 50%
- TRANSITION AT 12%

○ AS52
△ MEASURED DATA FOR CLEAN WING
☐ MEASURED DATA FOR FORCED TRANSITION

Re_C ≈ 23 × 10⁶ FOR OPEN SYMBOLS
Re_C ≈ 28 × 10⁶ FOR SOLID SYMBOLS

TRANSITION LOCATION
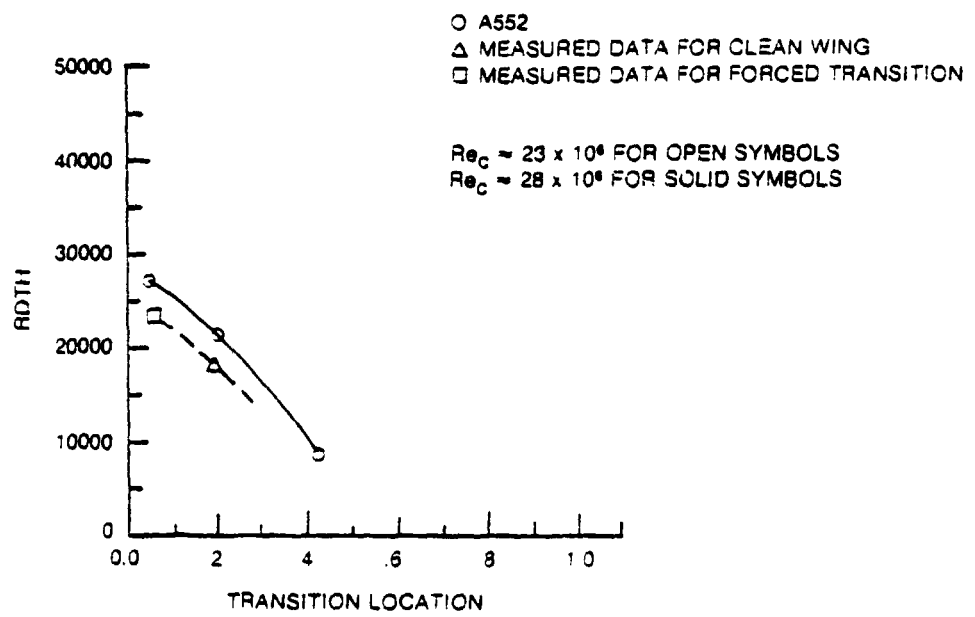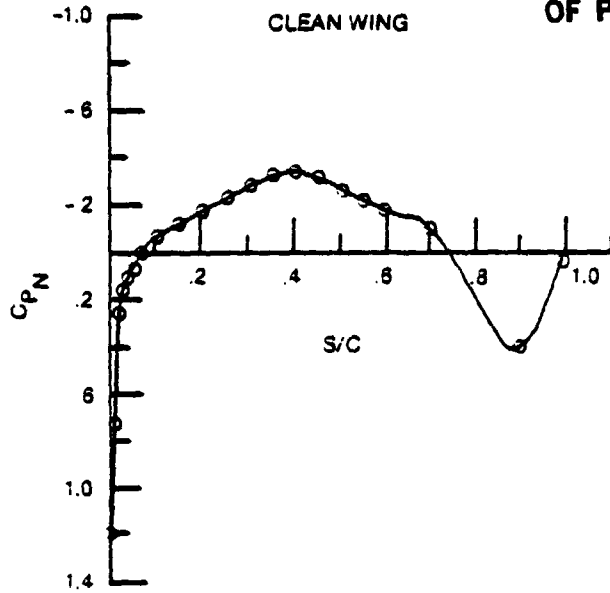
Figure C-4.   Transition Determination, Case 4 F-111 NLF Glove

CLEAN WING

- CASE 5
- FLIGHT 161, RUN 25
- LOWER SURFACE
- $\Lambda = 19°$, M = 83, C_L = 377
- RAKE AT 50%
- TRANSITION AT 3%

○ A552
△ MEASURED DATA FOR CLEAN WING
□ MEASURED DATA FOR FORCED TRANSITION

Re_C ~ 23 x 10⁶ FOR OPEN SYMBOLS
Re_C ~ 28 x 10⁶ FOR SOLID SYMBOLS
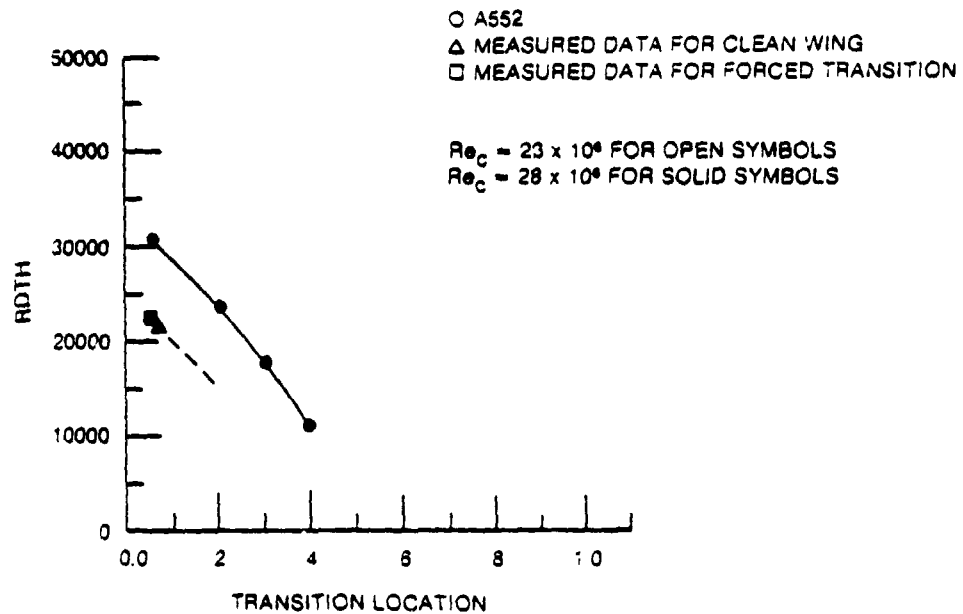
Figure C-5.   Transition Determination, Case 5 F-111 NLF Glove

- CASE 6
- FLIGHT 161, RUN 11
- LOWER SURFACE
- Λ = 19° M = 83, C_L = 394
- RAKE AT 50%
- TRANSITION AT 13%

○ A552
△ MEASURED DATA FOR CLEAN WING
□ MEASURED DATA FOR FORCED TRANSITION

Re_c = 23 x 10⁶ FOR OPEN SYMBOLS
Re_c = 28 x 10⁶ FOR SOLID SYMBOLS

Figure C-6.   Transition Determination, Case 6 F-111 NLF Glove

CLEAN WING

C_{P_N}

S/C

- CASE 7
- FLIGHT 161, RUN 281
- LOWER SURFACE
- $\Lambda = 22°$, M = 85, $C_L = 285$
- RAKE AT 50%
- TRANSITION AT 0%

○ A552
△ MEASURED DATA FOR CLEAN WING
□ MEASURED DATA FOR FORCED TRANSITION

$Re_c = 23 \times 10^6$ FOR OPEN SYMBOLS
$Re_c = 28 \times 10^6$ FOR SOLID SYMBOLS

RDTH

TRANSITION LOCATION
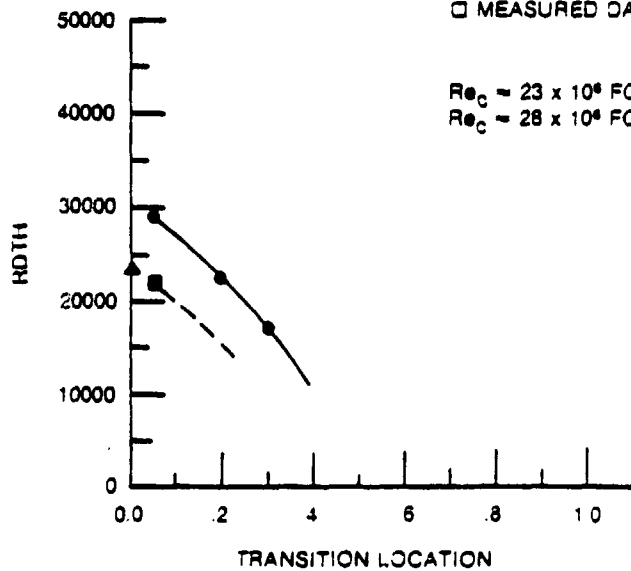
Figure C-7. Transition Determination. Case 7 F-111 NLF Glove

Case 8:

This case was for the lower surface with the rake at 50% chord. The sweep angle was 21.7 deg, and C_L was 0.382. Displacement thickness Reynolds number at the rake location versus the transition location is plotted in Figure C-8. Transition was at 3% chord.

Case 9:

This case was for the lower surface with the rake at 50% chord. The sweep angle was 25.2 deg, and C_L was 0.275. Displacement thickness Reynolds number at the rake location versus the transition location is plotted in Figure C-9. Transition was at 2% chord.

Case 10:

This case was for the lower surface with the rake at 50% chord. The sweep angle was 25.0 deg, and C_L was 0.373. Displacement thickness Reynolds number at the rake location versus the transition location is plotted in Figure C-10. Transition was at 5% chord.

Case 11:

This case was for the upper surface with the rake at 60% chord. The sweep angle was 9.0 deg, and C_L was 0.416. Displacement thickness Reynolds number at the rake location versus the transition location is plotted in Figure C-11. Transition for this case was at 46% chord. The cause of transition was probably the adverse pressure gradient, which began at 43% chord. This adverse gradient resulted in large growth rates of Tollmien-Schlichting disturbances.

Case 12:

This case was for the upper surface with the rake at 60% chord. The sweep angle was 15.9 deg, and C_L was 0.397. Displacement thickness Reynolds number at the rake location versus the transition location is plotted in Figure C-12. Transition was at 23% chord.

CLEAN WING
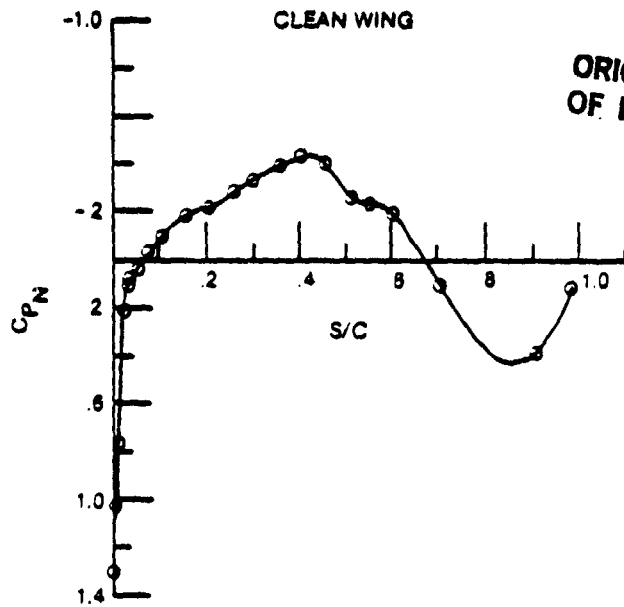
- CASE 8
- FLIGHT 161, RUN 112
- LOWER SURFACE
- $\Lambda = 22°$, M = 84, $C_L = 382$
- RAKE AT 50%
- TRANSITION AT 8%

O   A552
△   MEASURED DATA FOR CLEAN WING
□   MEASURED DATA FOR FORCED TRANSITION

$Re_c = 23 \times 10^6$ FOR OPEN SYMBOLS
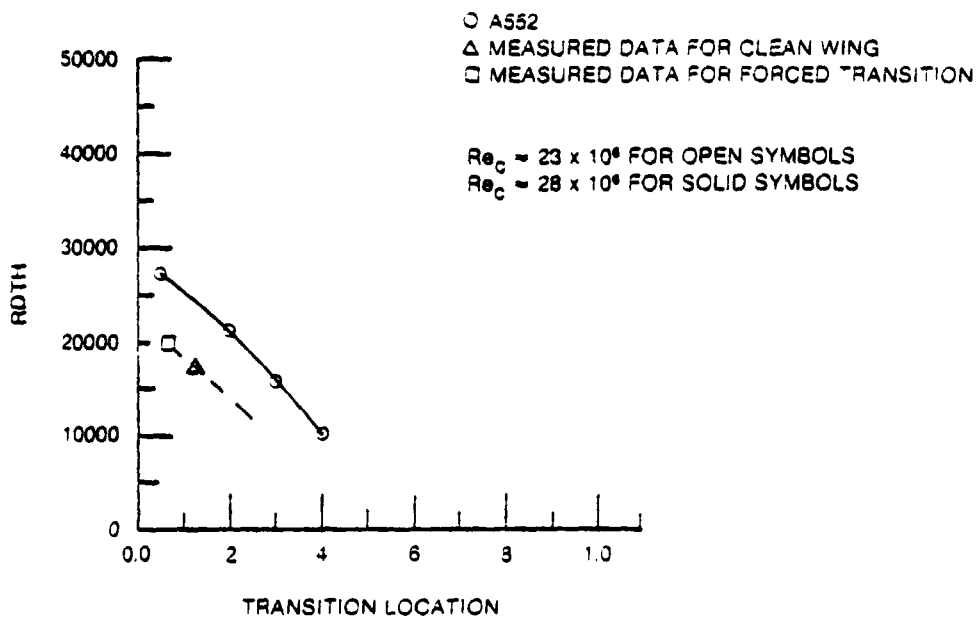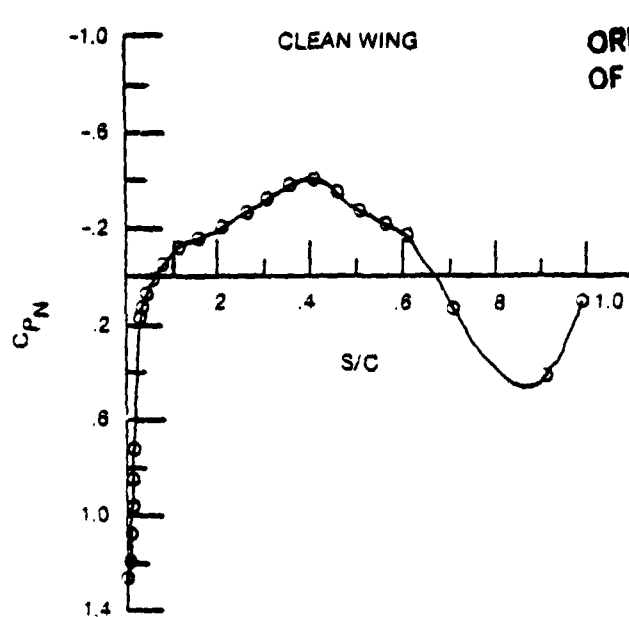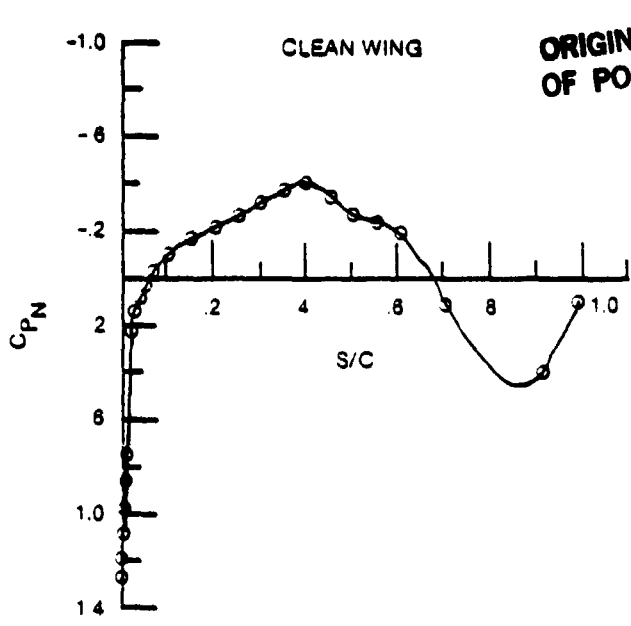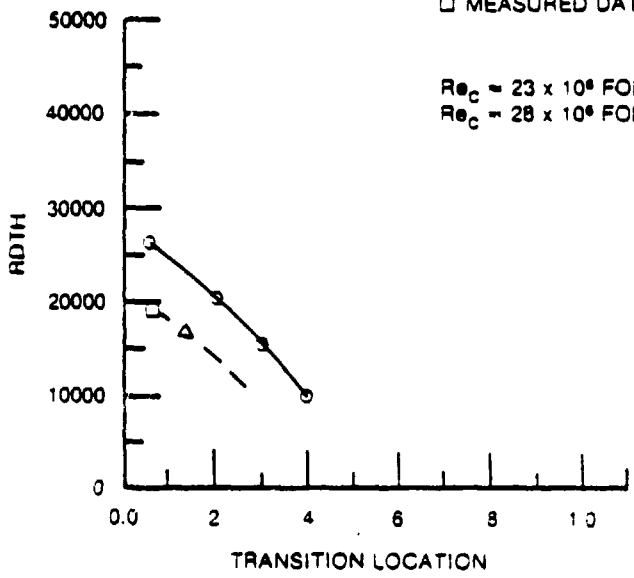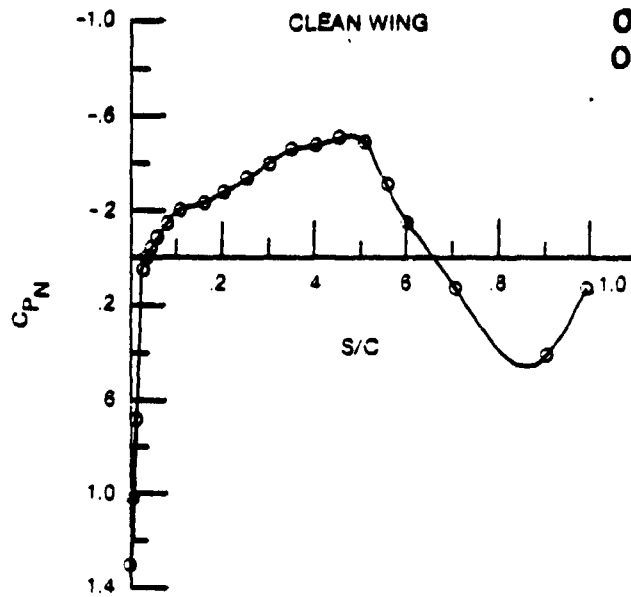$Re_c = 28 \times 10^6$ FOR SOLID SYMBOLS

TRANSITION LOCATION
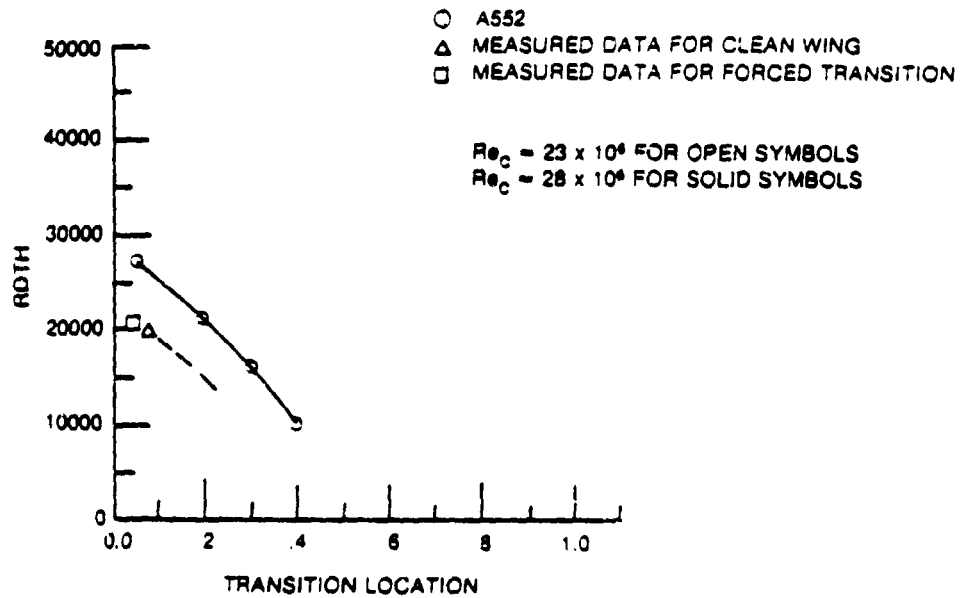
Figure C-8. Transition Determination, Case 8 F-111 NLF Glove

CLEAN WING
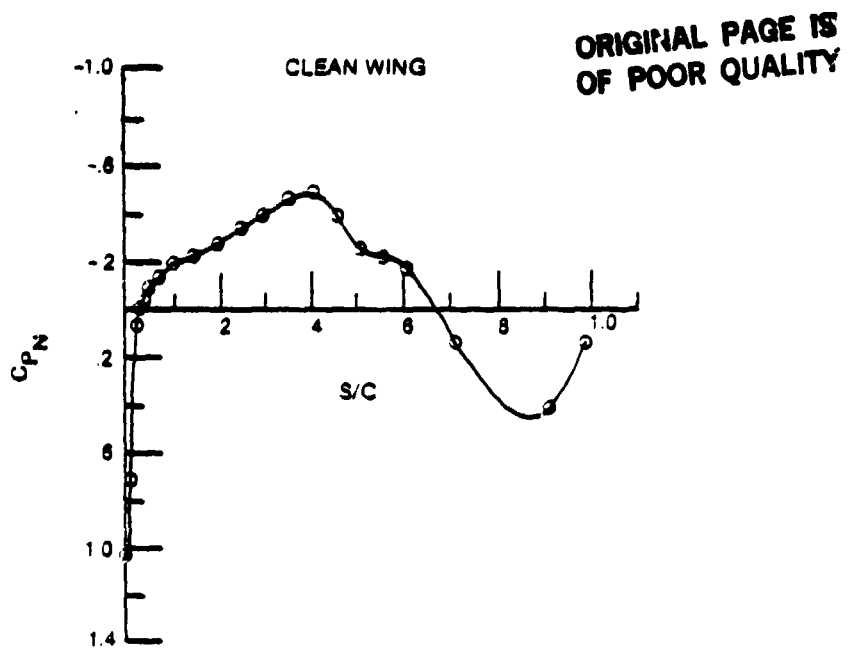
- CASE 9
- FLIGHT 161, RUN 23
- LOWER SURFACE
- $\Lambda = 25°$, M = 85, C_L = 275
- RAKE AT 50%
- TRANSITION AT 2%

C A552
△ MEASURED DATA FOR CLEAN WING
□ MEASURED DATA FOR FORCED TRANSITION

Re_c ~ 23 x 10⁶ FOR OPEN SYMBOLS
Re_c ~ 28 x 10⁶ FOR SOLID SYMBOLS

TRANSITION LOCATION
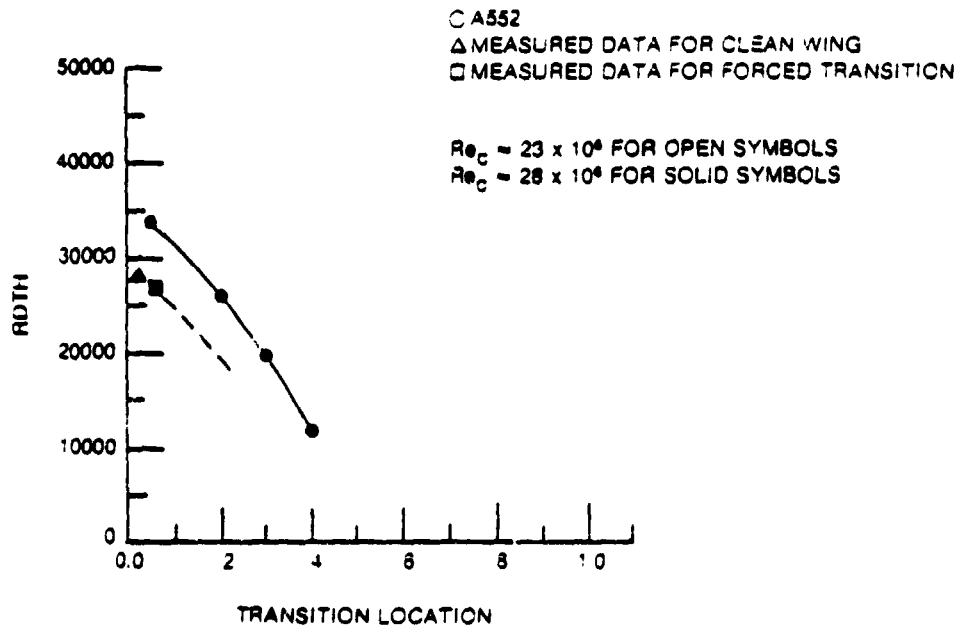
Figure C-9.   Transition Determination, Case 9 F-111 NLF Glove
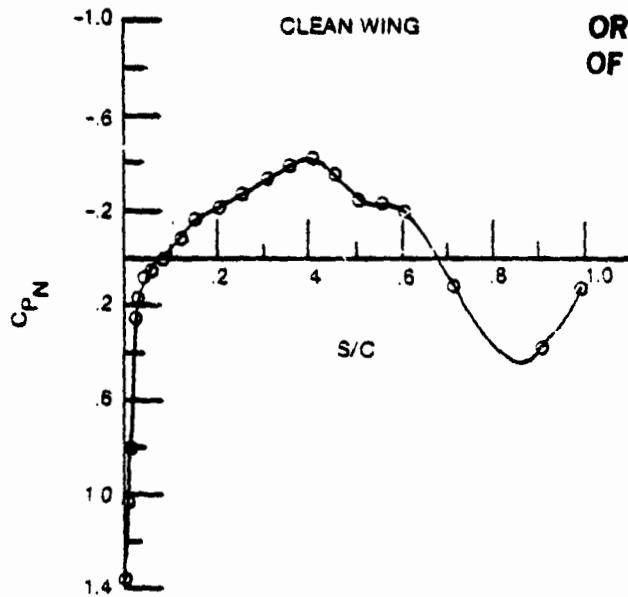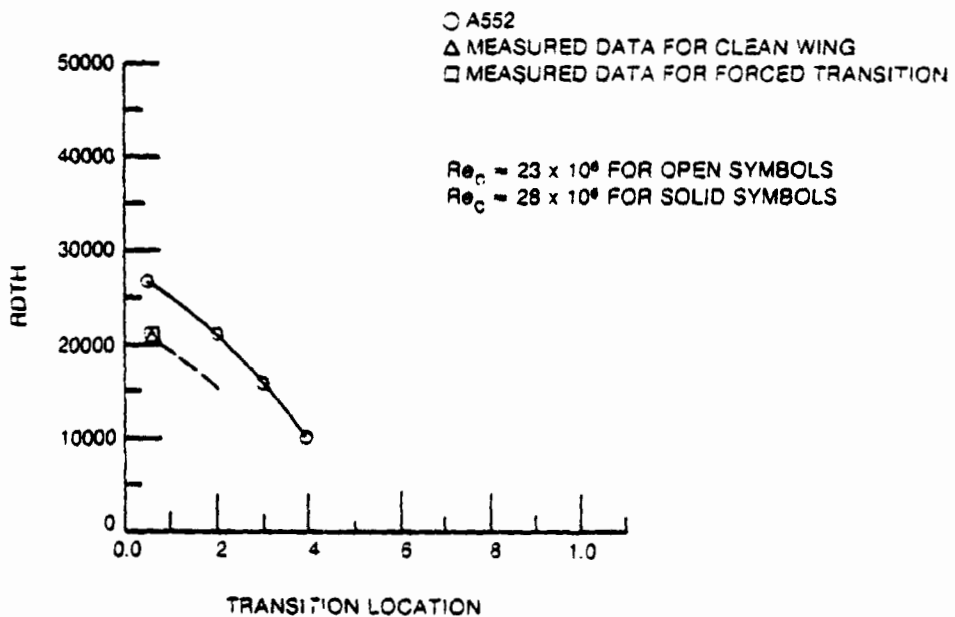
Figure C-10. Transition Determination, Case 10 F-111 NLF Glove

CLEAN WING
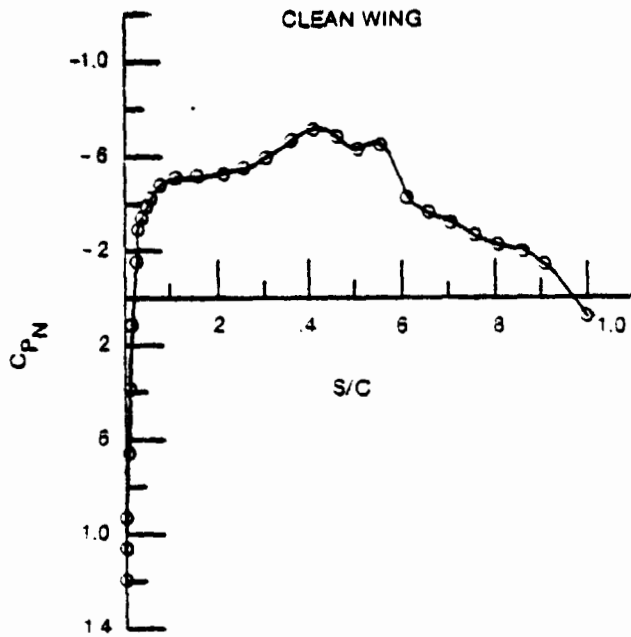
CASE 11
FLIGHT 161. RUN 15
UPPER SURFACE
Λ = 9° M = 82. C_L = 416
RAKE AT 60%
TRANSITION AT 46%

○ A552
△ MEASURED DATA FOR CLEAN WING
□ MEASURED DATA FOR FORCED TRANSITION

Re_C = 23 x 10⁶ FOR OPEN SYMBOLS
Re_C = 28 x 10⁶ FOR SOLID SYMBOLS
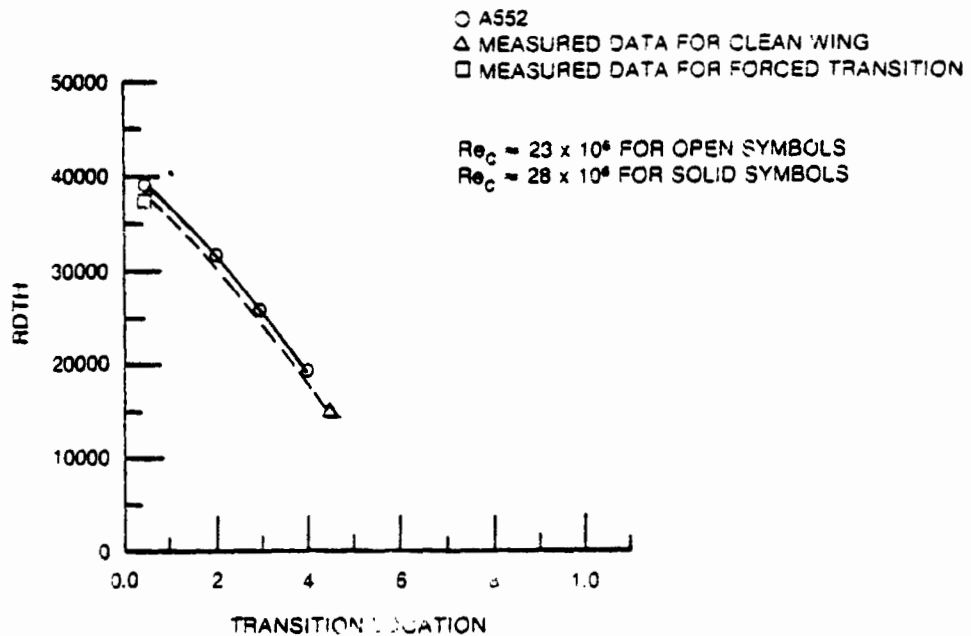
Figure C-11.   Transition Determination, Case 11 F-111 NLF Glove

CLEAN WING

C_{P_N}

S/C
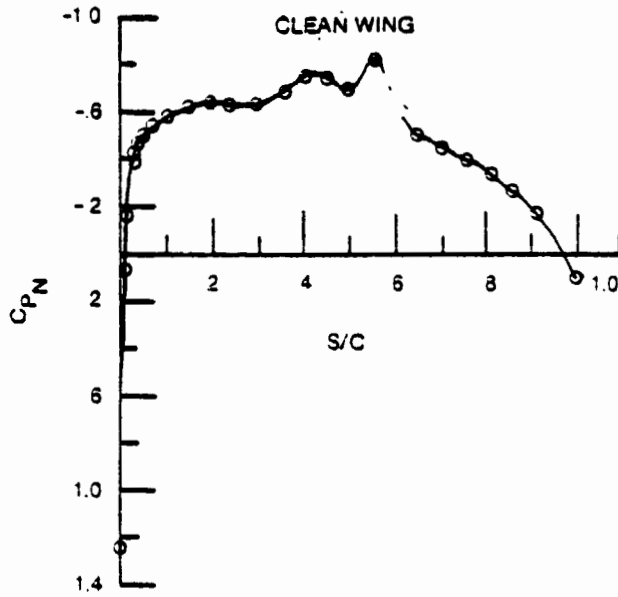
CASE 12
FLIGHT 161. RUN 7
UPPER SURFACE
Λ = 16°. M = 83. C_L = 397
RAKE AT 60%
TRANSITION AT 23%

O A552
△ MEASURED DATA FOR CLEAN WING
□ MEASURED DATA FOR FORCED TRANSITION

Re_C = 23 x 10⁶ FOR OPEN SYMBOLS
Re_C = 28 x 10⁶ FOR SOLID SYMBOLS
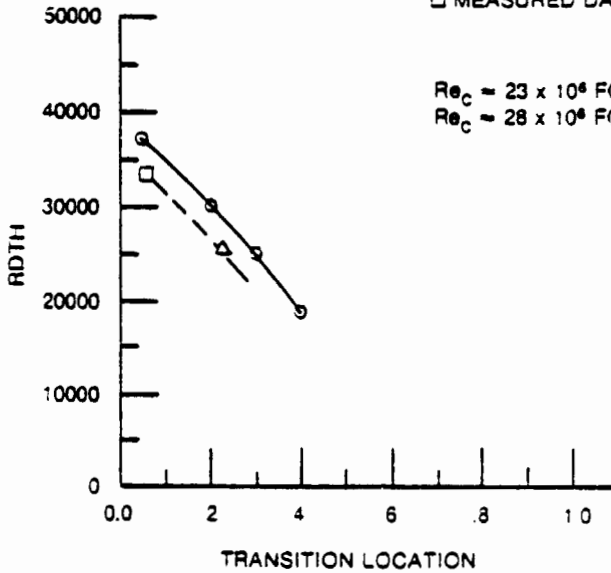
RDTH

TRANSITION LOCATION

Figure C-12.   Transition Determination, Case 12 F-111 NLF Glove

Case 13:

This case was for the upper surface with the rake at 60% chord. The sweep angle was 18.8 deg, and C_L was 0.377. Displacement thickness Reynolds number at the rake location versus the transition location is plotted in Figure C-13. Transition was at 17%.

Case 14:

This case was for the upper surface with the rake at 60% chord. The sweep angle was 22.0 deg, and C_L was 0.358. Displacement thickness Reynolds number at the rake location versus transition location is plotted in Figure C-14. Transition was at 7% chord.

Case 15:

This case was for the upper surface with the rake at 60% chord. The sweep angle was 25.2 deg, and C_L was 0.373. Displacement thickness Reynolds number at the rake location versus the transition location is plotted in Figure C-15. Transition was at 21%.

Case 16:

This case was for the upper surface with the rake at 90% The sweep angle was 9.0 deg, and C_L was 0.379. Displacement thickness Reynolds ber at the rake location versus the transition location is plotted in Figure C-16. For each of the aft-rake cases, five forced transition flights were made. For this case, three of the forced transition flights were at a chord Reynolds number of about 28 million and two were at a chord Reynolds number of about 23 million. Because the clean wing flight was at a chord Reynolds number of about 23 million, the results of the forced transition flights at 29 million have been adjusted to the clean wing Reynolds number using A552. There is quite a bit of scatter in the forced transition results. In fairing a curve through those points parallel to the A552 curve, the low Reynolds number points have been given more weight than the high Reynolds number points. Transition was at 36% chord. This case had more laminar flow than any other case analyzed. However, the extent of laminar flow would probably have been greater if there had not been an
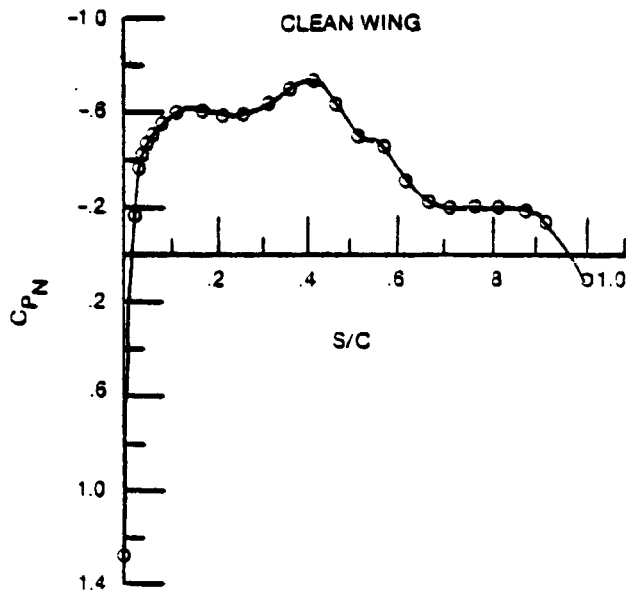
CLEAN WING

- CASE 13
- FLIGHT 161, RUN 25
- UPPER SURFACE
- $\Lambda = 19°$ M = 83. C_L = 377
- RAKE AT 60%
- TRANSITION AT 17%

O A552
△ MEASURED DATA FOR CLEAN WING
□ MEASURED DATA FOR FORCED TRANSITION
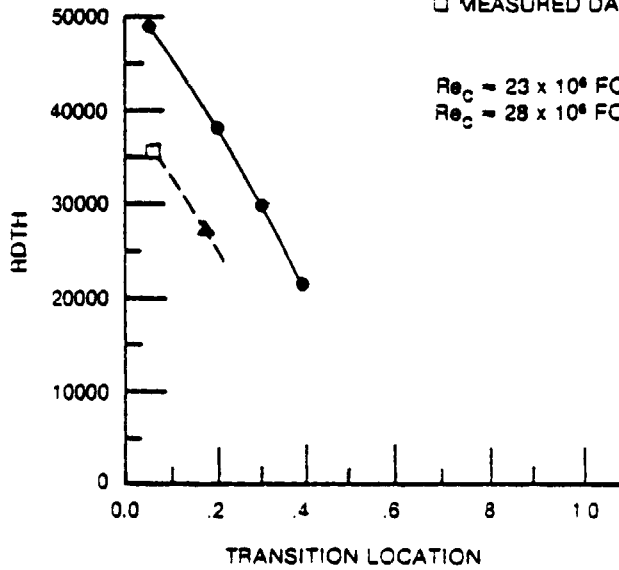
$Re_c = 23 \times 10^6$ FOR OPEN SYMBOLS
$Re_c = 28 \times 10^6$ FOR SOLID SYMBOLS

Figure C-13.   Transition Determination. Case 13 F-111 NLF Glove

CLEAN WING

CASE 14
- FLIGHT 161. RUN 28
- UPPER SURFACE
- $\Lambda = 22°$, M = 35. C_L = 358
- RAKE AT 60%
- TRANSITION AT 7%

○ A552
△ MEASURED DATA FOR CLEAN WING
□ MEASURED DATA FOR FORCED TRANSITION

$Re_C \approx 23 \times 10^6$ FOR OPEN SYMBOLS
$Re_C \approx 28 \times 10^6$ FOR SOLID SYMBOLS
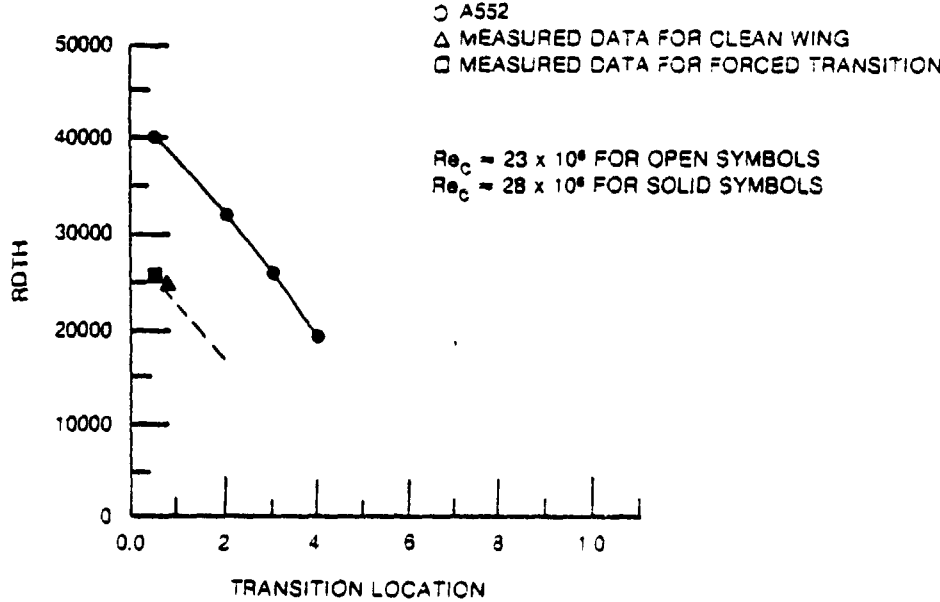
Figure C-14.   Transition Determination. Case 14 F-111 NLF Glove

CLEAN WING
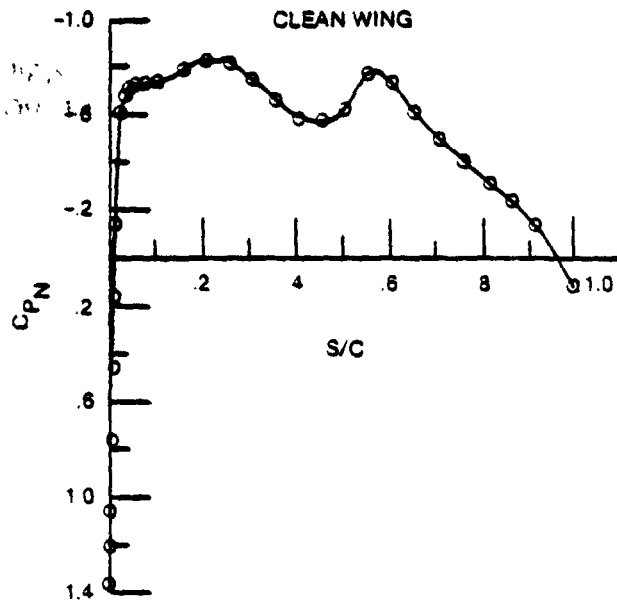
- CASE 15
- FLIGHT 161, RUN 12
- UPPER SURFACE
- Λ = 25, M! = 85, C_L = 373
- RAKE AT 60%
- TRANSITION AT 21%

O A552
△ MEASURED DATA FOR CLEAN WING
□ MEASURED DATA FOR FORCED TRANSITION

Re_C = 23 x 10⁶ FOR OPEN SYMBOLS
Re_C = 28 x 10⁶ FOR SOLID SYMBOLS

Figure C-15.   Transition Determination, Case 15 F-111 NLF Glove

CLEAN WING
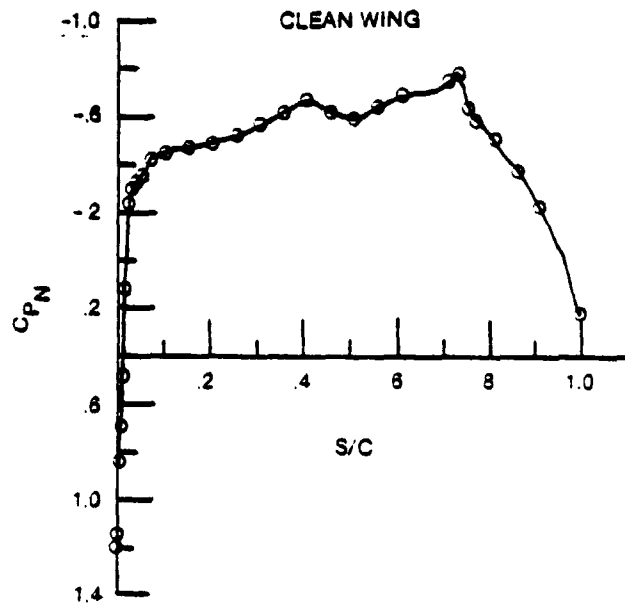
- CASE 16
- FLIGHT 147, RUN 8A
- UPPER SURFACE
- $\Lambda = 9°$, M = 82, C_L = 379
- RAKE AT 90%
- TRANSITION AT 56%

O A552
△ MEASURED DATA FOR CLEAN WING
□ MEASURED DATA FOR FORCED TRANSITION

$Re_c \approx 23 \times 10^6$ FOR OPEN SYMBOLS
$Re_c \approx 28 \times 10^6$ FOR SOLID SYMBOLS

Figure C-16.   Transition Determination, Case 16 F-111 NLF Glove

adverse pressure gradient in the region from 40% to 50% chord, which resulted in very large amplification of Tollmien-Schlichting disturbances.

Case 17:

This case was for the upper surface with the rake at 90% chord. The sweep angle was 9.0 deg, and C_L was 0.432. Displacement thickness Reynolds number at the rake location versus transition location is plotted in Figure C-17. Transition was at 55% chord.

Case 18:

This case was for the upper surface with the rake at 90% chord. The sweep angle was 9.0 deg, and C_L was 0.504. Displacement thickness Reynolds number at the rake location versus the transition location is plotted in Figure C-13. Transition for this case is at 45% chord.

Case 19:

This case was for the upper surface with the rake at 90% chord. The sweep angle was 16.1 deg, and C_L was 0.379. Displacement thickness Reynolds number at the rake location versus transition location is plotted in Figure C-19. Transition location was at 36% chord. Figure C-19 shows that the high Reynolds number flight with a trip at 30% chord apparently has transition at about 19% chord. This probably resulted from higher crossflow and Tollmien-Schlichting disturbance growth rates at the higher Reynolds number.

Case 20:

This case was for the upper surface with the rake at 90% chord. The sweep angle was 16.1 deg, and C_L was 0.436. Displacement thickness Reynolds number at the rake location versus the transition location is plotted in Figure C-20. Transition was at 42% chord. The three forced transition flights, which were at higher Reynolds number of about 23 million, apparently had transition at about 7% chord. This probably was due to higher disturbance growth at the higher Reynolds number.

CLEAN WING
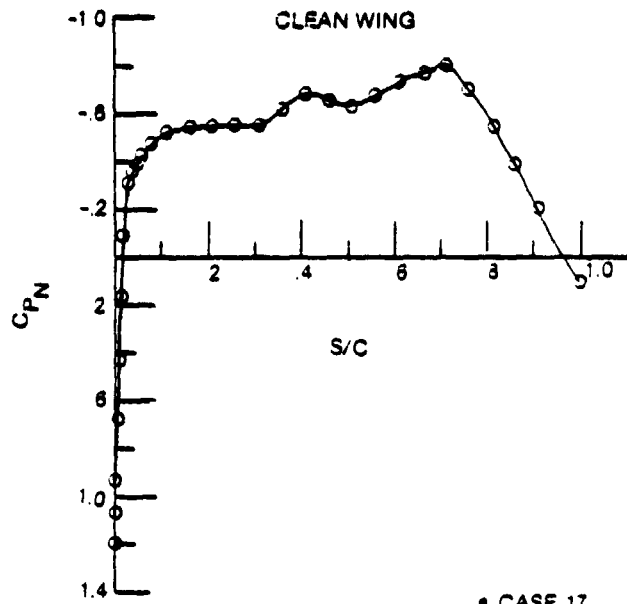
- CASE 17
- FLIGHT 155. RUN 18
- UPPER SURFACE
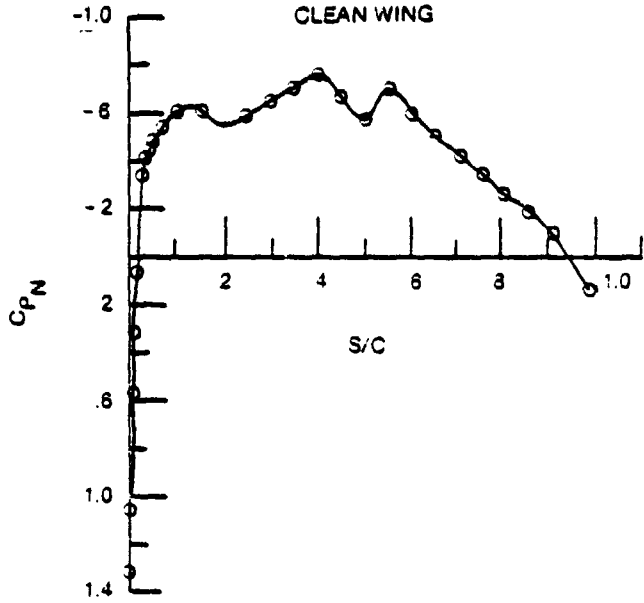- $\Lambda = 9°$ M = 82. $C_L = 432$
- RAKE AT 90%
- TRANSITION AT 55%

O A552
△ MEASURED DATA FOR CLEAN WING
☐ MEASURED DATA FOR FORCED TRANSITION

$Re_c = 23 \times 10^6$ FOR OPEN SYMBOLS
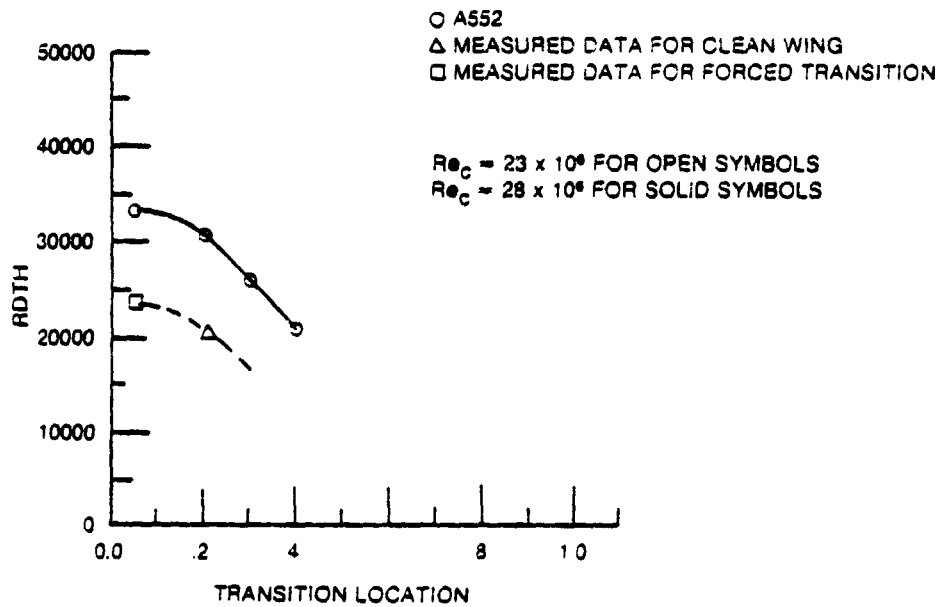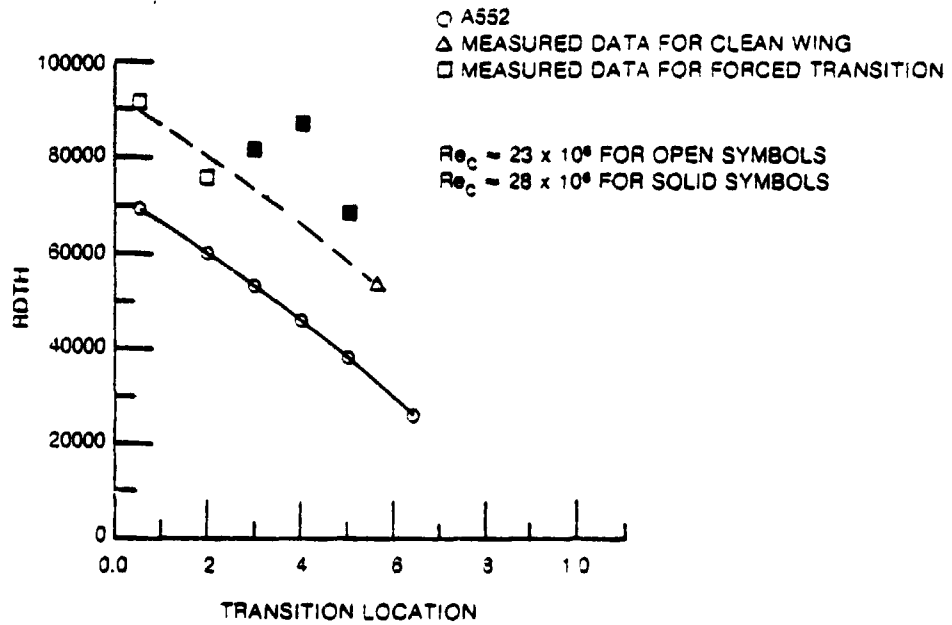$Re_c = 28 \times 10^6$ FOR SOLID SYMBOLS

TRANSITION LOCATION
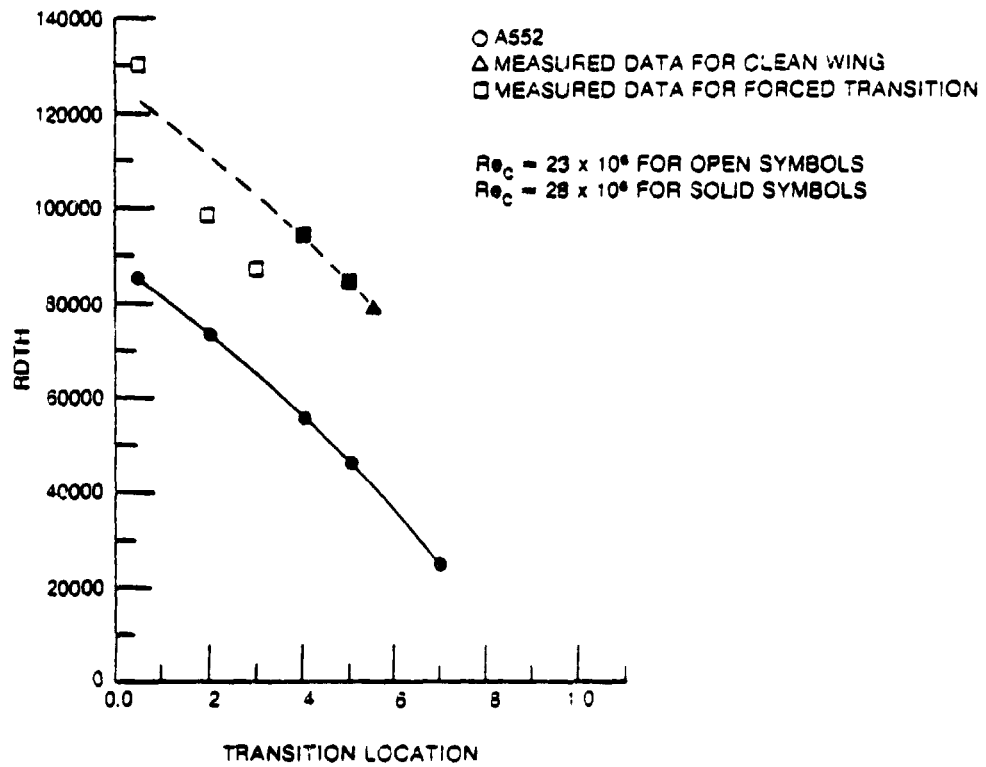
Figure C-17.   Transition Determination, Case 17 F-111 NLF Glove
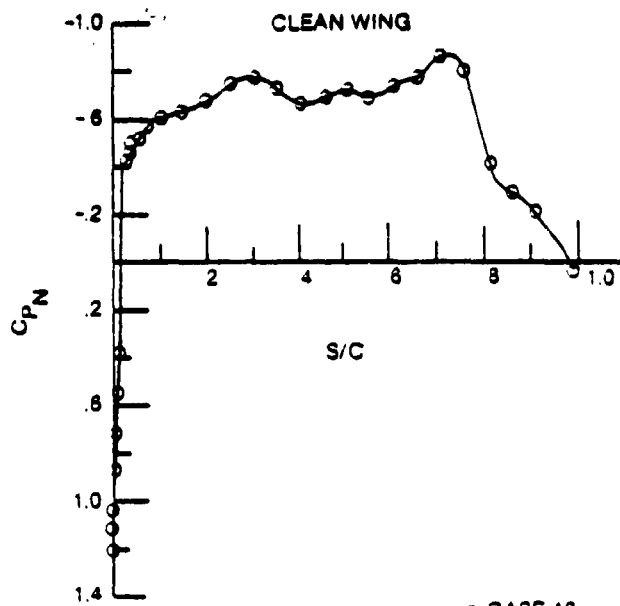
- CASE 18
- FLIGHT 158. RUN 3
- UPPER SURFACE
- $\Lambda = 9°$, M = 82, $C_L = 504$
- RAKE AT 90%
- TRANSITION AT 45%

O A552
△ MEASURED DATA FOR CLEAN WING
□ MEASURED DATA FOR FORCED TRANSITION

$Re_C = 23 \times 10^6$ FOR OPEN SYMBOLS
$Re_C = 28 \times 10^6$ FOR SOLID SYMBOLS
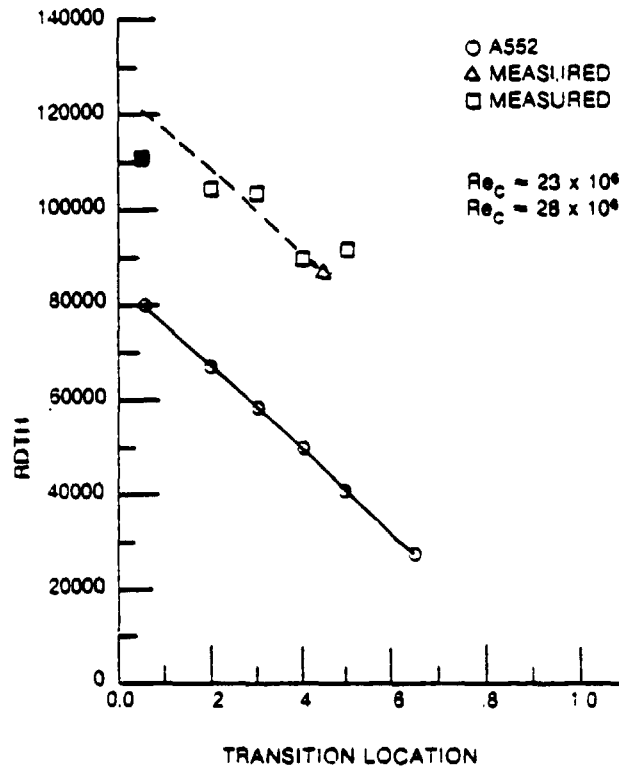
Figure C-18.   Transition Determination, Case 18 F-111 NLF Glove

CLEAN WING

(graph: C_{P_N} vs S/C)
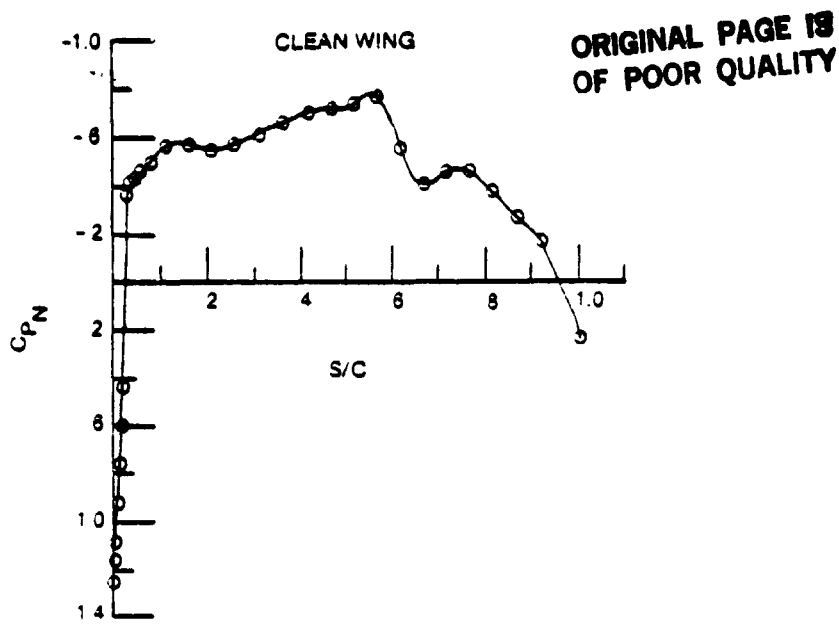
- CASE 19
- FLIGHT 147 RUN 14
- UPPER SURFACE
- $\Lambda = 16°$, M = 83, $C_L = 379$
- RAKE AT 90%
- TRANSITION AT 36%

○ A552
△ MEASURED DATA FOR CLEAN WING
□ MEASURED DATA FOR FORCED TRANSITION

$Re_C = 23 \times 10^6$ FOR OPEN SYMBOLS
$Re_C = 28 \times 10^6$ FOR SOLID SYMBOLS

(graph: RDTH vs TRANSITION LOCATION)

RDTH

TRANSITION LOCATION
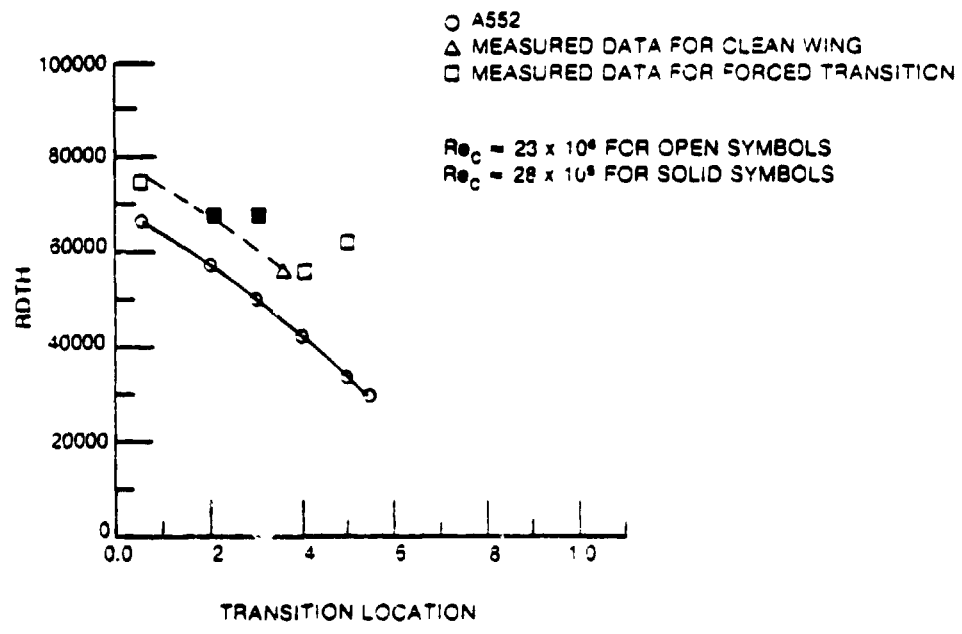
Figure C-19.   Transition Determination, Case 19 F-111 NLF Glove

CLEAN WING

- CASE 20
- FLIGHT 147, RUN 15
- UPPER SURFACE
- Λ = 16°, M = .83, C_L = 436
- RAKE AT 90%
- TRANSITION AT 42%

○ A552
△ MEASURED DATA FOR CLEAN WING
□ MEASURED DATA FOR FORCED TRANSITION

Re_C = 23 x 10⁶ FOR OPEN SYMBOLS
Re_C = 28 x 10⁶ FOR SOLID SYMBOLS

TRANSITION LOCATION
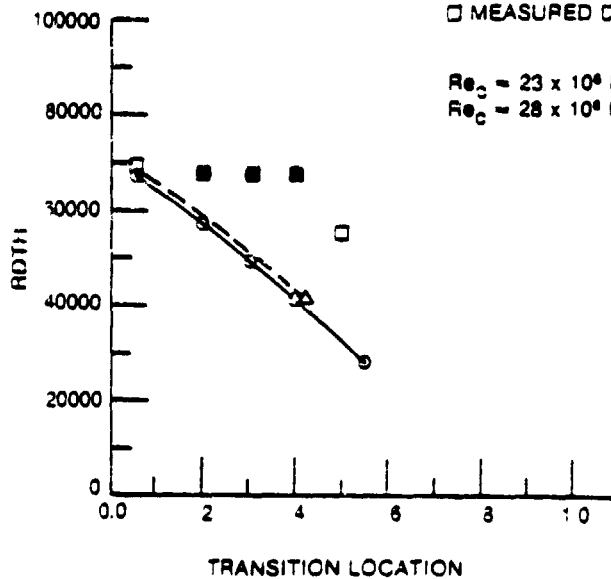
Figure C-20. Transition Determination, Case 20 F-111 NLF Glove

Case 21:

This case was for the upper surface with the rake at 90% chord. The sweep angle was 16.1 deg, and C_L was 0.550. Displacement thickness Reynolds number at the rake location versus the transition location is plotted in Figure C-21. Transition was at 43% chord.

Case 22:

This case was for the upper surface with the rake at 90% chord. The sweep angle was 25.2 deg, and C_L was 0.276. Displacement thickness Reynolds number at the rate location versus transition location is plotted in Figure C-22. Transition was at 20% chord. The flights with transition forced at 20%, 30%, and 40% chord all appear to have transition in the vicinity of 5% to 10% chord. This indicates that, at this high Reynolds number and sweep angle, transition is very sensitive to pressure distribution.

Case 23:

This case was for the upper surface with the rake at 90% chord. The sweep angle was 25.1 deg, and C_L was 0.357. Displacement thickness Reynolds number at the rake location versus transition location is plotted in Figure C-23. Transition was at 13% chord. A552 indicated laminar separation at 31% for the flight with forced transition at 40%. Therefore, in Figure C-23 the point for the 40% forced transition flight was moved from 40% to 31% chord. A similar move was made for the flight with forced transition at 50%. The laminar separation ahead of the trip for these two flights was the result of adverse gradients in the region from 25% to 40% chord for the flight with the trip at 40% chord and in the region from 20% to 30% chord for the flight with the trip at 50% chord (fig. 3-13 in app. B).

Case 24:

This case was for the upper surface with the rake at 90% chord. The sweep angle was 25.2 deg, and C_L was 0.429. Displacement thickness Reynolds number at the rake location versus the transition location is plotted in Figure C-24. A552 indicated laminar separation at 36% for the flight in which transition was forced at 40% chord. That point was adjusted accordingly in Figure C-24.

- CASE 21
- FLIGHT 147, RUN 16
- UPPER SURFACE
- $\Lambda = 16°$, M = 83, C_L = 550
- RAKE AT 90%
- TRANSITION AT 43%

O A552
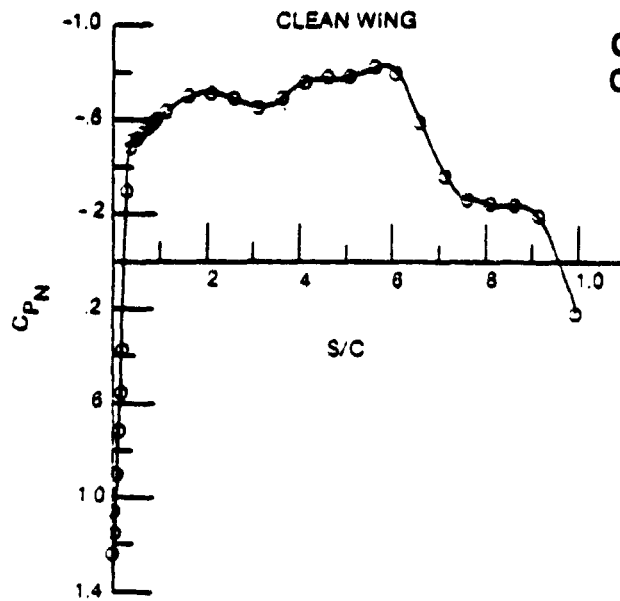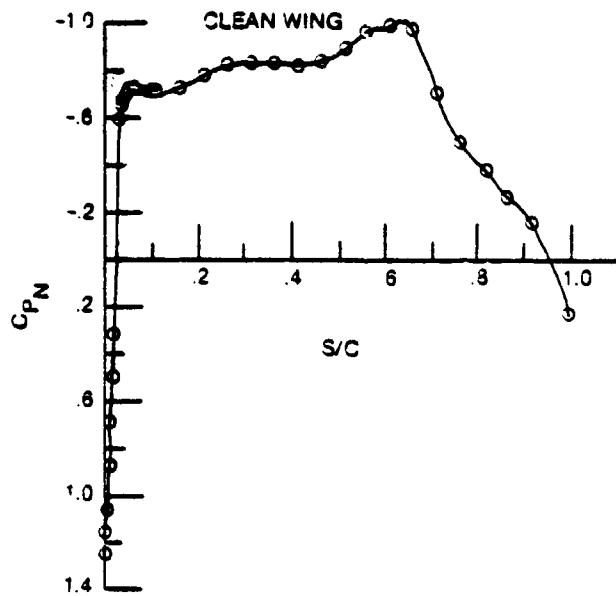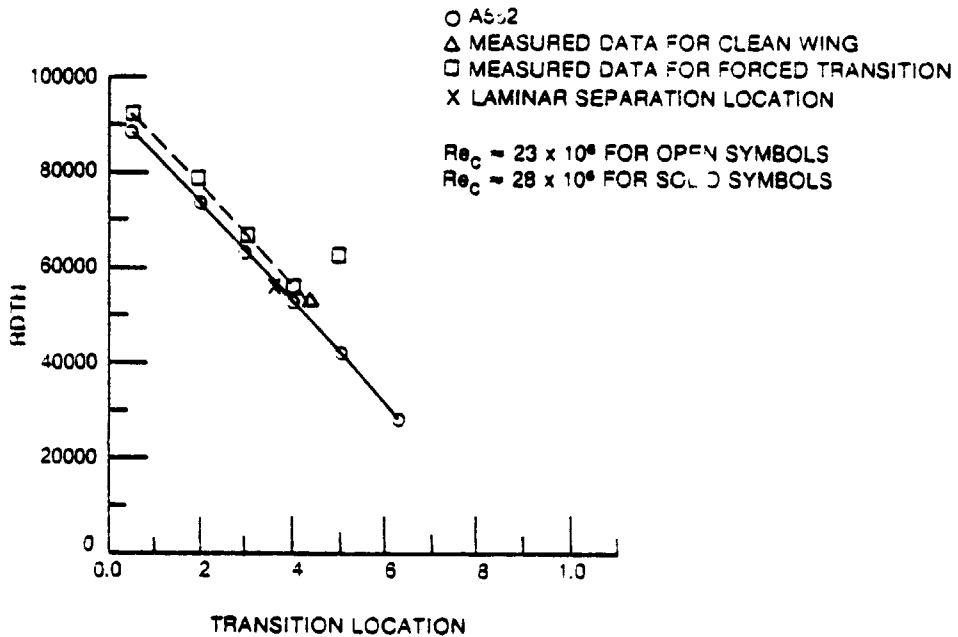△ MEASURED DATA FOR CLEAN WING
□ MEASURED DATA FOR FORCED TRANSITION
X LAMINAR SEPARATION LOCATION

Re_C ≈ 23 x 10⁶ FOR OPEN SYMBOLS
Re_C ≈ 28 x 10⁶ FOR SOLID SYMBOLS

Figure C-21.   Transition Determination, Case 21 F-111 NLF Glove

CLEAN WING

S/C

- CASE 22
- FLIGHT 158, RUN 23
- UPPER SURFACE
- Λ = 25°, M = 85, C_L = 276
- RAKE AT 90%
- TRANSITION AT 20%

O A552
△ MEASURED DATA FOR CLEAN WING
□ MEASURED DATA FOR FORCED TRANSITION

$Re_c \approx 23 \times 10^6$ FOR OPEN SYMBOLS
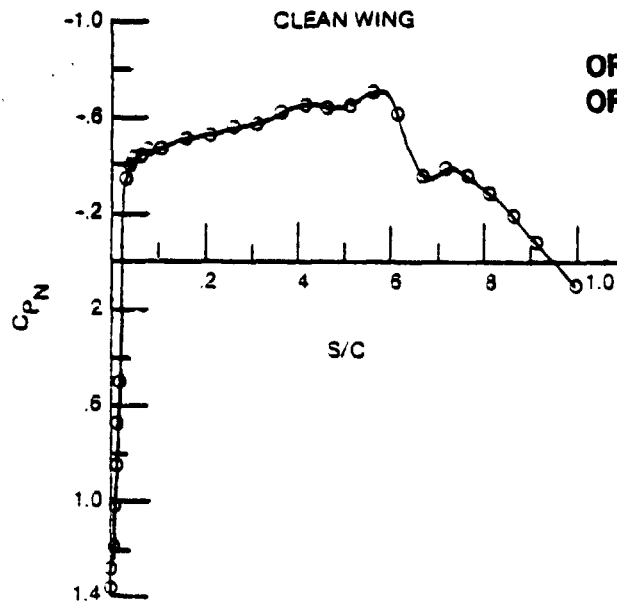$Re_c \approx 28 \times 10^6$ FOR SOLID SYMBOLS

. TRANSITION LOCATION
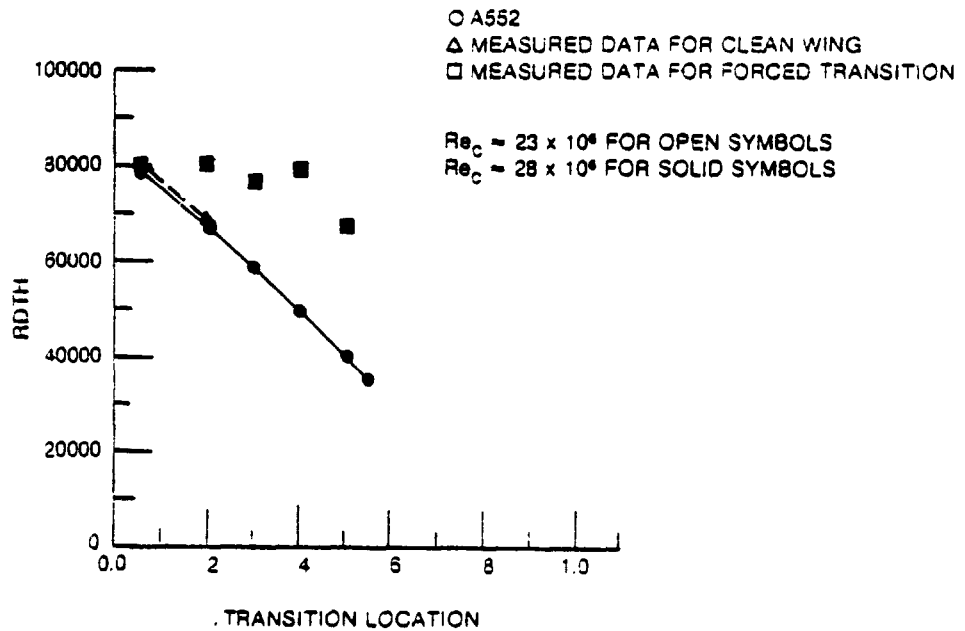
Figure C-22. Transition Determination, Case 22 F-111 NLF Glove

- CASE 23
- FLIGHT 147, RUN 21
- UPPER SURFACE
- $\Lambda = 25°$, M = 35. C_L = 357
- RAKE AT 90%
- TRANSITION AT 18%

O A552
△ MEASURED DATA FOR CLEAN WING
□ MEASURED DATA FOR FORCED TRANSITION
X LAMINAR SEPARATION LOCATION

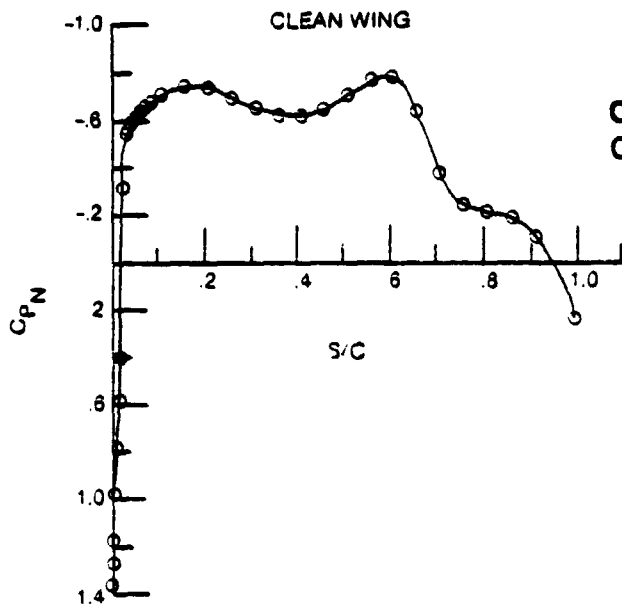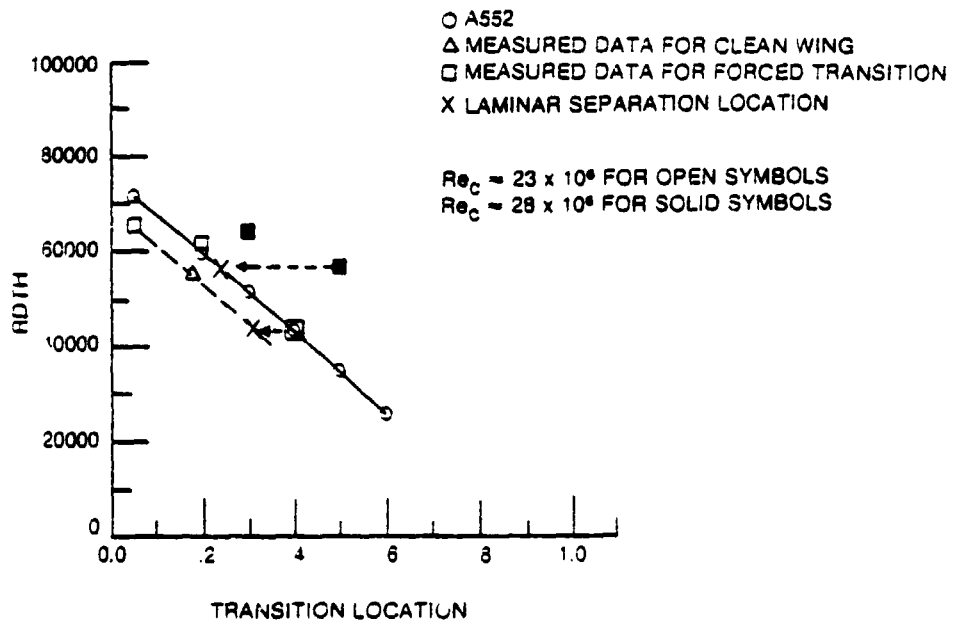$Re_C = 23 \times 10^6$ FOR OPEN SYMBOLS
$Re_C = 28 \times 10^6$ FOR SOLID SYMBOLS

Figure C-23.   Transition Determination, Case 23 F-111 NLF Glove

CLEAN WING

C_{P_N}

S/C

-1.0

-.6

-.2

.2

.6

1.0

1.4

2 4 6 8 10

- CASE 24
- FLIGHT 155, RUN 13
- UPPER SURFACE
- $\Lambda = 25°$, M = 85, $C_L = 429$
- RAKE AT 90%
- TRANSITION AT 15%

O A552
△ MEASURED DATA FOR CLEAN WING
□ MEASURED DATA FOR FORCED TRANSITION
X LAMINAR SEPARATION LOCATION

$Re_C = 23 \times 10^6$ FOR OPEN SYMBOLS
$Re_C = 28 \times 10^6$ FOR SOLID SYMBOLS

RDTH

100000

80000

60000

40000

20000

0

0.0 2 4 6 8 10

TRANSITION LOCATION

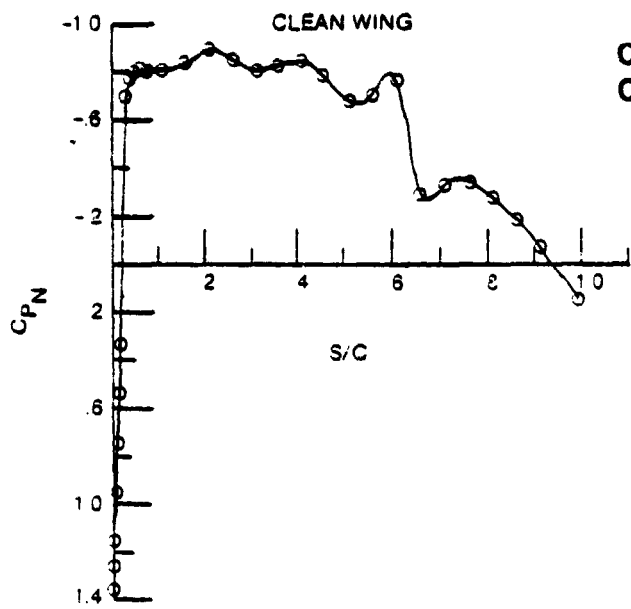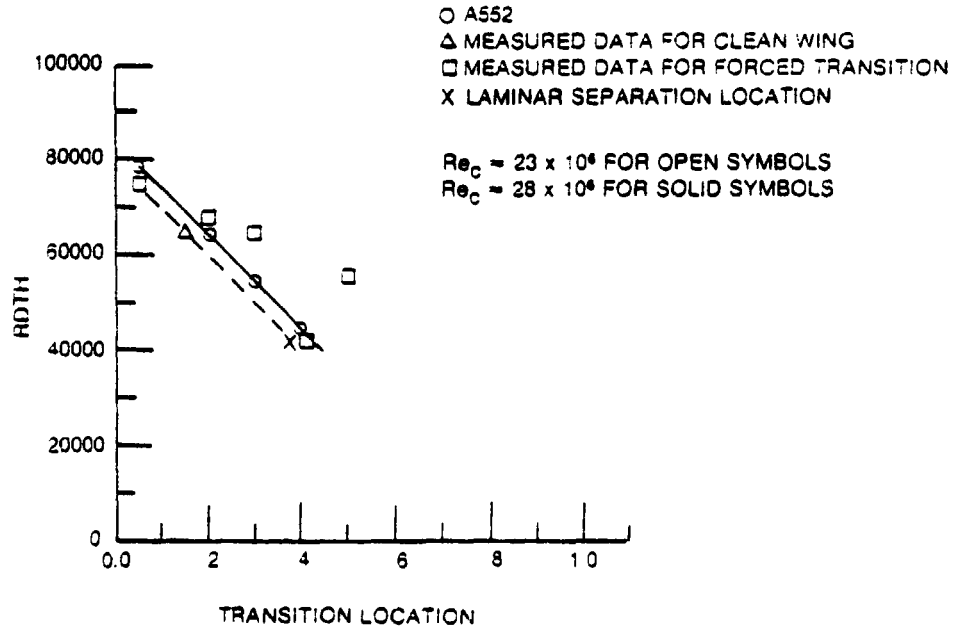Figure C-24.   Transition Determination, Case 24 F-111 NLF Jove

Case 25:

This case was for the lower surface with the rake at 90% chord. The sweep angle was 9.0 deg, and C_L was 0.416. Displacement thickness Reynolds number at the rake location versus the transition location is plotted in Figure C-25. Transition was at 23% chord.
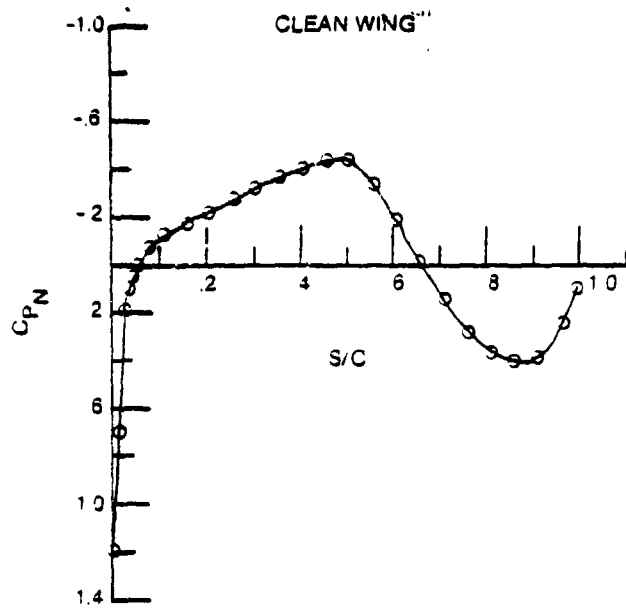
Case 26:

This case was for the lower surface with the rake at 90% chord. The sweep angle was 15.6 deg and C_L was 0.353. Displacement thickness Reynolds number at the rake location versus the transition location is plotted in Figure C-26. Transition for this case was at 51% chord. This was just slightly past the beginning of the adverse pressure gradient, which was the probable cause of transition.

Cases 27 Through 31:

These were lower surface cases with the rake at 90% chord and a wing sweep of 10 deg. Cases 27 through 29 had a C_L near 0.41 and a chord Reynolds number near 23 million. Cases 30 and 31 had a C_L near 0.32 and a chord Reynolds number of about 27 million. Figures C-27 through C-31 show the displacement thickness Reynolds number at the rake versus transition location. Transition varied from 31% chord for case 27 to 49% for case 31. The flights with forced transition at 40% and 50% indicated premature transition, so the RDTH point from the 5% forced transition flight was weighed most heavily in determining the clean wing transition location.

Cases 32 Through 34:

These cases were from the lower surface with the rake at 90% chord and sweep near 15 deg. Figures C-32 through C-34 show the displacement thickness Reynolds number at the rake versus transition location. Again, the result of the forced transition at 5% was the primary determiner of the clean wing transition location. Each of these three cases experienced transition at the beginning of the adverse pressure gradient, 51% chord.
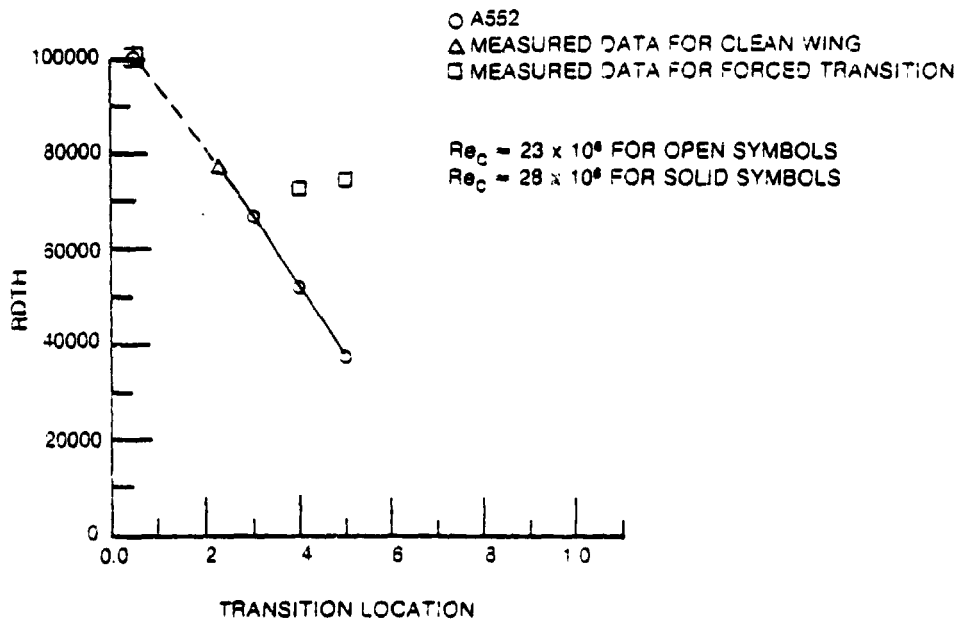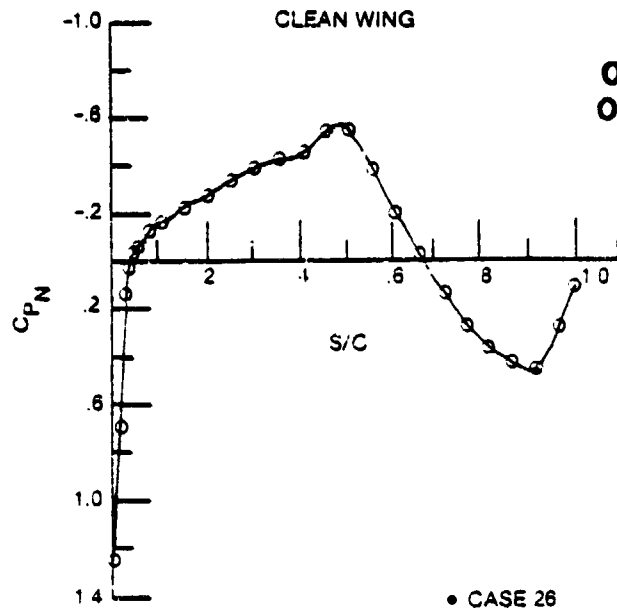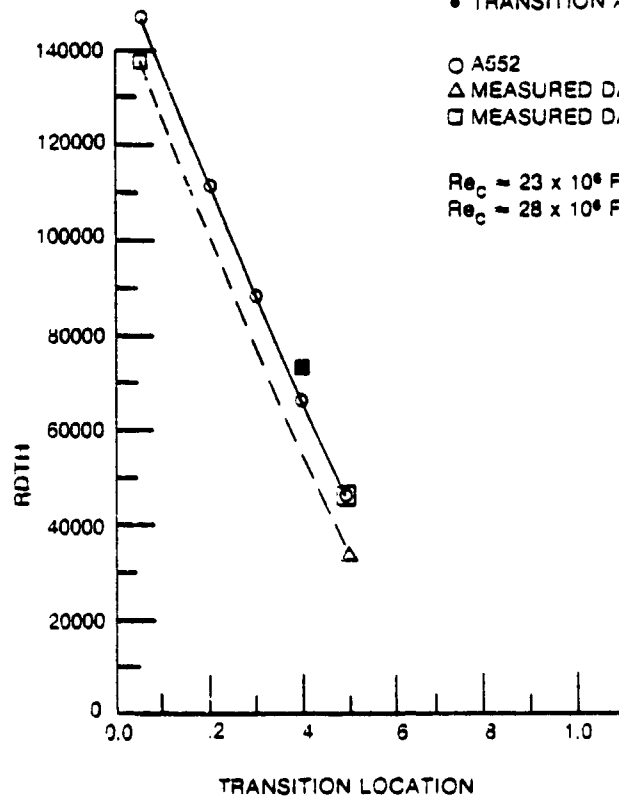
Figure C-25. Transition Determination, Case 25 F-111 NLF Glove

CLEAN WING
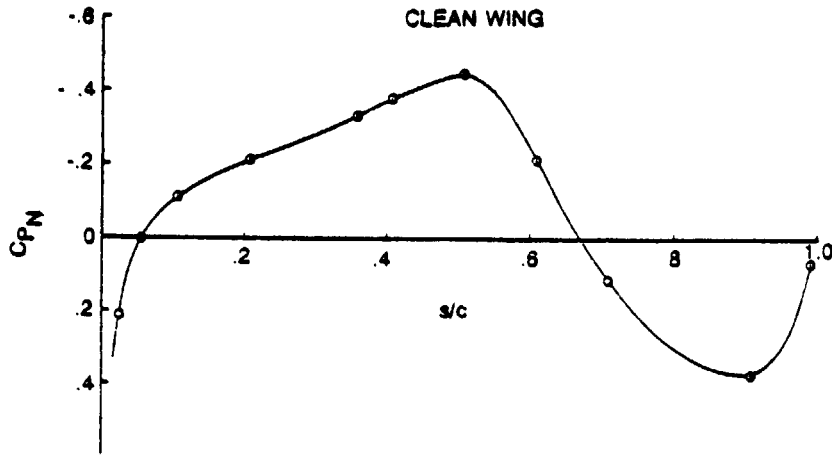
- CASE 26
- FLIGHT 146, RUN 18.
- LOWER SURFACE
- Λ = 16°, M = 83, C_L = 353
- RAKE AT 90%
- TRANSITION AT 51%

○ A552
△ MEASURED DATA FOR CLEAN WING
□ MEASURED DATA FOR FORCED TRANSITION

Re_C = 23 x 10⁶ FOR OPEN SYMBOLS
Re_C = 28 x 10⁶ FOR SOLID SYMBOLS

TRANSITION LOCATION

Figure C-26. Transition Determination, Case 26 F-111 NLF Glove

CLEAN WING

CASE 27
FLIGHT 148, RUN 2
LOWER SURFACE
$\Lambda_{LE} = 10^0$, M = .80, C_L = .425

RAKE AT 90%
TRANSITION AT 31%

A552
MEASURED DATA FOR CLEAN WING
MEASURED DATA FOR FORCED TRANSITION

$Re_c = 23 \times 10^6$

Figure C-27. Transition Determination, Case 27 F-111 NLF Glove

C-33

Figure C-28. Transition Determination, Case 28 F-111 NLF Glove

CLEAN WING

- CASE 29
- FLIGHT 146, RUN 4
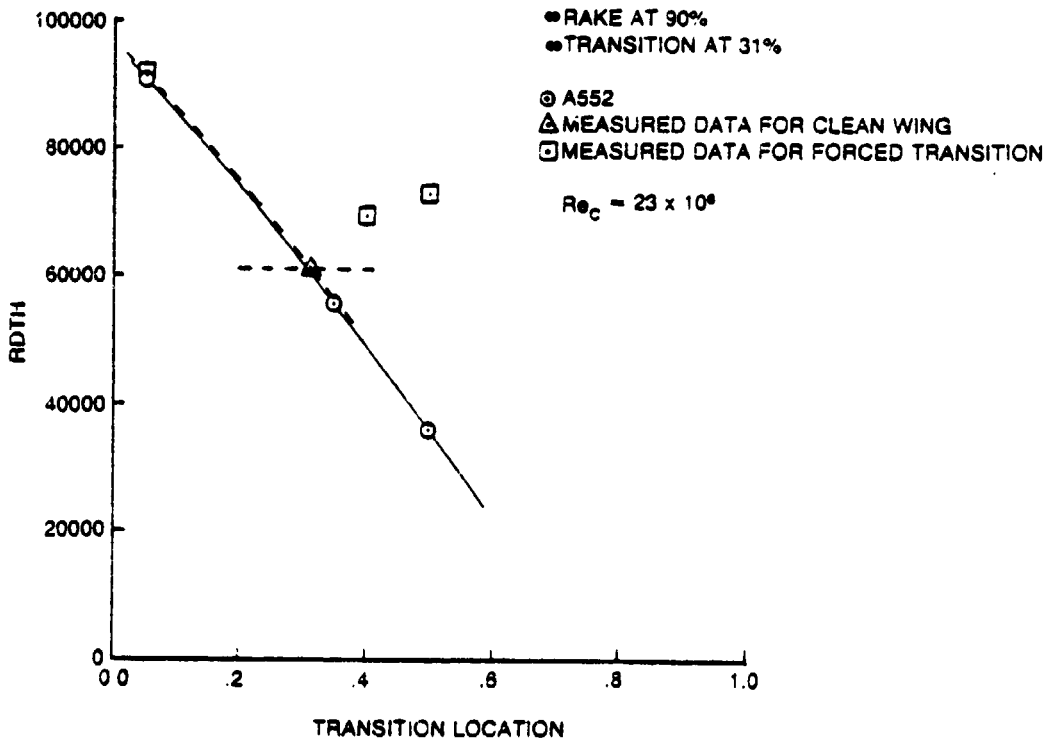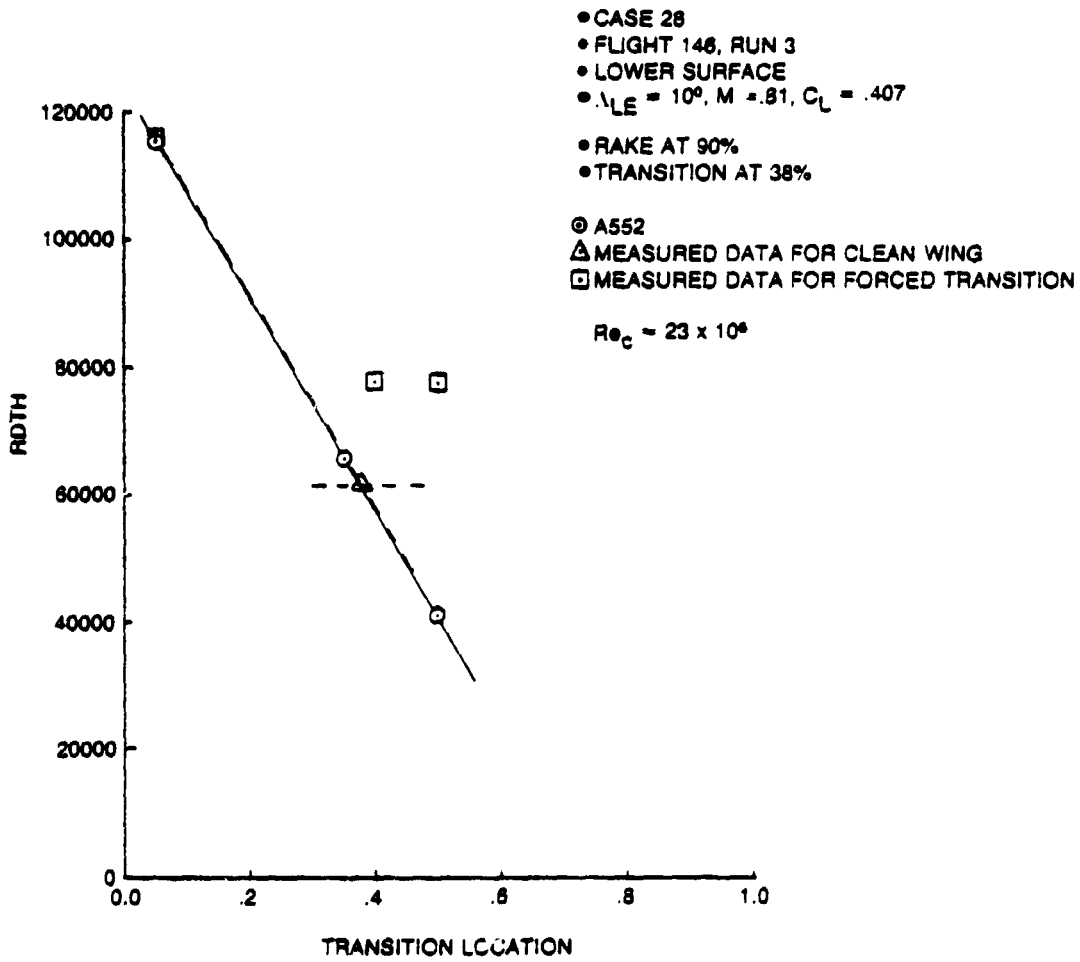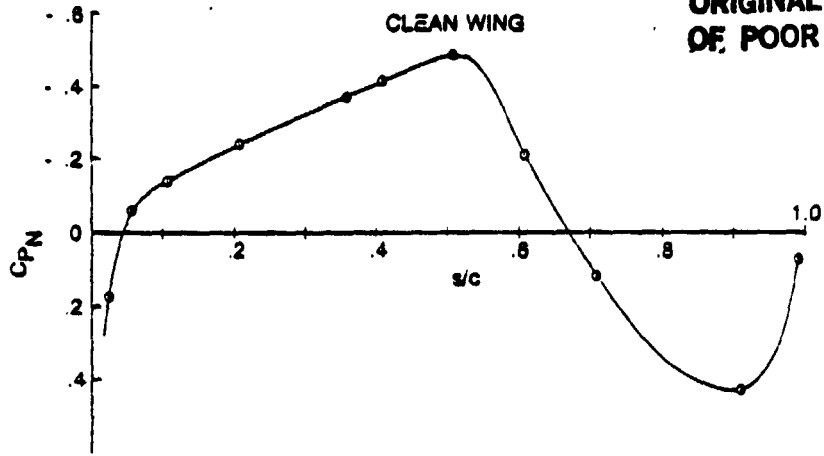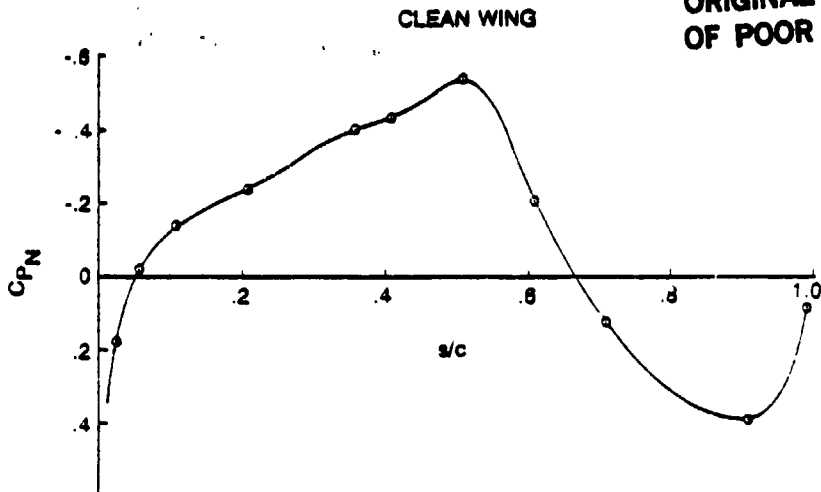- LOWER SURFACE
- $\lambda_{LE} = 10°$, M = .82, C_L = .414

- RAKE AT 90%
- TRANSITION AT 34%

⊕ A552
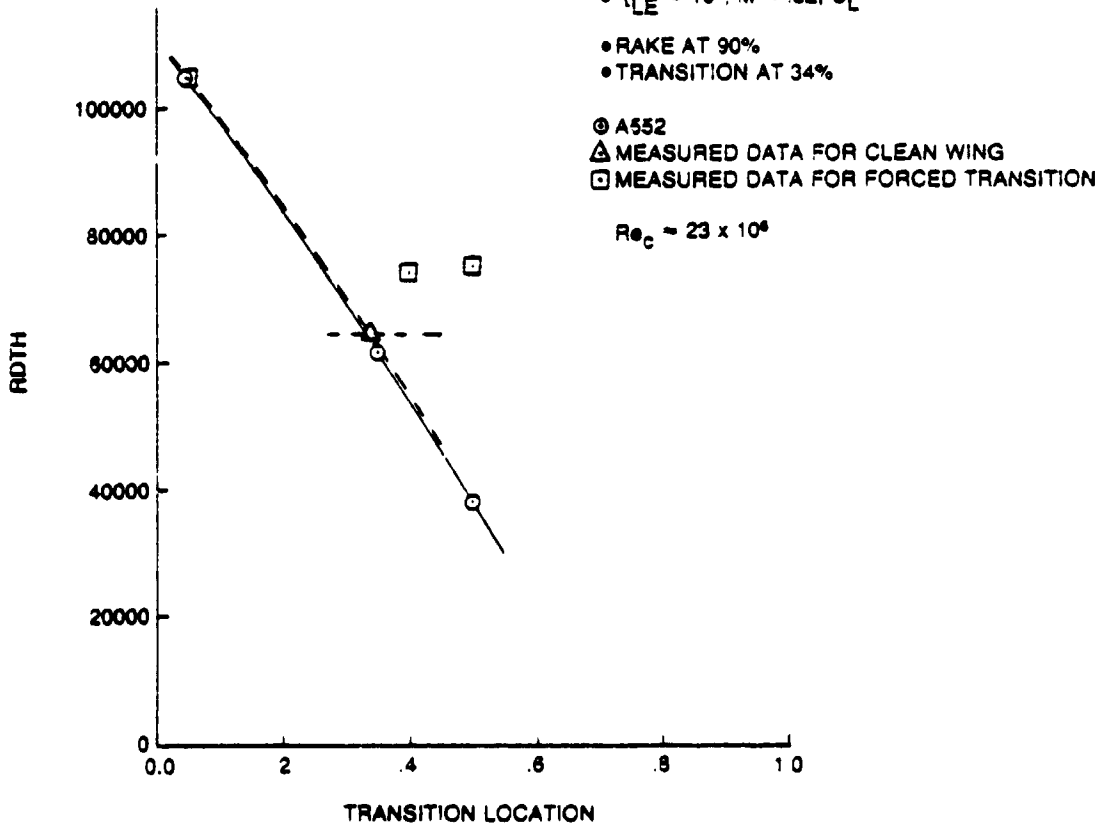△ MEASURED DATA FOR CLEAN WING
⊡ MEASURED DATA FOR FORCED TRANSITION

$Re_c \approx 23 \times 10^6$

Figure C-29. Transition Determination, Case 29 F-111 NLF Glove

CLEAN WING

CASE 30
FLIGHT 146, RUN 8
LOWER SURFACE
$\Lambda_{LE} = 10°$, M = .81, C_L = .322

RAKE AT 90%
TRANSITION AT 48%

A552
△ MEASURED DATA FOR CLEAN WING
□ MEASURED DATA FOR FORCED TRANSITION

$Re_c \approx 23 \times 10^6$ FOR OPEN SYMBOLS
$Re_c \approx 28 \times 10^6$ FOR SOLID SYMBOLS
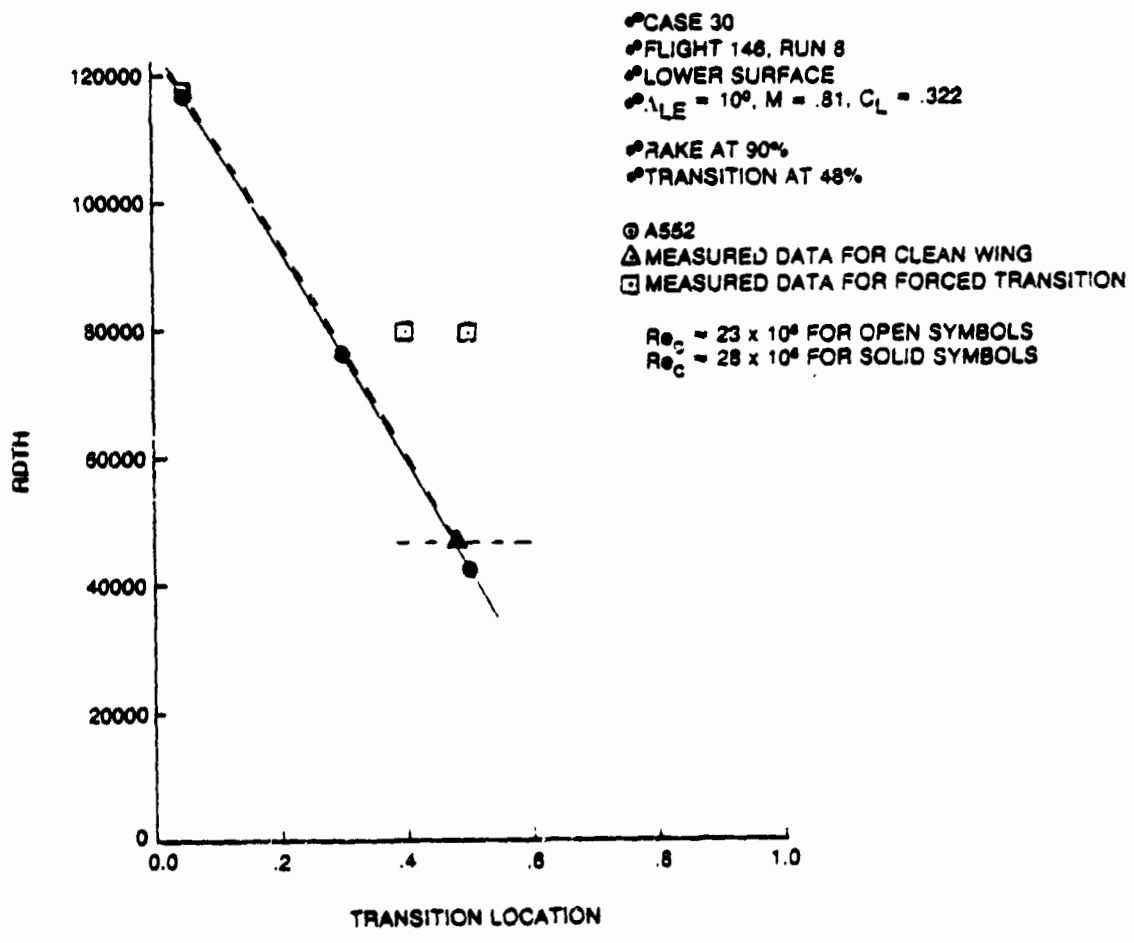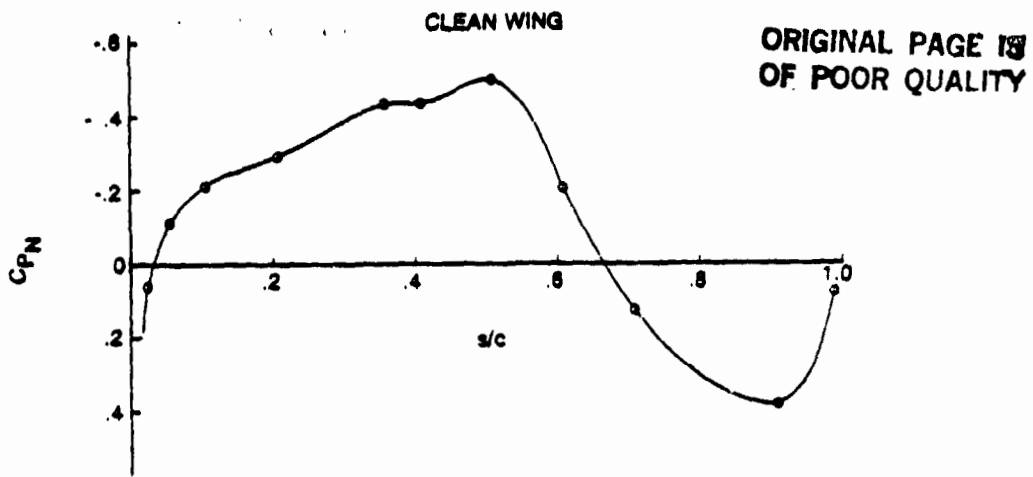
Figure C-30. Transition Determination, Case 30 F-111 NLF Glove

CLEAN WING

CASE 31
FLIGHT 146, RUN 9
LOWER SURFACE
$\Lambda_{LE} = 10°$, $M = .82$, $C_L = .314$

RAKE AT 90%
TRANSITION AT 49%

A552
MEASURED DATA FOR CLEAN WING
MEASURED DATA FOR FORCED TRANSITION

$Re_c \approx 23 \times 10^6$ FOR OPEN SYMBOLS
$Re_c \approx 27.5$ FOR SOLID SYMBOLS

TRANSITION LOCATION

Figure C-31. Transition Determination, Case 31 F-111 NLF Glove

CLEAN WING

- CASE 32
- FLIGHT 146, RUN 17A
- LOWER SURFACE
- Λ_{LE} = 15°, M = .83, C_L = 292

- RAKE AT 90%
- TRANSITION AT 51%

○ A552
△ MEASURED DATA FOR CLEAN WING
□ MEASURED DATA FOR FORCED TRANSITION

Re_c ≈ 23 x 10⁶ FOR OPEN SYMBOLS
Re_c ≈ 27.6 FOR SOLID SYMBOLS
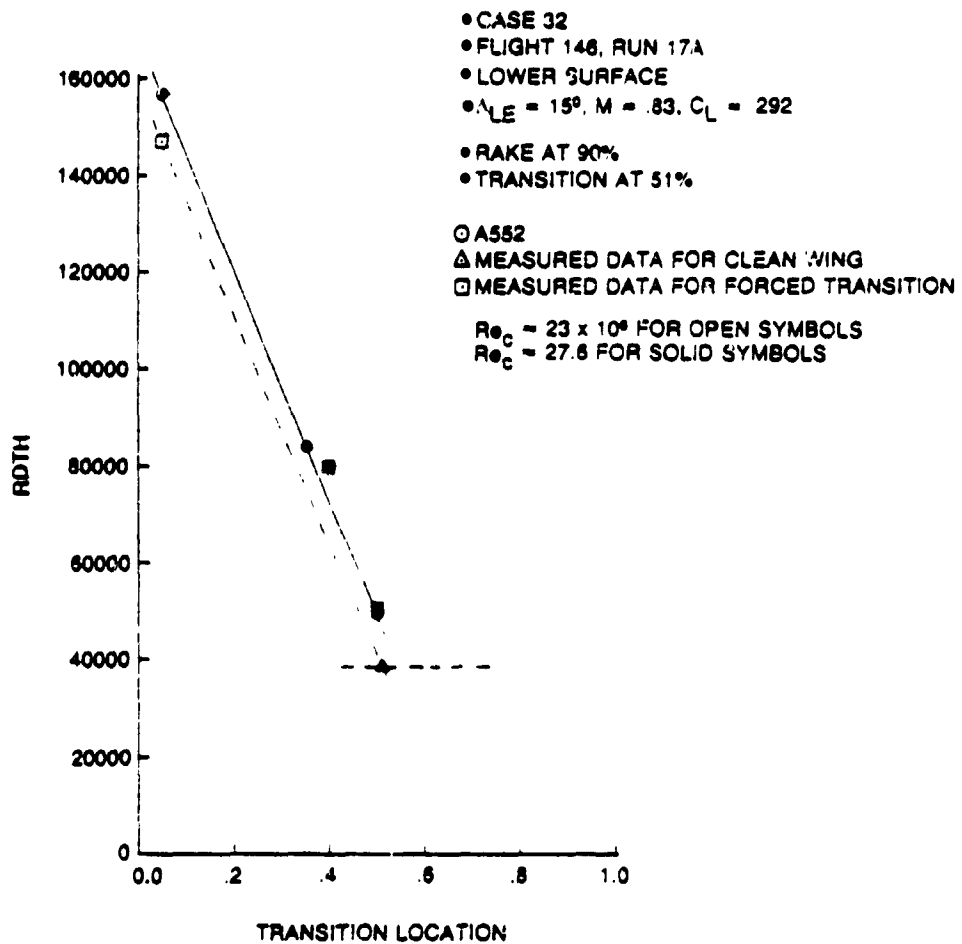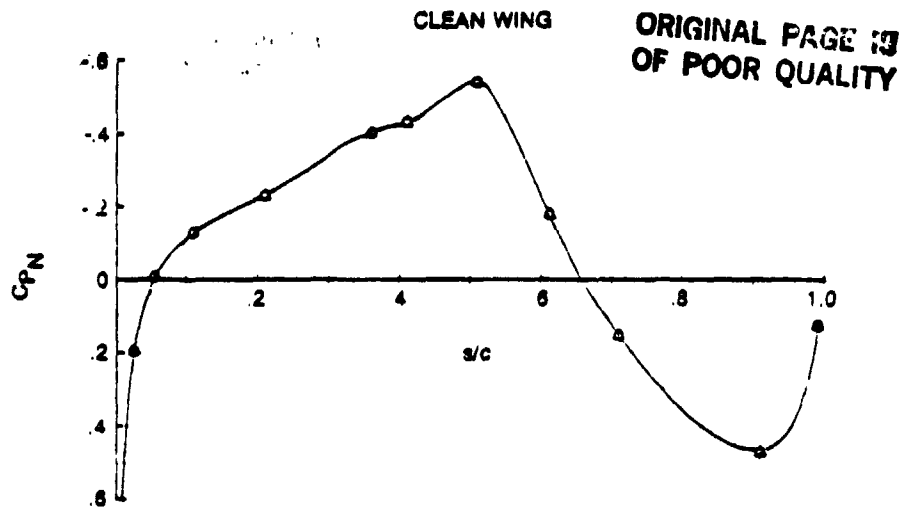
Figure C-32. Transition Determination, Case 32 F-111 NLF Glove

CLEAN WING

CASE 33
FLIGHT 146, RUN 17B
LOWER SURFACE
$\Lambda_{LE} = 15^\circ$, M = .83, $C_L = 415$

RAKE AT 90%
TRANSITION AT 51%

○ A552
△ MEASURED DATA FOR CLEAN WING
□ MEASURED DATA FOR FORCED TRANSITION

$Re_c = 23 \times 10^6$ FOR OPEN SYMBOLS
$Re_c = 28 \times 10^6$ FOR SOLID SYMBOLS
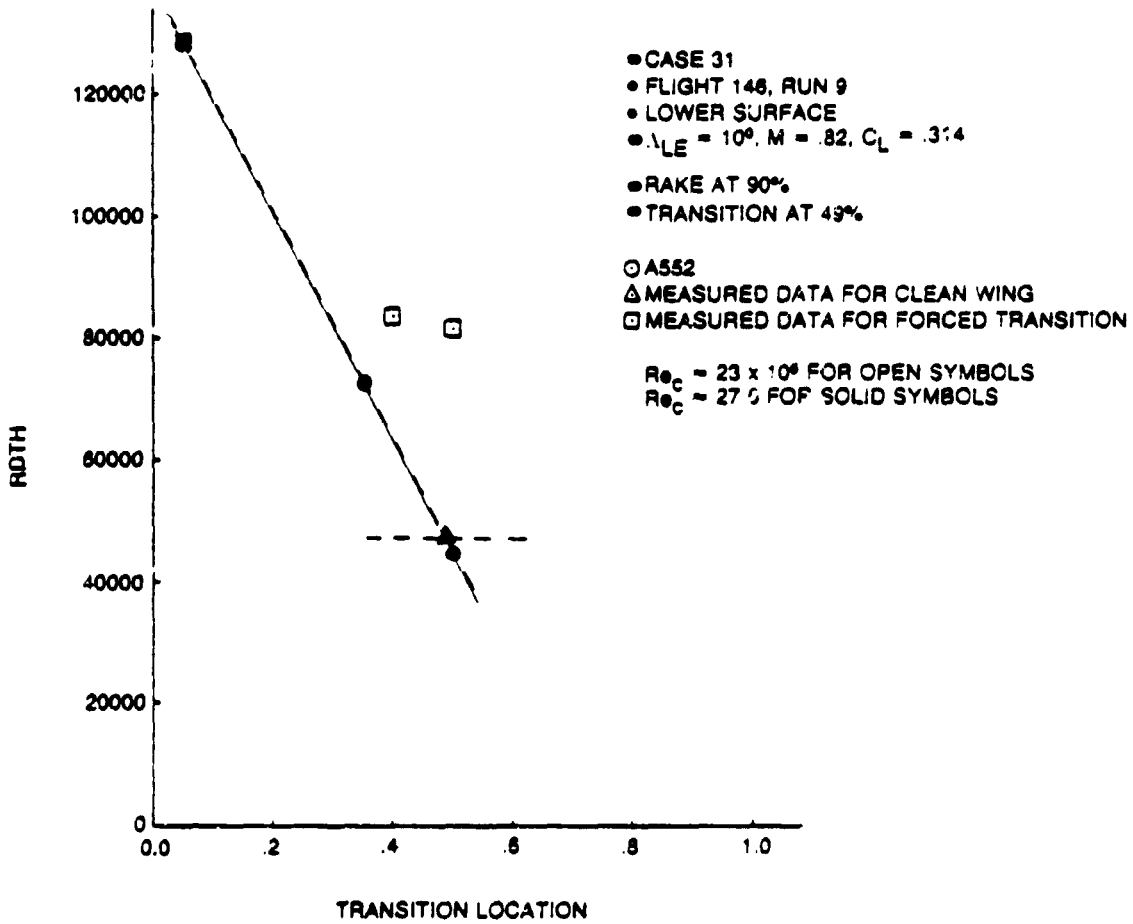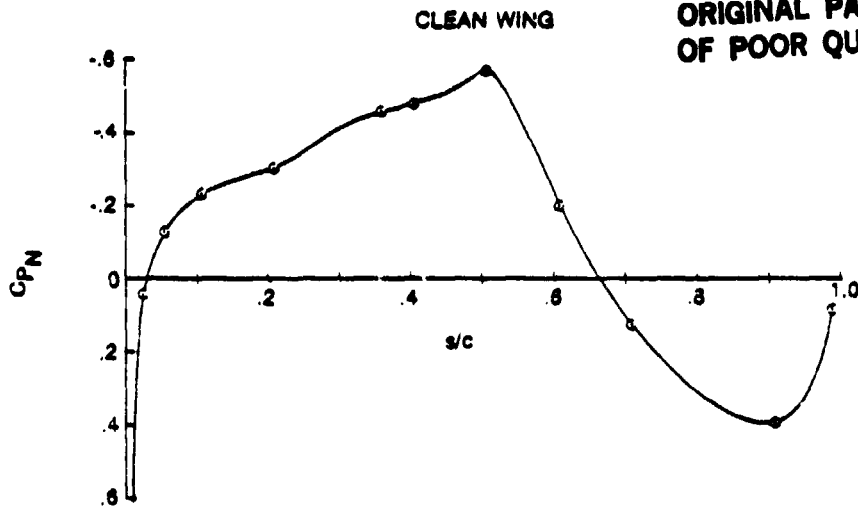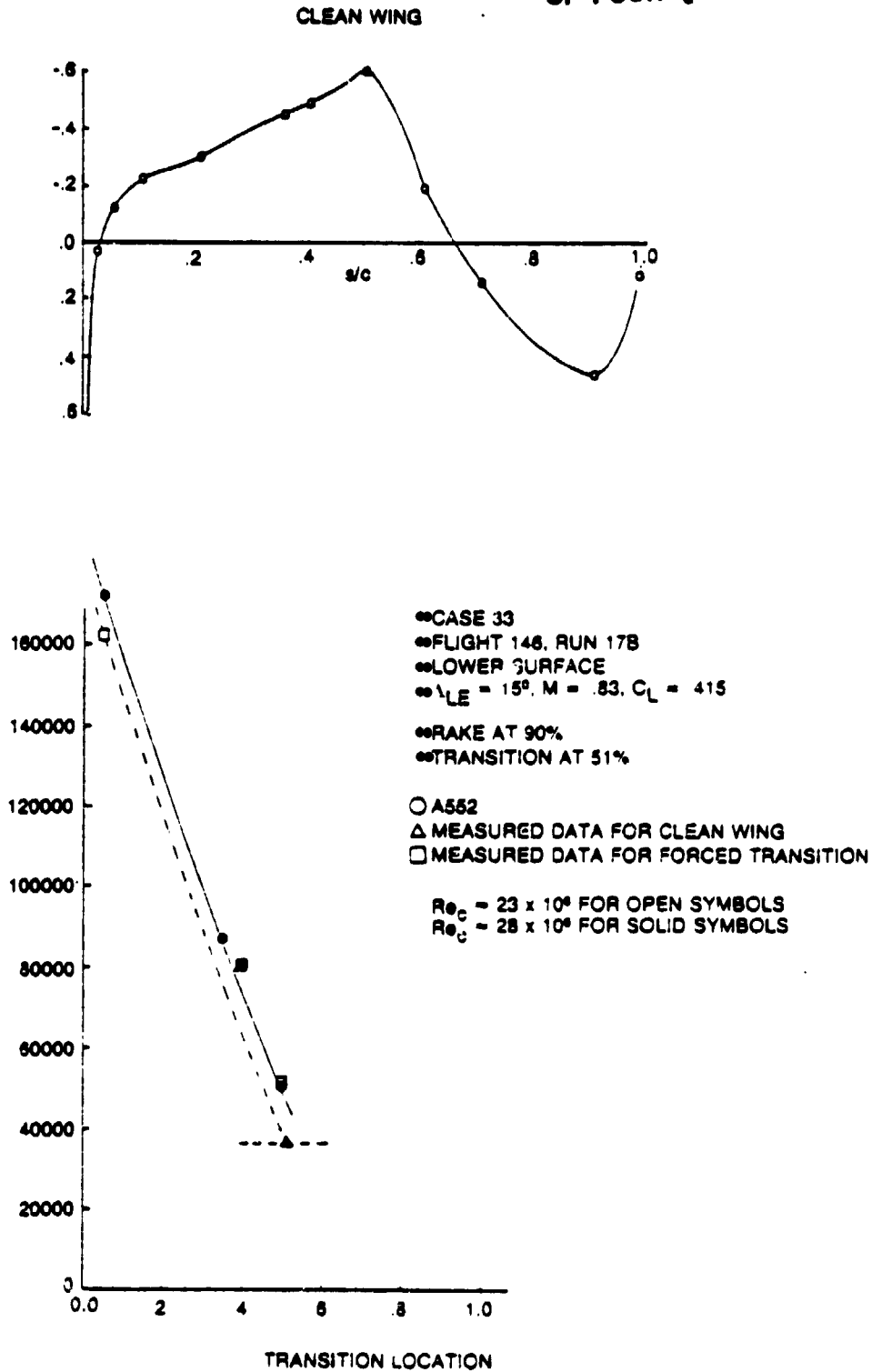
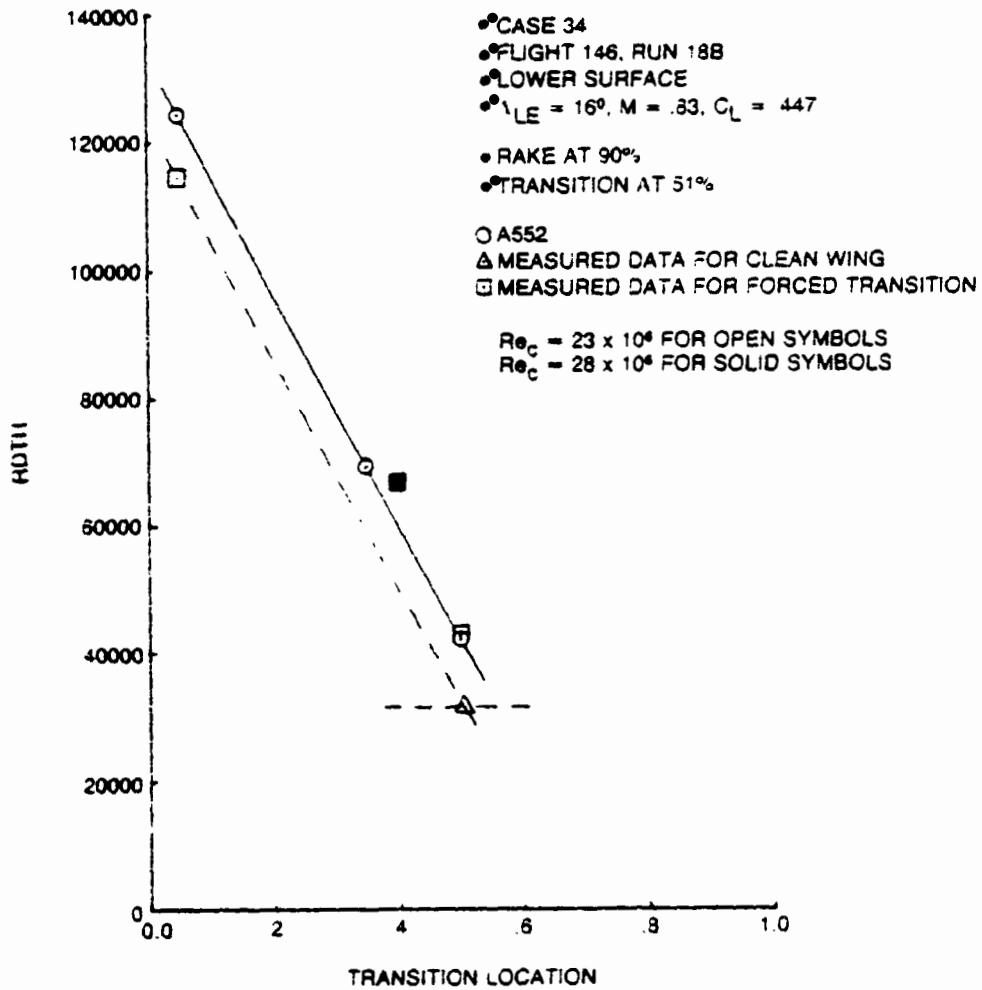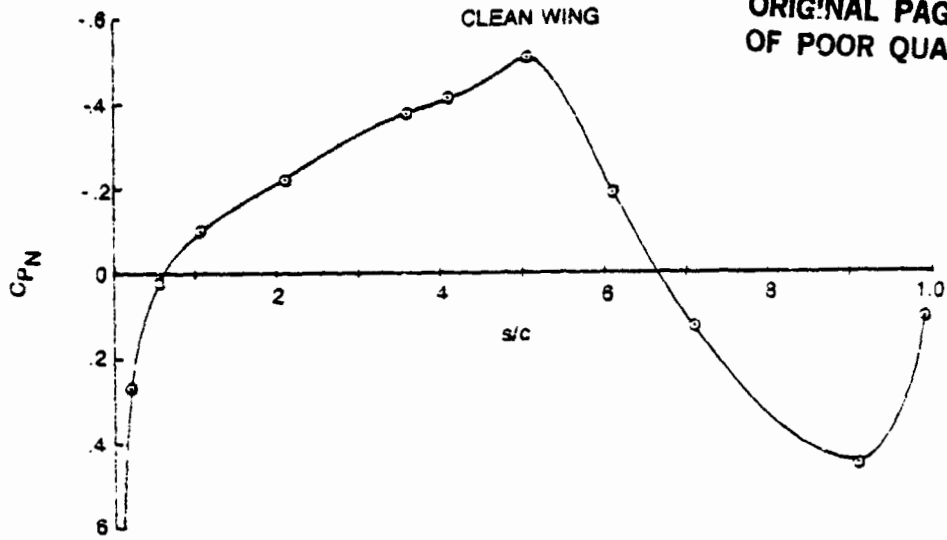TRANSITION LOCATION

Figure C-33. Transition Determination, Case 33 F-111 NLF Glove

Figure C-34. Transition Determination, Case 34 F-111 NLF Glove

APPENDIX D

C-F AND T-S DISTURBANCE GROWTH CURVES

Page

PRECEDING PAGE BLANK NOT FILMED

PAGE _D-2_ INTENTIONALLY BLANK

APPENDIX D: C-F AND T-S DISTURBANCE GROWTH CURVES

This appendix contains the C-F and T-S disturbance growth curves used to define the envelopes for each case. As explained in Section 6.1.2, for the T-S disturbances, a range of frequencies was analyzed, and for the C-F disturbances, a range of values of $\alpha *_{r_s}$ (spanwise component of the dimensional wavenumber) was analyzed. In the plots shown here, $KS = \alpha *_{r_s}$. For the T-S disturbances, wave angle was kept fixed at 40 deg for the upper surface cases and at 25 deg for the lower surface cases. These angles closely correspond to the direction of peak amplification. The frequencies corresponding to the T-S disturbances analyzed are listed in each figure. These frequencies can be related to the T-S curves using the one curve in each case for which the frequency has been noted by an arrow. The higher frequencies in the list correspond, in order, to the curves that peak ahead of the indicated curve, and the lower frequencies correspond, in order, to the curves that peak behind the indicated curve.

PAGE $D-4$ INTENTIONALLY BLANK
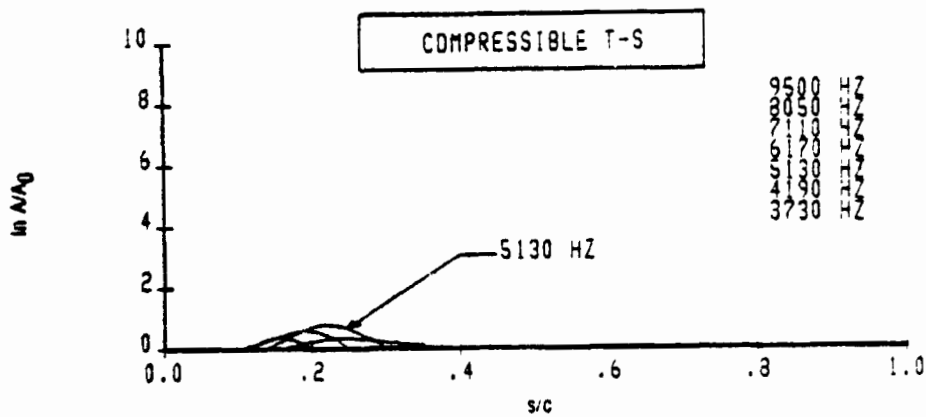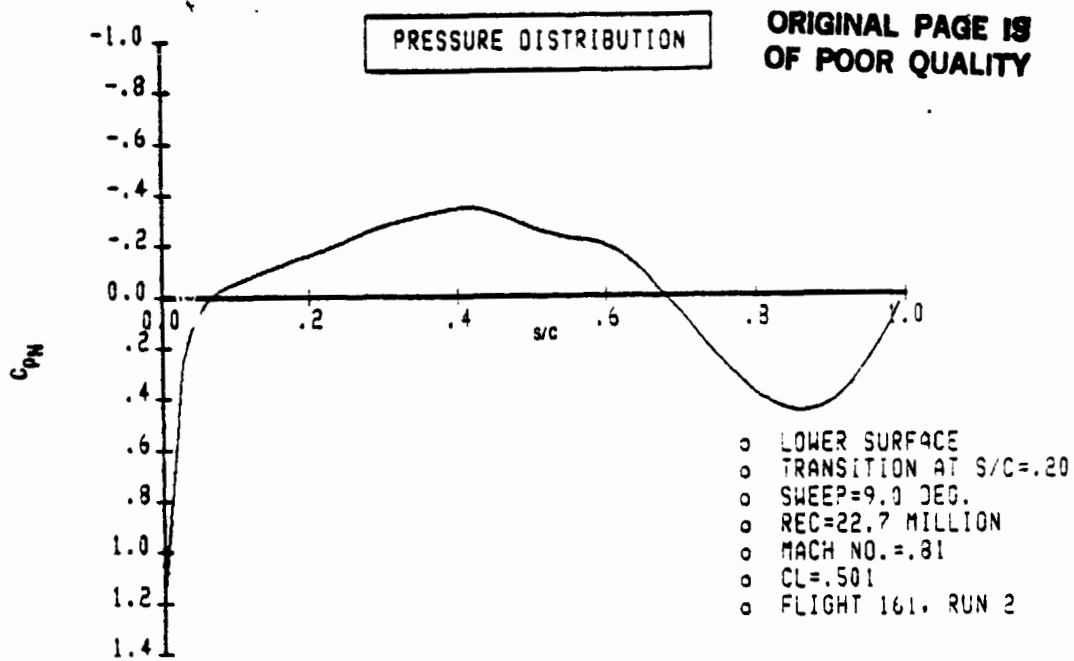
Figure D-1.   F-111 Stability Analysis Results Case 2, Lower Surface

PRESSURE DISTRIBUTION

o LOWER SURFACE
o TRANSITION AT S/C=.14
o SWEEP=16.0 DEG.
o REC=28.2 MILLION
o MACH NO.=.83
o CL=.387
o FLIGHT 161. RUN 20

COMPRESSIBLE T-S

5550 HZ

12700 HZ
11630 HZ
10730 HZ
9480 HZ
8230 HZ
6800 HZ
5550 HZ
4000 HZ

COMPRESSIBLE C-F

o RANGE OF KS VALUES: 300 TO 1600
o FREQUENCY=0 HZ
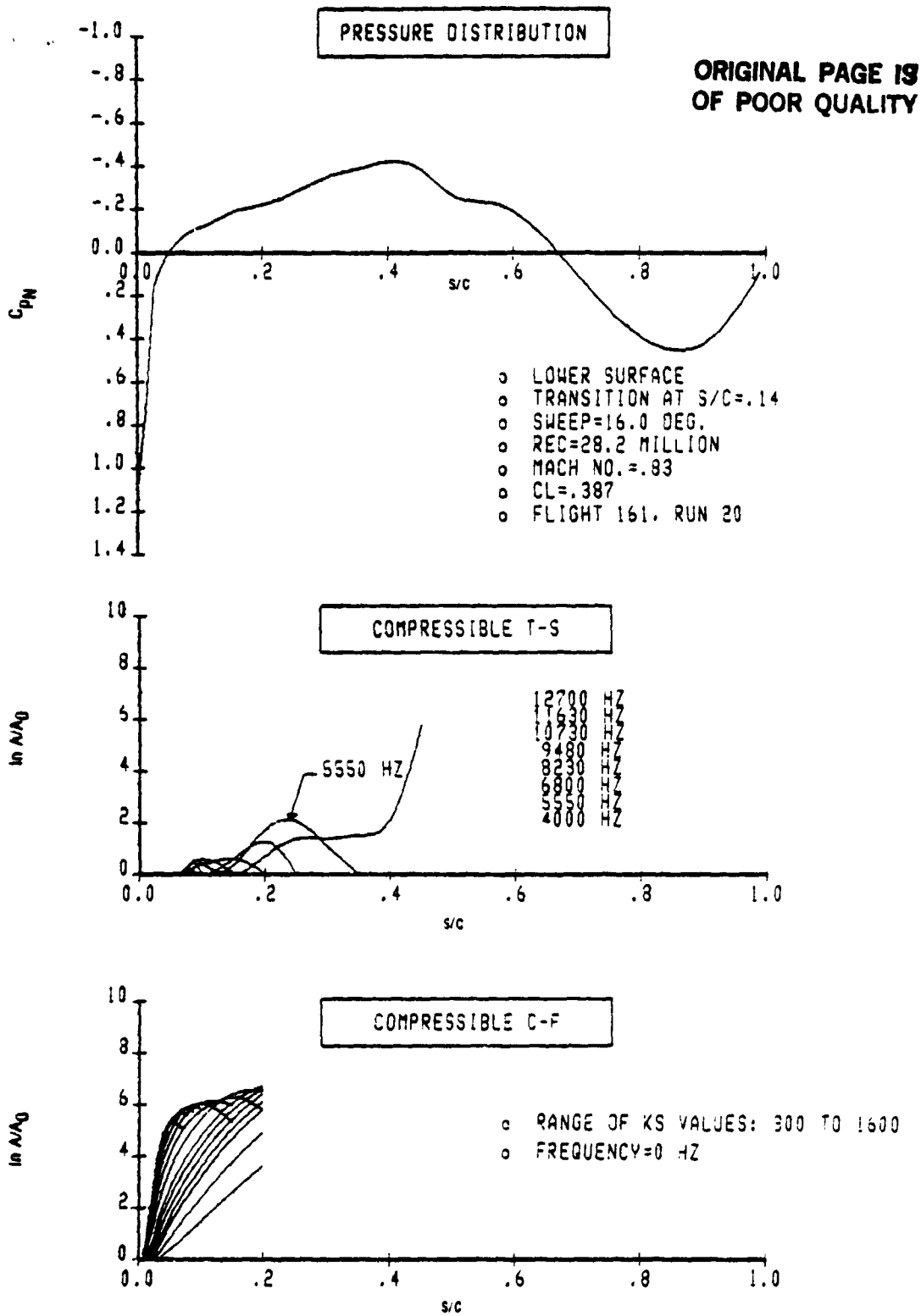
Figure D-2.   F-111 Stability Analysis Results Case 3, Lower Surface

PRESSURE DISTRIBUTION

C_{p_N}

s/c

o LOWER SURFACE
o TRANSITION AT S/C=.13
o SWEEP=19.0 DEG.
o REC=23.3 MILLION
o MACH NO.=.83
o CL=.394
o FLIGHT 161, RUN 11

COMPRESSIBLE T-S

$\ln A/A_0$

4370 HZ

8400 HZ
7560 HZ
6440 HZ
5350 HZ
4370 HZ
3890 HZ

s/c

COMPRESSIBLE C-F

$\ln A/A_0$

o RANGE OF <S VALUES: 300 TO 1600
o FREQUENCY=0 HZ

s/c

Figure D-3.   F-111 Stability Analysis Results Case 6, Lower Surface

PRESSURE DISTRIBUTION

ORIGINAL PAGE IS
OF POOR QUALITY

o LOWER SURFACE
o TRANSITION AT S/C=.08
o SWEEP=21.7 DEG.
o REC=23.6 MILLION
o MACH NO.=.94
o CL=.382
o FLIGHT 161, RUN 112

COMPRESSIBLE T-S

4840 HZ

COMPRESSIBLE C-F

o RANGE OF KS VALUES: 50 TO 1400
o FREQUENCY=0 HZ
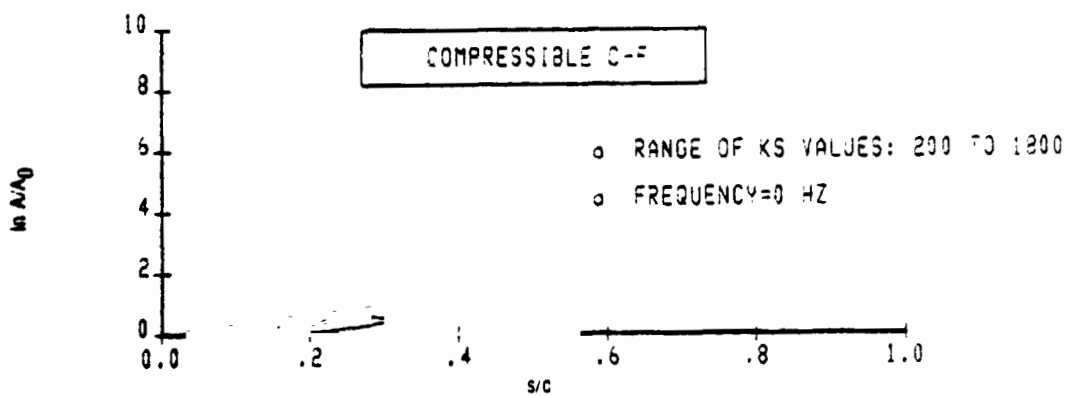
Figure D-4.   F-111 Stability Analysis Results Case B, Lower Surface

PRESSURE DISTRIBUTION

o UPPER SURFACE
o TRANSITION AT S/C=.23
o SWEEP=15.9 DEG.
o REC=23.3 MILLION
o MACH NO.=.83
o CL=.397
o FLIGHT 161, RUN 7

COMPRESSIBLE T-S

7000 HZ
6000 HZ
5000 HZ
4000 HZ

5000 HZ

COMPRESSIBLE C-F

o RANGE OF KS VALUES: 200 TO 1600
o FREQUENCY=0 HZ

Figure D-5.   F-111 Stability Analysis Results Case 12, Upper Surface

PRESSURE DISTRIBUTION

o UPPER SURFACE
o TRANSITION AT S/C=.17
o SWEEP=18.8 DEG.
o REC=27.1 MILLION
o MACH NO.=.93
o CL=.377
o FLIGHT 161, RUN 25

COMPRESSIBLE T-S

5000 HZ

7000 HZ
6000 HZ
5000 HZ
4000 HZ

COMPRESSIBLE C-F

o RANGE OF KS VALUES: 300 TO 1500
o FREQUENCY=0 HZ

Figure D-6.   F-111 Stability Analysis Results Case 13, Upper Surface

PRESSURE DISTRIBUTION

o UPPER SURFACE
o TRANSITION AT S/C= 21
o SWEEP=25.2 DEG.
o REC=23.9 MILLION
o MACH NO.=.85
o CL=.373
o FLIGHT 161, RUN 12

COMPRESSIBLE T-S

7000 HZ
6000 HZ
5000 HZ
4000 HZ

5000 HZ

COMPRESSIBLE C-F
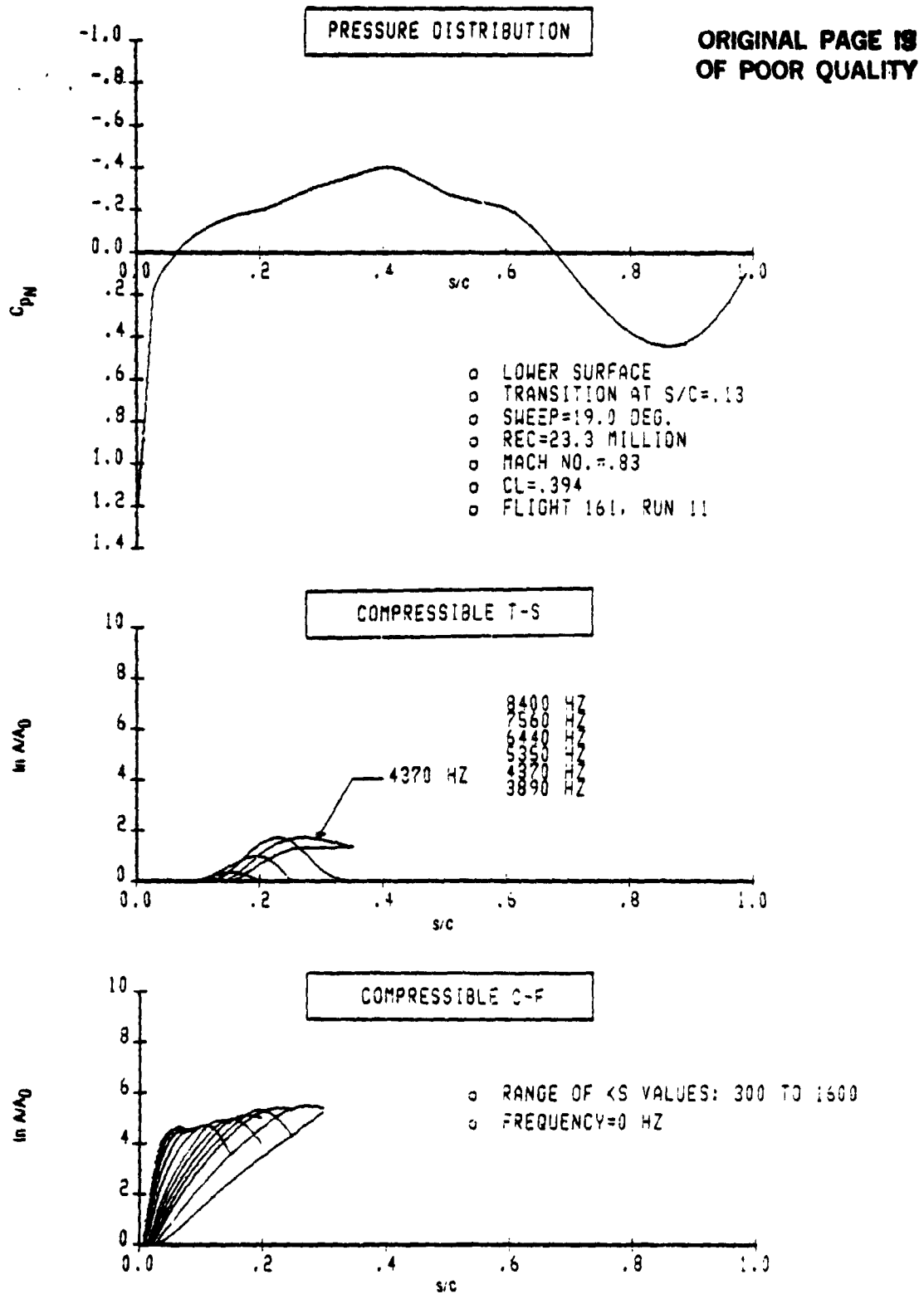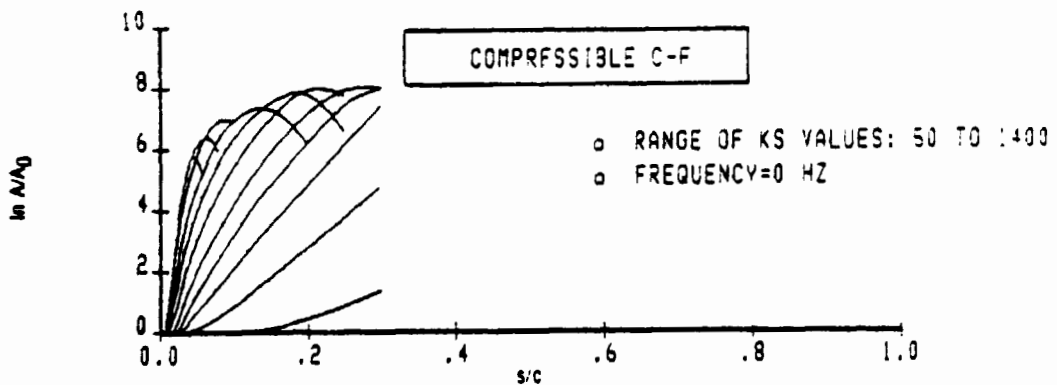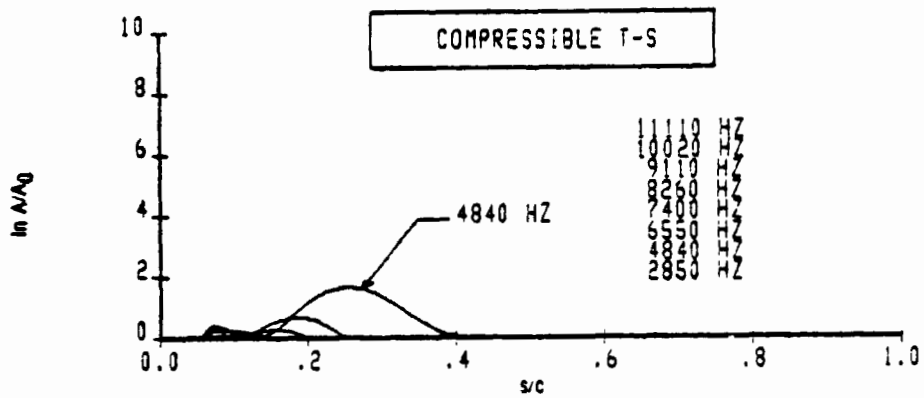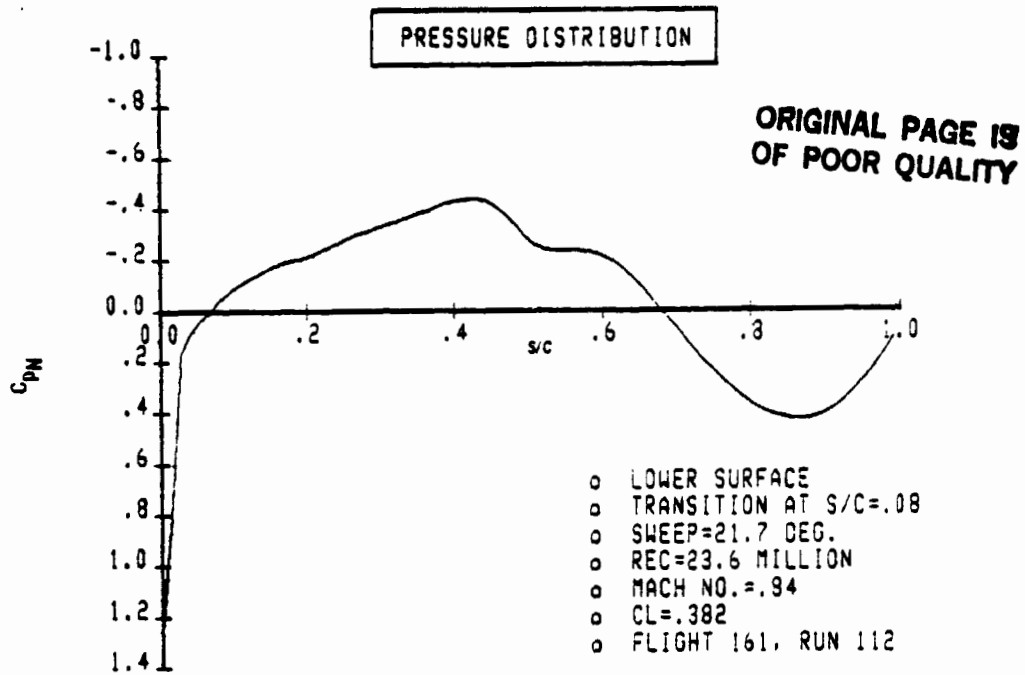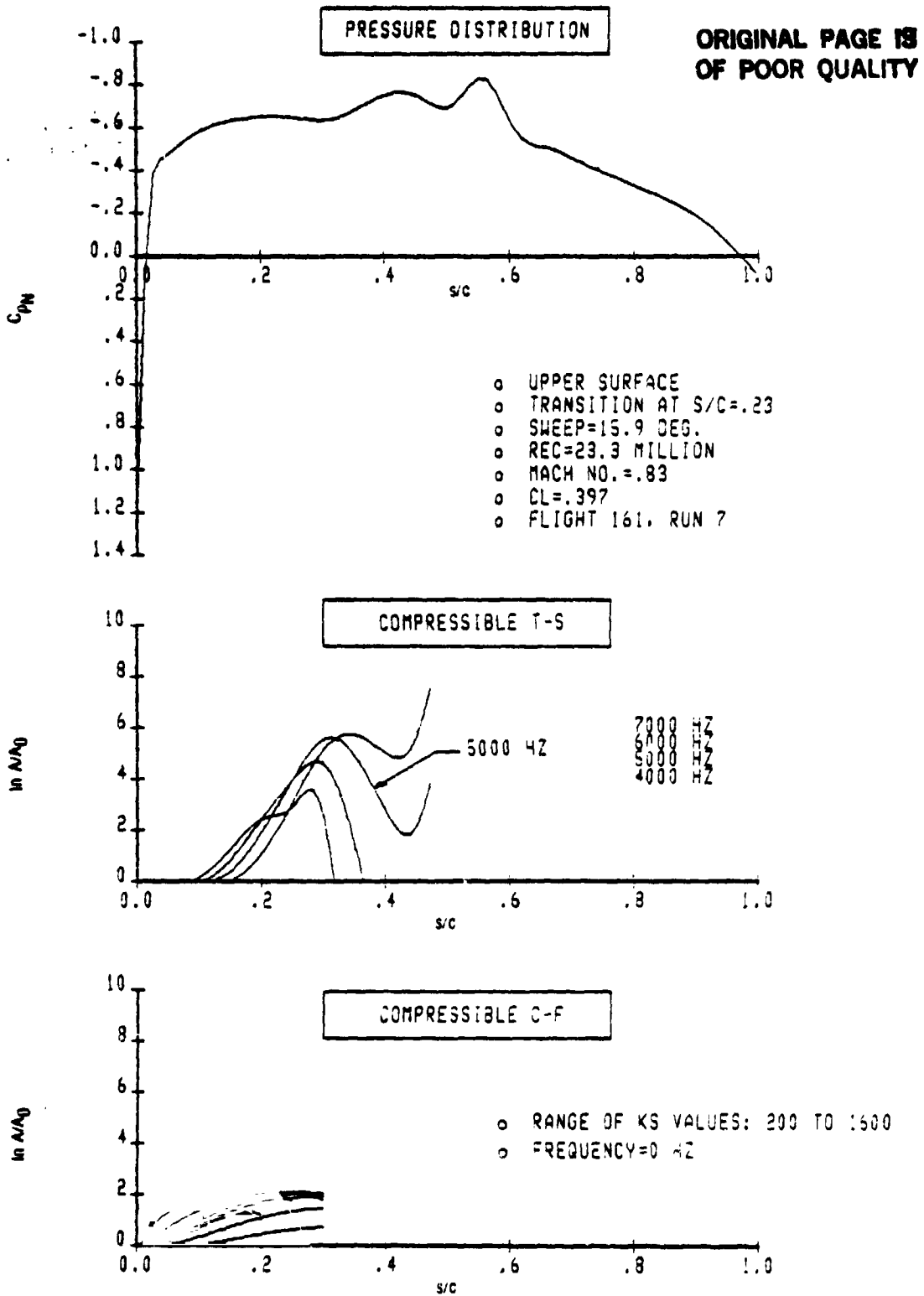
o RANGE OF KS VALUES: 200 TO 1600
o FREQUENCY=0 HZ
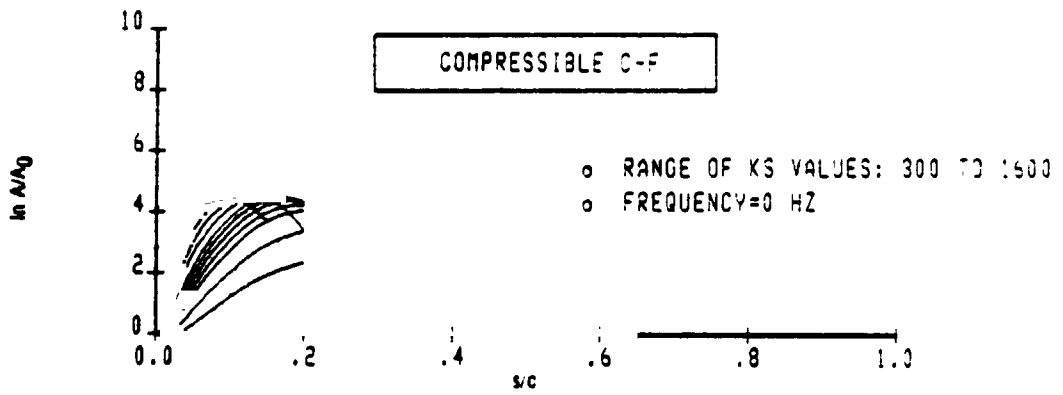
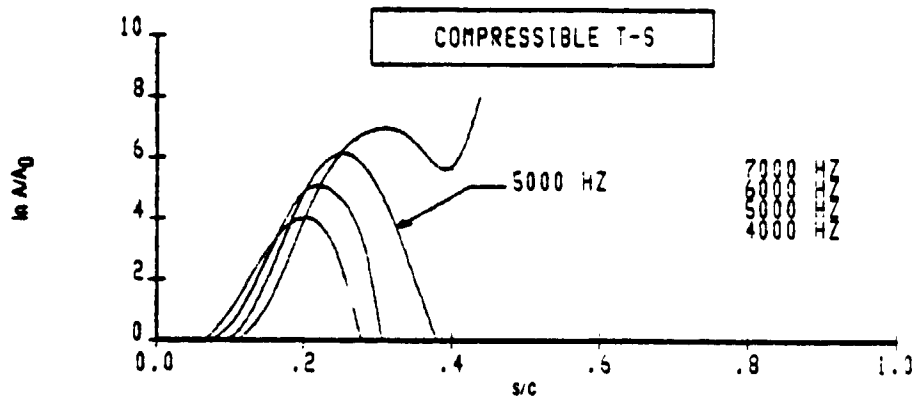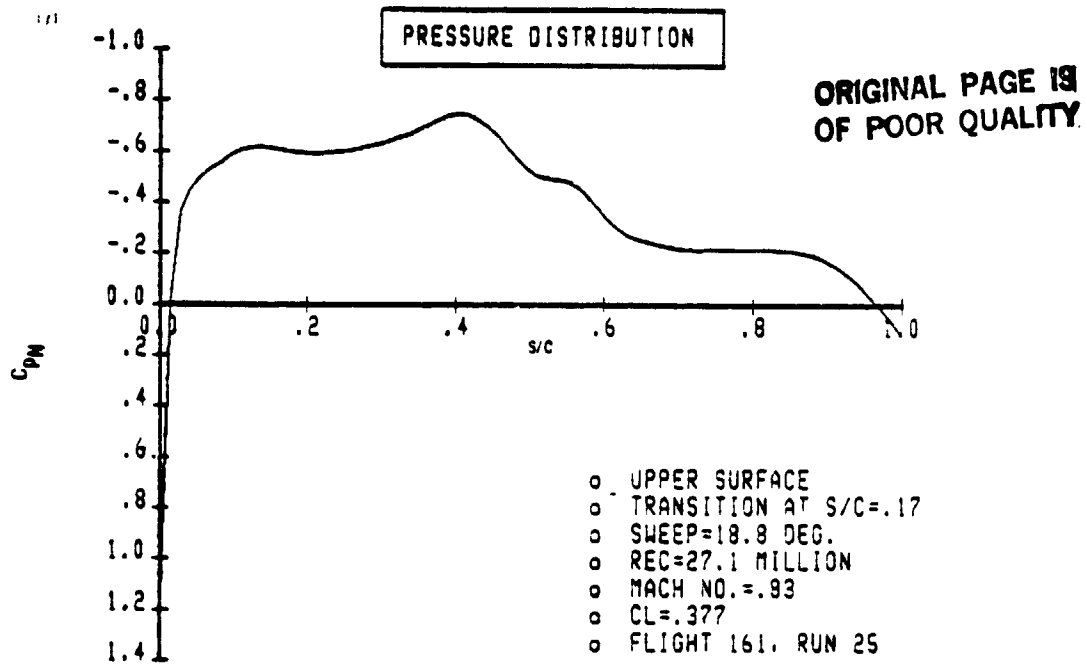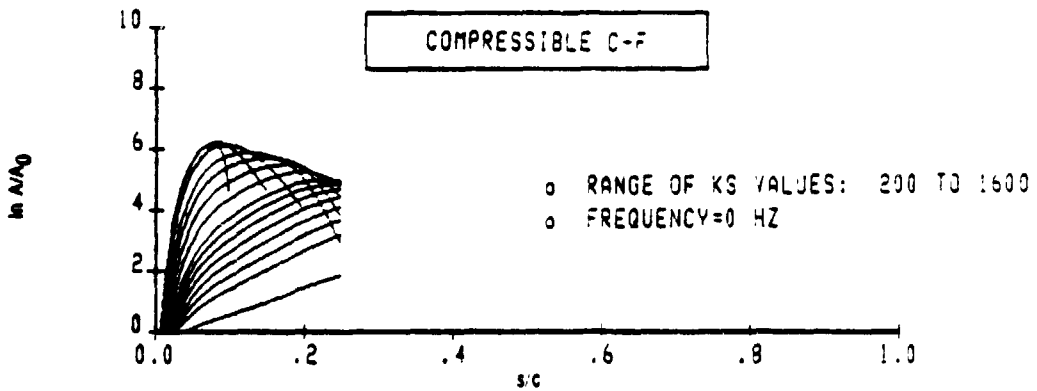Figure D-   F-111 Stability Analysis Results Case 15, Upper Surface
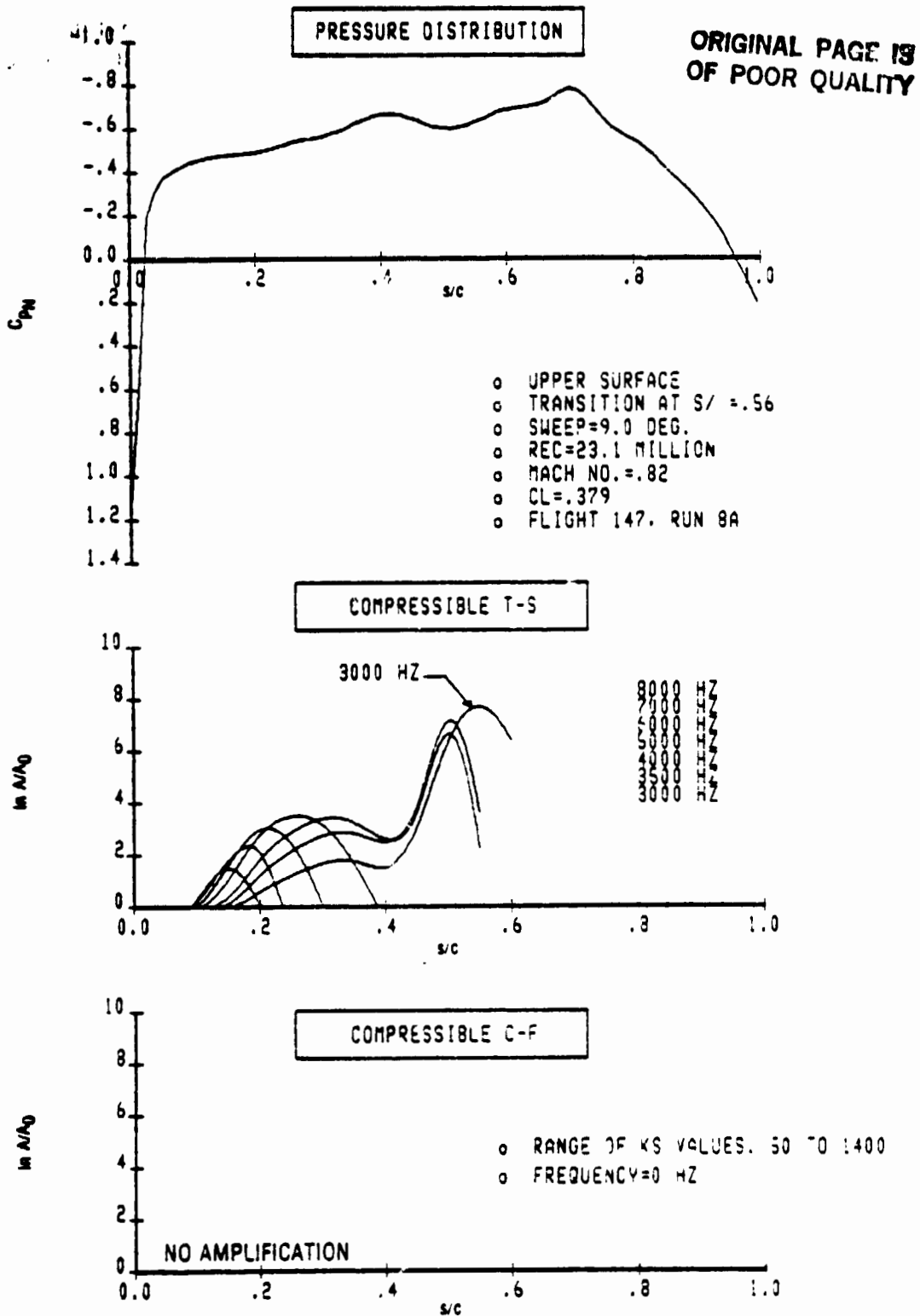
Figure D-8.   F-111 Stability Analysis Results Case 16, Upper Surface

PRESSURE DISTRIBUTION

- o UPPER SURFACE
- o TRANSITION AT S/C=.55
- o SWEEP=9.0 DEG.
- o REC=27.9 MILLION
- o MACH NO.=.82
- o CL=.432
- o FLIGHT 155, RUN 18

COMPRESSIBLE T-S

3100 HZ

COMPRESSIBLE C-F

- o RANGE OF KS VALUES: 50 TO 1400
- o FREQUENCY=0 HZ

NO AMPLIFICATION

Figure D-9.   F-111 Stability Analysis Results Case 17, Upper Surface

PRESSURE DISTRIBUTION

C_{p_N}

-1.0
-.8
-.6
-.4
-.2
0.0
.2
.4
.6
.8
1.0
1.2
1.4

.2 .4 .6 .8 1.0
s/c

o UPPER SURFACE
o TRANSITION AT S/C=.45
o SWEEP=9.0 DEG.
o REC=23.0 MILLION
o MACH NO.=.82
o CL=.504
o FLIGHT 158, RUN 3

COMPRESSIBLE T-S

$\ln A/A_0$

14
12
10
8
6
4
2
0

4000 HZ

7000 HZ
6000 HZ
5000 HZ
4000 HZ
3000 HZ
2000 HZ

0.0 .2 .4 .6 .8 1.0
s/c

COMPRESSIBLE C-F

$\ln A/A_0$

10
8
6
4
2
0

o RANGE OF KS VALUES: 50 TO 1400
o FREQUENCY=0 HZ

NO AMPLIFICATION

0.0 .2 .4 .6 .8 1.0
s/c

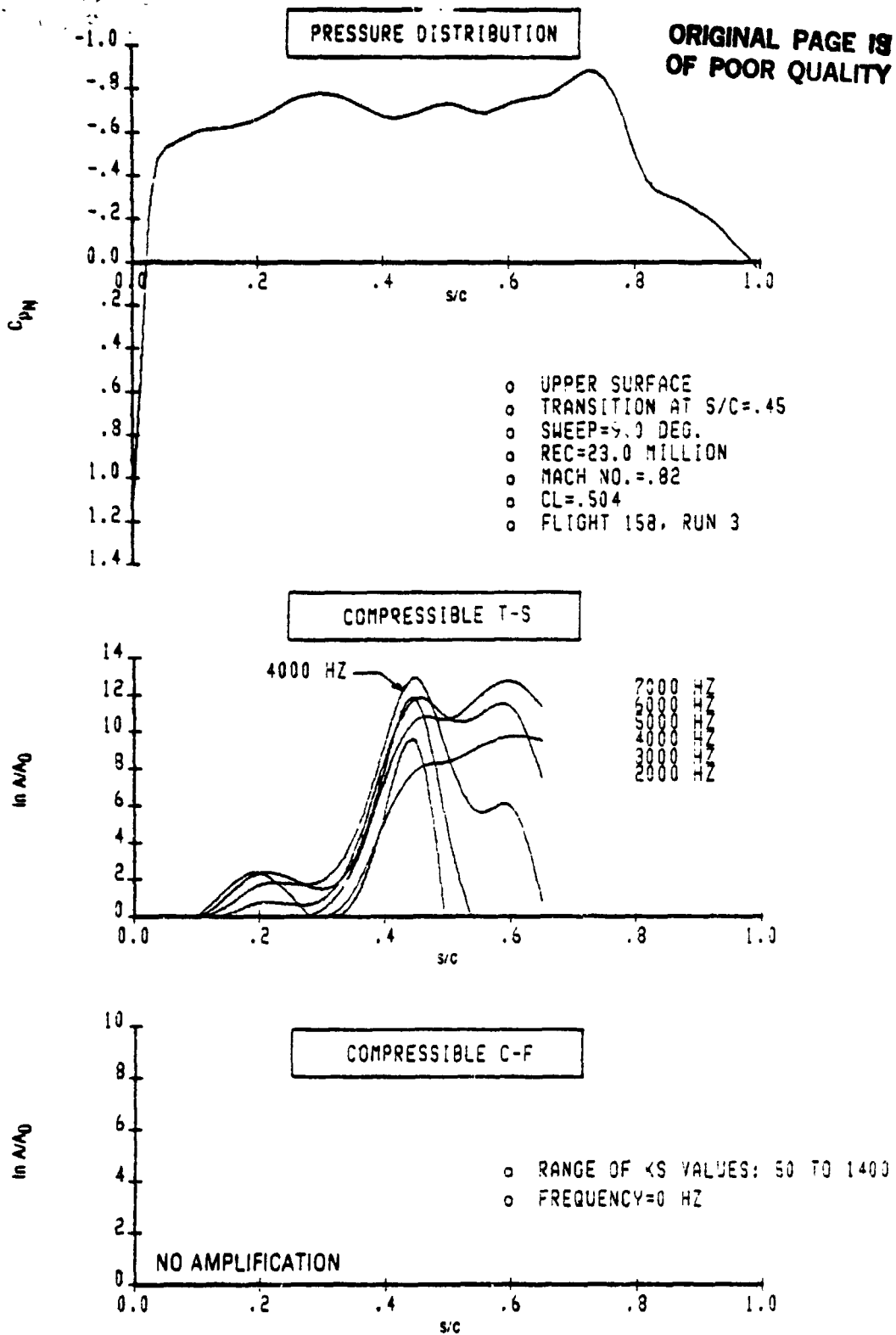*Figure D-10.   F-111 Stability Analysis Results Case 18, Upper Surface*

PRESSURE DISTRIBUTION

o UPPER SURFACE
o TRANSITION AT S/C=.36
o SWEEP=16.1 DEG.
o REC=23.3 MILLION
o MACH NO.=.83
o CL=.379
o FLIGHT 147, RUN 14

COMPRESSIBLE T-S

5000 HZ

7000 HZ
6000 HZ
5000 HZ
4000 HZ

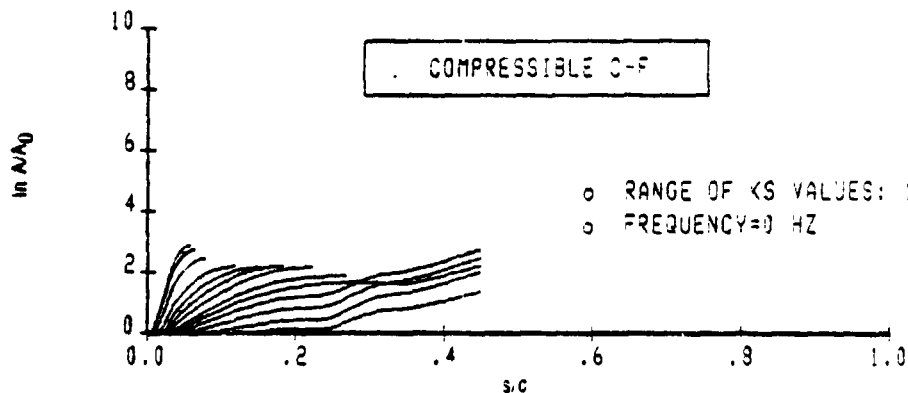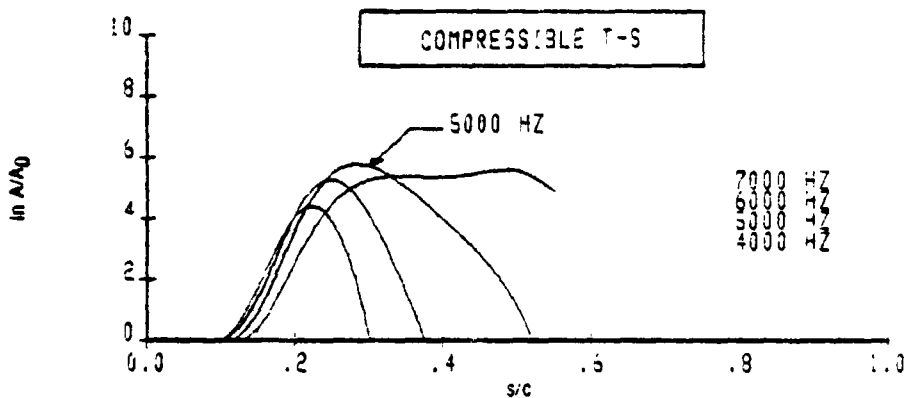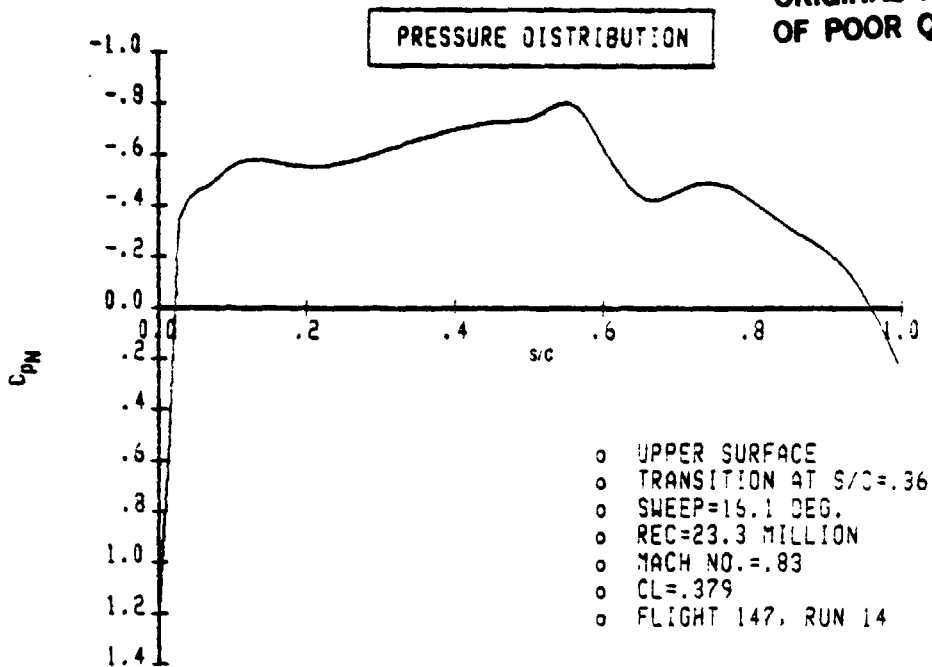**COMPRESSIBLE C-F**

o RANGE OF KS VALUES: 150 TO 1400
o FREQUENCY=0 HZ

Figure D-11.   F-111 Stability Analysis Results Case 19, Upper Surface

PRESSURE DISTRIBUTION
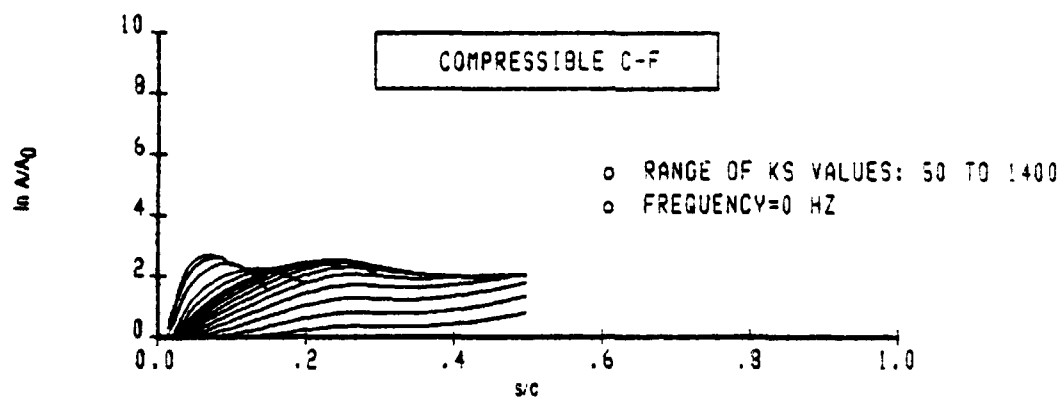
C_{p_N}

s/c

o UPPER SURFACE
o TRANSITION AT S/C=.42
o SWEEP=15.1 DEG.
o REC=23.3 MILLION
o MACH NO.=.83
o CL=.436
o FLIGHT 147, RUN 15

COMPRESSIBLE T-S

ln A/A$_0$

3500 HZ

8000 HZ
7000 HZ
6000 HZ
5000 HZ
4000 HZ
3500 HZ
3000 HZ

s/c

COMPRESSIBLE C-F

ln A/A$_0$

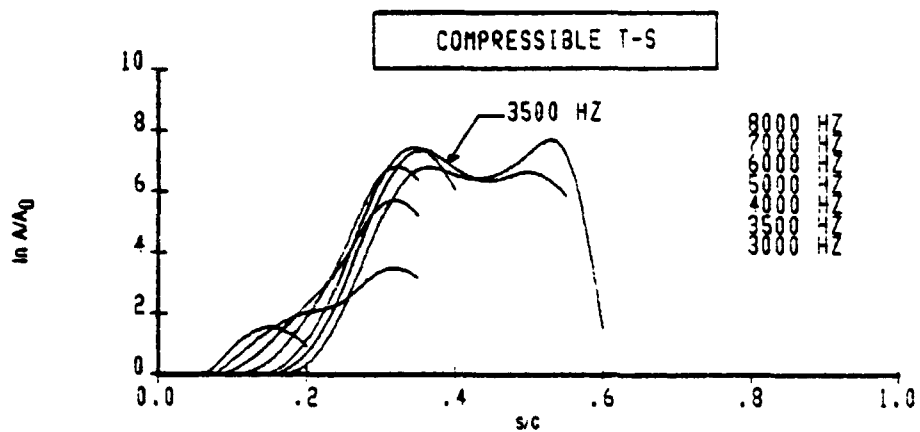o RANGE OF KS VALUES: 50 TO 1400
o FREQUENCY=0 HZ

s/c

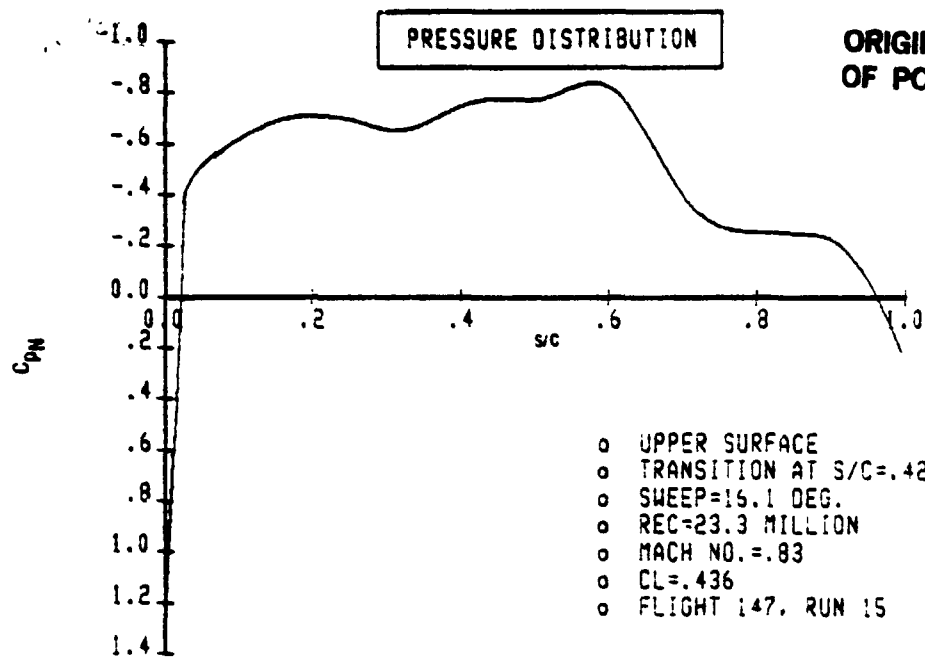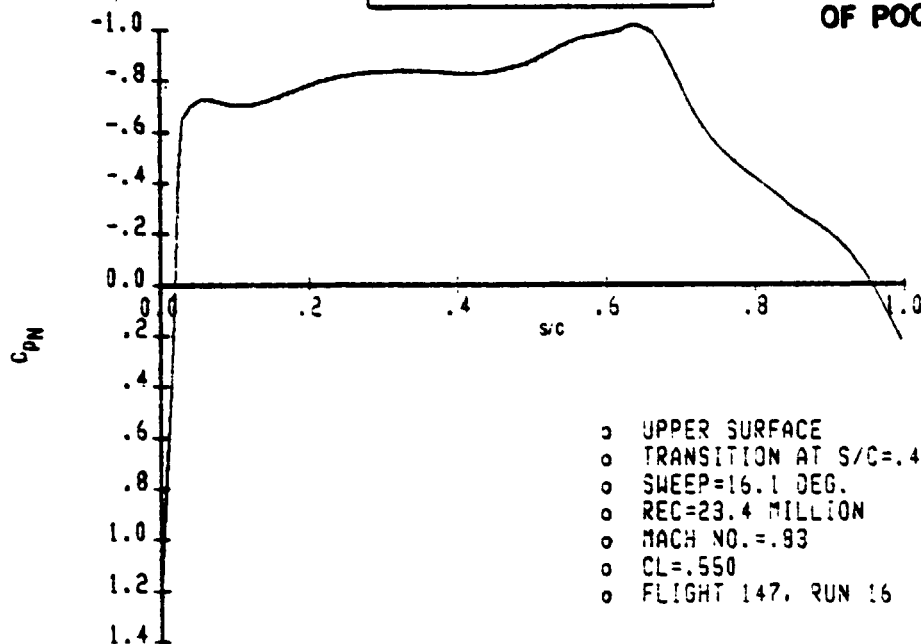Figure D-12.   F-111 Stability Analysis Results Case 20, Upper Surface

PRESSURE DISTRIBUTION

o UPPER SURFACE
o TRANSITION AT S/C=.43
o SWEEP=16.1 DEG.
o REC=23.4 MILLION
o MACH NO.=.93
o CL=.550
o FLIGHT 147, RUN 16

COMPRESSIBLE T-S

4000 HZ

7000 HZ
6000 HZ
5000 HZ
4000 HZ
3500 HZ
3000 HZ

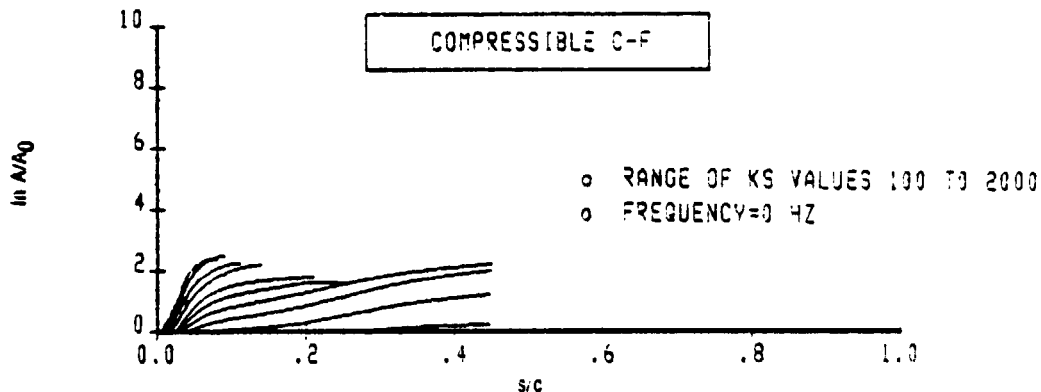## COMPRESSIBLE C-F

o RANGE OF KS VALUES 100 TO 2000
o FREQUENCY=0 HZ

Figure D-13.   F-111 Stability Analysis Results Case 21, Upper Surface

PRESSURE DISTRIBUTION

- o UPPER SURFACE
- o TRANSITION AT S/C=.20
- o SWEEP=25.2 DEG.
- o REC=28.9 MILLION
- o MACH NO.=.85
- o CL=.276
- o FLIGHT 158, RUN 23

COMPRESSIBLE T-S

4000 HZ

7000 HZ
6000 HZ
5000 HZ
4000 HZ

COMPRESSIBLE C-F

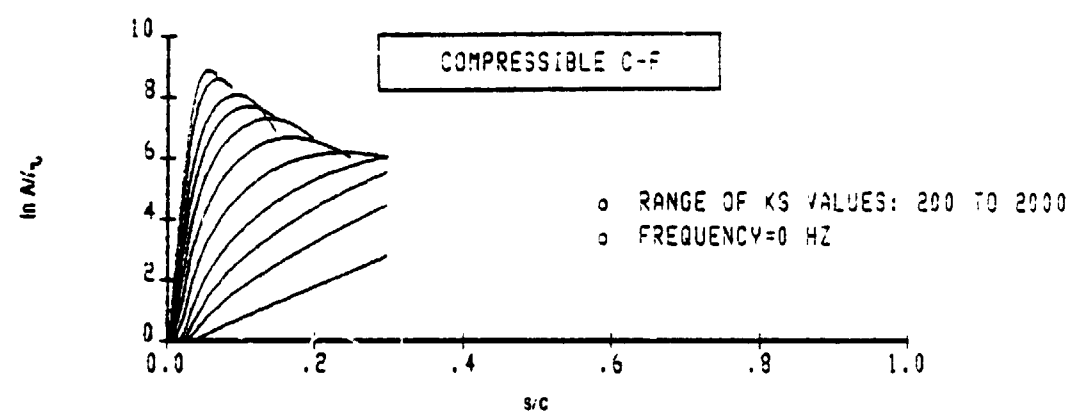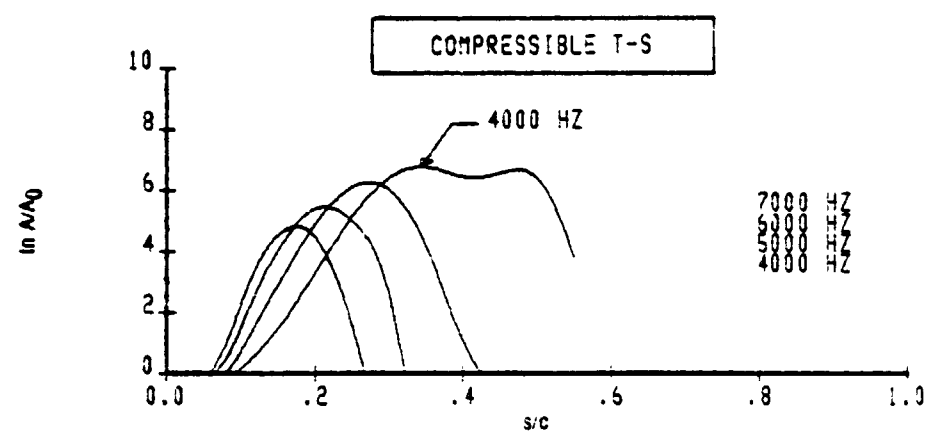- o RANGE OF KS VALUES: 200 TO 2000
- o FREQUENCY=0 HZ

Figure D-14.   F-111 Stability Analysis Results Case 22, Upper Surface

PRESSURE DISTRIBUTION

o   UPPER SURFACE
o   TRANSITION AT S/C=.15
o   SWEEP=25.2 DEG.
o   REC=23.8 MILLION
o   MACH NO.=.85
o   CL=.429
o   FLIGHT 155, RUN 13

COMPRESSIBLE T-S

6000 HZ

7000 HZ
6000 HZ
5000 HZ
4000 HZ

COMPRESSIBLE C-F

o   RANGE OF KS VALUES: 300 TO 1600
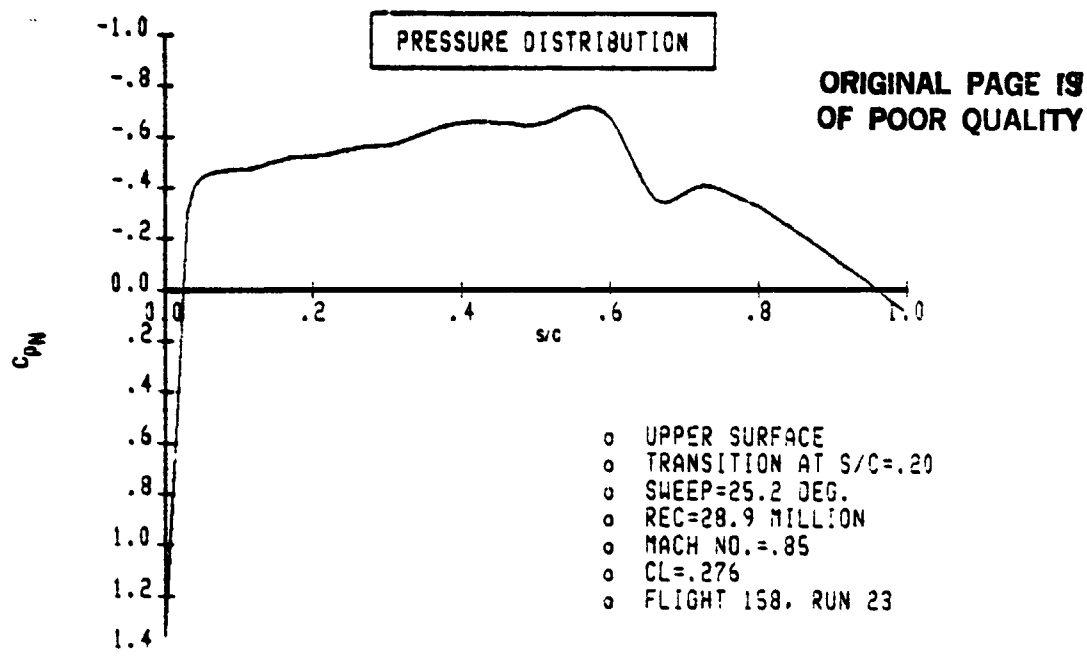o   FREQUENCY=0 HZ

Figure D-15.   F-111 Stability Analysis Results Case 24, Upper Surface

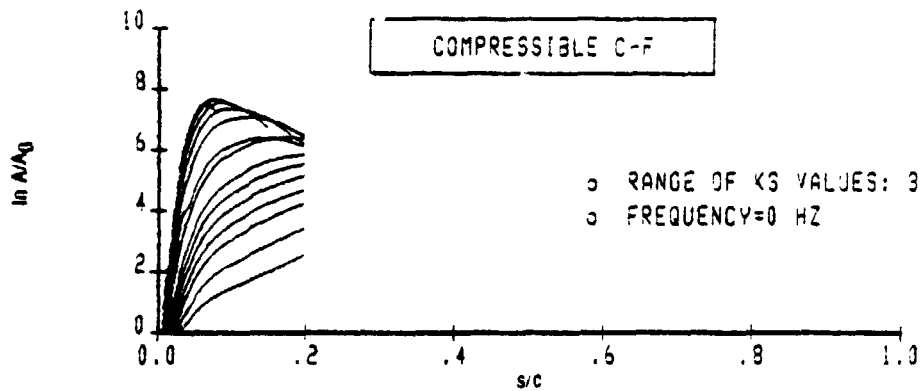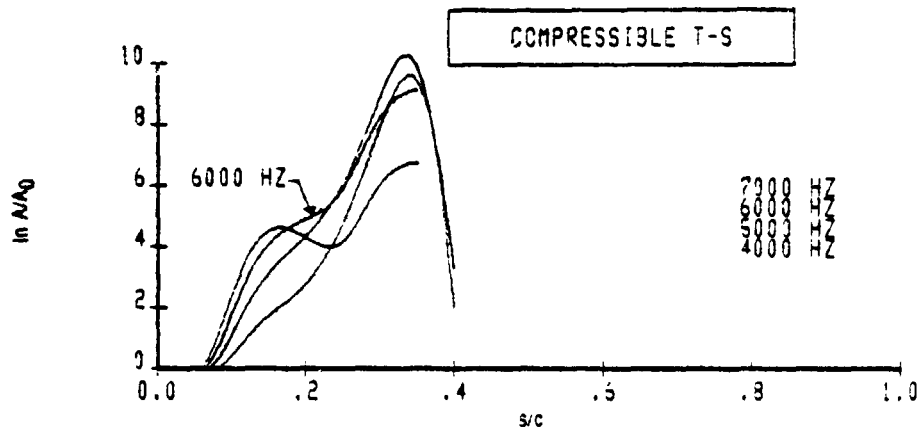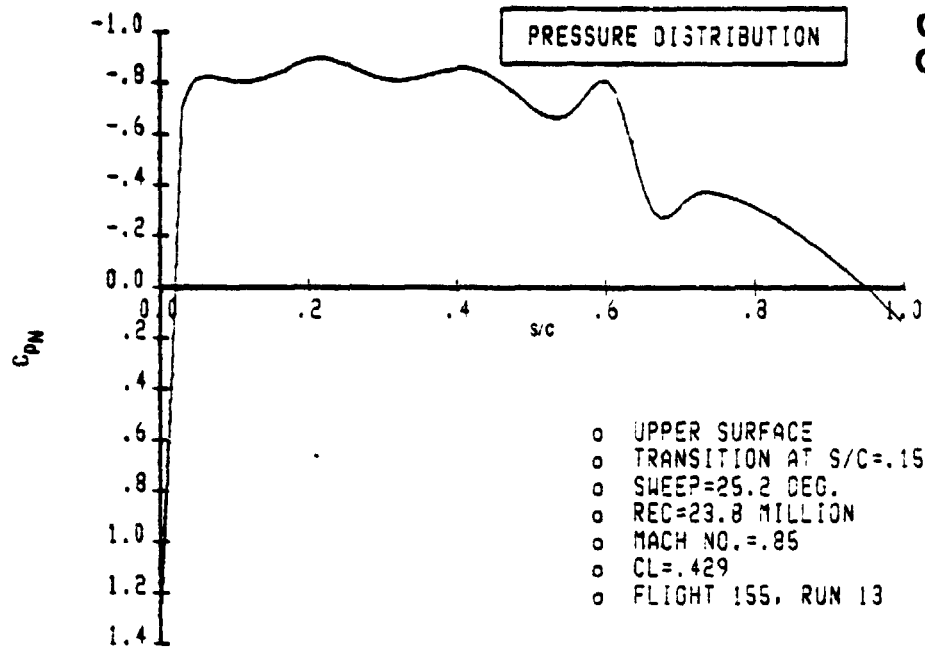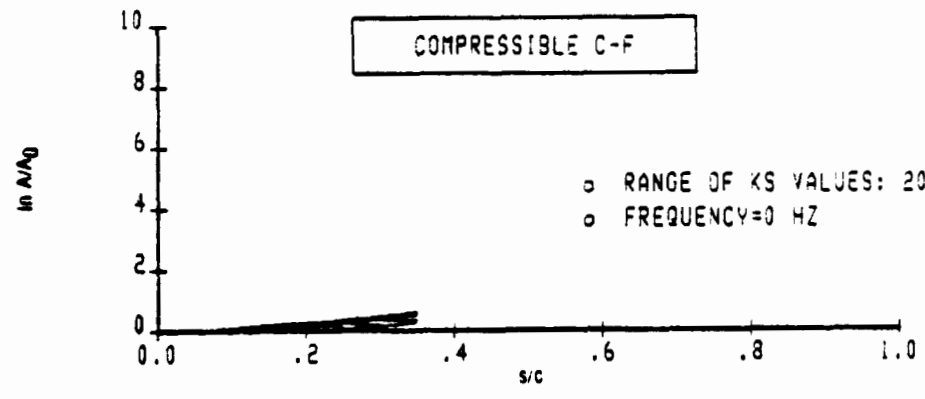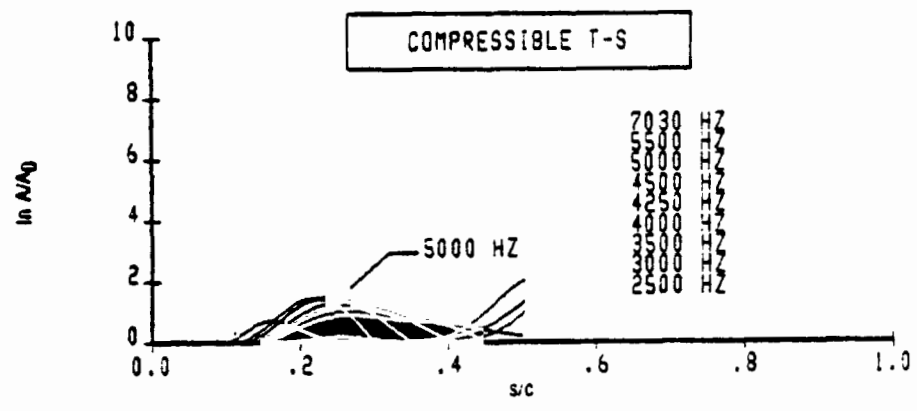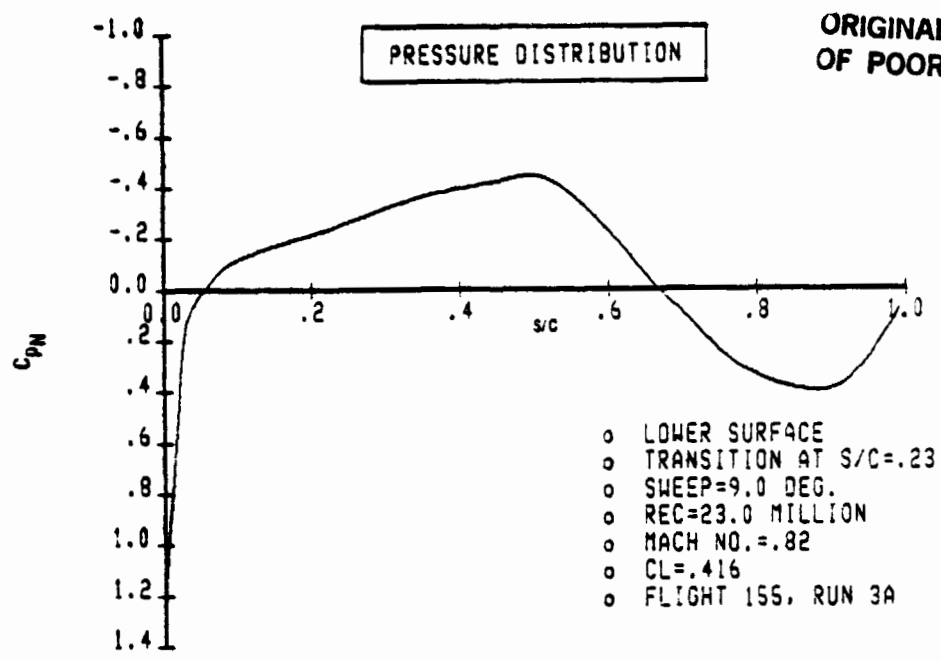Figure D-16.   F-111 Stability Analysis Results Case 25, Lower Surface

Figure D-17.   F-111 Stability Analysis Results Case 26, Lower Surface

Figure D-18. F-111 Stability Analysis Results Case 27, Lower Surface

PRESSURE DISTRIBUTION

- LOWER SURFACE
- TRANSITION AT S/C = .38
- SWEEP = 10 DEG.
- REC = 23.1 MILLION
- MACH NO. = .81
- CL = .407
- FLIGHT 146, RUN 3

COMPRESSIBLE T-S

5525 HZ

3516 HZ
4020 HZ
4521 HZ
5525 HZ
7031 HZ
10000 HZ

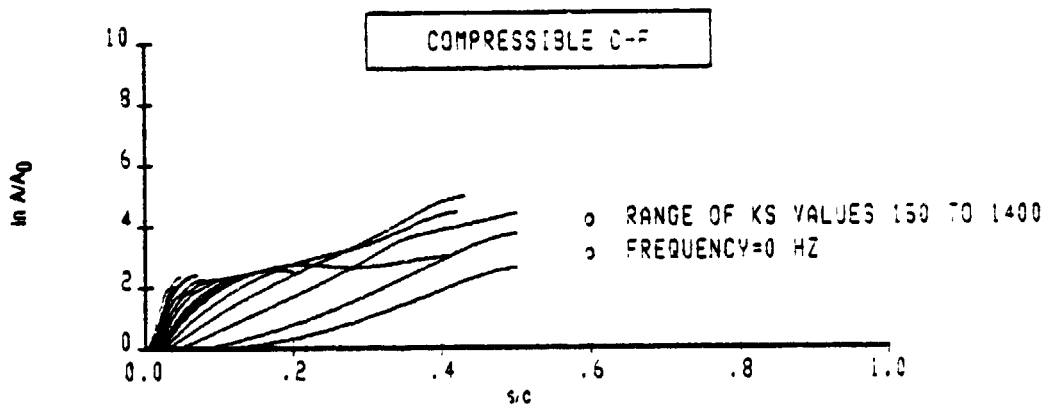S/C

- C-F IS NOT CALCULATED FOR THIS CASE.
  SEE TEXT, PAGE 41.

Figure D-19. F-111 Stability Analysis Results Case 28, Lower Surface

PRESSURE DISTRIBUTION

●LOWER SURFACE
●TRANSITION AT S/C = .34
●SWEEP = 10 DEG.
●REC = 23.4 MILLION
●MACH NO. = .82
●CL = .414
●FLIGHT 146, RUN 4

COMPRESSIBLE T-S

3021 HZ
3778 HZ
4029 HZ
4533 HZ
5037 HZ
5540 HZ
7051 HZ
10050 HZ

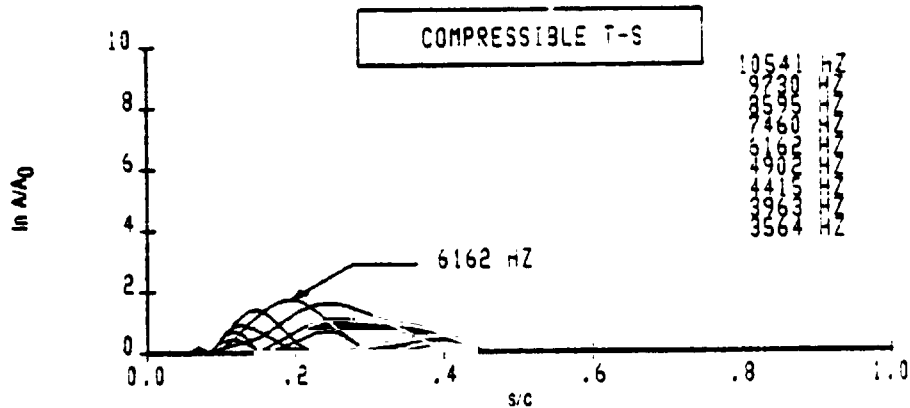5037 HZ

●●C-F IS NOT CALCULATED FOR THIS CASE.
SEE TEXT, PAGE 41.

Figure D-20. F-111 Stability Analysis Results Case 29, Lower Surface

PRESSURE DISTRIBUTION
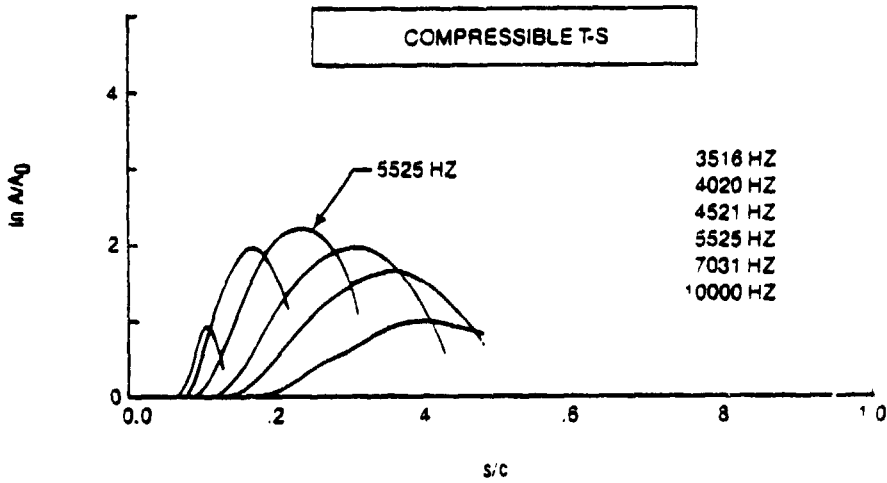
- LOWER SURFACE
- TRANSITION AT S/C = .48
- SWEEP = 10 DEG.
- REC = 26.9 MILLION
- MACH NO. = .81
- CL = .322
- FLIGHT 146, RUN 8

COMPRESSIBLE T-S

4189 HZ

5747 HZ

3670 HZ
3900 HZ
4189 HZ
4709 HZ
5196 HZ
5747 HZ
7304 HZ
10270 HZ

- C-F IS NOT CALCULATED FOR THIS CASE.
  SEE TEXT, PAGE 41.

Figure D-21. F-111 Stability Analysis Results Case 30, Lower Surface

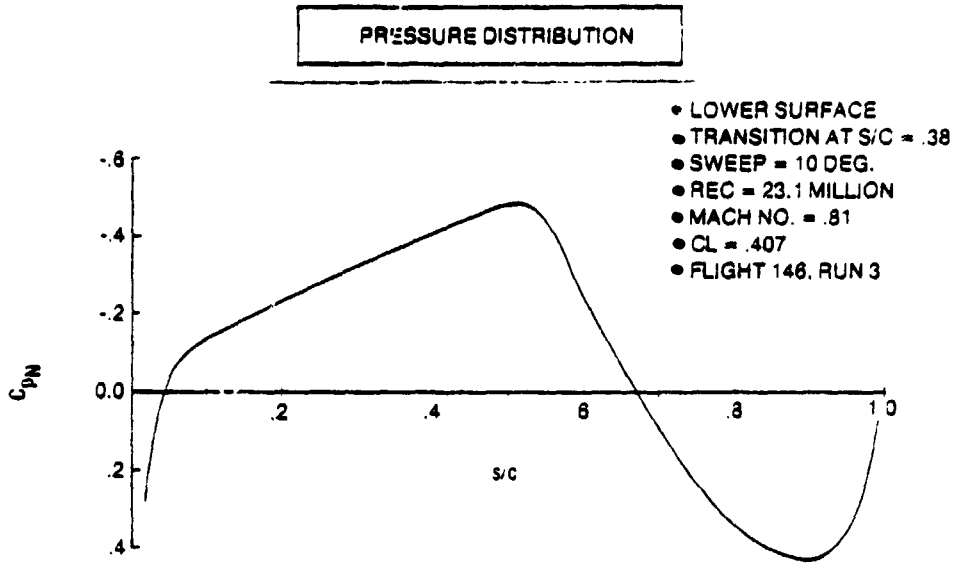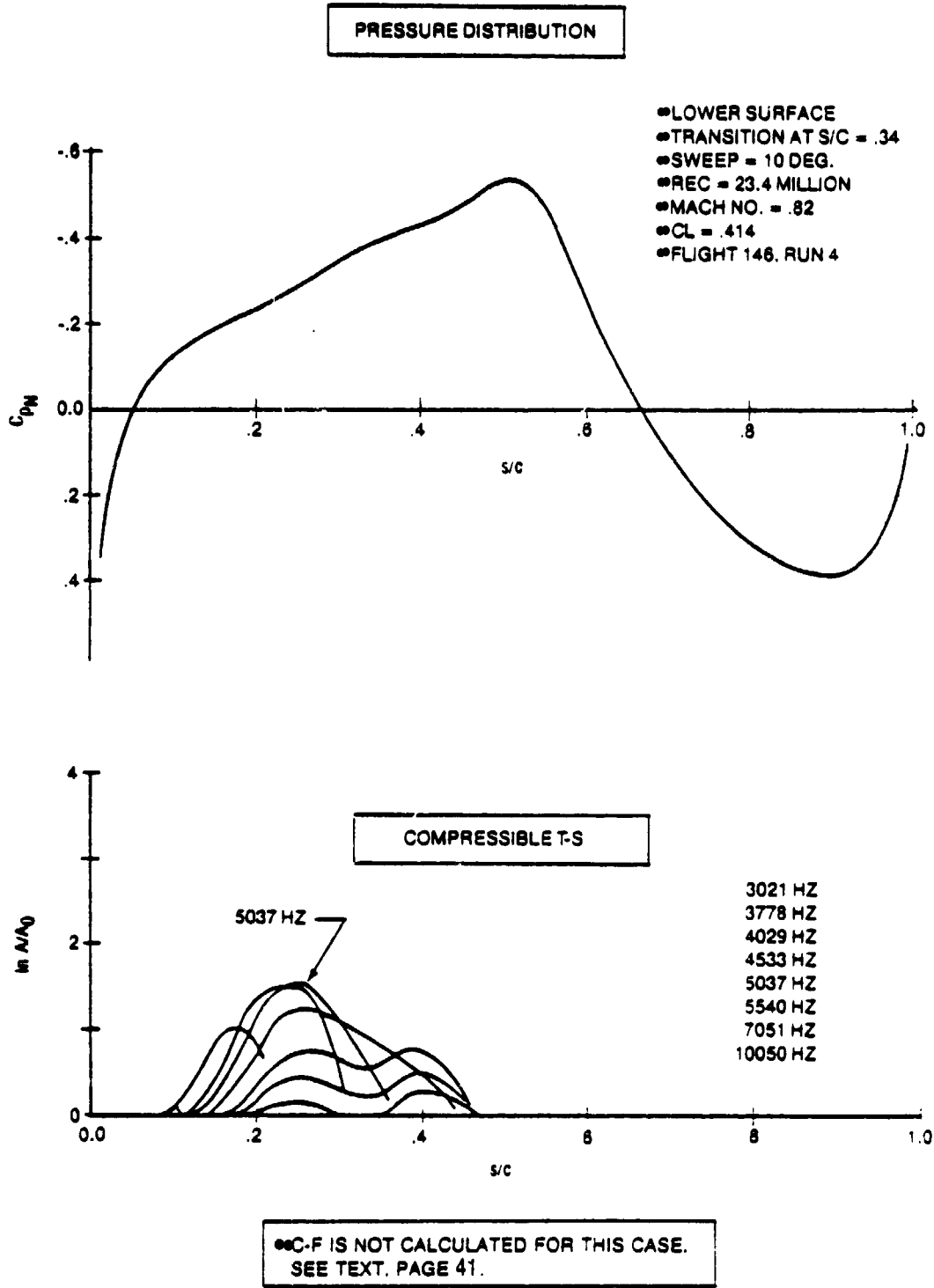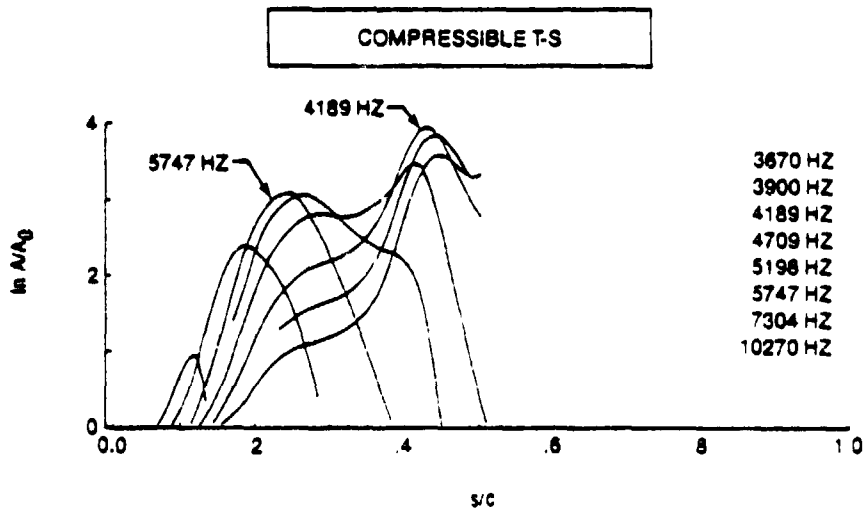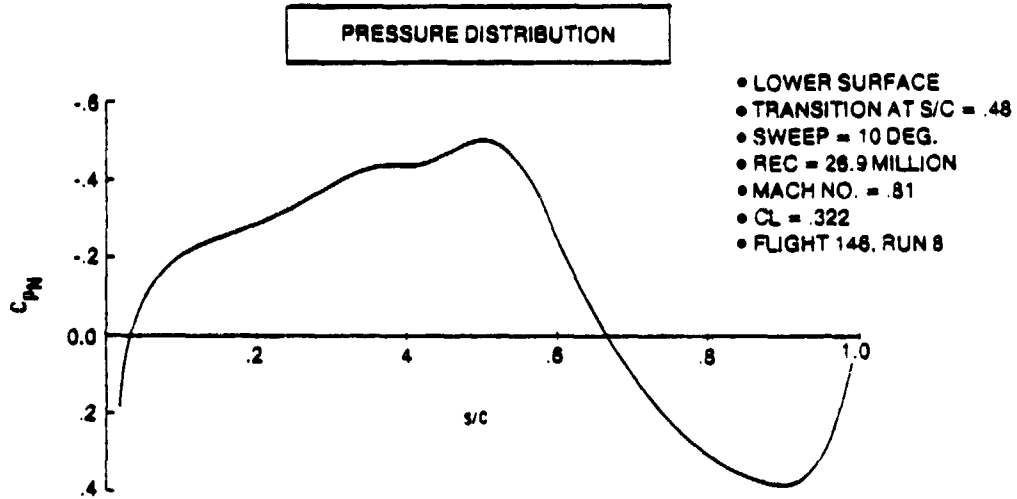**PRESSURE DISTRIBUTION**

- LOWER SURFACE
- TRANSITION AT S/C = .49
- SWEEP = 10 DEG.
- REC = 27.3 MILLION
- MACH NO. = .82
- CL = .314
- FLIGHT 148, RUN 9

COMPRESSIBLE T-S

5394 HZ
4319 HZ

4007 HZ
4319 HZ
4630 HZ
4938 HZ
5394 HZ
5864 HZ
7400 HZ
8800 HZ
11100 HZ

COMPRESSIBLE C-F

- RANGE OF KS VALUES 100 TO 1400
- FREQUENCY = 0 HZ
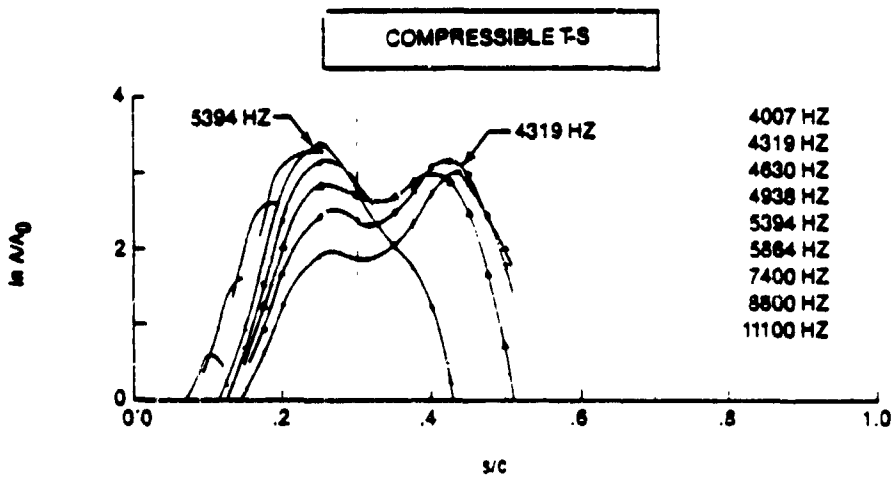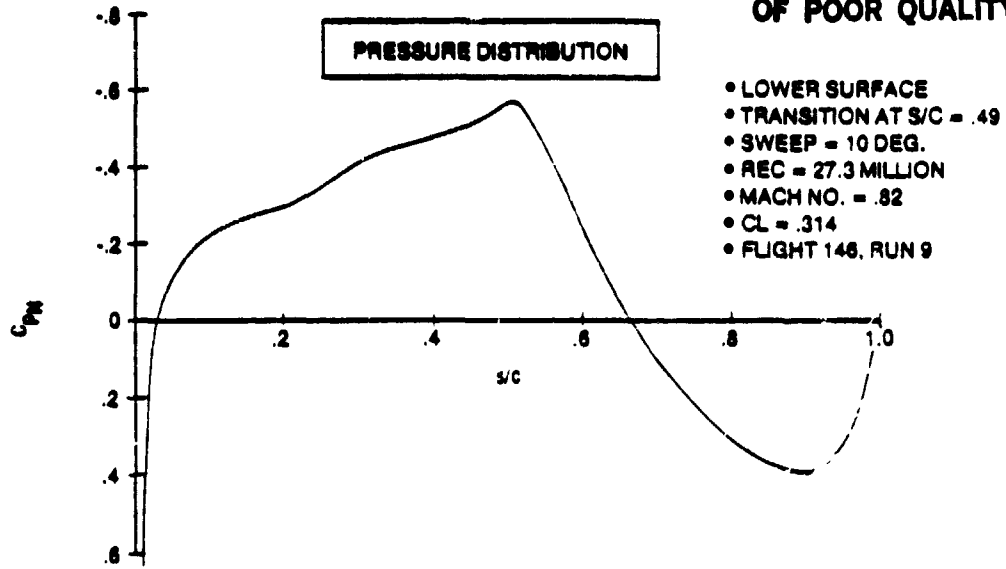
Figure D-22. F-111 Stability Analysis Results Case 31, Lower Surface

PRESSURE DISTRIBUTION

- LOWER SURFACE
- TRANSITION AT S/C = .51
- SWEEP = 15 DEG.
- REC = 27.7 MILLION
- MACH NO. = .83
- CL = .292
- FLIGHT 146, RUN 17A

COMPRESSIBLE T-S

3574 HZ
4083 HZ
4593 HZ
4900 HZ
5612 HZ
6501 HZ
7144 HZ
10000 HZ

5612 HZ

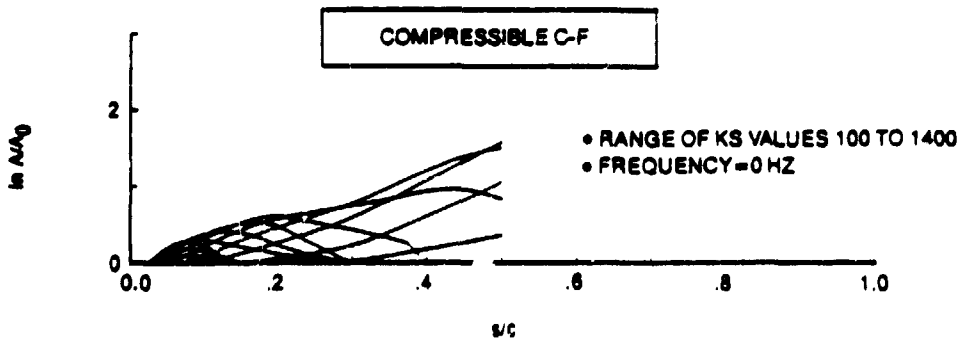**COMPRESSIBLE C-F**

- RANGE OF KS VALUES 100 TO 1400
- FREQUENCY = 0 HZ

Figure D-23. F-111 Stability Analysis Results Case 32, Lower Surface

PRESSURE DISTRIBUTION

- LOWER SURFACE
- TRANSITION AT S/C = 5¹
- SWEEP = 15 DEG.
- REC = 27.9 MILLION
- MACH NO. = .83
- CL = .415
- FLIGHT 146, RUN 17B

COMPRESSIBLE T-S

5503 HZ

3886 HZ
4129 HZ
4435 HZ
4984 HZ
5503 HZ
6083 HZ
7732 HZ
10871 HZ

COMPRESSIBLE C-F

RANGE OF KS VALUES 100 TO 1400
FREQUENCY = 0 HZ
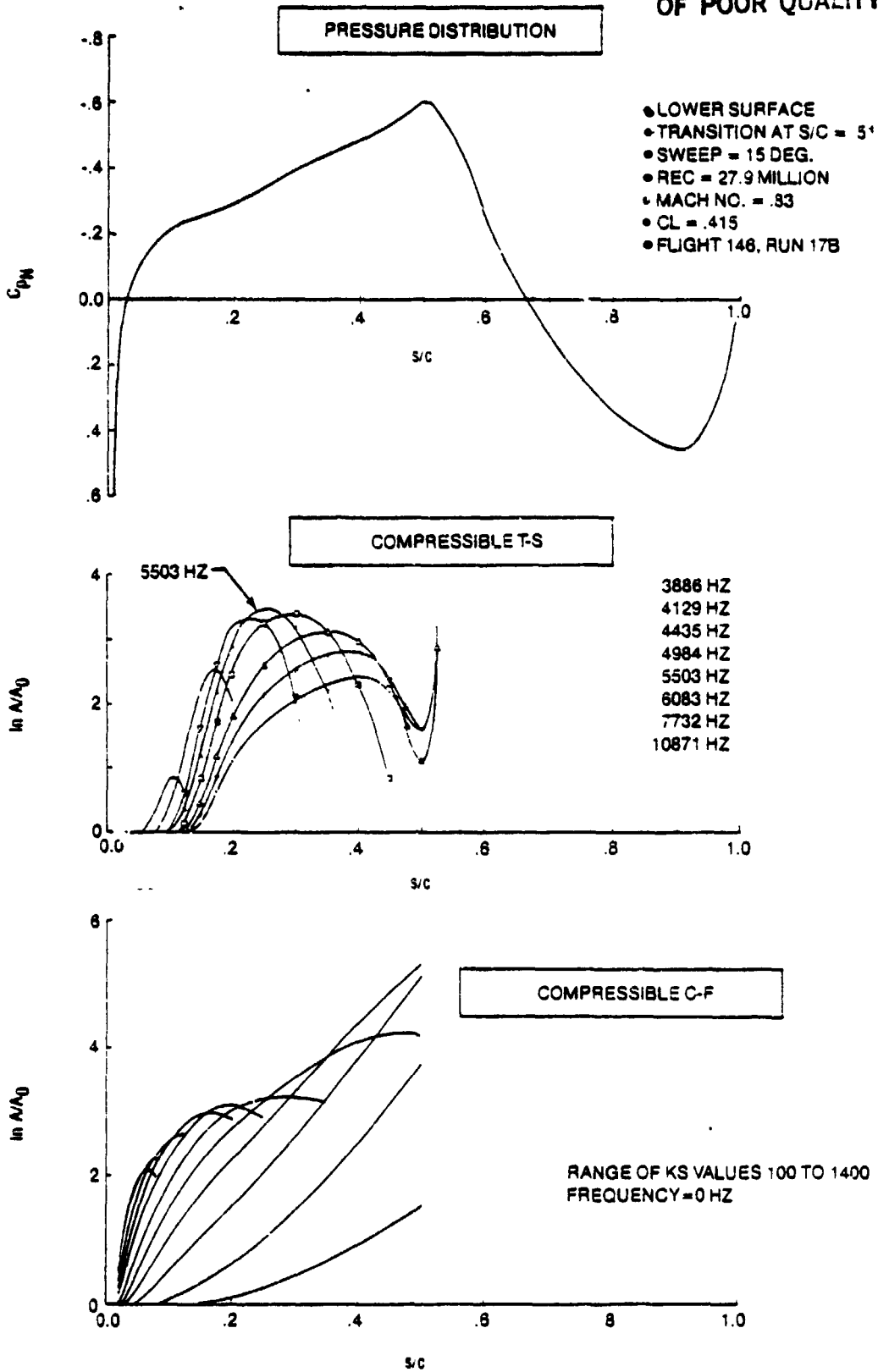
Figure D-24. F-111 Stability Analysis Results Case 33, Lower Surface

PRESSURE DISTRIBUTION
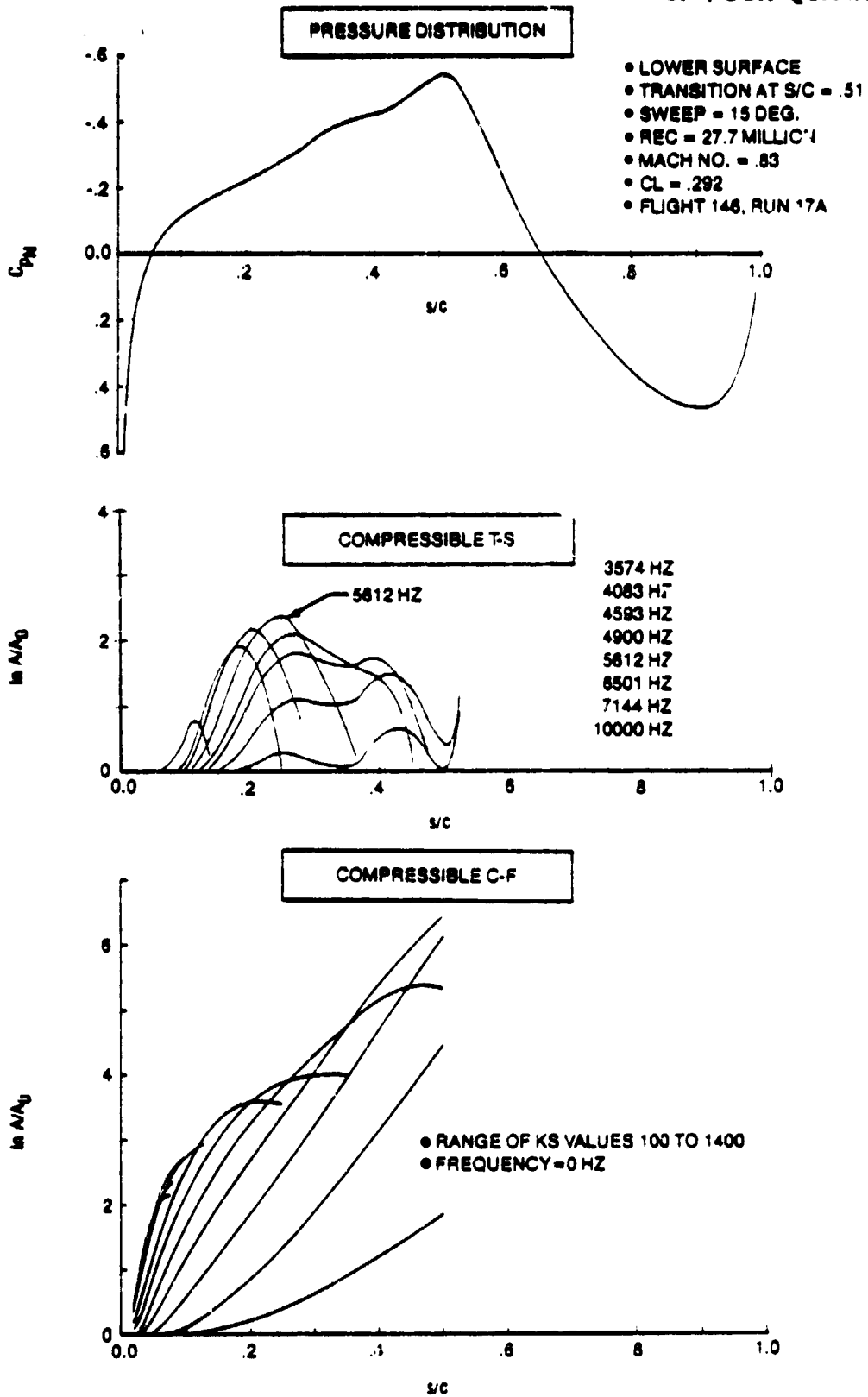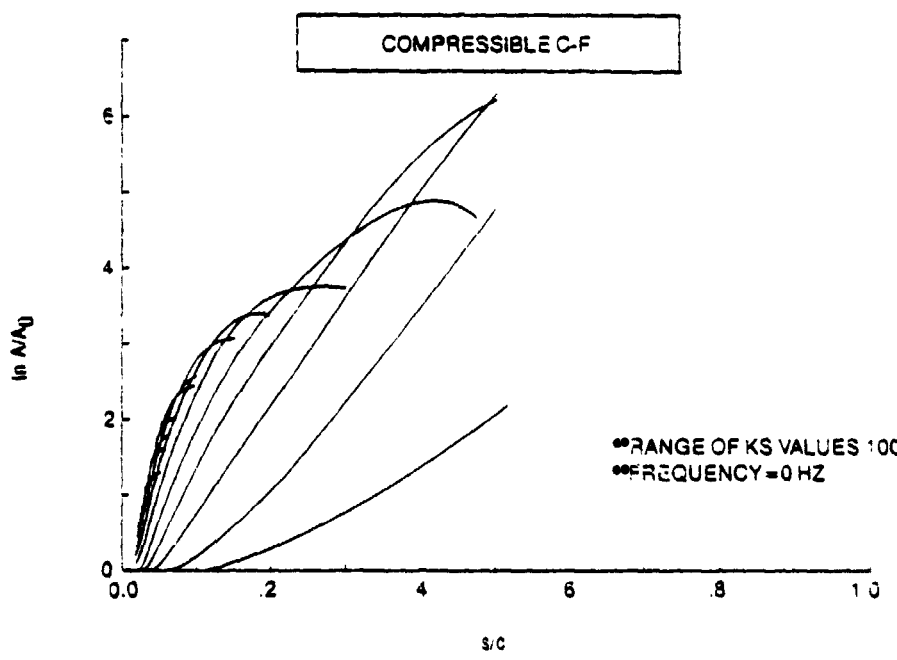
- LOWER SURFACE
- TRANSITION AT S/C = 51
- SWEEP = 16 DEG.
- REC = 23.2 MILLION
- MACH NO. = .83
- CL = .447
- FLIGHT 146, RUN 18B

C_{pN}

S/C

COMPRESSIBLE T-S

2859 HZ
3330 HZ
3800 HZ
4300 HZ
4800 HZ
5000 HZ
6632 HZ
8000 HZ
9510 HZ

5000 HZ

$\ln A/A_0$

S/C

COMPRESSIBLE C-F

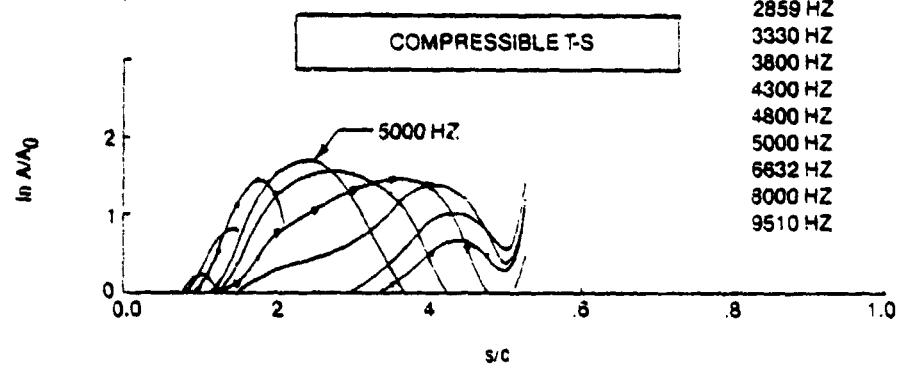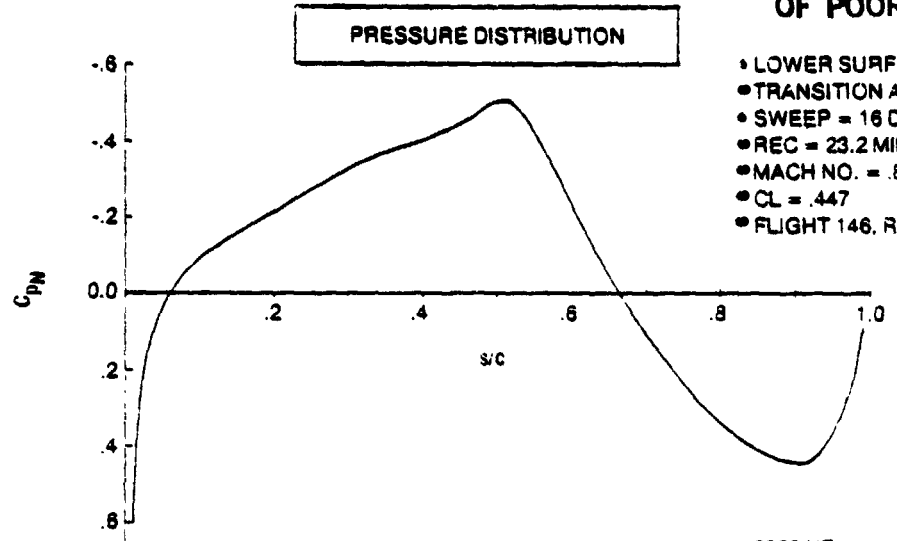$\ln A/A_0$

- RANGE OF KS VALUES 100 TO 1400
- FREQUENCY = 0 HZ

S/C

Figure D-25. F-111 Stability Analysis Results Case 34, Lower Surface